RHEOLOGICAL PROPERTIES AND STRUCTURE OF A
SEMI-SOLID TIN-LEAD ALLOY

by

PASCAL ADRIEN JOLY

Ingénieur Civil des Mines, Nancy, France
(1969)

M.S., Massachusetts Institute of Technology
(1971)

Submitted in partial fulfillment of the requirements

for the degree of

DOCTOR OF PHILOSOPHY

at the

Massachusetts Institute of Technology

June, 1974

.

Signature of Author . . . .

Certified by . . . .
Thesis Supervisor

Certified by . . . . Thesis Co-Supervisor

Accepted by . . . .
Chairman, Departmental Committee on Graduate Students

ABSTRACT

RHEOLOGICAL PROPERTIES AND STRUCTURE OF A
SEMI-SOLID TIN-LEAD ALLOY

by

PASCAL ADRIEN JOLY

The effect of various thermomechanical treatments on the structure and rheological behavior of Sn-15%Pb alloy in its solidification range was investigated using a concentric cylinder viscometer. The apparatus was designed to permit wide ranges of cooling rates up to 25°C/minute and shear rates up to 750 sec^{-1}. Initially, the alloy was continuously sheared as it cooled from above the liquidus to a desired fraction solid. In one series of experiments, shear was stopped and the alloy quenched. In a second series, the alloy was held isothermally and subjected to various mechanical treatments.

The size and morphology of primary solid particles during continuous cooling is influenced by both shear and cooling rates. Faster cooling results in finer structures while increased rate of shear reduces the amount of entrapped liquid in individual particles. At high cooling rate, 25°C/minute, primary solid particles size is $\simeq 50\mu$ and is independent of shear rate. Changes in the size of primary solid particles with shear rates (e.g. a decrease of size from 280 to 180μ for an increase in shear rate from 230 to 750 sec^{-1}) were only observed in slow cooled, 0.33°C/minute, specimens.

The viscosity of the slurry, at a given fraction solid, decreases with decreasing cooling rate and increasing shear rate. Exercising the full range of shear and cooling rates possible in the viscometer, the apparent viscosity of a 0.55 fraction solid slurry varied from 3 to 80 poise. The apparent viscosity of continuously cooled slurries obeys a "state equation" of the type proposed for non-metallic systems:

$$\eta_a = A \exp Bf_s$$

relating the apparent viscosity, η_a, to the fraction solid, f_s, the coefficients A and B are dependent on structure.

The structure and viscosity of isothermally held slurries follow the same trends as slowly cooled slurries, i.e. at a given fraction solid, particle size, amount of entrapped liquid and viscosity decrease with increasing shear rate. Furthermore, their viscosity at a given fraction solid is consistently lower than that of continuously cooled slurries.

Isothermally held slurries are pseudoplastic, i.e. variations up or down of shear rate result in a corresponding decrease or increase in measured viscosity. Over wide ranges of shear rate, the apparent viscosity of the slurries obeys a power law equation:

$$\eta_a = k\dot{\gamma}^n$$

relating the apparent viscosity, η_a, to shear rate, $\dot{\gamma}$. The coefficients k and n depend on the initial structure of the slurries.

The slurries are thixotropic and show a hysteresis loop phenomenon similar to other well known thixotropic systems. Measured areas of hysteresis loops increase with increasing fraction solid, initial viscosity (structure) and time at rest. For instance, the area for a slurry held at 0.45 fraction solid with an initial viscosity of 15 poise, varies between 2.0 and 8.0 X 10^5 dyne.$cm^{-2}sec^{-1}$ for rest times between 30 seconds and 30 minutes, respectively. These areas are comparable to measured areas for honey and epoxy mixed with silica flakes which are 1.5 and 3.0 X 10^5 dyne. $cm^{-2}sec^{-1}$, respectively. Isothermally held slurries follow "equations of state" relating the area of hysteresis loop, A, to the process variables (e.g. up time, t_u, and maximum shear rate, $\dot{\gamma}_m$). For instance, the slurries obey the equation:

$$A = A_o - Nt_u$$

where the coefficients A_o and N depend on fraction solid and structure.

A model is proposed to explain the thixotropic behavior. It is based on the formation and fracture of bonds between primary solid particles. The driving force for the formation of these bonds is the lowering of the interfacial energy of the liquid-solid interface whereas fracture results from the action of fluid flow forces on the particles. The model shows that at low shear rates (below a critical shear rate) agglomerates can form resulting in large particles with entrapped liquid, hence high slurry viscosity.

Finally a mechanism is proposed for the formation of particulate non-dendritic structure generated under vigorous agitation. It is one where, above a certain fraction solid of $\approx$0.15, a multiplication mechanism

breaks up initially formed dendrites into degenerate dendritic primary particles. Subsequently, coalescence and/or ripening occurs, driven by the lowering on the interfacial energy of the primary solid particles.

Thesis Supervisors: Robert Mehrabian
Assistant Professor of Metallurgy

Merton C. Flemings
Abex Professor of Metallurgy

TABLE OF CONTENTS

LIST OF FIGURES AND ILLUSTRATIONS

LIST OF TABLES

ACKNOWLEDGEMENTS

At the end of this long work,I would like to thank many people.

My advisors, Professor R.Mehrabian for his guidance and unfailing encouragement throughout the course of this thesis,Professor M.C.Flemings for his enthusiasm and his understanding during my graduate career at M.I.T.

My colleagues of the solidification group;my friends E.S.Palmer and J.P.Ibar for their constructive remarks; Ed Backan and Barbara Rich for their assistance ;Karen Seriff for the typing of this thesis;all my friends for their help.

The Army Research Office in Durham,North Carolina and the Army Research Project Agency in Washington,D.C., for their financial support.

Finally,my wife Nancy for her understanding and patience ,the value of which is beyond estimate.

CHAPTER I: INTRODUCTION

Rheology[1], the science of deformation, comprises the study of the flow behavior of liquids, the deformation and flow of semi-liquids or heterogeneous systems, and the deformation of solids under shear stress. So defined, rheology encompasses theoretically the study of the viscosity of liquid metals, the creep and fatigue of metals, and includes any aspect of deformation or flow of metal in its solidifying range.

One important contribution of rheology has been in the study of dispersions[2], and heterogeneous systems. Examples of such studies are: suspensions of pigments in oil (i.e. paint[3] and ink[4]), latex[5], and polymers[6]. In comparison the rheology of metals in their solidification range has received little attention. Exceptions would be the study of hot tearing[7] and fluid flow[8] during solidification (i.e. flow induced by mechanical or electromagnetic stirring, vibration, ultra-sonics and gas bubbling). It also includes the work on aluminum alloys by Galkin and Lomazov[9] who measured, at different fractions solid, the viscosity and its dependence upon the shear rate.

More recently, work at MIT[10,11,12,13] has shown that when alloys are subjected to vigorous agitation in their solidification range, they behave as low viscosity slurries. The fluid nature of the semi-solid alloys permits them to be cast at fractions solid as high as .50.

This process has been called "Rheocasting". In another related process, "Thixocasting", the thixotropic (shear-thinning) nature of metal slurries is utilized. The solid-liquid mixture, when left at rest, thickens

and behaves like a solid until it is sheared, as in die casting. It then behaves like a slurry and flows to fill the die cavity.

In order to apply these phenomena successfully, however, a better fundamental understanding of the rheological behavior of partially solidified, vigorously agitated metal slurries is necessary. It is to this end that the present study was undertaken. The first goal of the work is to relate the structure of a "Rheocast" ingot (i.e. particle size, shape, distribution of size, and degree of agglomeration of primary solid particles) to solidification parameters (i.e. cooling rate, shear rate, and fraction solid at which shear is stopped). The second goal is to describe the nature of the pseudoplasticity and thixotropy of metal slurries as they are maintained at a constant fraction solid.

CHAPTER II: LITERATURE SURVEY

A. Rheology

1. Definitions

Rheology is defined as the science which studies the flow characteristics of materials; its purpose is to find for every system a rheological equation[14] of the type $\Phi = \Phi(\tau,\dot{\tau},\ldots,\gamma,\dot{\gamma},\ldots,t) = 0$. Different materials show different rheological properties corresponding to their ability to deform under shear. One might say that the action of a force causes an elastic material to be strained, a plastic material to be deformed, and a liquid to flow. This difference in rheological behavior is due to the shear components of the stress, τ, since the isotropic pressure, σ, causes all of these materials to behave in the same way, i.e. elastically.

Most materials exhibit both elastic and viscous properties. Theoretically it is possible to represent any material (homogeneous or heterogeneous, solid or liquid) by an arrangement of viscous and elastic elements which, put together either in parallel and/or in series, would describe its flow behavior. This is the field of "body representation" or phenomenological rheology[15], and is mainly used for viscoelastic bodies (polymeric materials).

The drawbacks of this approach are the increasing difficulty of analyses as the number of elements is increased, and mostly the lack of physical interpretation for each new element. It is simpler to define classes of material according to the way their viscosity depends on shear

rate, or according to the shape of their flow curves   (obtained by plotting the shear rate versus the stress necessary to generate this shear rate).

2. Newtonian Material

The first class of materials is made up of liquids where the shear rate, $\dot{\gamma}$, is proportional to the shear stress, τ. They are referred to as Newtonian, since they satisfy Newton's law, $\tau = \eta\dot{\gamma}$, where, η, the viscosity is a constant (not dependent on the shear rate). It is the viscosity that is resisting flow, and dissipating the mechanical energy necessary to set the liquid in motion. On a graph of shear stress versus shear rate, Figure 1, the "flow curve" is a straight line starting from zero, whose slope is equal to the viscosity. Examples of Newtonian materials are water, (η = .01 poise at T = 25°C), and some oils (motor oil, η = 5-15 poise).

3. Non-Newtonian

In general the viscosity, η, is not a constant and depends on the rate of shear; the problem is to know what function of $\dot{\gamma}$, is the viscosity.

i) Power Law

A   power formulation $\eta = k\dot{\gamma}^n$, has been proposed[16]; it usually does not describe the system over the whole range of shear rates and the coefficient, n, has never been given a physical interpretation. It is best suited for pseudoplastic systems (with a negative coefficient) and dilatant systems (with a positive coefficient).

ii) Power Series

Power series have been suggested[16]

$$\eta = \eta_0 + \sum_{n=1}^{\infty} \alpha_{2n} \, \dot{\gamma}^{2n} \tag{1}$$

where η_0 is the value of viscosity at zero shear, and α_{2n} is the coefficient of the series. This formulation has two advantages: firstly, it can be applied on a wider range of shear, and, secondly, it relates the change of viscosity to the square of the shear rate, $\dot{\gamma}^2$, which is the dissipated strain power per unit viscosity. The drawbacks of this approach are: (a) computation of the coefficients is a lengthy task, especially for pseudoplastic materials where positive and negative coefficients must alternate, and (b) it does not ascribe a physical meaning to the coefficients.

iii) Closed Forms

Reiner[16] introduced a coefficient of structural stability, χ, defined as:

$$\chi = (\phi_{\infty} - \phi)/(dy/d\tau^2) \tag{2}$$

where ϕ is the fluidity (i.e. the inverse of viscosity), ϕ_{∞} and ϕ_0 are the fluidities at infinite stress and at zero stress, respectively. Integrating equation (2) gives:

$$(\phi_{\infty} - \phi)/(\phi_{\infty} - \phi_0) = \exp(-\tau^2/\chi) \tag{3}$$

and now χ can be determined from a semi-log plot of $\phi_{\infty} - \phi$ versus the square of the shear stress, τ^2. This equation is best suited for pseudoplastic materials.

There is no unique equation that can represent non-Newtonian systems. Even pseudoplastic materials, which are one class of non-Newtonian

materials, are represented by many different equations and only over a small range of shear rates.

4. Flow Curves

As mentioned above, the viscosity of most materials is not constant (their flow curves are not straight lines). Some, however, have time-independent rheological properties as do Newtonian materials. These materials are divided into four main classes[17,18] and will be described herein. There are two additional classes of materials whose rheological properties are time-dependent; these two groups of materials will be described last.

i) Bingham Bodies or Ideal Plastics

Some fluids exhibit a yield stress, τ_y, below which they behave elastically, but above which the shear rate is directly proportional to the difference between the applied stress and the yield stress, Figure 1. These fluids are termed Bingham bodies or ideal plastics. Their rheological equation is $\tau - \tau_y = \eta_{pl} \dot{\gamma}$. Substances which exhibit this type of behavior include oil-well drilling muds, sewage sludge, tooth paste, greases and fats.

ii) Pseudoplastic or Quasi-plastic Bodies

Materials which show behavior intermediate between Newtonian and Bingham fluids are called Pseudoplastics. In these materials, the viscosity is a function of the shear rate and decreases as the shear rate increases. Their flow curve is represented in Figure 1.

Materials in which pseudoplasticity is readily observed include paints, printing inks, polymer melts and some dispersed systems. In these systems

the shear stress is supposed to break down progressively the random ground state "structure" to an extent determined by the shear rate. There is a progressive build-up of a shear orientated "structure" and therefore easier flow.

iii) Dilatant Bodies

Dilatancy, often called shear thickening, is the opposite of pseudoplasticity, Figure 1. The viscosity increases as the shear rate increases. Examples of dilatant materials are some polymer melts and some very concentrated dispersed systems. No theory has yet been offered to explain dilatant behavior. However, this behavior is always described as the result of a structural build-up.

iv) Some materials can be described by a combination of the classes outlined above, each class operating on a small range of shear rates. Their flow curve has the shape shown on Figure 2a. It can be divided into four regions; I, Newtonian, II, Pseudoplastic, III, Dilatant, and IV, Newtonian. This phenomenon of variable viscosity is called structural viscosity[19] and the curve referred to as an Ostwald curve. Many materials exhibit this phenomenon but practical difficulties sometimes prevent their study at either very low or very high shear rates.

v) In another group of materials, called thixotropic materials, the shear stress does not reach a steady state value immediately after the application of shear. Instead, the shear stress decreases over a period of time due to structure breakdown until it eventually reaches a steady state value: an equilibrium is then established between the rate of breakdown and the rate of structure redevelopment. The time interval required for

equilibrium to be established decreases as the shear rate increases. If the shear rate is brought back to zero, the structure redevelops over a period of time. Many dispersed systems are thixotropic.

vi) Another, rather rare, class of fluids also exhibit a time dependent type of behavior which is the reverse of thixotropy and is called rheopexy. The shear stress increases with time until it becomes measurably independent of it.

The flow curve of thixotropic or rheopectic fluids cannot be represented on a conventional τ versus $\dot{\gamma}$ curve. The specific conditions under which a curve is obtained must be specified. For instance, in an experiment described by John-Pryce Jones[20], three different fluids are brought to rest after having been sheared, and are then sheared again after a time, t, at rest. Jones measured the deflection angle, θ, of the torque measurement device, as a function of the time at rest, Figure 2b, for each fluid. As shown in Figure 2b, Jones had to introduce another class of materials whose viscosities are also time dependent, false bodies, which are equivalent to thixotropic materials with a very short recovery time.

Since thixotropic materials are of primary interest to this study they are treated in detail in a subsequent section, II.C.

In summary, dispersed systems are not expected to be Newtonian; as will be seen in the next chapter some are pseudoplastic, and some are dilatant. Should rearrangement of structure be possible in metal suspensions, both an Ostwald curve and a time-dependency of the thixotropic type can be expected.

B. Rheology of Dispersions

1. Definitions

The feature common to all dispersed systems is their hetero-geneity[21] (i.e. there is a discontinuity in their physico-chemical properties - at least two phases are present). Examples of dispersed systems include the following: coarse suspensions, and coarse emulsions, where the size of second phase particles is greater than 10 microns; colloidal systems where the particle size varies between 10 Å and .1 micron and finally molecular and supermolecular dispersions where the size of the second phase element is below 10 Å. The term 'emulsion' refers to a mixture of a liquid in a liquid and the term 'suspension' to a mixture of a solid in a liquid[21]. Therefore, slurries of solid metal particles in equilibrium with liquid metal are suspensions and more precisely very coarse suspensions; solid particles vary in size from 30 to 500 microns[10,13].

2. Viscosity of Suspensions: Theory

The theoretical calculation of the viscosity of suspensions of solid particles can be approached in several ways[22,23]. Firstly, the viscosity may be determined from the velocity gradient

$$\tau_{ik} = -\eta(\frac{\partial u_i}{\partial x_k} + \frac{\partial u_k}{\partial x_i}) \tag{4}$$

and, secondly, from the energy dissipation in the bulk of the liquid

$$E_v = -\eta \int_v \frac{\partial u_i}{\partial x_k} (\frac{\partial u_i}{\partial x_k} + \frac{\partial u_k}{\partial x_i})dv \tag{5}$$

where τ_{ik} is the shear stress on the plane i in the direction k. The u's

are the velocities at the locations x, and E_v is the energy dissipated in the bulk of the fluid by the viscous forces.

For the case of dilute suspensions, less than .01 in concentration, there is good agreement[24,25] among the different theoretical studies that the viscosity, η_a, is a simple linear function of the volume concentration, g_s,

$$\eta_r = \eta_a/\eta_0 = 1 + k_1 g_s \tag{6}$$

where η_0 is the viscosity of the pure fluid without particles. For solid spheres the commonly accepted value of k_1 is 2.5[26]. Other calculations carried out for ellipsoidal particles[27] result in k_1 values lower than 2.5; similar calculations are reported for rod shaped particles[28].

With more concentrated suspensions, it is necessary to account for the hydrodynamic interaction of particles, particle rotations, collisions between particles, mutual exclusion, doublet and higher order agglomerate formation, and ultimately mechanical interference between particles as packed bed concentrations are approached. Perhaps the greatest difficulty in arriving at a theory for these concentrated suspensions is the fact that the random structure of the suspension cannot in general be represented by a simple model[34].

Many of the existing theories can be expressed as power series

$$\eta_r = \eta_a/\eta_0 = 1 + k_1 g_s + k_2 g_s^2 + \cdots \tag{7}$$

in which η_r is the relative viscosity and the k's are constants to be determined; k_1 is generally assumed to be 2.5 and k_2 has been calculated to be 14.1[29], 12.6[30], 7.35[31], and 10.0[32].

Several expressions have been proposed which give the relative viscosity of a suspension as a function of concentration in a closed form. Mooney[33] arrived at a functional equation for the relative viscosity by considering two successive additions of uniform spheres to a pure fluid. In this way he accounted for the possible interactions and the mutual crowding effect of the two fractions of spheres on each other. Solution of the functional equation resulted in

$$\eta_r = \exp[2.5 \, g_s/(1 - k_3 g_s)] \qquad (8)$$

where the value of k_3 is determined experimentally. From a model based on the geometry of the cubic and face centered lattices, and the fact that for spheres in contact the relative viscosity must be infinite, Mooney suggested a value of k_3 between 1.35 and 1.91.

In summary, several quantitative descriptions of viscosities of concentrated suspensions have been attempted. However, the physical significance of the various terms used in the proposed equations is rarely verified.

For example, investigators have rarely addressed themselves to the problem of determining the effects of particle size, shape, or distribution of size on viscosity. Many researchers have found that it is better to use experimental data and develop empirical equations to interpret their findings.

3. Viscosity of Suspensions: Experimental Data

Many experiments have been done on suspensions of coarse particles in liquids of different viscosity. The best way to compare these data

is to plot the relative viscosity, η_r, versus the volume fraction solid of second phase. This was done by Thomas[34] and is shown in Figure 3. The particle materials include polystyrene, rubber latex, glass and methyl-methacrylate. In this work the density of the suspending medium was chosen to match the density of the suspended material. These data were obtained with both rotational and capillary viscometers and represent a range of spherical particle diameters from .1 to 435 microns.

The two main features of the curve in Figure 3 are: first, the slow rise at low fraction solid, and the fast rise as fraction solid exceeds 0.40; second, the small scatter of the data (13% at g_s = .50 and 6% at g_s = .40). Thomas[34], however, only reports data for closely sized systems and uses limiting values of the viscosity whenever it is affected by their size. For particles less than 1 micron in diameter, the limiting value of the relative viscosity is obtained as the intercept of a linear plot of 1/D versus η_r (where D denotes the particle diameter); for particles larger than 10 microns, the limiting value of the relative viscosity was obtained as the intercept of a linear plot of D versus η_r.

Thomas[34] was able to find an empirical equation to fit these data points

$$\eta_r = 1 + 2.5 \ g_s + 10.05 \ g_s^2 + A \ exp \ B \ g_s \qquad (9)$$

The first three terms in equation (9) take into account the hydrodynamic interaction; the last term is only to be added at concentrations higher than g_s = .25 and takes care of the rearrangement of particles in the suspension. This last term is proportional to the probability of a particle

transferring from one shear plane to another and its use was first suggested by Eyring[35]. Thomas calculated the values of A = .0027 and B = 16.6 from his data.

The large number of data points, the different nature of particle materials, and the good fit of the curve justify the use of his curve and equation as a standard for comparison with measurements carried out on metal slurries. Yet many other problems arise as the viscosity of some suspensions, including metal slurries, are found to be dependent on shear rate, and on particle size, shape and distribution. These effects are reviewed in the next paragraphs.

i) Effect of Shear Rate

Suspensions of particles in the size range .10 to 230 microns exhibit both pseudoplastic and dilatant types of behavior, depending on the viscosity of the suspending medium and the shear rate, Table I. Suspensions of glass spheres in the size range 50-230 microns in polyisobutylene were found[37] to be pseudoplastic at shear rates up to 1 sec^{-1}. Suspensions of glass beads in the size range 25-150 microns in a sucrose solution were found[36] to be Newtonian up to a volume fraction g_s = .65, at shear rates up to 1300 sec^{-1}. Suspensions of quartz grains, 50-200 microns, in water are found[38] to be dilatant between 0.10 and 0.30 fraction solid at 350 sec^{-1}.

ii) Effect of particle Size and Shape

The effects of particle size and shape on the viscosities of suspensions are listed in Table II.

Clarke[38] studied suspensions of quartz grains in water and found the

viscosity increased from .14 to .38 poise at g_s = .30 as the size increased from 10 to 200 microns. He explained this behavior as a result of the increased dissipation of energy in collisions. When there is a difference of density between the suspending medium and the suspended medium, inertial forces are not balanced during collisions and some energy is dissipated.

Other authors[40,41] have observed the reverse phenomenon with suspensions of irregularly shaped particles. One[40] has studied suspensions of coal (150 microns and under) in oil and reports that the viscosity is multiplied by 2.5 times as the size is decreased from 150 to 50 microns at .35 fraction solid. Other workers [41] report data on methyl-methacrylate particles in a modified glycerol covering the size range 40 to 280 microns. At 0.15 fraction solid they observed an increase in viscosity (by a factor of 2.5) as particle size decreased from 280 to 40 microns. In this study, the authors explain the observed behavior as a result of a layer of stagnant liquid, participating in the movement of each particle and thus increasing the effective fraction solid.

The data do not permit an isolated conclusion of the effect of particle size to be drawn but indicate that, whenever particles are not spherical, the relative viscosity is higher than that of a suspension of spheres and increases with increasing size[41]. In one study[42] (suspension of clay particles in water, .4 to .8 microns in size), the relative viscosity increased 39% at g_s = .20 from .018 to .025 as the axial ratio went from 1 to 10. This increase is due to the greater flow resistance of the particles themselves and to the larger probability of interference between the particles. As the axial ratio becomes very large $\simeq 10^4$ (long rod-like

particles), it is found[43] that viscosity increases tremendously. For instance, suspensions of SiO_2-SiC whiskers have viscosities 20 times larger at g_s = .10 than those of spherical particles; this increase is due to the entanglement of the whiskers[43].

iii) Effect of Particle Size Distribution

In general, as the size of particles becomes non-uniform, the viscosity of a suspension decreases. The distribution does not have to be multimodal (discontinuous) but can be monomodal (continuous) and cover a certain range from the smallest to the largest particle.

For monomodal distribution of particle size, the viscosity of the corresponding suspension is at a minimum whenever the size ratio, R, (ratio of the smallest to the largest particle) is lower than 1/1.4[44]. This is true for dilute ($g_s \leq$ .20) as well as very dilute suspensions.

For bimodal distribution (distribution made of two different sizes, each of which has a size ratio of 1/1.4 or less), the blend ratio (ratio of the concentration of smaller particle to the concentration of larger particle, g_{s1}/g_{s2}) and the size ratio, R_{12}, (ratio of the smallest to the largest size) have each an effect of their own on the viscosity of the suspension[45]. Results of this study are shown in Figure 4, for particles of glass ranging in size from 25 to 250μ suspended in polyisobutylene[37]. The volume fraction of the smaller particles, 25 to 40μ in size, was kept constant at g_{s1} = .25. Thus, at each given total volume fraction solid, the blend ratio is constant and the different curves show the effect of the size ratio, R_{12}. Whereas, for each size ratio, the variation of viscosity with the blend ratio and fraction solid is indicated by the curve denoting

this specific size ratio.

In general at a given blend ratio, viscosity increases with increasing size ratio. When the size ratio is less than 1/10, the optimum blend ratio is 1 (50%-50% in volume of solid phase of each size).

For trimodal and multimodal distributions, the optimum blend corresponds to optima for the corresponding bimodal systems[45]. So for a trimodal distribution, one would have a blend ratio of 1 (i.e. 33% in volume of each size). The finer particles in a bimodal suspension are believed[45] to behave essentially as a fluid toward the coarser particles, seeming to play a "ball bearing" role for the larger particles and decrease the energy dissipated in collisions.

iv) Effect of Aggregation

Aggregation of particles always results in higher viscosity[46]. Differences in viscosity of up to two orders of magnitude are found for aggregates containing up to 300 particles. This is primarily due to the increase of effective volume fraction solid as more and more liquid is entrapped in the aggregates.

v) Settling and Non-Settling Suspensions

The major problem in studying the rheology of settling suspensions is to avoid sedimentation and plug flow. Clarke[38] studied suspensions of quartz and glass spheres in water. He used a concentric cylinder viscometer, which he placed in a stirred vessel to keep all the solids uniformly dispersed. He observed that slippage occurred at high shear rate ($\dot{\gamma} > 250$ sec^{-1}) for large particles (D > 150 microns). To prevent slippage he used vertical grooves on the wall of the cup and bob, .0625 inch wide,

.04 inch deep, and .1 inch apart and showed that the Reynolds Number was still compatible with laminar flow. But he added that it has not yet been established whether local turbulence takes place owing to the movement of particles (see Appendix E on turbulence).

His major contribution was that he demonstrated the difference between settling and non-settling suspensions. When the density of the solid particles is greater than that of the suspending medium, the viscosity increases with increasing particle density; it increased from .06 to .24 poise at g_s = .40 as the difference in density increased from .172 to 1.96 g/cm^3.

Ward[47] modified equation (6) and added another term, K, to account for density differences between the particles and the suspending medium. He found an empirical relationship between K and the difference in density, $\Delta\rho$,

$$K = 1.6 \times 10^{-3} \ \Delta\rho/\eta_0 \tag{10}$$

His modification of equation (6), relating relative viscosity to fraction solid, becomes

$$\eta_r = (1 - k_1 \ g_s - K)^{-1} \tag{11}$$

where η_0 is the viscosity of the suspending medium. His data were obtained from suspensions of solid particles in the size range 60-100 microns in solutions of glycerol in water. Figure 5 shows a plot of equation (10) with data from Ward[47], Clarke[38] and DeBruijn[48]. If equation (10) is rewritten as

$$K = (2.3 \pm 1.4) \times 10^{-3} \, \Delta\rho/\eta_o \qquad (12)$$

it will cover the whole range of particle sizes from 50 to 700 microns.

In general, the viscosity of a suspension increases with increasing density difference between the particles and the suspending medium. Clarke[38] attributed this phenomenon to the decreased viscous drag forces experienced by colliding particles when their density exceeds that of the suspending medium. Consequently the particles easily move around and rebound from one another increasing the number of interactions, the total energy dissipated, therefore the viscosity. This competition of viscous and inertial forces is reflected in equation (10) where the important parameter is the ratio of the difference of density to the viscosity of the suspending medium.

In summary it is apparent that many factors have an effect on the viscosity of suspensions. It is very difficult to isolate the observed effect of a single parameter and to predict its sole effect on the viscosity of a new system. The problem becomes more complicated when predictions are to be made using the combined effect of two or more parameters. Yet it is possible to describe the general mechanisms operating when a suspension is sheared. This is done in the following section. An understanding of the mechanisms involved and their contribution to the viscosities of suspensions will permit certain predictions about the rheological behavior of a given system.

4. Mechanisms of Non-Linear Behavior

The behavior of a dispersed system can be explained[49] by the fact that suspended particles interfere with the mobility of part of the

suspending medium. There are two sorts of interference: 1. Disturbance
and 2. Immobilization.

Disturbance is a hydrodynamic problem which can be defined as an
interference experienced by the suspending medium as it moves by the parti-
cles of the suspension. For dilute suspensions of rigid spheres the problem
was solved by A. Einstein[26]. Non-spherical particles have been treated by
Jeffery[27] and others[50] who observed that particle rotation should also
be considered. If anisotropic particles rotate, the volume of fluid dis-
placed in their rotation is much larger than their own volume. The parti-
cle motion is then equivalent to the motion of a sphere of higher diameter
and the effective volume fraction is much higher than the actual one.

One can thus explain now why suspensions of elongated particles are
more viscous. Furthermore, at higher shear rates, the particles can orient
themselves in a direction such that they do not rotate, their motion
becomes limited, and the lesser disturbance results in lower viscosities.
This, for instance, explains why suspensions of ellipsoids are pseudo-
plastic.

As the volume fraction of particles in the suspension increases, there
is a further contribution to disturbance due to the interaction between
particles. To ascertain this contribution to the viscosity of a suspension,
it is necessary to differentiate between attracting and non-attracting
particles.

The interaction of non-attracting particles is usually limited if
particles and liquid have the same density; the particles are then con-
strained by the viscous drag of the fluid and exchange no inertial forces.

Should their density not be the same, each collision absorbs some energy and as the number of collisions increase with shear rate, dilatant behavior will be observed.

Attracting particles, per se, are not different from non-attracting particles in suspension. However their potential to create aggregates whenever they enter the domain of attraction of another particle, results in a change in the structural configuration of the suspension that can lead to higher interference[65] (i.e. disturbance). Attracting particles can also cause the dissipation of energy through the breaking or forming of bonds. Michaels and Bolger[68] explain that it takes energy to pull two particles apart, yet when they recombine by collision, the separation energy is not recovered but rather dissipated in local disturbances around the contact point. This would explain why some suspensions made of attracting particles are more viscous than those of non-attracting particles at equivalent fraction solid[68]. It is extremely difficult to predict how this contribution (dissipated energy) varies with shear rate.

Immobilization is due to the fact that suspended particles generally bind part of the suspending medium so that an effective larger particle is formed which is suspended as a whole in the suspending medium.

Immobilization can be an important contributing factor to the viscosity of a suspension[47]. Many particles absorb a certain layer of liquid which participates in their motion and increases the effective fraction solid. Should this layer be sheared off as shear rate increases, pseudo-plasticity will be observed[49].

Liquid can also be immobilized if it permeates or is entrapped in the

loose structure of a giant molecule or of an aggregate. This is why suspensions of aggregates give higher viscosities[46].

The effect of shear rate on immobilization is generally time dependent. As shear forces are increased, aggregates break up and release entrapped liquid. Yet, the number of collisions increases with increasing shear, thus increasing the probability of aggregate formation. Very often a dynamic equilibrium is reached between the rate of break-up and the rate of build-up[64]. More details are given in Appendix G, specially on how to compute the kinetic constants. It is possible to conclude that it will take a finite amount of time for this equilibrium to be attained, resulting in time dependent rheological properties. This phenomenon is further discussed in the section under: Thixotropy.

The brief discussion above deals with suspensions of attracting or non-attracting particles but it always assumes that there is no reaction taking place between the liquid and the solid. Should the latter be true, other phenomena, such as the requirement of a thermodynamic equilibrium at the solid-liquid interface, come into play and an analysis of the rheological behavior of such a suspension is more difficult.

In the next section, a survey of the known cases where such reactions occur, between the liquid and the solid, is presented.

5. Rheology of Bodies in Their Melting Range

A few studies have dealt with the rheological systems where changes of phase, such as solidification, precipitation, and dissolution take place[10,51,52].

Basalt[51] was investigated at different temperatures; at .25 fraction

solid, the measured viscosity is 2000 poise (2 orders of magnitude higher than that of the liquid). The system was found to be highly pseudoplastic, over the range of shear rates 0-10 sec^{-1}.

The rheological behavior of a partially crystalline polyethylene has been studied in a Couette viscometer[52]. It was found that viscosity increases sharply as the crystallinity increases and that it is shear rate dependent. Measured viscosities decreased as shear rate was increased from 30 to 10,000 sec^{-1}, Figure 6a. This pseudoplastic behavior was attributed to the formation of crystallites or aggregates at low shear rate. Some liquid crystals[53], just below their melting point, exhibit an equivalent flow behavior, Figure 6b.

Partially solidified, vigorously agitated, slurries of tin-lead alloys were first studied at M.I.T. in 1971[10]. A Couette viscometer was used to measure induced torque, hence viscosity, at given shear rates and fractions solid. A major finding of that work was that the partially solidified slurries exhibited a "shear thinning phenomenon". This was explained in terms of the size and shape of the primary solid particles in the slurry. It was found that with increasing shear rates these particles became elipsoidal in shape and were oriented in the flow direction. While it was recognized that this "shear thinning phenomena" could be ascribed to the thixotropy of the system, few controlled dynamic experiments were carried out to verify this fact.

The study reported here was undertaken to verify, expand and explain these previous observations. To this end, the apparatus was modified to permit controlled large variations in shear rate. Experimental

measurements were coupled with detailed metallographic studies. Finally,

the rheological behavior of the partially solidified tin-lead

alloys was   compared with other well known thixotropic systems.

C.   Thixotropy

1. Definition

In his introduction to thixotropy, H. Freundlich[54] describes

thixotropy as an isothermal, reversible sol-gel transformation, i.e. "if it

is possible to liquify a certain gel into a sol, simply by shaking or

stirring, and if the sol sets into a gel again when left at rest" then this

system (sol or gel) is a thixotropic material. So defined it would narrow

the range of thixotropy to sol and gel (i.e. suspensions of ultra-micro-

scopic particles); but he adds that the same phenomenon, time-dependent

shear-thinning, has been observed on suspensions made up of much larger

particles such as clay or pastes[55]. In present day terminology, a

thixotropic system is one which features a time dependent, shear thinning,

reversible viscosity.

2. Thixotropy Characterization

Even though Freundlich[54] defined thixotropy as a reversible

isothermal shear-thinning mechanism, he proposed very crude tests to

observe and measure it. Some of the more advanced experimental techniques

used to characterize thixotropic systems are as follows:

i) "Equivalent Flow Curve"

Alfrey[56] devised an experiment whereby one applies a

constant stress, τ, to a material and measures the variations of shear, γ,

as a function of time, Figure 7a. For each new shear stress, a new curve,

γ versus time, is obtained. On each of these curves the initial rate of increase of the shear is measured (i.e. the shear rate at time zero), Figure 7a. The experiment is repeated after leaving the system at rest for different times,t, and a surface in the three-dimensional space, $\dot{\gamma}$, τ, t is generated, Figure 7b. The disadvantages of this method are: first, the requirement of having a constant stress viscometer, second, the long times necessary to generate sufficient data, and finally the difficulty involved in measuring $\dot{\gamma}_o$. Furthermore this procedure does not give any information about the nature of the structural breakdown or about its kinetics.

ii) Hysteresis Loop

An excellent method used to characterize thixotropy is that developed by Green and Weltmann[57], and consists of measuring a hysteresis loop. They used a rotational viscometer in which the angular velocity could be varied continuously. The procedure commences with an up-curve, starting at zero speed. The speed is then increased continuously and rapidly while measuring the change in induced torque. At some specified upper rotational limit, the speed is either maintained constant and then reversed or simply reversed to zero and a down-curve is measured. If the material is thixotropic, the up- and down-curves (i.e. torque versus shear rate) when plotted together will not coincide, thus forming a loop. This condition is ascribed to a thixotropic breakdown. A large loop means considerable breakdown, while a small loop signifies small breakdown or little thixotropy, Figure 8a. This quantitative description of thixotropy (i.e. area of the hysteresis loop) is also affected by the time it takes to attain the desired maximum shear rate itself.

The hysteresis phenomenon is the result of the time element involved in the breakdown of the structures of the thixotropic systems. It was already mentioned that pseudoplasticity is the result of a structural breakdown due to shear - the main difference is the relaxation time: it is infinitesimally small for pseudoplastic systems and finite for thixotropic ones.

Having indicated that thixotropy is a problem of kinetics (the kinetics of structural breakdown) it will now be shown how, from the loop measurements, one can derive useful information as to the exact conditions of the process. This is done in the next section.

3. Hysteresis Loop Analysis

There are two methods for breaking down thixotropic structures: by increasing the shear rate and by prolonging the time duration of the applied torque. It is thus important to follow how the area of the hysteresis loop is affected by the time it takes to attain a desired maximum shear rate as well as by the value of this maximum itself.

i) Effect of Time

Figure 8b shows how the time it takes on the up-curve to reach the maximum shear rate, $\dot{\gamma}_{max}$, affects the corresponding maximum torque value. For short times, $t = t_0$, the path followed is denoted as T_2B_0. With increasing times the torque necessary to sustain a given shear rate decreases (e.g. for $t = t_1$), the path followed is T_2B_1. After reaching the maximum shear rate the corresponding torque decreases to a steady state value with time, at B_n, Figure 8b. The down-curve, B_nT_2, is then obtained by decreasing shear rate back to zero. For printing ink suspensions[57],

the experimentally measured areas of hysteresis loops (e.g. the area

enclosed by $T_2B_1B_nT_2$) are found to be a linear function of the time spent

in the up-curve

$$A = A_0 - Nt \qquad (13)$$

where A = the measured area of the hysteresis loop

　　t = the time spent in the up-curve,

　A_0 and N are constants.

No theory has been proposed to explain this linear relationship and it

probably depends on the system investigated. (Other systems may not give

a linear relationship.)

ii) Effect of Shear Rate

If the rate of increase of the shear rate is kept constant,

while the magnitude of the maximum shear rate is increased, the area of the

loop increases. For example, thixotropic material sheared along the path

T_2B_1 reaches a maximum shear rate of $\dot{\gamma}_1$, and has a corresponding hysteresis

loop area enclosed by $T_2B_1B_2T_2$, Figure 8b. With increasing maximum shear

rates, $\dot{\gamma}_2$ and $\dot{\gamma}_3$, the area enclosed by the hysteresis loop increases. An

empirical relationship is found to exist for the same system as before[57]

$$A = Q(\dot{\gamma}_{max})^2 \qquad (14)$$

where Q is a proportionality constant.

Equation (14) can be derived theoretically if it is assumed that the

loss in torque resulting from thixotropic breakdown is directly proportional

to the shear rate. But no one as yet has proposed a theory to verify this

latter assumption.

4. Thixotropy and Its Possible Mechanism

Even though Green and Weltmann[57] devised a method to character-
ize thixotropy, they did not give any equation to relate the rheological
properties to the structure. Other workers have proposed equations for
systems such as polymers[58,59], oils[60,61], and aqueous solutions[62-64].

In most of theses models, the rheological behavior is described in
terms of "scalar constitutive equations"[65], consisting of an equation of
state and a rate equation. The general form of the equation of state is:

$$\tau = \eta(\lambda,\dot{\gamma})\dot{\gamma} \tag{15}$$

in which the viscosity, η, is a function of the shear rate, $\dot{\gamma}$, as well as a
structural parameter, λ. The rate equation is expressed as

$$\frac{d\lambda}{dt} = f(\lambda,\dot{\gamma}) \tag{16}$$

which states that the rate at which the structure changes is a function of
both the shear rate and the structural parameter.

The physical significance of λ depends upon the structure ascribed to
the system. If the system is considered to contain "cells" having solid
properties moving in a Newtonian fluid, and growing in number or volume
when left undisturbed, λ may be the total volume of the cells contained in
one cubic centimeter. Alternatively, if links are formed between the
particles, λ may be considered as the concentration of the links. It is
therefore a measure of the internal structure present under a specific set
of conditions.

One of the proposed forms of the equation of state, equation (15),
is[66,67,69]:

$$\tau = (\eta_\infty + \tau_y/\dot{\gamma})\dot{\gamma} \qquad (17)$$

In equation (17) the term in the parenthesis is equivalent to the viscosity term in equation (15). At high shear rates, the second term in the parenthesis becomes zero, therefore, η_∞ is the viscosity of the system at very high shear rates; τ_y is the thixotropic contribution to shear stress and is structure dependent. Goodeve[66] and Gillespie[67] derived the following expression for τ_y:

$$\tau_y = \frac{1}{2} nv \, \sigma_M \qquad (18)$$

where σ_M is the value of the rupture stress of the link (i.e. ultimate tensile strength of the particle), v is the volume of a link and n is the number of links per unit volume. The equivalent rate equation to equation (16), by the same authors, is:

$$\frac{d\lambda}{dt} = An_0(1 - \lambda)^2 - B\lambda \qquad (19)$$

where A and B are kinetic constants for the formation and rupture of links, respectively, and are dependent on the shear rate; λ is the structural parameter equal to n/n_0. As can be seen in Appendix G, this model fails when the kinetic constants need to be exactly evaluated. These constants depend on geometrical factors (specially at high fraction solid) and on the nature of the forces involved in the bonding of the particles.

Other investigators[68,69] have also tried to compute the thixotropic contribution, τ_y, by relating it to the energy of the links between particles. The proposed models again fail to develop exact analytical solutions for the kinetic constants in their equations.

In summary, the successful quantitative descriptions of thixotropy are limited to empirical equations obtained from hysteresis loop measurements. Most of the existing theories approach the description of thixotropy in the same way (i.e. computation of the thixotropic contribution, τ_y, in equation (17)). However, the specific nature of the models and the impossible task to develop quantitative means of expressing the kinetic constants, make the proposed equations of little use except when verified by experiments.

D. Role of Convection in the Grain Refinement of Solidification Structures

Convection has been known to affect the presence and extent of the equiaxed zone of a casting. It also affects the size of the equiaxed grains and thus provides an excellent means for grain refining[8]. Convection takes place in the fluid either as a result of thermal and composition gradients (natural convection) or as a result of momentum transfer to the liquid such as in pouring a liquid into a mold or as in mechanical and electro-magnetic stirring (forced convection).

It is generally believed that convection promotes crystal multiplication and provides an excellent means for the transport of new crystals into the bulk of the fluid. However there is no agreement on the exact mechanism by which grain multiplication takes place.

One mechanism for grain multiplication is that of dendrite remelting whereby an arm is remelted at its base and then carried away, Figure 9. During dendritic growth of a binary alloy, a side branch (arm) is attached to the main stalk by a neck of lower melting point material which, in addition to the local curvature, favors remelting in the presence of thermal fluctuations[70]. Convection is then responsible for bringing about these

thermal fluctuations. This mechanism has been shown to operate in the coarsening of dendrites[71] and experimental proof has been given by Jackson, et.al. by direct observation of a freezing NH_4Cl[72] water melt.

Another theory has been advanced whereby segmentation is produced either directly by the shearing of a branch from the main stalk due to the fluid body forces[73], or indirectly by local heating due to local deformation[74]. This theory has been supported by the results of Garlick, et.al.[75] and those of Balandin, et.al.[76]. They showed that the degree of grain refinement is proportional to the difference of density between the liquid and the solid, and inversely proportional to the strength of the solid near the solidus temperature.

In practice, convection can be generated in many ways, either from a device exterior to the metal (vibration, rotation or the mold) or from a device inside the metal (induction, electromagnetic stirring or mechanical stirring). Experiments on aluminum and steel have shown that vibration or rotation of the mold during solidification was not enough to produce a fine equiaxed structure[77]. It was found that turbulence or acceleration of the liquid[78] and shear forces[79] in the solidifying metal were the significant factors to achieve grain refinement (i.e. if a uniform rotational motion was produced, only a columnar structure would develop[77]).

This suggests the importance of shear flow and the use of intermittent rotation or electromagnetic stirring during solidification to achieve equiaxed structures. Agitation of the solidifying metal, created by the insertion of blades in the liquid, is another technique which was used successfully to grain refine Al and Mg base alloys[80,81,82].

Recent work at M.I.T.[10,11,12,13] has shown the tremendous effect of high rates of shear on solidification structures and has shown the possibility of casting metals in the semi-solid state. Alloys studied were Sn-15%Pb alloy[10], aluminum base A-380 alloy[12], copper base Cu-10%Sn and Cu-5%Zn-5%Sn-5%Pb alloys and an iron base Fe-3%C-4%Si alloy[13].

The major finding of this work is that when metals are vigorously agitated during solidification, the usual dendritic structure is absent, and in its place are small rounded grains varying in size from 50 to 700 microns. In the case of the cast iron of approximately eutectic composition, the primary solid particles were two-phase, austenite and graphite[13].

Even though vigorous agitation was found to always produce the same type of structures on different alloys, only few and qualitative studies of the effects of shear rate and cooling rate on the "Rheocast" structures were done[11]. It is to this end that the study reported here was undertaken; (1) to characterize the structures in terms of the size of the primary solid particles, their shape, their distribution of size and the volume of liquid entrapped by these particles, (2) to relate these structures to the rheological properties, (3) to learn about the possible mechanisms by which shear affects solidification structures.

CHAPTER III: EXPERIMENTAL APPARATUS AND PROCEDURE

A. Viscometer

The viscometer used to study the rheological properties of metal slurries and the effect of shear on solidification, has been previously described[10], Figure 10. It is a rotating cylinder viscometer and the metal system is held in the annular gap between the two cylinders. The crucible is placed inside a furnace. Two holes in the furnace, one at the bottom and one at the top, make passage for the shaft used to rotate the crucible and for the torque bar connected to the fixed bob.

1. General Description

The rotation mechanism consists of a constant torque 5 horsepower D.C. motor, connected to the shaft (stainless steel) by a belt drive system. Attached to the shaft is a crucible (304 stainless steel, 4-3/16 inches in diameter and 6-3/16 inches long) inside which sits the cup locked into place by means of keyways.

Inside the cup hangs the bob that is screwed onto the torque bar (4140 steel, 3/4 inch diameter) used in combination with a torque dynamometer designed by the Instrumentation Laboratories at M.I.T., Figure 11b. Torques of up to 10^9 dyne-centimeter are measured in this way.

The furnace was constructed from four electric heating elements which were 34 inches high and formed a cylinder 12 inches in diameter. The elements were insulated by several layers of Fiberfrax insulation. The entire furnace was surrounded by a reflective shield. Top and bottom pieces were insulated with Fiberfrax, Fiberchrome and Transite. The

furnace was constructed in two sections which clamped together.

Temperature was recorded   by   calibrated Chromel-Alumel thermocouples, shielded with grounded 1/8 inch stainless steel tubing. Holes were drilled in the walls of the cup and the bob (1/8 inch diameter) to make place for the thermocouples at different locations around the melt, Figure 14. The thermocouples run through the shaft down to a Graphalloy slip ring and brush assembly; there, the rotating leads were connected through silver brushes to stationary leads, in turn connected to a Moseley two-pen recorder. When isothermally held, the thermal gradients were immeasurable both from top to bottom and across the radius (i.e. less than 0.25°C).

2. Modifications

The equipment was modified to achieve greater shear rates, up to 1000 sec^{-1}, as opposed to 450 sec^{-1}. A new spray cooling device was added to permit cooling rates up to 25°C/min.

The larger shear rates were obtained by building a new bob and cup arrangement with a smaller gap (3 mm as opposed to 9 mm), Figure 11a. This new geometry also improved the distribution of the particles (reduced flotation or settling) and reduced turbulence. The smaller gap size also assures better thermal uniformity and permits faster cooling rates. Grooves were again machined on the bob and cup walls.

Faster cooling rates were also obtained by incorporating a water spray jacket around the crucible, Figure 10b. The jacket is made of a double wall cylinder, sealed at the top and the bottom, with small holes on the inside wall. The water is injected under pressure through a pipe connected

-51-

to the jacket and is sprayed onto the crucible; the crucible can be stationary or rotating since the jacket surrounds it without touching it. The water runs down the crucible and is collected at the bottom.

Finally, control over the crucible rotation speed was improved via a D.C. generator whose output was exactly proportional to the rotational speed.

In summary, this special viscometer permits

1. rheological measurements on any metallic system whose melting point is lower than 300°C,

2. rapid quenching of the rheological structures that are then accessible to examinations,

3. testing of non-metallic systems such as honey, paint, epoxy and oils,

4. study of the effect of temperature on the rheology of these systems.

B.   Materials

1.   Metal

Most of the experiments were done on Sn-15 wt % Pb alloy. This alloy was chosen because some of its rheological properties have been previously studied[10], the low melting point of the alloy does not raise any equipment problems, and a good deal of thermodynamic, diffusion, viscosity, and surface tension data for the alloy are available. Finally, the density of the first solid forming is not too different from that of the liquid (see Appendix A).

2.   Experimental Set-Up

Tin and lead, 99.9% pure (see Appendix B), were first melted in a clay graphite crucible inside an electric furnace. To insure melt

homogeneity the molten alloy was stirred with a carbon rod for two minutes. The bob was screwed onto the torque bar and centered in the crucible by means of both a centering pin in the bottom of the bob, and a split ring centering device which fits into the cylinder. After the bob was secured in place, the alloy was poured into the annular space through a coated funnel and allowed to freeze. Both the cup and the bob were previously coated with zirconia-base mold wash, dried up for one half hour at 200°F. The lid was then bolted on the cylinder with silicone rubber gaskets in place, Figure 12. Insulation was placed between the crucible and the metal catch, which trapped any metal centrifuged out of the cylinder, Figure 12.

The torque bar was held in place through a high tolerance stainless steel bearing. The bearing assembly was bolted to horizontal rails which stretched across the furnace. The strain measuring device was placed atop the torque bar and bolted to horizontal rails.

3. Variables

The independent variables included the following:

a. Alloy composition,

b. Geometry of viscometer,

c. Initial cooling rate, ε

d. Initial rotation speed (or initial shear rate, $\dot{\gamma}$),

e. Final fraction solid (or temperature at quench), f_{sf},

f. Isothermal holding time,

g. Thermomechanical treatment

The dependent variables were:

a. Torque (viscosity) measurements,

b. Metallography: macro- and micro-structures were examined and the size, shape, and distribution of size of primary solid particles were determined by quantitative metallographic techniques.

C. Experimental Procedure

Basically two series of experiments were carried out, one in which the metal was brought up to a liquid state and then cooled at a given rate and sheared continuously at a constant rate. When the desired fraction solid was reached, the rotation of the cup was stopped and the specimen quenched.

In the second series of experiments, the metal would receive the above treatment first but would then gradually be brought to a specified temperature in the liquid-solid range. After the torque attained a constant "steady state" value, hysteresis loops were generated to study the thixotropy of the system. At the end of these isothermal experiments, rotation was stopped and the specimen quenched.

1. In the first series of experiments, aimed at studying the effect of shear on solidification structures, the three independent variables were: cooling rate, ε, shear rate, $\dot{\gamma}$, and the final fraction folid, f_{sf} (fraction solid at which rotation was stopped and the sample quenched).

The procedure employed and the measurements made are graphically illustrated in Figure 13.

Figure 13a shows an illustration of the thermal history of the alloy at two different cooling rates. The range of cooling rates employed was 0.33°C/minute to 25°C/minute. The lower rates were achieved by furnace

cooling the specimen. The high cooling rates were achieved by direct water cooling of the crucible utilizing the spray jacket shown in Figure 10b. Intermediate cooling rates were obtained by air cooling the crucible. Regardless of prior thermal history, at the desired final fraction solid, f_{sf}, rotation was stopped and specimens were quenched at 25°C/minute. Resulting from the difference in cooling rates, the slurries spent a different time in the liquid-solid range,e.g. for a final fraction solid, f_{sf} = 0.45, slurries cooled at ϵ = 25°C/minute, 1°C/minute and 0.33°C/minute spent a total time in the liquid-solid range of 2, 13, and 40 minutes, respectively.

A corresponding graph to the thermal cycle, for the rotation speed versus time is shown in Figure 13b. Rotation speeds were varied with the two cup and bob arrangements (3 mm and 9 mm spacings) such that shear rates in the range of 115 to 750 sec^{-1} were achieved.

2. In the second series of experiments, rheological measurements were made at a specified temperature in the liquid-solid range in order to determine the thixotropic nature of the slurries. Initially the alloy was sheared and cooled at 0.33°C/minute from above the liquidus temperature. Furnace temperature was subsequently controlled and the alloy was isothermally held, under shear, at the desired temperature. This thermal history of the alloy is illustrated in Figure 14a. As a result of this procedure, the total time spent in the liquid-solid range is the sum of two times (1) time spent in the liquid-solid range during the cooling (2) the isothermal holding time.

Initial shear rate, denoted as $\dot{\gamma}_0$ in Figure 14b, was maintained

constant throughout the cooling cycle and the initial isothermal holding until a steady state value of torque was achieved. Different cycles of rotation and rest were then applied while the temperature of the system was maintained constant. Figure 14b shows a schematic example of variation in rotation speed versus time. Figure 14c shows the corresponding torque measurements.

i) Hysteresis loops

The significance of a hysteresis loop measurement has been described[57] in Chapter II.C. Figure 14b shows the procedure employed, rotation speed versus time, to generate a hysteresis loop; five independent variables had to be controlled (one shear rate and four different times). Maximum shear rate, $\dot{\gamma}_{max}$ in Figure 14b, could be varied as desired; it was usually 115 sec^{-1}. The time variables were: (1) Down-time, the time it took to bring the shear rate to zero, t_0 in Figure 14b (minimum time attainable was 4 seconds from 250 R.P.M. to zero); (2) Time at rest, time duration at which no shear was applied, t_1 in Figure 14b; (3) Up-time, the time it took to go to the desired $\dot{\gamma}_{max}$ at a constant rate of increase, t_2 in Figure 14b; (4) The time during which $\dot{\gamma}_{max}$ was maintained, t_3 in Figure 14b.

The number of loops was varied; as many as 75 loops were performed during one experiment; all loop measurements of shear rate versus torque were recorded on an X-Y recorder.

ii) Other experiments were carried out to study the pseudo-plasticity of the metal slurries. To this end, once a steady state was reached, the shear rate was changed up or down and the new steady state

value of torque was measured. In this way a flow curve of the slurry, at a given fraction solid, was obtained.

D. Measurements

1. Flow

Torque values are always proportional to the dynamometer cell output. The proportionality constant, 2.54×10^6 dyne cm/volt, was measured using calibrated weights acting at measured distance and verified using an Instron Machine. On the other hand, only for Newtonian materials is the shear rate proportional to the rotation speed of the cup. For materials of unknown behavior, trial and error methods have to be used to derive the value of the shear rate at a given location in the viscometer[83] (see Appendix D); that is, the shear rate varies across the gap of the viscometer.

Whenever giving values of rheological properties, the aim is to use variables independent of the geometry of the apparatus and relative to the same location. Such variables are called consistency variables[84]. In the concentric cylinder viscometer, the maximum shear stress is encountered on the wall of the bob, hence it is relevant to choose that location as the reference point (rather than an average location). So the torque, T, is expressed as

$$\tau = T/2\pi h \; \kappa^2 R^2 \qquad (20a)$$

$$\tau = CT \qquad (20b)$$

where h, the bob height, is equal to 8.9 cm, R, the cup radius, is equal to either 3.01 or 3.17 cm and κ, the ratio of the bob to cup radius, is equal to .74 or .90 and C, the instrument constant, is equal to 3.65×10^{-3} or

2.40×10^{-3} cm^{-3} according to the bob and cup arrangement used, respectively.

The rotation speed of the cup, Ω, is replaced by the shear rate

$$\dot{\gamma} = 2\Omega/(1 - \kappa^2) \qquad (21)$$

which is the shear rate at the bob wall only for Newtonian materials and is such that $\dot{\gamma} = .46\Omega$ for $\kappa = .74$ and $\dot{\gamma} = 1.01\Omega$ for $\kappa = .90$ where Ω is in r.p.m. These expressions for the shear rate are used throughout this work. The relative error committed using equation (21) is calculated in Appendix D.

The apparent viscosity is given by

$$\eta_a = \tau/\dot{\gamma} \qquad (22)$$

This is the viscosity a Newtonian fluid would have if, placed in the viscometer and sheared at the same rate, it gave rise to the same torque T. This expression is used throughout this work whether or not the word apparent is mentioned. The relative viscosity could also be used and is defined as

$$\eta_r = \eta_a/\eta_0 \qquad (23)$$

where η_0 is viscosity of the segregated liquid at that temperature. For instance, it is $\eta_0 = 0.025$ poise[85] at $f_s = 0.50$ for Sn-15%Pb alloy.

2. Corrections for End Effect and Wall Effects

In an actual rotating viscometer, there is always a viscous drag due to the stress on the bottom surface of the bob. Its effect has been shown[86] to be equivalent to an increase in the height of the bob, Δh. This correction is minimum by making cup radius large, the gap small and

the bob tall. For instance[87], it is about 1.5% for a bob height of 5.10 cm, a ratio κ = .90 and a cup radius of 1.30 cm. Since the height of the bob used in these experiments was 8.9 cm, no correction was made.

In a rotating viscometer, it is found that wall slippage is very unlikely to occur. No slippage was observed[44] with a suspension of particles 38 to 380 microns in size, in a viscometer where R = 7.10 cm and the gap was equal to 0.21 cm. In another study[38], slippage occurred when particles were larger than 150 microns at shear rates greater than 250 sec^{-1}. It was shown that slippage could be avoided by the use of vertical grooves on both walls[38,88]. Vertical grooves were thus incorporated in this viscometer.

3. Stability of Flow

Couette[89] pointed out that even though exact solutions of the Navier-Stokes equations were known in the case of a fluid, held between two indefinitely long coaxial cylinders, he proved that there were two different behaviors in the actual apparatus where the cylinders are finite in length. He also showed that the behavior at low speed of rotation conforms to the solution of Navier-Stokes equation while the behavior at high speed was different.

From the different studies of the turbulence of flow in a concentric viscometer (Appendix E) the following conclusions were reached:

(1) Theoretically there is no limit to the laminar flow when the outer cylinder is rotating[90],

(2) It is only when the outer cylinder is set impulsively into motion that there are chances for turbulence to develop and only when the Reynolds

Number reaches a critical value of R_e = 66 X 10^3.

(3) From experience, it is found that this critical value depends on the size of the gap and mostly on the eccentricity of the bob with respect to the cup[91].

Using these data, it is found that slurries of the Sn-15%Pb alloy with viscosities above 0.1 poise will have laminar flow at shear rate up to 1000 sec^{-1}.

4. Hysteresis Loop

In the hysteresis loop measurement, the cup is set impulsively into motion, and the corresponding plot of torque versus shear rate is measured. Before attributing the loop to thixotropy, one must be sure that the hysteresis phenomenon is not due to some experimental artifact.

For instance, it has been shown[94] that, for a Newtonian fluid, an artificial hysteresis could be observed if the maximum shear rate was reached in a time, t, less than $R(1-\kappa)/2\pi\nu$. For a metal slurry with a viscosity of 10 poise, this time is .03 second and rules out this possibility.

Two other studies[95,96] showed that the inertia of the bob could only result in anti-thixotropy and that a gradual increase of the rotation speed of the cup could not lead to any observable transient period of flow.

5. Hysteresis Loop of Concentrated Non-Stable Suspensions

Very little is known about the thixotropy of systems where the solid and liquid have different densities. No hydrodynamic studies have been done of their settling or floating, and no one can predict what would be the result of a non-stable suspension as rotation is started. Since

laminar flow is prevalent, no mixing is possible.

The question is to know whether   the increase in viscosity, observed after the metal slurry has been left at rest, results from an apparent increase in fraction solid (due to flotation) or from a real structural rearrangement such as bonding of particles.

When the laws of hindered settling are applied to metal slurries (Appendix F), it is found that it takes 5 minutes for the slurry to rise 1 cm (i.e. there is 1 cm of liquid at the bottom and the solid is concentrated in the rest of the space); the fraction solid has increased (for instance from .45 to .50); the corresponding increase in viscosity (as seen from Chapter IV.B) is always smaller than that observed actually when the shear is resumed (a factor of 2 compared to a factor of 5 or 10). This rules out the possibility that the hysteresis phenomenon observed is due to the flotation of primary solid particles in the slurry.

In addition, experiments were done on alloys of different composition, especially Pb-rich alloys where the difference in density is about twice   that of Sn-rich alloys (ρ_s = 10.65g/cc, ρ_{liquid} = 9.8g/cc at f_s = 0.45 for Pb-10%Sn alloy compared to ρ_s = 7.0g/cc, ρ_L = 7.4g/cc at f_s = .45 for the Sn-15%Pb alloy). It was found that the areas of the hysteresis loops in these experiments were generally smaller than those of Sn-rich alloys.

Furthermore, experiments were also carried out on well-known thixotropic systems to verify the accuracy of the viscometer.

E.   Calibration

The viscometer was calibrated with U.S. National Bureau of Standards

oils (standard number S-60, S-600 and S-2000, conforming to ASTM oil standard). The data agreed within 4% and it was decided not to add any correction for end effect (see Appendix D). In tests with oil, turbulence was not recorded, even when motion was set impulsively (e.g. 2 seconds to reach 250 rpm).

F. Metallography

The hollow cylindrical sample obtained in each experiment was removed and sectioned in half longitudinally. One half section was transversely cut at locations 1 inch from the top and 1/2 inch from the bottom. Each longitudinal and transverse cross-section was polished, etched and metallographically examined (see Appendix C for the method employed).

For each specimen, an average shape of the primary solid particle was measured and assumed to be constant. Using this value of the axial ratio, q, (ratio of the minor axis to the major axis), the distribution of size (minor axis, X) was measured using the Schwartz-Saltykov[97] method as modified by DeHoff[108] for ellipsoidal shape (see Appendix D).

Once the distribution of size was obtained, the average size, $\bar{X}$, of the primary solid particle and the standard deviation of the distribution, σ_X, were easily derived as well as the number of particles per unit volume, N_V. A minimum of 100 particles were counted on each specimen, at at least two different locations.

The volume fractions of either primary solid particle, g_{sf}, or entrapped liquid, g_{Le}, were counted using a point count on a grid. The point count of primary solid particle (not counting the secondary solid appearing as small dendrites at the edge of primary solid) gives a value V_V.

Experimental verifications of the equality

$$V_V = g_{sf} \qquad\qquad (24)$$

were carried out at two different fractions solid and agreed within 1% (see Appendix A). In summary, it is possible to characterize the structures of Rheocast specimens by their fraction solid, f_{sf}, their volume fraction of entrapped liquid, g_{Le}, the average size of the primary solid particles, $\bar{X}$, their shape (axial ratio), q, their number per unit volume, N_V, and their distribution of size, N(X) versus X or σ_X.

CHAPTER IV: RESULTS

A. Tests in Which the Alloy was Sheared Continuously from Above the
    Liquidus to the Desired Fraction Solid

   1. Effect of Shear Rate, Cooling Rate and Fraction Solid on the
       Apparent Viscosity

   In these experiments the alloy was initially cast in the annulus

of the viscometer, then heated up above the liquidus and cooled at a

controlled rate as shear was induced and maintained constant.

   The independent variables were: (1) shear rate, $\dot{\gamma}$, (2) cooling rate,

ϵ, and (3) final fraction solid, f_{sf}, at which shear was stopped and the

alloy quenched.

   The following observations were made. At the liquidus temperature,

the apparent viscosity is low; as the temperature drops and liquid freezes,

the viscosity begins to rise. The rate of increase is low at first but

increases rapidly as the fraction solid increases.

   Figures 15 to 18 show the effects of cooling rate and shear rate on

the viscosity of the Sn-15%Pb alloy continuously sheared from above the

liquidus. Figures 15 and 17 show that, at a given cooling rate, ϵ, the

viscosity decreases with increasing shear rate whereas Figures 16 and 18

show that, at a given shear rate, the viscosity decreases as the cooling

rate decreases (i.e. as the total time spent in the liquid-solid range

increases).

   At a high cooling rate, ϵ = 25°C/minute, an increase in shear rate

from $\dot{\gamma}$ = 230 to $\dot{\gamma}$ = 750 sec^{-1} results in a moderate decrease in the viscosity

of the slurry, Figure 15. For example, at f_s = 0.45, the viscosity decreases

from η = 37 to η = 12 poise (by a factor of $\simeq$ 3).

At the higher shear rate, $\dot{\gamma}$ = 750 sec^{-1}, the viscosity of the slurry can be further reduced by decreasing the cooling rate, Figure 16. For example, at f_s = 0.45, as the cooling rate is decreased from ε = 25 to ε = 0.33°C/minute, the viscosity is reduced from η = 12 to η = 2 poise (by a factor of 6).

At a slow cooling rate, 0.33°C/minute, the viscosity of the slurry at a given fraction solid decreases markedly as the shear rate is increased, Figure 17. At f_s = 0.45, as the shear rate is increased from 230 to 750 sec^{-1}, the corresponding measured viscosities are 15.0 and 2.0 poise (by a factor of 7.5).

Some of the data generated in these experiments are listed in Table III. A composite plot of some of the data presented in Figures 15-18 and Table III is presented in Figure 19 to show the relative change in measured viscosity as a function of cooling rate, shear rate and fraction solid.

In general, viscosity increases with increasing fraction solid, increasing cooling rate and decreasing shear rate. However, the relative change in measured viscosity due to variation of cooling rate and shear rate increases drastically with increasing fraction solid. Figure 19 establishes criteria for preparation of low viscosity slurries, e.g. η < 5 poise, for fractions solid as high as 0.45. At low fraction solid, up to f_s = 0.35, all different combinations of cooling and shear rates, within the ranges specified earlier, result in viscosities less than 5 poise, whereas slow cooling rates, ε = 0.33°C/minute, coupled with high shear rates, $\dot{\gamma}$ = 750 sec^{-1}, are necessary if the viscosity of a 0.45 fraction

solid slurry is to be maintained at the same relatively low level.

2. Effect of Cooling Rate, Shear Rate, and Final Fraction Solid on the Structure of Quenched Specimen

i) Effect of Cooling Rate and Shear Rate

At the highest cooling rate used, ε = 25°C/minute, the average size of primary solid particles* (average minor axis, $\bar{X}$) is about 50 ± 15 microns for a final fraction solid f_{sf} = 0.55 and does not appear to be affected by the shear rate employed, Figure 20. The corresponding microstructures are shown in Figure 22. The primary solid particles are of the same average size; however, there is less entrapped liquid in the particles that have experienced the higher shear rate, $\dot{\gamma}$ = 750 sec^{-1}. Measurements of entrapped liquid carried out on high magnification pictures, Figures 22b and 22d, show that there is more entrapped liquid at the lower shear rates (e.g. the volume fractions of entrapped liquid are 0.13 and 0.08 at $\dot{\gamma}$ = 230 and 750 sec^{-1}, respectively).

The distributions of size of primary solid particles are rather broad and do not change much over the range of shear rates used. A typical distribution is shown in Figure 21a. The standard deviation, σ_x, was calculated for each specimen and the ratio, $\sigma_x/\bar{X}$, where $\bar{X}$ is the average size (minor axis) of primary solid particles, varies between 0.70 and 0.90. These large values of the ratio, $\sigma/\bar{X}$, are again an indication of the broad range of particle sizes obtained.

At the lowest cooling rate used, ε = 0.33°C/minute, the average size (minor axis) of primary solid particles depends on the shear rate.

---

* Primary solid particles are the particles solidified during shear in the liquid-solid range prior to quench.

Figure 25 shows how the measured size decreases from 275 microns at $\dot{\gamma}$ = 230 sec^{-1} to 175 microns at $\dot{\gamma}$ = 750 sec^{-1} for a final fraction solid f_{sf} = 0.55. The corresponding microstructures are shown in Figure 23. Even though the primary solid particles sizes are different, the particle shape remains the same.

The amount of entrapped liquid, at this slow cooling rate, is less than that at the higher cooling rate. For example, at f_{sf} = 0.55 and $\dot{\gamma}$ = 230 sec^{-1}, the amounts of entrapped liquid are 0.13 and 0.02 for cooling rates of 25°C/minute and 0.33°C/minute, respectively. With increasing shear rate, the amount of entrapped liquid in the slow cooled samples becomes negligible, see Figure 23.

In general then, the effect of shear rate on the amount of entrapped liquid is the same at high or low cooling rate - as the shear rate increases the amount of entrapped liquid decreases.

The distributions of size are represented in Figures 21b and 21c. The ratios of standard deviation to average size of primary solid particles, $\sigma_x/\overline{X}$, are equal to 0.47 and 0.21 at $\dot{\gamma}$ = 230 and 750 sec^{-1}, respectively. At a given shear rate, e.g. 750 sec^{-1}, the size distribution of primary solid particles decreases with decreasing cooling rate, Figures 21b and 21c.

ii) Effect of Fraction Solid

In specimens that were initially cooled at 0.33°C/minute and quenched at final fractions solid, f_{sf}, less than 0.30, the primary solid particles were distinguishable from the surrounding matrix, Figure 24a. This was not true for specimens that had experienced the higher cooling rate of 25°C/minute, Figure 24b.

Comparison of the low fraction solid structure, Figure 24a, with that of a slurry sheared and cooled at the same rates but quenched at $f_{sf} = 0.55$, Figure 23, reveals that the average size (minor axis) of primary solid particles increases from 115 to 175 microns. The number of primary solid particles per unit volume increases from 0.25×10^6 to 0.36×10^6 cm^{-3} as the final fraction solid increases from $f_{sf} = 0.30$ to 0.55.

The size distribution of the primary solid particles for specimens quenched at $f_{sf} = 0.30$ is shown in Figure 21d; 67% of the primary solid particles are smaller than 120 microns as opposed to 11% at $f_{sf} = 0.55$, Figure 21c.

Thus, as the fraction solid in the liquid-solid range increases, the existing primary solid particles coarsen and the total number of primary solid particles increases.

Figure 24c shows the structure of a fast cooled specimen, for $\varepsilon = 25°C/minute$, at $f_{sf} = 0.25$, near the outside wall of the crucible. In addition to the equiaxed dendrites, there are some columnar dendrites growing from the wall which were not observed at higher fraction solid.

B. Experiments in Which the Alloys was Sheared Continuously from Above the Liquidus and Held Isothermally at a Given Fraction Solid

The procedure was the same as that described in section A, but the cooling rate was gradually brought to zero to achieve a constant temperature within the liquid-solid range while rotation was maintained constant. Next, two different types of isothermal (constant fraction solid) experiments were performed: (1) Constant shear rate experiment-in which rotation was maintained constant and the corresponding "steady state" value of torque was recorded; (2) Pseudoplasticity experiments-in which the rotation

speed was changed up or down and the new "steady state" value of torque was measured.

All viscosity measurements reported here are "steady state" viscosities. That is, each slurry, regardless of previous thermomechanical history was held at a given fraction solid and shear rate, until no further observable changes in measured torque occurred with time.

In these experiments the total time spent in the liquid-solid range signifies time spent during cooling to reach a certain fraction solid plus isothermal holding time at that fraction solid. In the previous continuously cooled experiments, the total time spent in the liquid-solid range signified time spent during cooling to reach the desired final fraction solid at which rotation was stopped and the specimen quenched.

1. Constant Shear Rate Experiments

Figures 25 and 26 show that at low shear rates (e.g. 115 and 230 sec^{-1}) the viscosity of a slurry at a given fraction solid above about $f_s = 0.35$ is lower when the slurry is held isothermally and reaches a "steady state" than when the slurry is continuously cooled. For example, data on Figure 26 show that, at 0.45 fraction solid, the viscosity of a slurry continuously cooled at 0.33°C/minute and sheared at 230 sec^{-1} was 15 poise compared to 9 poise when the slurry was isothermally held; the total times spent in the liquid-solid range were 40 and 90 minutes, respectively.

No change in viscosity of a slurry was observed at a given fraction solid with increasing isothermal holding time after the slurry had spent about sixty minutes in the liquid-solid range.

Similar experiments carried out at higher shear rates showed that differences in viscosity of a continuously cooled slurry and   an isothermally held slurry ("steady state" viscosity) decreased with increasing shear rates. For example, the viscosities of continuously cooled and isothermally held slurries, at 0.45 fraction solid sheared at 350 sec^{-1}, were 6 and 4 poise, respectively. The corresponding viscosities at 750 sec^{-1} were 2.0 and 1.0 poise, respectively. These data points are shown in Figures 16 and 27. Figure 27 also shows how the "steady state" viscosity of an isothermally held slurry, f_s = 0.45, decreases with increasing shear rate. Each data point on the curve was obtained in a separate experiment.

In summary then, results of these experiments show that the viscosity of a slurry, for fractions solid above $\simeq$ 0.35, decreases, with increasing total time spent in the liquid-solid range. Furthermore, there is a "steady state" lower limit of viscosity which is recorded when total time spent in the liquid-solid range reaches 60 minutes. Finally, variations in viscosity   with time spent in the liquid-solid range and with shear rates decrease with increasing shear rates.

2. Pseudoplasticity Experiments (changing shear rate experiment)

These experiments were identical to those reported in the preceding section, except shear rates were changed during isothermal holding in the liquid-solid range, once a "steady state" had been reached.

Figure 23 shows how changes in shear rate affect the viscosity of a slurry. Again, measured viscosities are "steady state" viscosities as previously defined. For a given fraction solid, the "steady state" viscosity of the slurry increases with decreasing shear rate. For example,

the viscosity of a slurry, initially sheared at 115 sec^{-1} and isothermally

held at f_s = 0.50 increases from 16 to 75 poise as the shear rate is

changed over the range of 250 to 30 sec^{-1}.

The effect of prior mechanical treatment, i.e. initial shear rate, on

the viscosity at a certain shear rate is also shown in Figure 28. For

example, at f_s = 0.45, viscosities of a slurry initially sheared at 350

sec^{-1} are consistently lower than those of a slurry at the same fraction

solid but initially sheared at 115 sec^{-1}. These observations are in line

with those previously reported in Figure 27. Finally, as before, changes

in viscosity are more significant when a slurry is subjected to the lower

shear rate. The changes in viscosity reported in Figure 28 were reversible

but time dependent. For instance, the time to reach a new "steady state"

value of viscosity from 150 to 400 sec^{-1} was 5 minutes for a slurry

initially sheared at 350 sec^{-1} and held at f_s = 0.45. The dependence of

this reversibility will be further described in a following section on

thixotropy.

3. Structures of Isothermally Held Slurries

i) Comparison Between Structures of Continuously Cooled and Isothermally Held Slurries

Figure 29 shows the structures of three slurries that have

been sheared at the same constant shear rate of $\dot{\gamma}$ = 230 sec^{-1} but have

spent different times in the liquid-solid range. Two slurries in Figures

29a and 29b were continuously cooled at 1°C/minute and 0.33°C/minute and

quenched at a final fraction solid f_{sf} = 0.45; they spent total times in

the liquid-solid range of 13 and 40 minutes, respectively. The slurry in

Figure 29c was isothermally held at f_s = 0.45 and spent a total time in the

liquid-solid range of 90 minutes prior to quench.

As seen from Figure 29, the major difference between the structures of these three slurries is the amount of entrapped liquid within the primary solid particles. Figure 31a shows the decrease in measured volume fraction of entrapped liquid versus time spent in the liquid-solid range. Thus, the effective volume fraction of primary solid particle decreases with time spent in the liquid-solid range. This could explain the lower measured viscosities of isothermally held slurries reported in Figures 25 and 26.

The other two variables affecting viscosity at a given fraction solid are the size distribution and the size of the primary solid particles. Measured average particle size (minor axis, $\bar{X}$) for all three slurries and size distribution for two of the slurries of Figure 29 are shown in Figures 31a, 31b and 31c. There is no significant variation in particle size with total time spent in the liquid-solid range. However, Figures 31b and 31c show that the size distribution becomes narrower with this total time. The ratios, $\sigma_X/\bar{X}$, of standard deviation of the distribution of size to the average size are 0.70 and 0.45 for the two slurries with total times spent in the liquid-solid range of 40 and 90 minutes, respectively.

ii) Effect of Initial Shear Rate on the Structures of Iso-
thermally Held Slurries

Figure 30 shows the microstructures of three slurries sheared over the range of 115 to 750 sec^{-1}, that were held isothermally at f_s = 0.45 and spent the same total time in the liquid-solid range. The size of primary solid particles decreases with increasing shear rate: the size decreases from 200 to 85 microns over the range of applied shear rates, Figure 32a. The measured size distribution of two of the specimens are

shown in Figures 32b and 32c. The calculated ratio of standard deviation to average size, $\sigma_x/\bar{X}$, does not vary much with shear rate - it is $\simeq 0.45$ in both cases.

The important trend established here is that the amount of entrapped liquid within the primary solid particles decreases with increasing total time spent in the liquid-solid range. This phenomenon was previously reported for the continuously cooled slurries (Chapter IV.A, Figures 20, 22 and 23). The other observation is that the particle size of slurries isothermally held at a constant fraction solid decreases with increasing shear rate; this was also observed with the continuously cooled slurries that spent at least 40 minutes in the liquid-solid range, Figure 23.

C. Experiments on Non-Metallic Systems

To verify the ability of the viscometer used in this study to detect and measure thixotropy, experiments were done on well known thixotropic materials; epoxy mixed with silica flakes, unprocessed honey and paint were used.

Thixotropy was studied using the hysteresis loop technique of Green and Weltmann[57] described earlier. The critical variables used in obtaining the loops, e.g. the maximum shear rate, and the time to reach that maximum, are listed in Table IV. The results are as follows:

1. Rheological Properties of Honey

The honey used was natural unprocessed honey (New England blend). The experiments were carried out at room temperature. An example of the hysteresis loop obtained is shown in Figure 33, where the shear rate was changed from zero to 55 sec^{-1} in 1 second. The loop area is 1.5 X 10^5 dyne

$cm^{-2}sec^{-1}$. Similar experiments were carried out after leaving the system at rest for different times at a higher temperature, 30°C. The initial viscosity increased from 85 to 130 poise as the time at rest was increased from 0 to 48 hours, Figure 44.

The results obtained here are in qualitative agreement to those reported in the literature[100]. However, no relative viscosity values were available to permit a quantitative comparison.

2. Rheological Properties of Epoxy Mixed with Silica Flakes

Both pure epoxy (Shell EPON 828) and epoxy containing 2.95 wt% (1.30% in volume) of SiO_2 flakes (Cab-O-Sil) were used in these experiments. The mixture was made by stirring the flakes into the epoxy for 10 minutes at 60°C.

Tests with pure epoxy were run at different temperatures. It was found out that pure epoxy behaves as a Newtonian fluid in the temperature range of 24 to 32°C when subjected to shear rates of up to 150 sec^{-1}.

The viscosity and the thixotropy of the mixture were measured, i.e. hysteresis loops were generated, after the mixture had been left at rest for 12 hours. A typical loop is shown in Figure 35; the time it took to reach the maximum shear rate, 115 sec^{-1}, was 1.5 seconds, Table IV; the corresponding loop area is 3.00×10^5 dyne $cm^{-2}sec^{-1}$.

3. Rheological Properties of Paint

The thixotropic data obtained (hysteresis loop) of the paint (Sherwin-Williams, white, flat tone-alkyd base) is shown in Figure 36. It took 10 seconds to reach the maximum shear rate of 270 sec^{-1}, Table IV. The area of the loop is 0.15×10^5 dyne $cm^{-2}sec^{-1}$.

The small relative decrease in viscosity is the result of the limited shear rates available in the viscometer. Shear rates of up to 20,000 sec^{-1} are reported in brushing conditions[101] which, if attained, would permit a larger loop to be generated. The results obtained (values of viscosity and yield stress) are in good agreement with those of Doherty and Hurd[102].

D. Thixotropic Experiments on Sn-15%Pb Slurries

Results here reported were obtained from slurries held isothermally at a given fraction solid in the liquid-solid range. The initial procedure to reach the desired temperature (fraction solid) was that described earlier in section B. Hysteresis loops were then generated using the Green and Weltmann[57] method described earlier.

The effect of the following parameters on the area of the hysteresis loops is presented herein:

(1) the fraction solid at which the loops are generated, f_s,

(2) the previous mechanical history (initial shear rate), $\dot{\gamma}_0$,

(3) the time during which the slurry was left at rest, rest time, t_r,

(4) the time needed to bring the slurry to rest, down time, t_d,

(5) the time needed to increase the shear rate to its maximum, up time, t_u,

(6) the maximum shear rate, $\dot{\gamma}_{max}$

1. Effect of Fraction Solid

All the slurries reported here were sheared at an initial shear rate of $\dot{\gamma}_0 = 115 \ sec^{-1}$ and spent a total time of 90 minutes in the liquid-solid range prior to thixotropic measurements. The curves in Figure 37 show the effect of fraction solid on the hysteresis loop obtained with an up time of 2 seconds to reach a maximum shear rate, $\dot{\gamma}_{max}$, of 115 sec^{-1}.

Figures 37a and 37b show the effect of two different times at rest, 30 and 120 seconds, respectively.

For a given rest time the area of the hysteresis loop increases with increasing fraction solid. For example, at t_r = 30 seconds, the measured areas for fractions solid f_s = 0.40 and f_s = 0.45 are 1.15 X 10^5 and 2.05 X 10^5 dyne $cm^{-2}sec^{-1}$, respectively.

For fraction solid lower than t_s = 0.35 the appearance of thixotropy, i.e. hysteresis loop, depends on the time the slurry is left at rest. Figure 37c shows the domains where thixotropy and no thixotropy are observed. For example, at f_s = 0.25, slurries initially sheared at 115 sec^{-1} did not exhibit thixotropy (i.e. the difference in stress is lower than the accuracy of the stress recorder, $\simeq 10^2 dyne/cm^2$) for rest times of up to about 2 minutes. Evidence of thixotropy, hysteresis loops, was observed after a rest time of 5 minutes. The data presented are for an up time of 2 seconds to reach a maximum shear rate of 115 sec^{-1}.

2. Effect of Initial Shear Rate

The effect of initial shear rate, $\dot{\gamma}_0$, on thixotropy is shown in Figure 38. Two slurries, f_s = 0.45, were left at rest for 30 seconds. Up time to reach a maximum shear rate of 250 sec^{-1} was 3 seconds. The area of the hysteresis loops decreases with increasing initial shear rate. It is 6 X 10^5 and 1.55 X 10^5 dyne $cm^{-2}sec^{-1}$, for corresponding initial shear rates of 115 and 350 sec^{-1}.

3. Effect of Time at Rest

The curves in Figures 37a and 37b, and 39a show the effect of rest time on the hysteresis loops obtained with an up time of 2 seconds to reach

a maximum shear rate of 115 sec^{-1}. The recorded area of the loop increases with increasing time at rest. Figure 39b shows measured areas of the loops from Figure 39a.

The same phenomenon was observed when the fraction solid and the initial shear rate were varied, Figures 39c and 39d.

4. Effect of Down Time

The down time referred to here is time spent in decreasing the shear rate of the slurry from its initial value to zero prior to hysteresis loop measurements. In the loops reported above this down time was kept to a minimum of 4 seconds. Figure 40 shows that the areas of the loop increases with increasing down time. For example, in slurries initially sheared at $\dot{\gamma}_0$ = 115 sec^{-1}, held at f_s = 0.45, the area increases from 2.00 X 10^5 to 3.50 X 10^5 dyne $cm^{-2}sec^{-1}$ as the down time increases from 4 to 60 seconds, Figure 40b. The rest time in these experiments was 45 seconds.

5. Effect of Up Time

The up time is the time spent in increasing the shear rate from zero to its maximum, $\dot{\gamma}_{max}$. Figure 41 shows that the area of the hysteresis loop decreases with increasing up time. For instance, for slurries initially sheared at $\dot{\gamma}_0$ = 115 sec^{-1} and held isothermally at f_s = 0.45, the are of the loop goes from 1.50 X 10^5 to 0.50 X 10^5 dyne $cm^{-2}sec^{-1}$ as the up time goes from 2 to 10 seconds, $\dot{\gamma}_0$ was 115 sec^{-1} and rest time prior to shear was 45 seconds. The areas of the loops become zero for up times greater than 15 seconds. The same effect was observed on a 0.40 fraction solid slurry, Figure 41b.

6. Effect of Maximum Shear Rate

The effect of maximum shear rate on the area of the hysteresis loop is shown in Figure 42. The area of the loop increases with increasing maximum shear rate, $\dot{\gamma}_{max}$. For instance, at t_r = 30 seconds for slurries held at f_s = 0.45 and initially sheared at $\dot{\gamma}_0$ = 350 sec^{-1}, the measured areas are 0.80, 1.50 and 2.20 X 10^5 dyne $cm^{-2}sec^{-1}$ for maximum shear rates of 115, 250 and 300 sec^{-1}, respectively.

In summary, it has been shown that metal slurries are thixotropic, regardless of rest time, for fractions solid higher than f_s = 0.35 and that the area of hysteresis loop is dependent on the thermomechanical history and on the conditions under which the measurements are carried out. For fractions solid less than 0.35 the occurrence of thixotropy is a function of the time spent at rest.

The general trends established here are:

(1) The area of the hysteresis loop increases with increasing fraction solid, rest time, down time and maximum shear rate.

(2) The area of the hysteresis loop decreases with increasing initial shear rate and up time.

CHAPTER V: DISCUSSION

The results of viscosity measurements presented in the previous
section are compared to other well-known rheological systems. The feasi-
bility of applying equations of state, proposed for non-metallic systems,
to Sn-15%Pb slurries is tested. Coarsening and coalescence mechansims are
proposed for the aggregation of primary solid particles in the Sn-15%Pb
slurries. Finally, the effect of shear flow on the formation of primary
solid particles is discussed.

A.   Rheological Properties

In this section, some general correlations are drawn between the
rheological properties of Sn-15%Pb slurries and other well-known systems.
Attempts are made to test the applicability of different equations of
state, developed for non-metallic systems, to this metallic system. For the
Sn-15%Pb alloy, weight fraction solid and volume fraction solid are used
interchangeably since there is a difference of only $\simeq 1\%$ between the two
values as shown in Appendix A.

1. Effect of Fraction Solid on Viscosity

When compared to suspensions of non-interacting spheres of poly-
styrene, rubber latex, glass and methylmethacrylate[34], the relative vis-
cosity of the metal slurries, at a given fraction solid are larger by 1 to
2 orders of magnitude, Figure 43. The data points plotted for the Sn-15%Pb
slurries cover all ranges of thermomechanical treatments reported earlier
in the results section. The data points for non-interacting spherical
particles are for a range of sizes from 0.1 to 435 microns.

When compared to suspensions of kaolin (clay) particles[68], 0.2 to 2 microns in size, in water, the relative viscosity of the metal slurries at a given fraction solid is of the same order of magnitude, Figure 43. The data points for kaolin suspensions cover the range of shear rates from 0.5 to 42 sec^{-1}. The high viscosity of these suspensions has been explained on the basis of an aggregation mechanism[68]. Network bonds are formed between kaolin particles to lower their surface energy. At a given shear rate, it takes a certain amount of energy to pull two particles apart (i.e. the energy necessary to break the network bonds). Yet when particles recombine by collision, the separation energy is not recovered but rather dissipated in local disturbances around the contact point.

This model can be applied to metal slurries of Sn-15%Pb alloy. Welds are formed between primary solid particles to lower their interfacial energy; upon rupture of the welds, some energy is dissipated (i.e. the change of surface energy incurred upon rupture of a weld) and becomes part of the viscosity of the slurry. The following equation is derived in Appendix H for the added viscosity

$$\eta_2 = \frac{3}{2\pi} \cdot \sigma \cdot g_s^2 \cdot \frac{R_2^2}{R_1^3} \cdot \frac{1}{\dot{\gamma}} \qquad (25)$$

where σ is the interfacial energy between the solid and the liquid metal, g_s is the volume fraction solid, $\dot{\gamma}$ is the shear rate, R_1 and R_2 are the radii of the primary solid particle and of the weld, respectively. At $g_s = 0.50$, for $R_1 = 50$ and $R_2 = 5$ microns, at a shear rate of 100 sec^{-1}, the added viscosity is $\simeq 2$ poise.

Table V compares relative viscosity data of a partially crystalline

polymer[52] (low molecular weight polyethylene) to that of the Sn-15%Pb
slurries. The relative viscosities of the two systems are of the same
order of magnitude. The high viscosity of partially crystalline poly-
ethylene is due to the formation of crystallites. However, in contrast to
metallic systems, the degree of crystallinity at a given temperature is a
function of shear rate. Therefore, instead of using the degree of crystal-
linity as a parameter, one may use the degree of molecular association[52]
(the molecular weight of the same but amorphous polymer resulting in the
same viscosity as that of the partially crystalline polymer). For instance,
it is found that the equivalent molecular weight of this polymer increases
seven times between the melting point and 80°C at a shear rate of 30 $\sec^{-1}$
and 3.5 times at a shear rate of 1000 $\sec^{-1}$.

2. Effect of Structure on Viscosity

In general, the viscosity of a suspension is an indication of the
energy consumed in shear flow. It is made up of the resistance of the
fluid to shear flow, the change in streamlines due to the existence of
solid particles and to the rotation of the particles, and the energy of
collisions with or without interactions.

The general trends established in this study relating viscosity of
Sn-15%Pb slurries to their structure are summarized in Table VI. The
dependence of the internal structure upon the conditions of the thermo-
mechanical processing (i.e. cooling rate and shear rate) will be left aside
for the moment and the dependence of particle size and the amount of
entrapped liquid upon the thermomechanical processing will be examined.

In all the continuously cooled and isothermally held slurries, the

viscosity at a given fraction solid increases with increasing primary solid particle size. The same trend has been previously established for suspensions of quartz particles, ranging in size from 25 to 175 microns, in water[38]. In that work, the increase of viscosity was attributed to the increasing magnitude of the inertial forces involved in the collisions of the larger particles. It was further demonstrated that the observed effect of change in particle size on viscosity becomes more pronounced as the density difference between the solid particle and the suspending medium increases.

Table VI also shows that a decrease in the amount of entrapped liquid results in a corresponding decrease in viscosity. The same effect has been reported for suspensions of aggregates of glass beads, 35 microns in size, in Aroclor (chlorinated biphenyl, η_0 = 80 poise) by Lewis and Nielsen[46]. Each suspension contained only aggregates of a given size (i.e. made up of a fixed number of glass beads) and therefore with a constant amount of entrapped liquid. It was shown that by increasing the amount of entrapped liquid (i.e. increasing the size of aggregates) the viscosity of the suspensions increased. Furthermore, it was shown that the viscosities of these aggregate suspensions obey Mooney's equation

$$\eta_r = \exp \left[k_1 g_s / (1 - k_2 g_s) \right] \qquad (26)$$

where η_r is the relative viscosity (apparent viscosity/viscosity of the suspending medium). The coefficients k_1 and k_2 are functions of the aggregate size; k_1 increases and k_2 decreases with increasing size of aggregate, i.e. increasing amount of entrapped liquid. Similar attempts to apply Mooney's equation to the Sn-15%Pb slurries were unsuccessful.

3. Equations of State

The apparent viscosity of continuously cooled Sn-15%Pb slurries, plotted versus fraction solid on semi-log paper shows a linear dependence over certain ranges of fraction solid (Figure 44). These portions can be described by an equation of the type:

$$\log \eta_a = \alpha + \beta f_s \tag{27}$$

where η_a is the apparent viscosity, and f_s is the fraction solid. The coefficients α and β are given in Table VII as a function of cooling rate and shear rate. Also listed in Table VII are the ranges of fraction solid over which equation (27) is applicable. The coefficient β is constant at a given cooling rate and does not change with increasing shear rate, whereas, α always decreases with increasing shear rate. Equation (27) can be rewritten as

$$\eta_a = A \exp B f_s \tag{28}$$

where $A = \exp(2.3\alpha)$ and $B = 2.3\beta$. Equation (28) is identical to the last term of equation (9) of the literature survey from Thomas's work[34]

$$\eta_r = 1 + 2.5 \, g_s + 10.05 \, g_s^2 + A \exp B \, g_s \tag{29}$$

Thomas proposed that, at fractions solid greater than 0.25, this term becomes the major contributor to the viscosity of a suspension and is due to the rearrangement of particles under shear. Eyring[35] developed the same kind of relationship assuming that particle rearrangement is proportional to the probability of transfer of particles from one plane of shear to the next.

Experimental values of A and B in equation (28) reported by Thomas[34],

for suspensions of spheres ranging in size from 0.1 to 435 microns, are

16, 6 and 0.0016, respectively. These correspond to $\alpha = -0.25$ and $\beta =$

7.21, which are close to those obtained in rapidly cooled (25°C/minute)

slurries of Sn-15%Pb alloy, Table VII.

4. Pseudoplasticity

The apparent viscosity of isothermally held slurries of Sn-15%Pb

alloy, plotted versus shear rate on a log-log scale shows a linear

dependence over certain ranges of shear rates (Figure 45). The viscosity

obeys the following equation:

$$\eta_a = k \, \dot{\gamma}^n \tag{29}$$

where η_a is the apparent viscosity, and $\dot{\gamma}$ is the shear rate. The values of

the coefficients k and n, calculated from Figure 45, are given in

Table VIII. Equation (29) is the classical power law equation used to

describe the flow behavior of shear rate dependent materials with a nega-

tive coefficient, n, for pseudoplastic materials and a positive coef-

ficient, n, for dilatant materials.

The values of n calculated for the Sn-15%Pb slurries are of the same

order of magnitude as those reported for suspensions of TiO_2[39] and of

kaolin[68] particles in water, Table VIII. Kaolin particles were shown to

form aggregates whose size decreases with increasing shear rates. Reducing

the size of the aggregates results in lowering of the effective fraction

solid (reduced entrapped liquid) and a corresponding decrease in viscosity.

It was also postulated[68] that the decrease in viscosity with increasing

shear rate corresponds to the decreasing contribution of the energy of

destruction of the network bond (See equation (25) and Appendix H).

The partially crystalline polymer (low molecular weight polyethylene) follows equation (29) over certain ranges of shear rates[52]. The calculated values of the coefficient n are given in Table VIII and are of the same order of magnitude as those for Sn-15%Pb slurries. Two mechanisms were proposed to explain this observation: (a) it was postulated that the high shear rates may "melt" or destroy the crystallites (it was found that the equivalent molecular weight decreases with increasing shear rate) and (b) it was proposed that high shear rates orient assymetric aggregates in the direction of flow.   This mechanism was also found to occur for liquid crystals that exhibit the same behavior[53].

Some of the proposed mechanisms outlined above are for agglomerates of micron size and needle shaped particles (kaolin, TiO_2) and some are for macromolecular aggregates (polyethylene). These mechanisms cannot be directly applied to metal slurries. However, the basic explanation of pseudoplasticity is based on models where there is an equilibrium between the rate of buildup and breakdown of aggregated structure; the buildup is due to the aggregation of particles or molecules to lower their surface energy and the breakdown is caused by the stresses due to the fluid flow forces acting on the aggregates (Figure 46).

Figure 47 shows the structures of isothermally held slurries of Sn-15%Pb alloy sheared at 230 sec^{-1} from the beginning of solidification till a steady state was reached at f_s = 0.45, then it was brought to zero and the specimen was quenched.

The initial shear rate of the specimen shown in Figure 47c and 47d

was 230 sec^{-1}. After steady state was reached, the shear rate was increased to 350 sec^{-1} for 5 minutes and decreased back to 230 sec^{-1} for 10 minutes. Finally it was brought back to zero and the specimen was quenched.

When an isolated particle of Figure 47b is viewed under polarized light, only one shade per particle is observed, Figure 47a. On the other hand, when an isolated particle of Figure 47d is viewed under polarized light, there is more than one shade per particle, Figure 47c.

One may thus conclude that each primary solid particle of the specimen in Figure 47a was originally one equiaxed dendrite that degenerated into the spheroidal shape under shear. If agglomeration occurred in this specimen, then the particles in the agglomerate had the same orientation. Whereas, in Figure 47c it is clear that several of the primary solid particles are agglomerates of particles with different orientations.

In these pseudoplasticity experiments, agglomerates of particles with different orientations were only observed when shear rates were changed after reaching a steady state under a certain constant shear rate. The change in measured viscosity corresponding to a change in shear rate results from changes in the structure of the initial slurry. One of these structural changes is the formation of agglomerates, lending credence to the proposed pseudoplasticity mechanism proposed for non-metallic suspensions as discussed above.

5. Thixotropy

The thixotropy of suspensions, for which solid and liquid are of different density, is complicated since there is a risk of floating or settling of the solid phase. Should this be the case, the increase of

torque after a certain period at rest could result from inhomogeneities in fraction solid, e.g. the local increase of the effective fraction solid. This possibility was ruled out for the metal slurries investigated here because the calculated settling velocity is too slow to give a significant amount of settling. For instance, at a fraction solid of 0.45, the calculated rate of hindered settling of 200 micron size particles is 1 cm in 5 minutes. The density difference between the liquid and the solid decreases as the fraction solid decreases, see Appendix F.

When compared to other thixotropic systems, metal slurries of Sn-15%Pb alloy exhibit a degree of thixotropy (area of hysteresis loop) of the same order of magnitude as that of the non-metallic systems used for comparison in this study, (Figure 48 and Table IV). As an example, the measured areas of hysteresis loops for the Sn-15%Pb slurries at a fraction solid of 0.45, honey, and epoxy with 2.95 wt % SiO_2 are 2-8, 1.5, and 3.0 X 10^5 dyne.cm^{-2} sec^{-1}, Table IV. Hysteresis loop areas of non-metallic systems reported by other investigators are listed in Table IX and are of the same order of magnitude as above.

The structure of a thixotropic material is both shear rate and time dependent, as is its measured viscosity. At low shear rates it is made up of aggregates with an effective volume fraction solid larger than the actual volume fraction solid present, due to entrapped liquid. With increasing shear rates, fluid flow forces break down the aggregates into smaller particles with less entrapped liquid, thus reducing the viscosity of the material. The observation of the hysteresis loop is a consequence of the time dependence of the dissociation of the aggregates.

In the case of chemically non-interacting particles, the aggregation (particle flocculation) at low shear rates is due to the attractive forces between the particles, e.g. long range electrical forces which permit the individual particles of, for example, clay to interact over distances of the order of 1000 $\overset{\circ}{A}$[54]. This aggregation can also be due to the formation of welds between chemically interacting particles such as the primary solid particles of Sn-15%Pb slurries. To differentiate between interacting and non-interacting particles, aggregation of the former is referred to as flocculation and the latter as agglomeration in this study.

For thixotropy to be observed, the concentration of the solid phase must be large enough to permit a significant number of particles to aggregate. In the case of chemically interacting particles, agglomerates form when two particles collide and stay in contact long enough for a weld to form. The probability of successful collisions (collisions followed by weld formation) depends on size, shape, number and distribution of size of primary solid particles as well as on shear rate.

The general trends established in this study relating the degree of thixotropy (area of hysteresis loop) to the structure and thermomechanical history of isothermally held slurries of Sn-15%Pb alloy are shown in Table XI.

i) For a given time at rest, there is a minimum fraction solid below which no thixotropy is observed (Figure 37). As the fraction solid is decreased the probability of successful collisions between particles decreases. For example, below fractions solid of 0.30, after times at rest up to 2 minutes, the areas of the hysteresis loops of Sn-15%Pb slurries,

initially sheared at 115 sec^- , are below the measurable minimum of 0.1 X 10^5 dyne.$cm^{-2}sec^{-1}$. The maximum shear rate used to generate the hysteresis loops in Figure 37 was the same as the initial shear rate, 115 sec^{-1}.

ii) The effect of initial shear rate on structure and viscosity of the Sn-15%Pb slurries are shown in Figures 30 and 31. Both the average primary particle size and viscosity increase with decreasing initial shear rate. The effect of initial shear rate on the area of the hysteresis loop follows the same trend; the area increases with decreasing initial shear rate (Figure 38). For instance, the areas of the hysteresis loops of two slurries held at 0.45 fraction solid and sheared at 350 and 115 sec^{-1}, after 30 seconds at rest, are 1.5 X 10^5 and 6.0 X 10^5 dyne.$cm^{-2}sec^{-1}$, respectively, an increase by a factor of 4.

iii) Increasing the rest time, t_r, or the down time, t_d, results in a corresponding increase in the area of the hysteresis loop (Figures 39 and 40 and Table XI). As the time at rest is increased, the time available for weld formation between particles increases. Alternatively, as the down time increases, longer times are spent at low shear rates. Thus the time available for weld formation increases and the fluid flow forces responsible for the dissociation of the agglomerates decrease. Consequently, more agglomerates or agglomerates of larger size are present at the beginning of the up curve, hence the higher the difference in torque. For example, the area of the hysteresis loop increases by a factor of 1.75 as the down time is increased from 4 to 60 seconds, Figure 40b.

A relationship between the rest time, t_r in minutes, and the area of hysteresis loops, A in dyne.$cm^{-2}sec^{-1}$, is given by

$$A = 3.0 \times 10^5 \ t_r^{.25} \qquad (30)$$

for the areas reported in Figure 39b and Table X.

iv) Finally the effect of the conditions of measurement on the degree of thixotropy follows the same trends as those reported for non-metallic systems[57] (Table X). The relationships are of the type

$$A = A_o - Nt_u \qquad (31)$$

relating the area of the hysteresis loop, A, and the up-time, t_u, and of the type

$$A = Q \ \dot{\gamma}_m^n \qquad (32)$$

relating the area, A, and the maximum shear rate, $\dot{\gamma}_m$. A_o, N, Q, and n are constant for a given system.

Even though no theoretical derivations have been reported for these equations they are always explained on the basis of the effect of shear rate on the number of fractured welds. For instance, as the up time decreases, so does the time during which the shear forces are operating; hence the number of fractured welds decrease and the viscosity increases.

B. Mechanism for Formation and Fracture of a Weld Between Two Primary Solid Particles

In the previous section the rheological properties of Sn-15%Pb slurries were compared with other well-known thixotropic systems. It was shown that (a) the Sn-15%Pb slurries behave like suspensions of interacting particles and (b) that their viscosity and hence their structure is shear rate and time dependent. Finally, some general relationships and trends were developed to describe the thixotropic behavior of the Sn-15%Pb

slurries. In the following sections, first a model is presented to quantitatively describe the formation of a weld between two primary solid particles of a Sn-15%Pb slurry after the particles have collided (Figure 49). Next, a model is presented to describe the magnitude of the shear forces necessary to break this weld.

1. Weld Formation

In this model the assumptions are:

(a) The two particles are in true contact - Whenever two particles collide, some liquid is left between them; if under the pressure exerted by the particles and caused by the fluid this liquid drains out then the particles establish a true contact. The time required by the liquid to drain will decrease with increasing shear rate, since the fluid flow forces increase with increasing shear rate.

(b) The dihedral angle between the two particles is 180°. This assumes that the interfacial energy between the solid particles is zero[125] (that is, there is no lattice mismatch between the two particles).

The equilibrium temperature of the liquid-solid interface, at the point of contact between the particles, depends on the local curvature, and for this surface of negative curvature, κ, the liquidus temperature is raised by[104]

$$\Delta T = -\frac{2\sigma\kappa T_L}{H} \tag{33}$$

where $\kappa = \frac{1}{2}(\frac{1}{R_2} - \frac{1}{R_3})$, see Figure 56,

σ = solid-liquid interfacial energy,

T_L = equilibrium liquidus temperature for a planar interface,

H is the volumetric heat of fusion.

Assuming equilibrium at the two liquid-solid interfaces (large primary solid particle of radius R_1 and area of contact with negative radius of curvature R_3 (Figure 56)) a diffusion couple is established in the liquid between these two interfaces. As shown in Appendix I, solvent (Sn) diffuses from the primary solid particle to the area of contact. Integration of the rate equation derived in Appendix I yields the following equation relating the radius of the weld, R_2, and the time of contact, t:

$$R_2^5 = 10\pi R_1^2 \ D\sigma T_L \ t/C_L(1 - k)mH \qquad (34)$$

where D is the diffusion coefficient, C_L is the weight percent of solute in the liquid, k is the partition ratio between solid and liquid, m is the liquidus slope, and the other terms are defined above.

Using selected values for the Sn-15%Pb alloy, listed in Table XII, equation (34) becomes

$$R_2^5 = 1.29 \times 10^{-9} \ R_1^2 \ t \qquad (35)$$

Equation (35) is plotted in Figure 50. For a primary particle of radius $R_1 = 100\mu$, the radius of the weld is $R_2 = 6.5\mu$ after a time $t = 10^{-3}$ seconds.

2. Mechanism for Fracture of a Weld Between Two Particles

A model is presented to describe the effect of shear rate on fracture of the weld formed between two primary solid particles. The fluid flow forces result in stresses that cause the metallic weld between the primary solid particles to deform (creep) and eventually fracture. Assumptions made are that this fracture occurs when the strain reaches a

critical limit of $0.10^{(126)}$. Whether this limiting value of strain is reached depends on the magnitude and duration of the stress generated by the motion of the fluid.

Assuming two primary solid particles in contact perpendicular to the flow direction, the force associated with the kinetic contribution of the fluid movement is calculated from Stokes's Law in Appendix J:

$$F = 12\pi R_1^2 \eta\dot{\gamma} \tag{36}$$

All terms in equation (36) have previously been defined. The shear stress due to the force operating on the total area of the weld, πR_2^2, is

$$\tau = 12(R_1/R_2)^2 \eta\dot{\gamma} \tag{37}$$

For a Sn-15%Pb slurry with a 5 poise viscosity (f_s = 0.45) containing 200μ primary solid particles (R_1 = 100μ) and a weld radius of R_2 = 6.5μ, calculated shear stress values from equation (37) are 20 and 100 psi for corresponding shear rates of 100 and 500 sec^{-1}. These values are of the same order of magnitude as those reported for strengths of semi-solid Sn-15%Pb alloy[10].

The duration over which this stress should be operative to induce a strain of 0.10 is calculated in Appendix J using the Larson-Miller parameter in extending previously reported creep data for a Sn-38%Pb alloy[111], Figure 52. These data yield the following equation:

$$t_f = \varepsilon/\dot{\varepsilon} = 4 \times 10^{10}\tau^{-2} \tag{38}$$

Calculated times for the example used above are 2.3×10^{-2} and 9×10^{-3} second for shear rates of 100 and 500 sec^{-1}, respectively, Table XIII.

Mason and Bartok[124] have developed an expression relating the rate of shear to duration over which two rigid (glass) spheres, of 50 to 300μ in size, stay in contact in a Couette viscometer. The average doublet life calculated and experimentally determined for fairly dilute solutions, $f_s \simeq 0.10$, is given by

$$\overline{t} = \pi/\dot{\gamma} \tag{39}$$

For a shear rate of 100 and 500 sec^{-1}, expression (39) yields average doublet lives of 5×10^{-2} and 6×10^{-3} seconds, respectively.

The mechanism proposed for agglomeration of primary solid particles predicts that very short times ($\simeq 10^{-3}$ second) are sufficient for a weld between two primary solid particles in true contact to grow to a size of 6.5μ. On the other hand, calculated times for fracture of these welds are rate dependent - the following equation is obtained combining equations (37) and (38)

$$t_f = 230 \, \dot{\gamma}^{-2} \tag{40}$$

Calculations of doublet lives and fracture times from equation (39) and (40) are shown in Table XIII and are plotted in Figure 53. Figure 53 shows, for this highly simplified model, shear rate conditions under which a given size weld formed between two primary solid particles will have time to fracture.

In summary then, the shear rate dependence of weld formation and fracture presented herein is in qualitative agreement with pseudoplasticity results reported in Figure 28. In general, low rates of shear favor formation of permanent welds, resulting in large particles or agglomerates with

entrapped liquid, hence high measured viscosities.

C. Formation of Rheocast Structures

The structures of Sn-15%Pb slurries consist of small primary solid particles well distributed in the remaining quenched liquid (Figures 22, 23, 29, 30). Similar Rheocast structures have been obtained in several alloy systems that have been subjected to vigorous agitation during solidification[10-13]. The general trends relating the structural parameters (average size of primary solid particles and amount of entrapped liquid) to the solidification parameters (cooling rate and shear rate) are summarized in Table VI.

In the following section, some mechanisms are proposed to explain the formation of these particulate non-dendritic structures generated under vigorous agitation.

At very low fractions solid, columnar or equiaxed dendrites form in the melt. These have well developed secondary and some tertiary arms (Figure 54a). As the fraction solid increases, these well developed dendrites experience grain multiplication by one of the following mechanisms.

(i) Grain multiplication is caused by dendrite remelting. Remelting comes about because some of the arms which form initially become unstable later in solidification and melt while others continue to grow. It is assumed that the roots of dendrite arms have a slightly higher solute content and have a greater curvature than the outer portions of the arms. Thus, their melting point is lower and thermal fluctuations induced by the vigorous agitation cause melting in this location.

(ii) It has also been suggested that mechanical fracture, resulting from the stress caused by fluid flow, might be enough to lead to grain multiplication. Should this mechanism be responsible for grain multiplication, the resulting structure will be shear dependent. That is, the size of the primary solid particles will decrease with increasing shear rate. This actually is the case for slowly cooled and isothermally held specimens, Figure 23, 30.

As fraction solid increases, these primary solid particles grow and coarsen. Coarsening can take place in the following ways:

(i) Each individual particle coarsens by one of the several mechanisms proposed for coarsening of dendritic structures[129]. Alternatively, spheroidization of the primary solid particles can take place by one of the two modes shown in Figures 55a and 55b.

(ii) Particles collide and coalesce (Figure 55c).

(iii) Larger particles coarsen at the expense of smaller ones, by an Ostwald ripening mechanism.

Whichever of the above mechanisms operates, coarsening is time dependent, which explains why slow cooled specimens under identical shear conditions have coarser structures with larger primary solid particles (Figures 22 and 23).

The driving force for coarsening is the lowering of the interfacial energy between solid and liquid. Any area of negative curvature will have a tendency to disappear and the equilibrium shape of a given primary particle will be a sphere with the largest possible radius. This explains why slow cooled slurries have less entrapped liquid than fast cooled slurries

and why isothermally held slurries have no entrapped liquid and are somewhat spheroidal in shape.

The coarsening mechanism is diffusion controlled so that any decrease in the boundary layer through which solute and solvent diffuse will result in an increase in the coarsening rate. Thus convection not only aids diffusion by simply increasing the diffusion flux (adding a term to Fick's first law) but also increases the solute gradient in front of a growing interface. This explains why, at any cooling rate, an increase in shear rate results in a decrease in entrapped liquid, lower effective volume fraction solid and hence lower viscosity.

CHAPTER VI: CONCLUSIONS

A. General

1. The apparent viscosity of Sn-15%Pb slurries increases with increasing fraction solid and is structure dependent. The structure and apparent viscosity are strongly influenced by the thermomechanical history of the alloy during solidification. The rheological behavior of vigorously agitated slurries of the alloy exhibit thixotropy.

B. Continuously Cooled Slurries

2. The viscosity of the slurry, at a given fraction solid, decreases with decreasing cooling rate and increasing shear rate. Exercising the full range of shear and cooling rates possible in the viscometer the apparent viscosity of a 0.55 fraction solid slurry was varied from 3 to 80 poise.

3. At a given shear rate and fraction solid, increasing the cooling rate results in finer primary solid particles with more entrapped liquid.

4. In both the fast and slow cooled slurries, the amount of entrapped liquid at a given fraction solid decreases with increasing shear rate. For instance, at 25°C/minute and a fraction solid of 0.55 the volume fraction of entrapped liquid are 0.13 and 0.08 for corresponding shear rates of 230 and 750 sec^{-1}.

5. At a given fraction solid, the average size of primary solid particles of fast cooled slurries, 25°C/minute, remains constant with changes in shear rate, while in the slowly cooled slurries, 0.33°C/minute, the average size of primary solid particles decreases with increasing shear

rate. At 0.55 fraction solid and a cooling rate of 0.33°C/minute, the size decreases from 280 to 180μ as shear rate increases from 230 to 750 sec^{-1}; at the same fraction solid but a cooling rate of 25°C/minute the size remains constant at 50μ.

6. Over wide ranges of fraction solid, the apparent viscosity of the continuously cooled slurries follow a state equation, relating the apparent viscosity, η_a, to the fraction solid, f_s:

$$\eta_a = A \exp B f_s$$

where A and B are constants for a given condition of shear and cooling rates. The coefficient B is of the same order of magnitude as that found for non-metallic systems such as suspensions of glass spheres ranging in size from 0.1 to .435μ.

7. Comparison of Sn-15%Pb slurries to suspensions of interacting and non-interacting particles, at the same fraction solid, shows that the viscosity of metal slurries is of the same order of magnitude as that of the former and consistently higher than that of the latter.

C. Isothermally Held Slurries

8. The structures and viscosity of isothermally held slurries follow the same trends as those of slowly cooled slurries, i.e. at a given fraction solid, particle size, amount of entrapped liquid and viscosity decrease with increasing shear rate. Furthermore, at a given fraction solid and shear rate, the viscosity of an isothermally held slurry is lower than that of a continuously cooled slurry.

9. Variations up or down of shear rate, at a given fraction solid, result in a corresponding decrease or increase in the measured viscosity.

For example, at 0.50 fraction solid, when shear rate is increased from 115 to 250 sec^{-1} viscosity decreases from 30 to 16 poise.

10. Over wide ranges of shear rates, the apparent viscosity of isothermally held slurries follows a state equation of the form:

$$\eta_a = k\dot{\gamma}^n$$

relating viscosity, η_a, to shear rate, $\dot{\gamma}$. The coefficients k and n depend on the initial structure of the slurries. The coefficient n varies between -0.3 and -0.82 for a wide range of conditions. A typical value for n in a non-metallic pseudoplastic system (clay in water) is between -0.65 and -0.86.

11. Slurries of Sn-15%Pb alloy are thixotropic and show a hysteresis loop phenomenon similar to other well-known non-metallic thixotropic systems. Measured areas of hysteresis loop increase with increasing fraction solid, initial viscosity (structure) and time at rest. For instance, the areas for a slurry held at 0.45 fraction solid and of initial viscosity 15 poise, varies between 2.0 and 8.0 X 10^5 $dyne.cm^{-2}sec^{-1}$ for rest times between 30 seconds and 30 minutes, respectively. These are comparable to measured areas for honey and epoxy mixed with 2.95 wt % SiO_2 which are 1.5 and 3.0 X 10^5 $dyne.cm^{-2}sec^{-1}$, respectively.

12. The occurrence of thixotropy (defined herein as a measurable minimum hysteresis loop area of 0.1 X 10^5 $dyne.cm^{-2}sec^{-1}$) is a function of fraction solid and time at rest. For fractions solid below 0.30 and rest times of up to 2 minutes, the areas of the hysteresis loops are below the measurable minimum.

13. Equations of state relating the area of hysteresis loop to the

process variables are similar to those of well-known non-metallic thixotropic systems. For instance, isothermally held slurries of Sn-15%Pb alloy obey an equation of the form:

$$A = A_o - Nt_u$$

relating area of hysteresis loop, A, and up time, t_u; the coefficients A_o and N depend on fraction solid and structure.

14. The proposed mechanism for thixotropic behavior of the isothermally held slurries is based on the formation and fracture of welds between primary solid particles. The driving force for the formation of these welds is the lowering of the interfacial energy of the liquid-solid interface, whereas fracture results from the action of the fluid flow forces on the particles. The model shows that, at low shear rates (below a critical shear rate) agglomerates form resulting in large particles with entrapped liquid, hence high slurry viscosity.

D. Formation of the Structures of Sn-15%Pb Slurries

15. The mechanism proposed for the formation of particulate non-dendritic structure generated under vigorous agitation is one where, above fractions solid of $\simeq$ 0.15, a multiplication mechanism breaks up initially formed dendrites, into degenerate dendritic primary solid particles. Subsequently, coalescence and/or ripening occurs, driven by the lowering of the interfacial energy of the primary solid particles.

CHAPTER VII: SUGGESTIONS FOR FUTURE WORK

1. The rheological behavior of isothermally held slurries should be studied over wider ranges of shear rates (gap size) and cooling rates.

2. Work should continue to relate structures to thermomechanical conditions during solidification. Effect of variations of the thermo-mechanical history on structures should be further studied. As example, the phenomenon of agglomeration of primary solid particles as affected by rate of shear should be investigated.

3. Application of the findings of this work to machine casting of semi-solid metals must include development of continuous apparatuses for production of the slurries. Therefore, the trends established here should be utilized in design of the continuous apparatuses.

4. The rheological properties of other metallic alloys (binary, ternary, two phase and multiphase. . .) should be studied.

5. In general, a much deeper understanding of this new field of rheology of metallic slurries is needed.
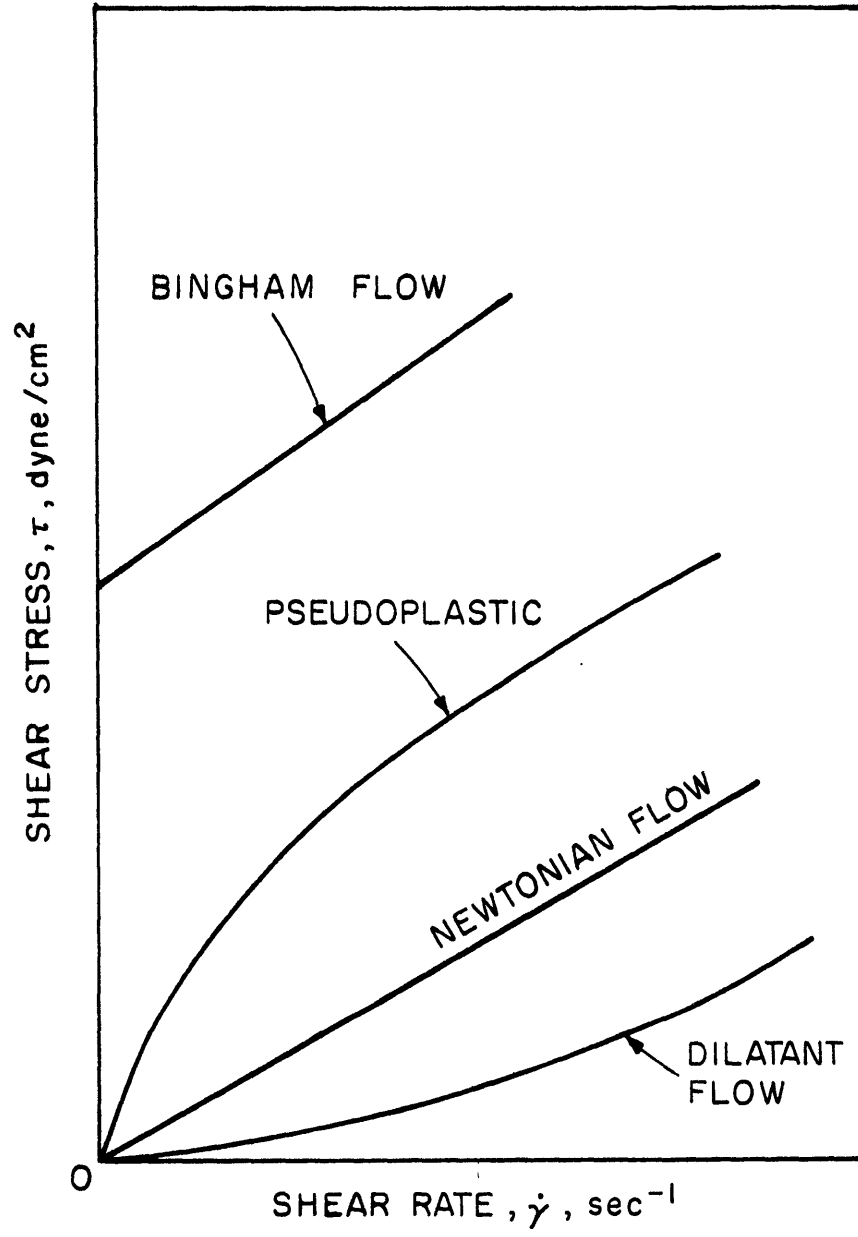
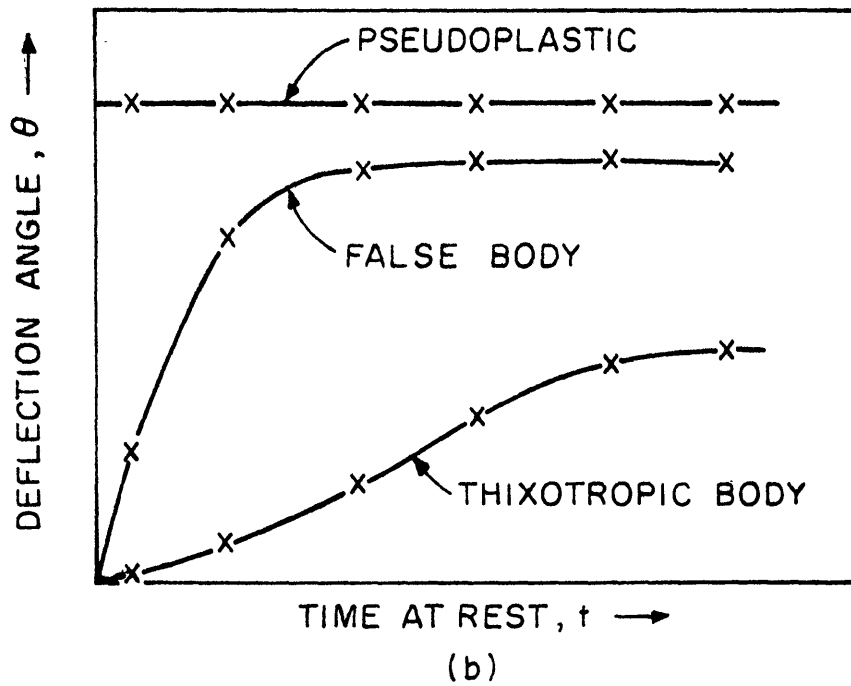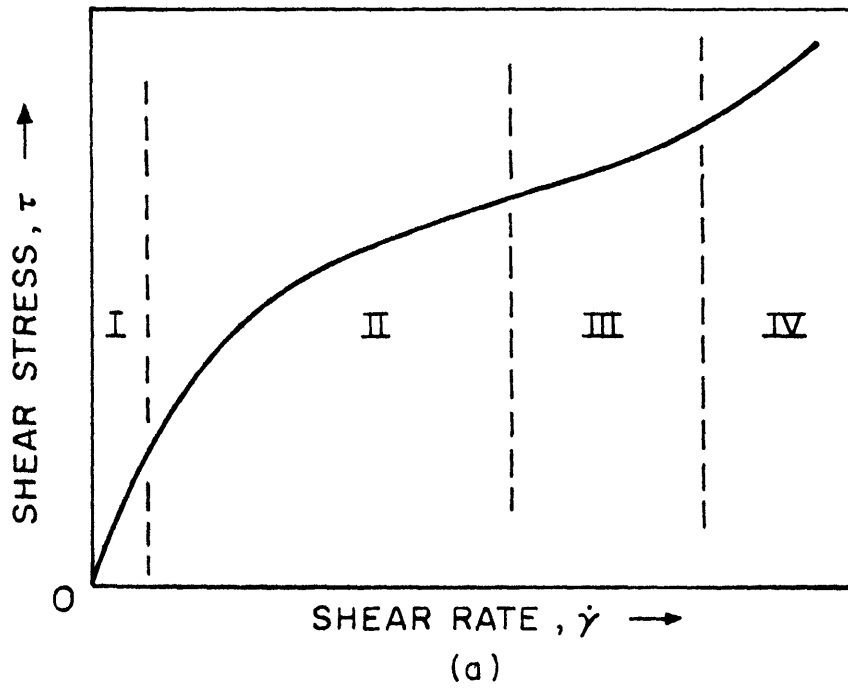Figure 1. Flow Behavior of Materials

Figure 2. Flow Curves (a) of a material showing structural viscosity
(Ostwald Curve); the four regions are I, Newtonian; II, Pseudoplastic;
III, dilatant and IV, Newtonian; (b) of three different materials (all
shear-thinning): pseudoplastic, thixotropic and false bodies, after
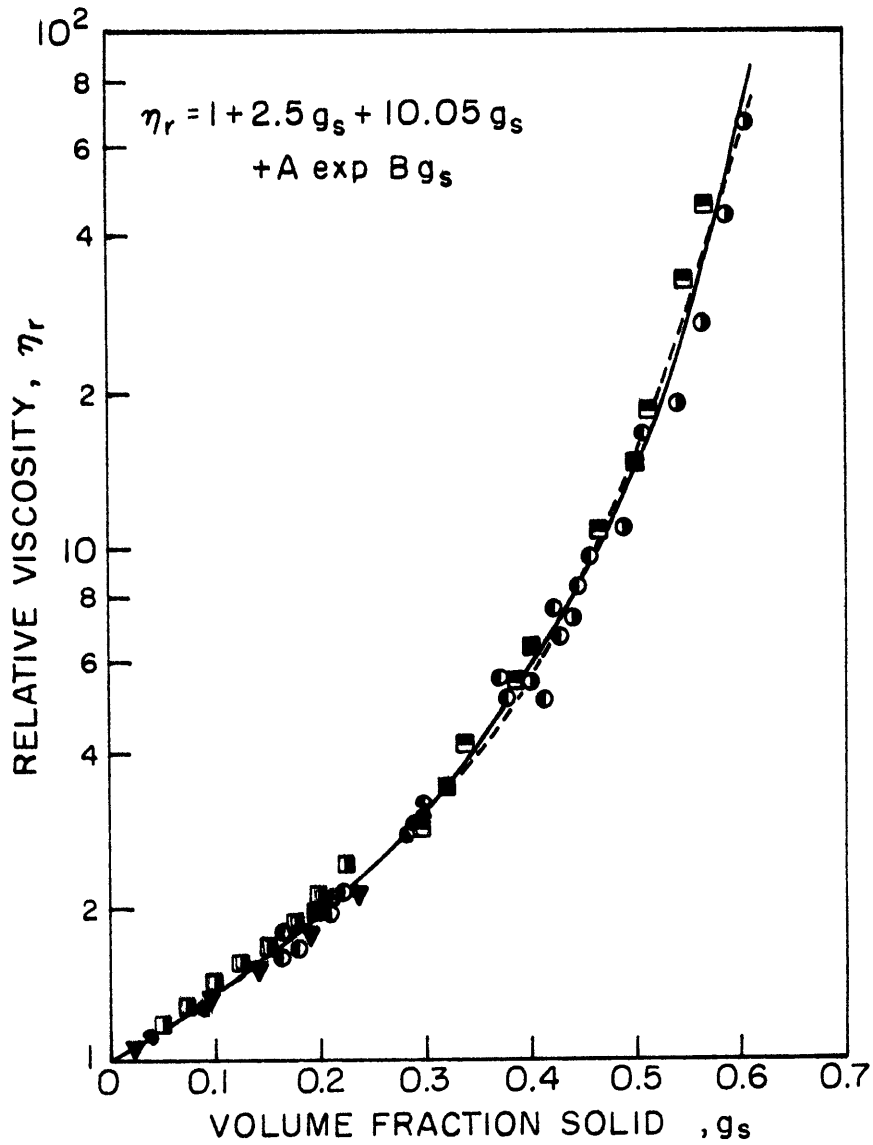J. Pryce-Jones[20].

Figure 3. Relative viscosity of suspensions of polystyrene, rubber latex, glass and methylmethacrylate in the size range from 0.1 to 435 microns, after Thomas[34].
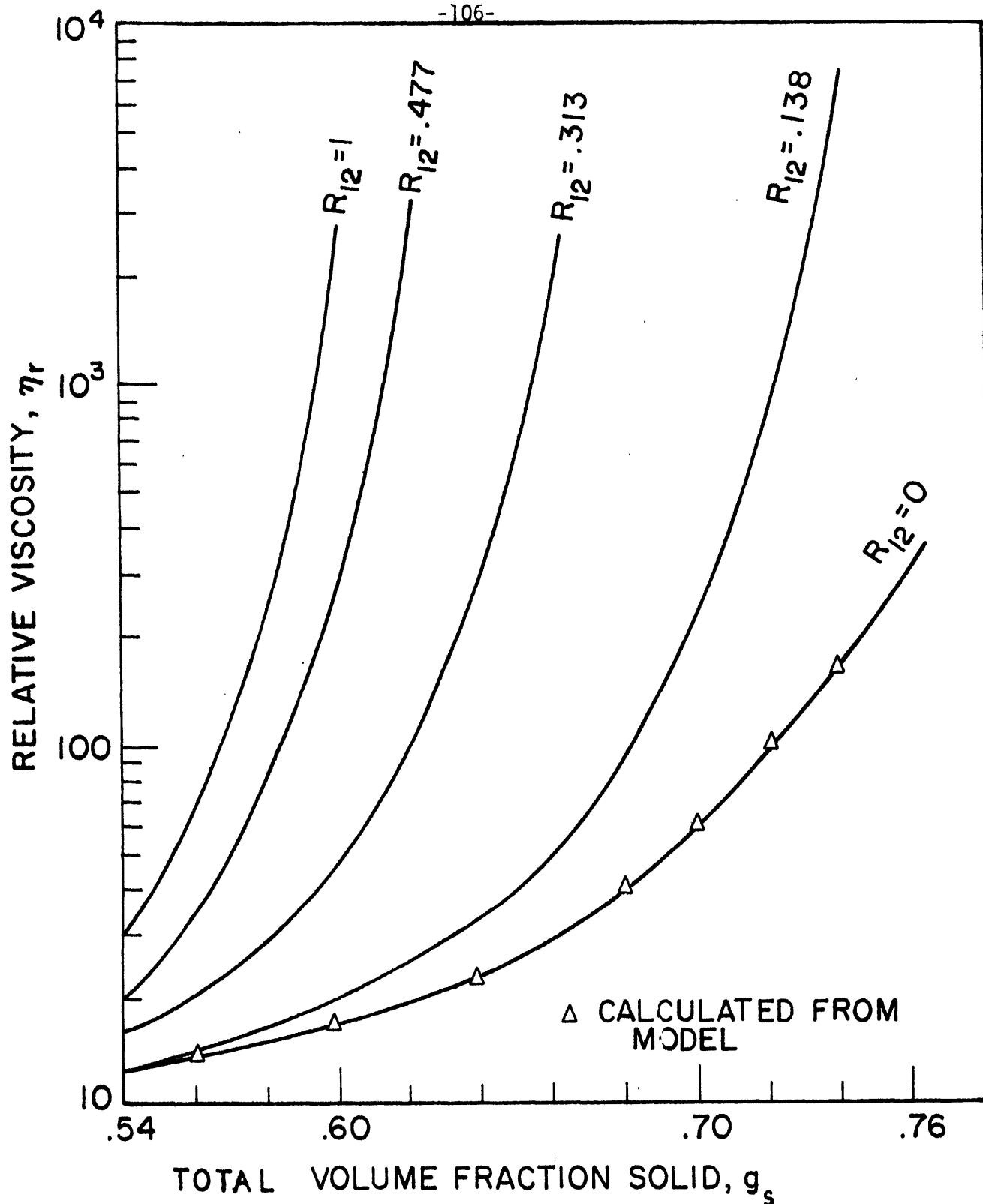
Figure 4. Relative viscosity of bidispersed suspensions of glass spheres in polyisobutylene, after Farris[45]. Each bimodal suspension has 25% by volume as small spheres. Each curve corresponds to a constant size ratio, R_{12}, ratio of the small sphere size (33,74,112 microns) by the large sphere size, 236 microns.
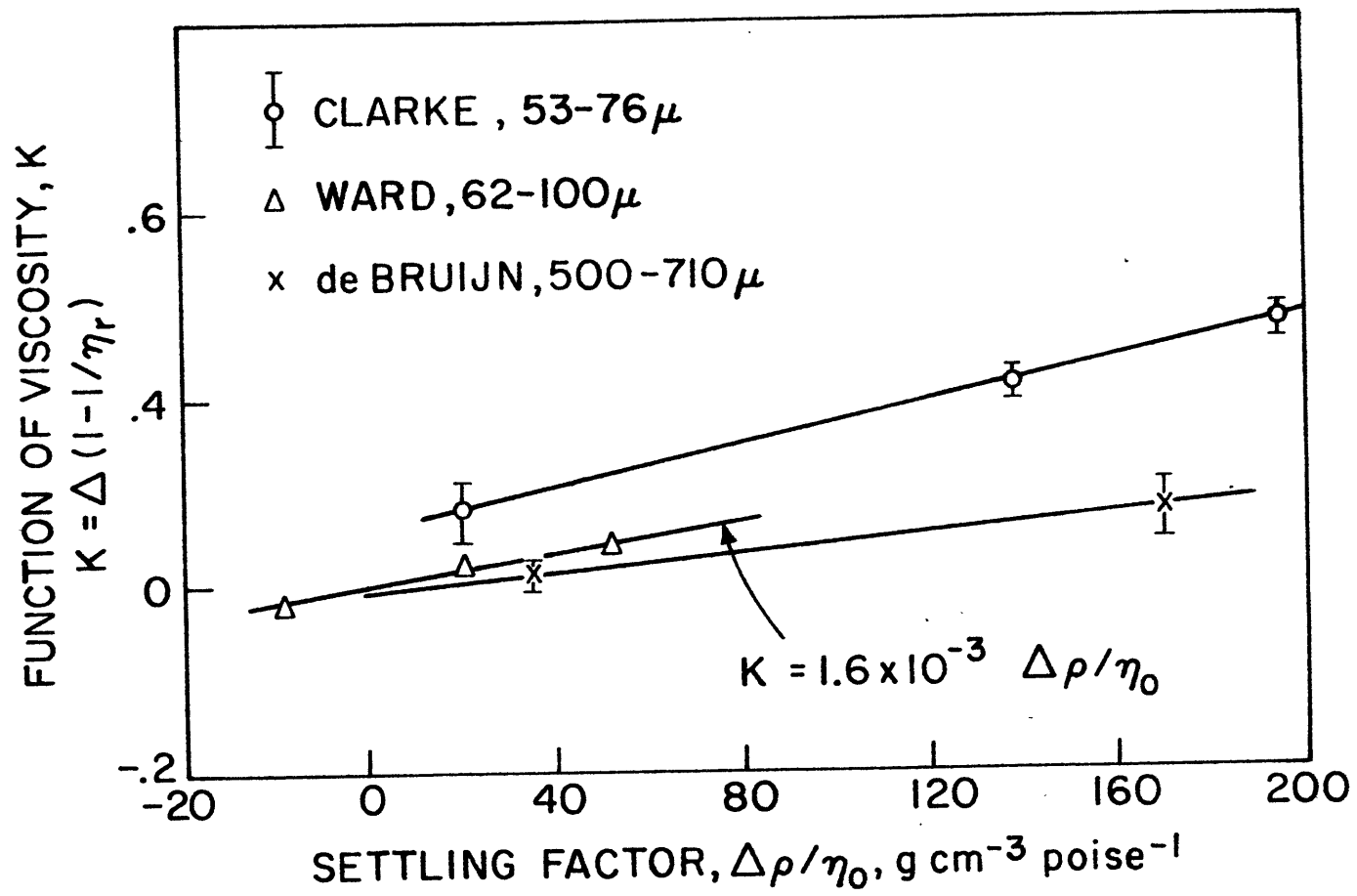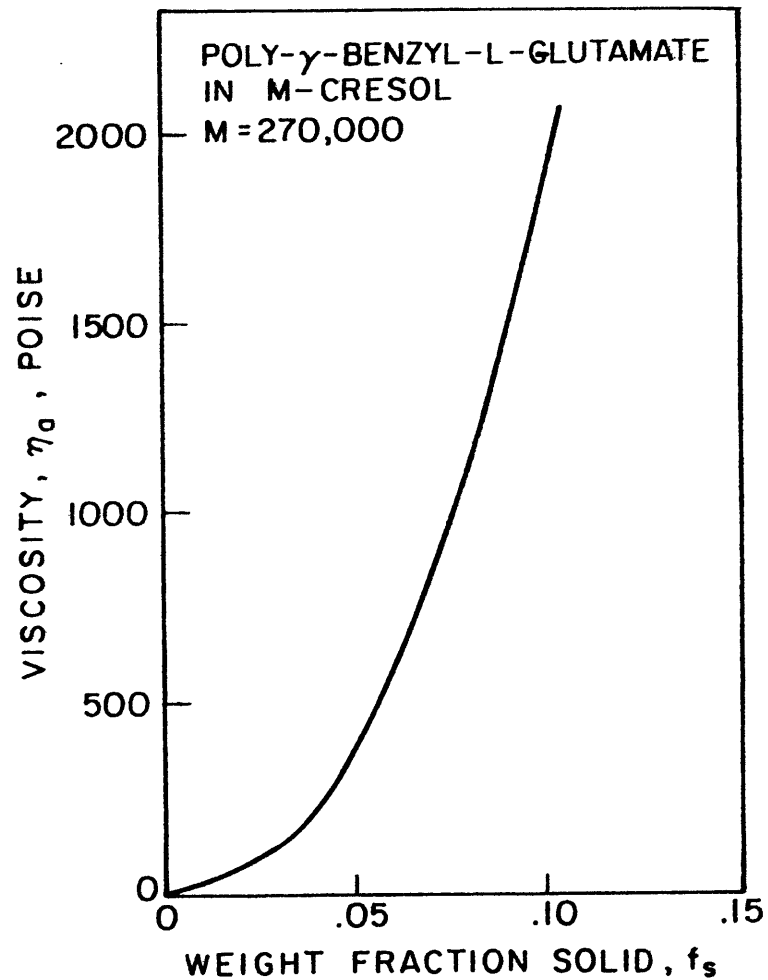
Figure 5. Effect of particle density on the relative viscosity, of coarse suspensions, after Ward[47].
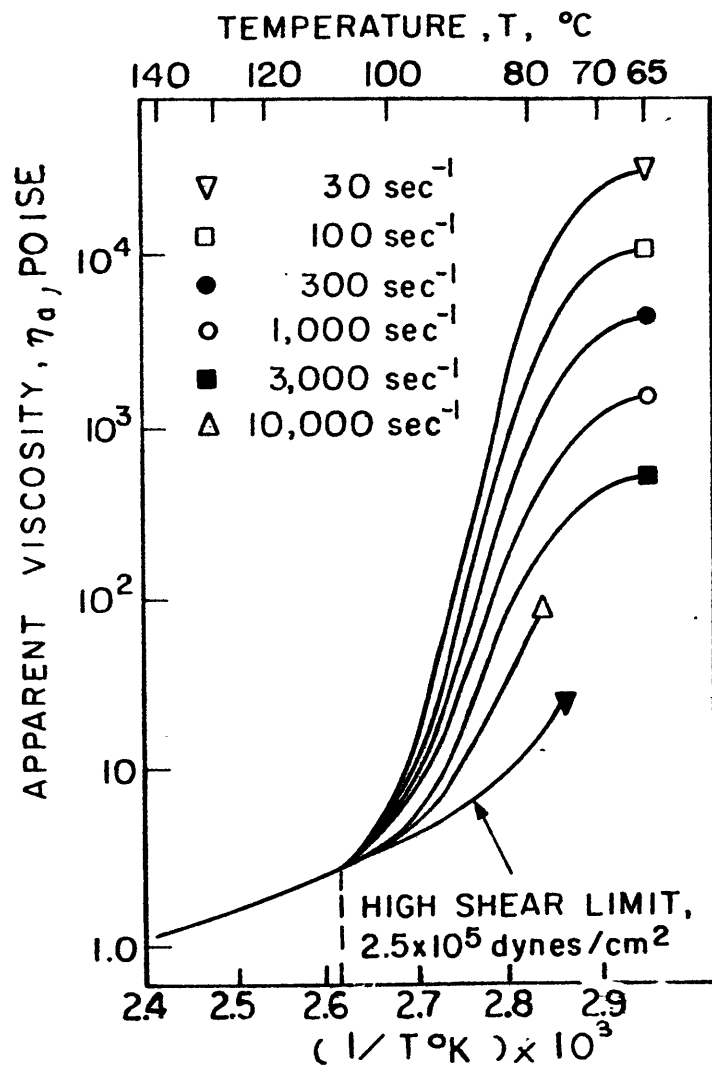
Figure 6a. Apparent viscosity of low molecular weight polyethylene at different temperatures below the melting point and different shear rates after Porter[52].
Figure 6b. Viscosity of a liquid crystal, after Hermann[53].

THIXOTROPIC MATERIAL
CONSTANT STRESS, τ

SHEAR, γ →

$\dot{\gamma}_0$

O

TIME, t →

(a)

SHEAR RATE, $\dot{\gamma}_0$ →

TIME AT REST, t →

SHEAR STRESS, τ →

(b)
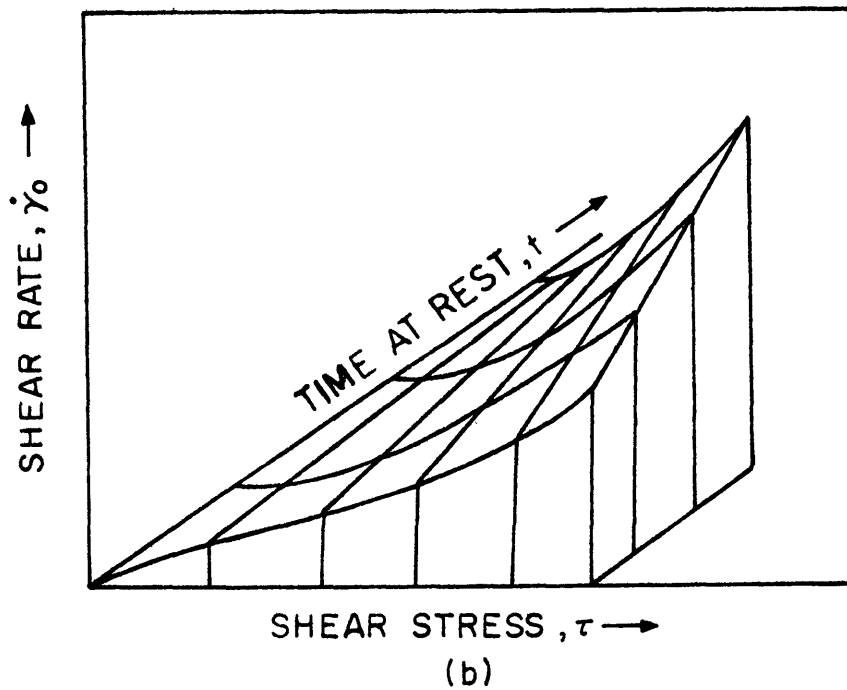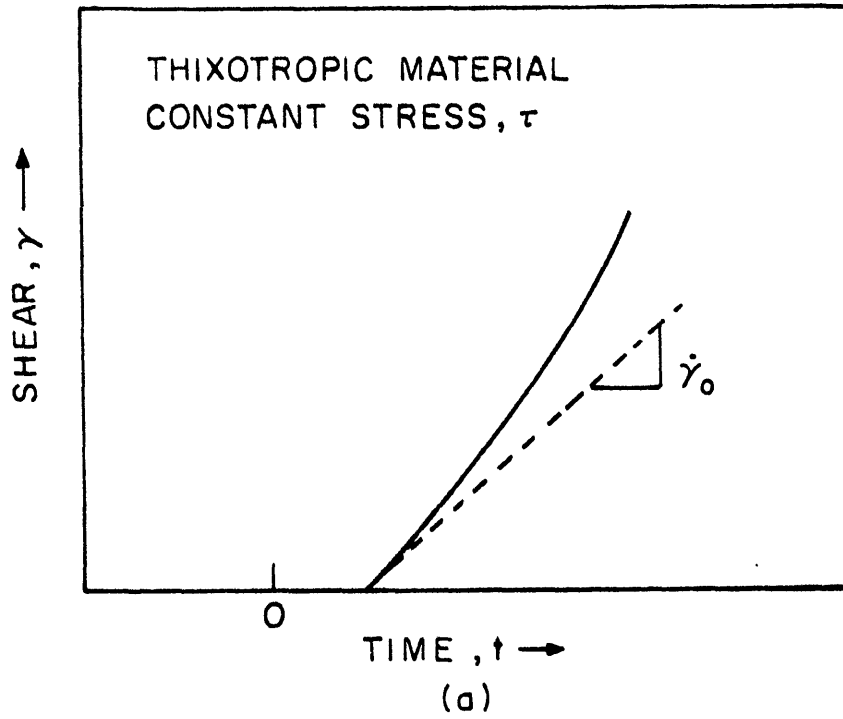
Figure 7. Characterization of a thixotropic material after Alfrey[56]:
(a) at constant stress by the measure of $\dot{\gamma}_0$; (b) as a function of the stress, τ, and the time at rest, t.
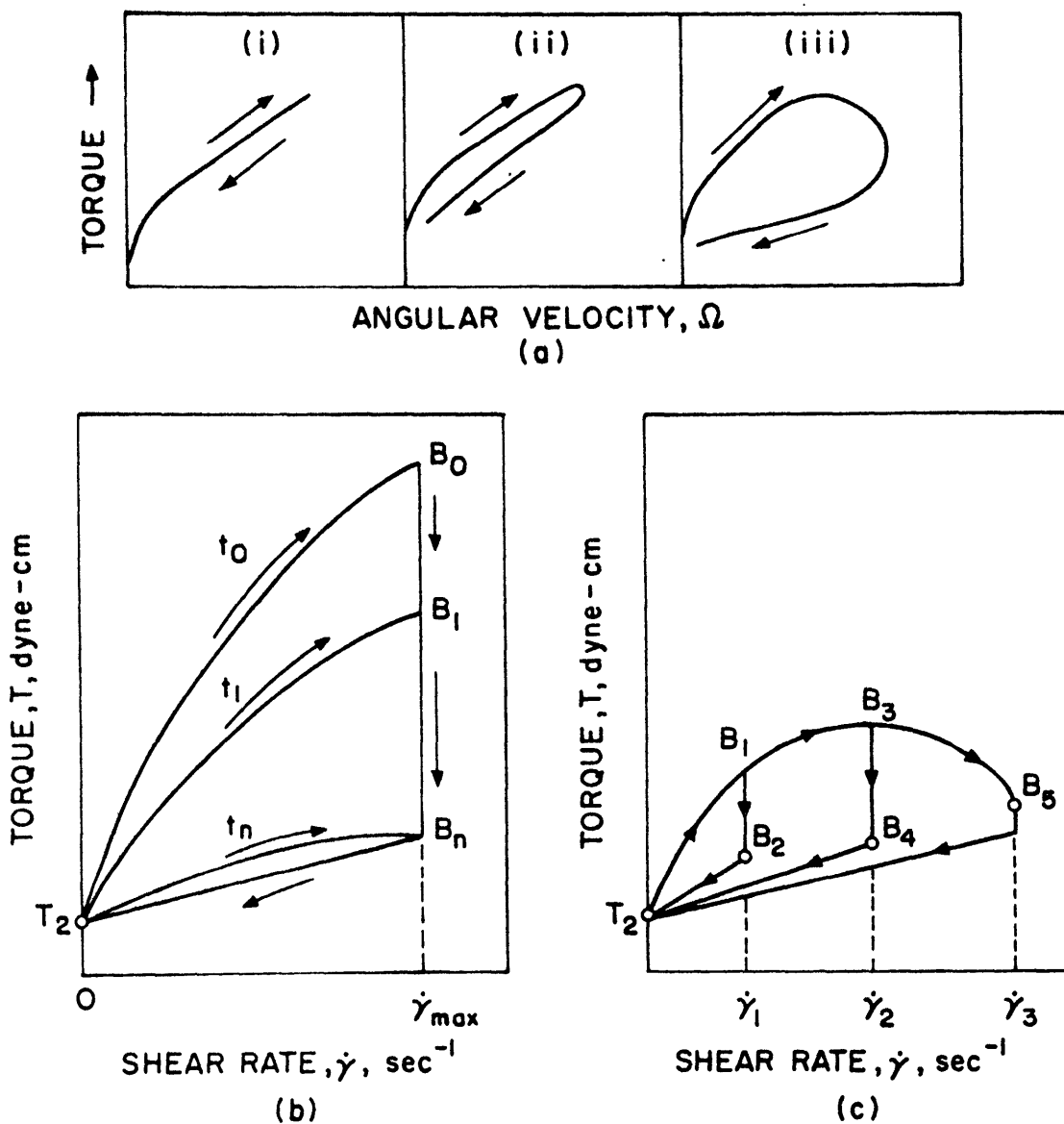
Figure 8. Hysteresis loops (a) of three different materials showing i) no, ii) little, iii) high thixotropy, (b) of a printing ink when the up time is increased, (c) of a printing ink when the maximum shear rate is increased, after Weltman[57].

START

CENTER ARM DISAPPEARING

END
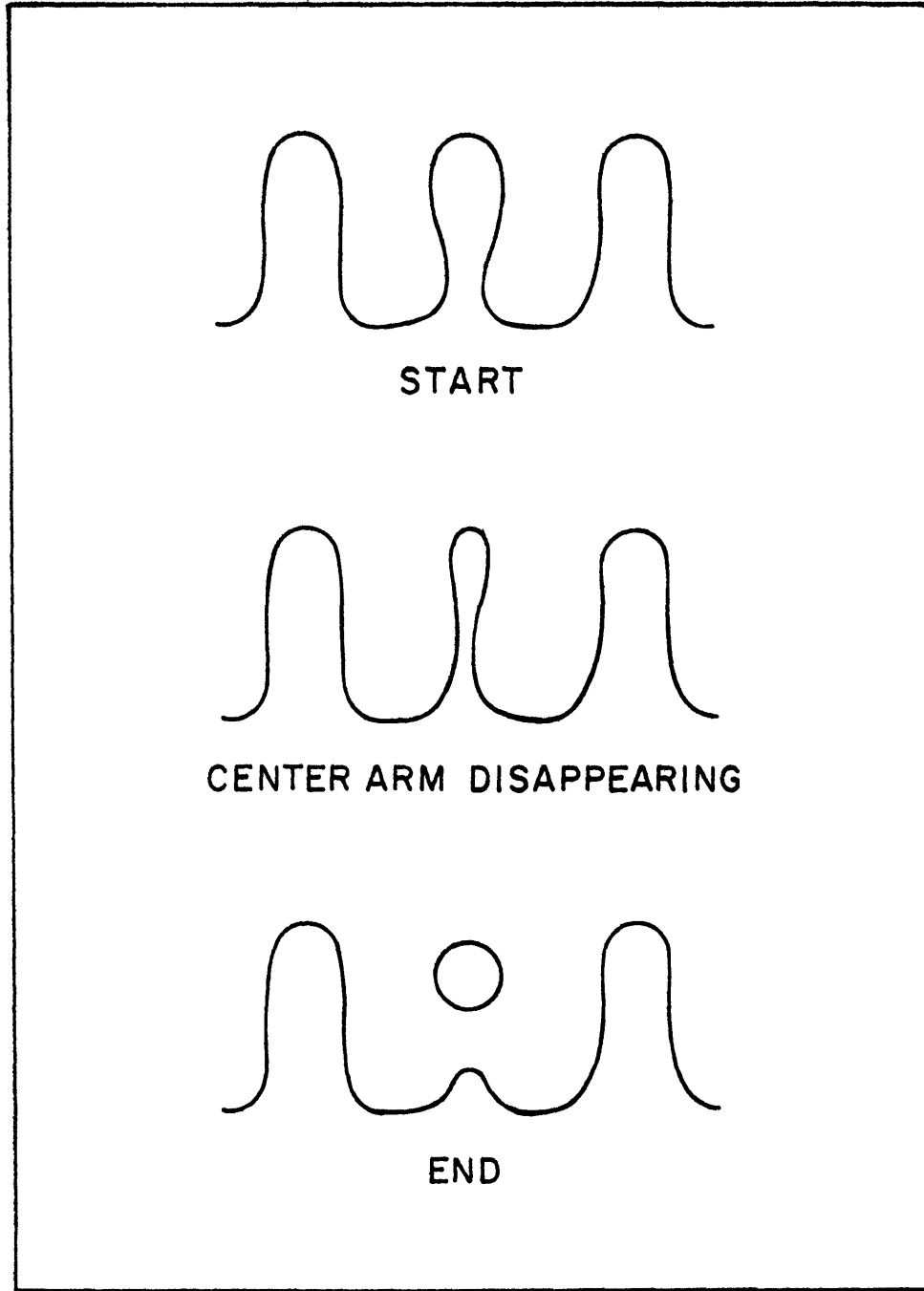
Figure 9. Dendrite Coarsening Model, after Kattamis, et al.[71].
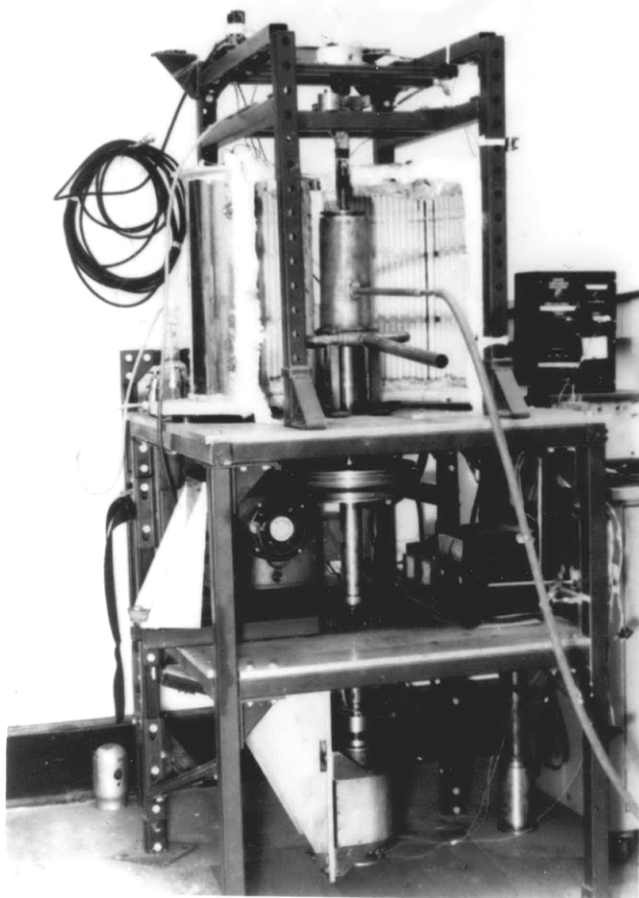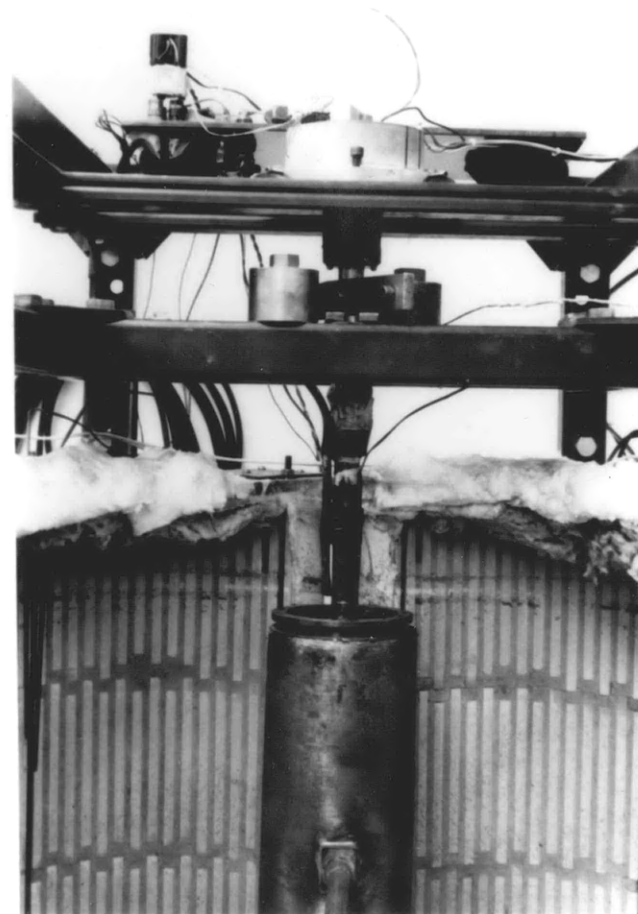
(a)   (b)

Figure 10 Photograph of main apparatus showing (a) from top to bottom,torque
          dynamometer,furnace,shaft and belt drive,thermocouple junction box
          and (b) enlarged view of furnace and water spray jacket.
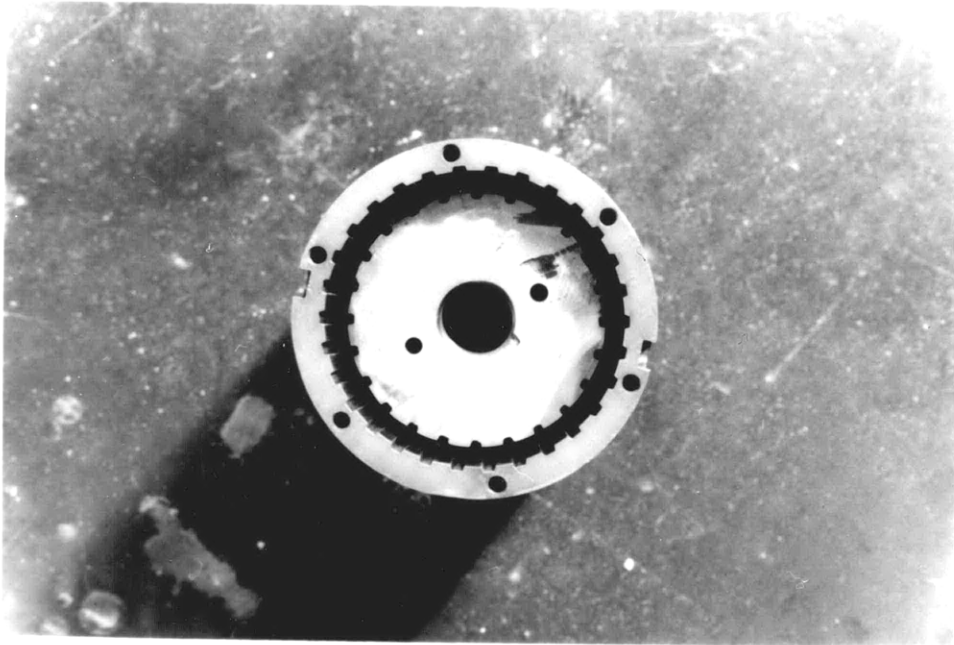
(a)
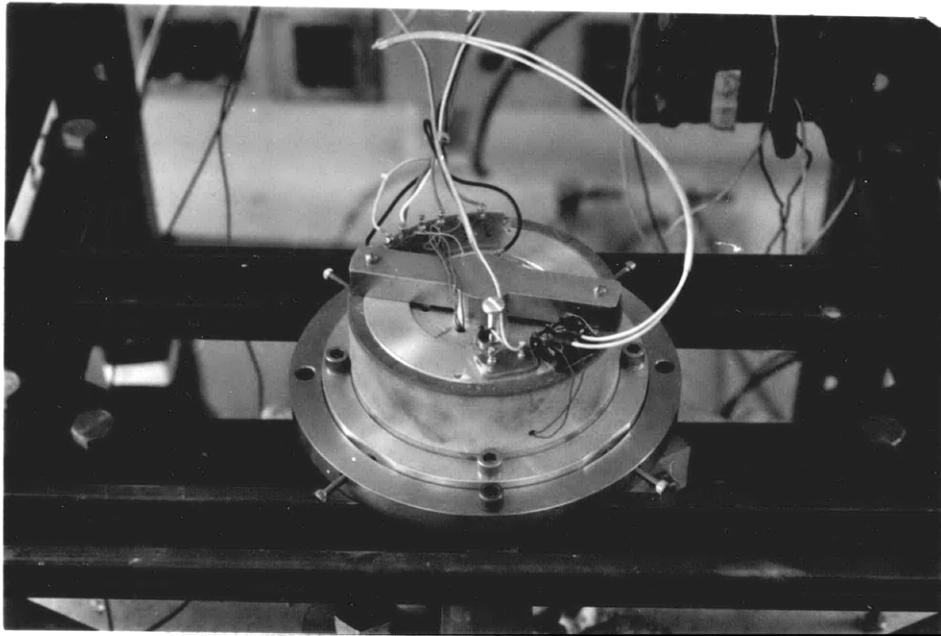
(b)

Figure 11a. Photograph of the cup and bob arrangement.

Figure 11b. Photograph of the torque dynamometer.
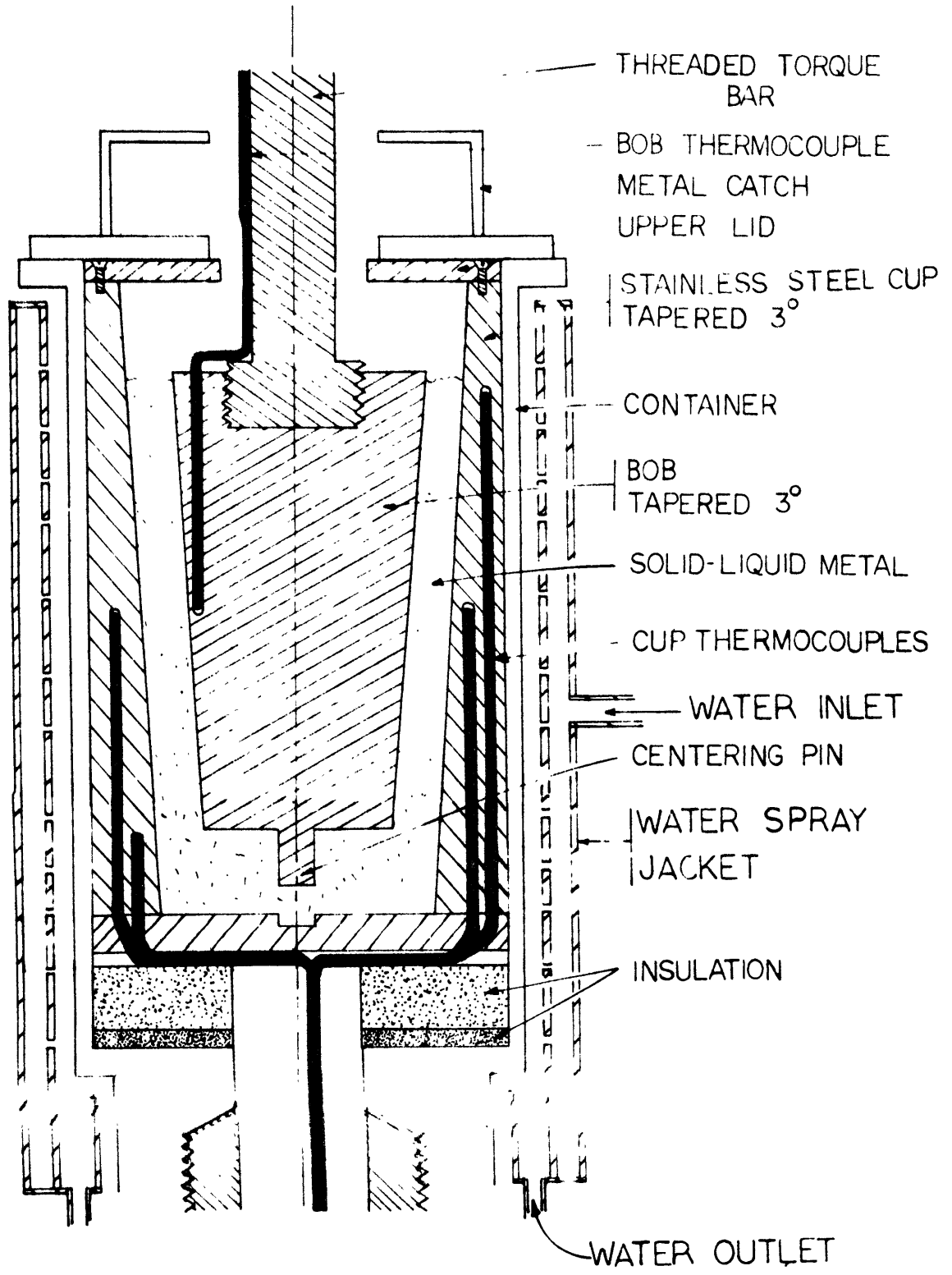
Figure 12.Schematic diagram of apparatus
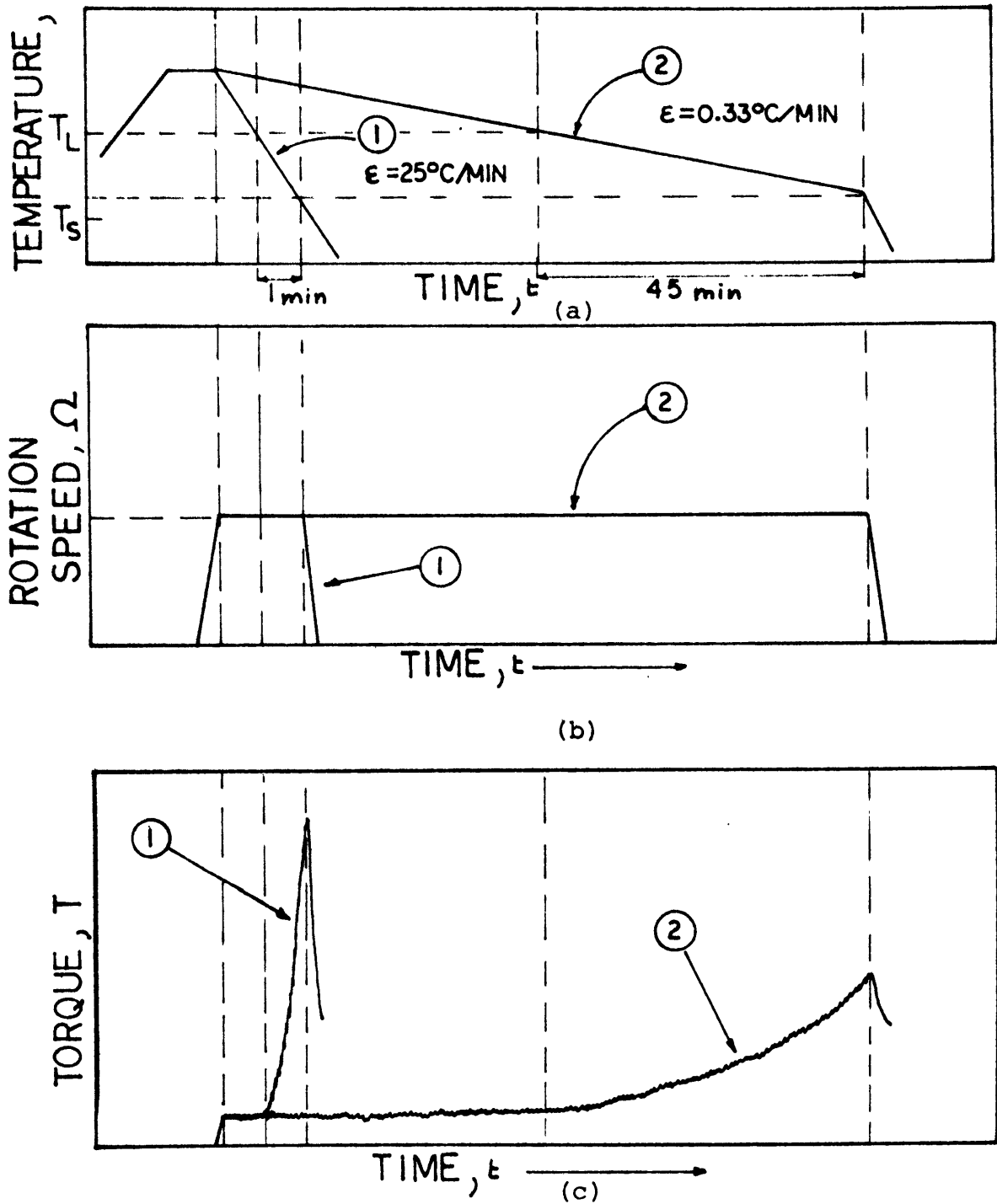
Figure 13. Procedure empoyed for continuously cooled Sn-15%Pb
slurries, showing (a) temperature versus time, (b)
rotation speed versus time and (c) the corresponding torque.
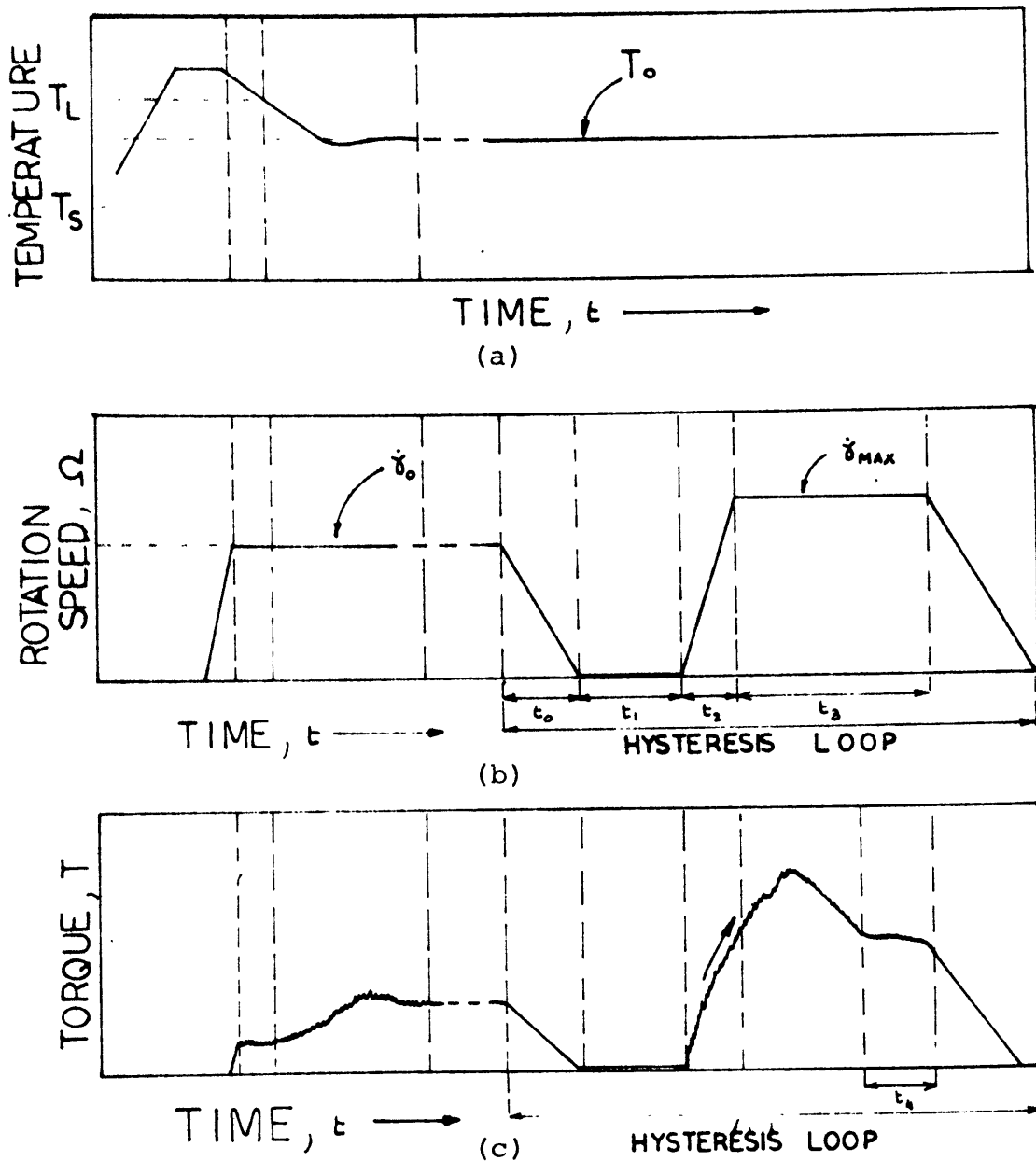
Figure 14. Procedure employed for isothermally held Sn-15%Pb
slurries, showing (a) temperature versus time, (b)
rotation speed cycles for a hysteresis loop and (c)
the corresponding torque.
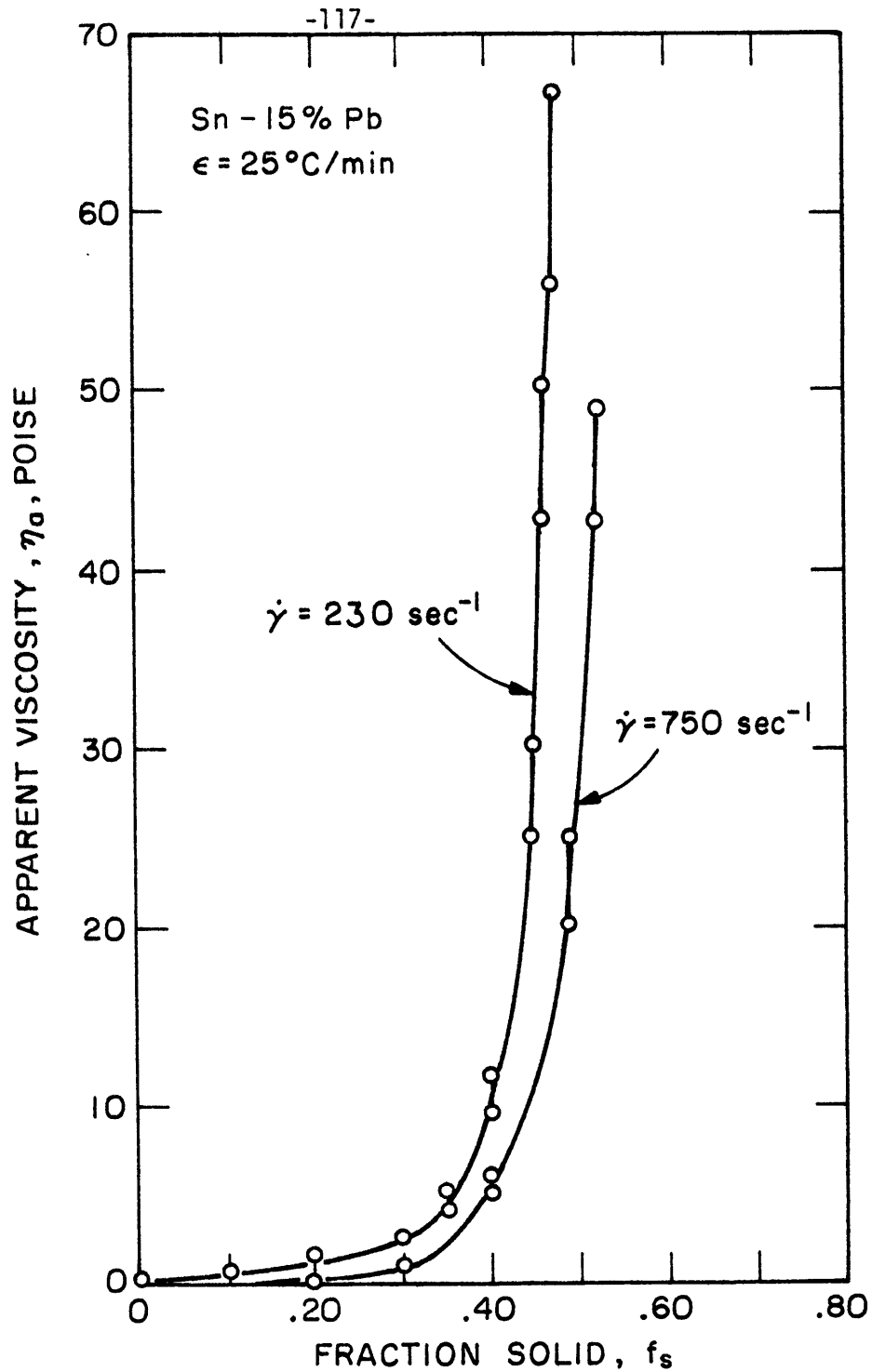
Figure 15. Effect of fraction solid on the apparent viscosity of a Sn-15%Pb slurry. Effect of two different shear rates, 230 and 750 sec^{-1}, at a high cooling rate 25°C/minute.
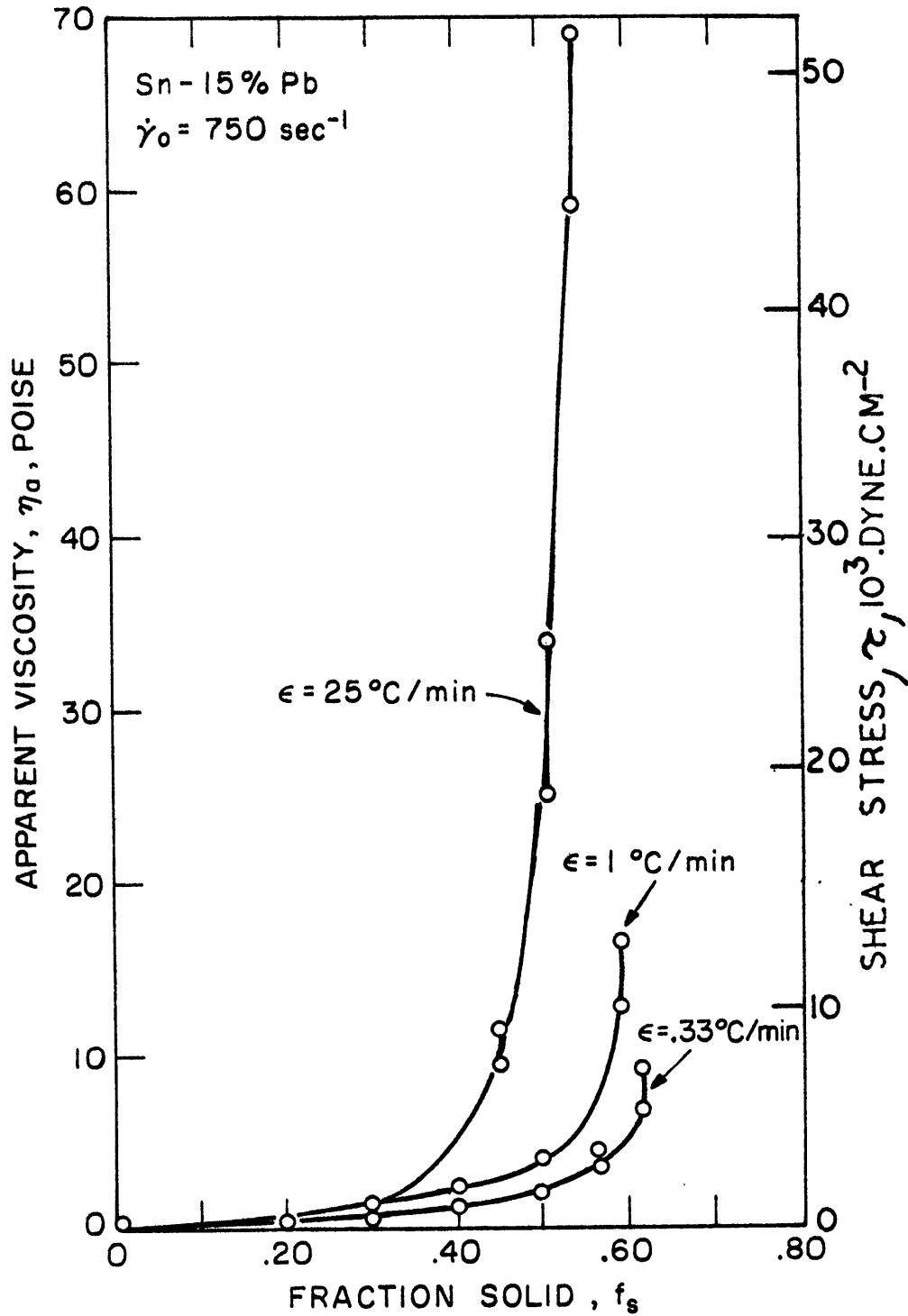
Figure 16. Effect of fraction solid on the apparent viscosity of a Sn-15%Pb slurry. Effect of three different cooling rates 25, 1.0 and 0.33°C/minute at a high shear rate of 750 sec^{-1}.
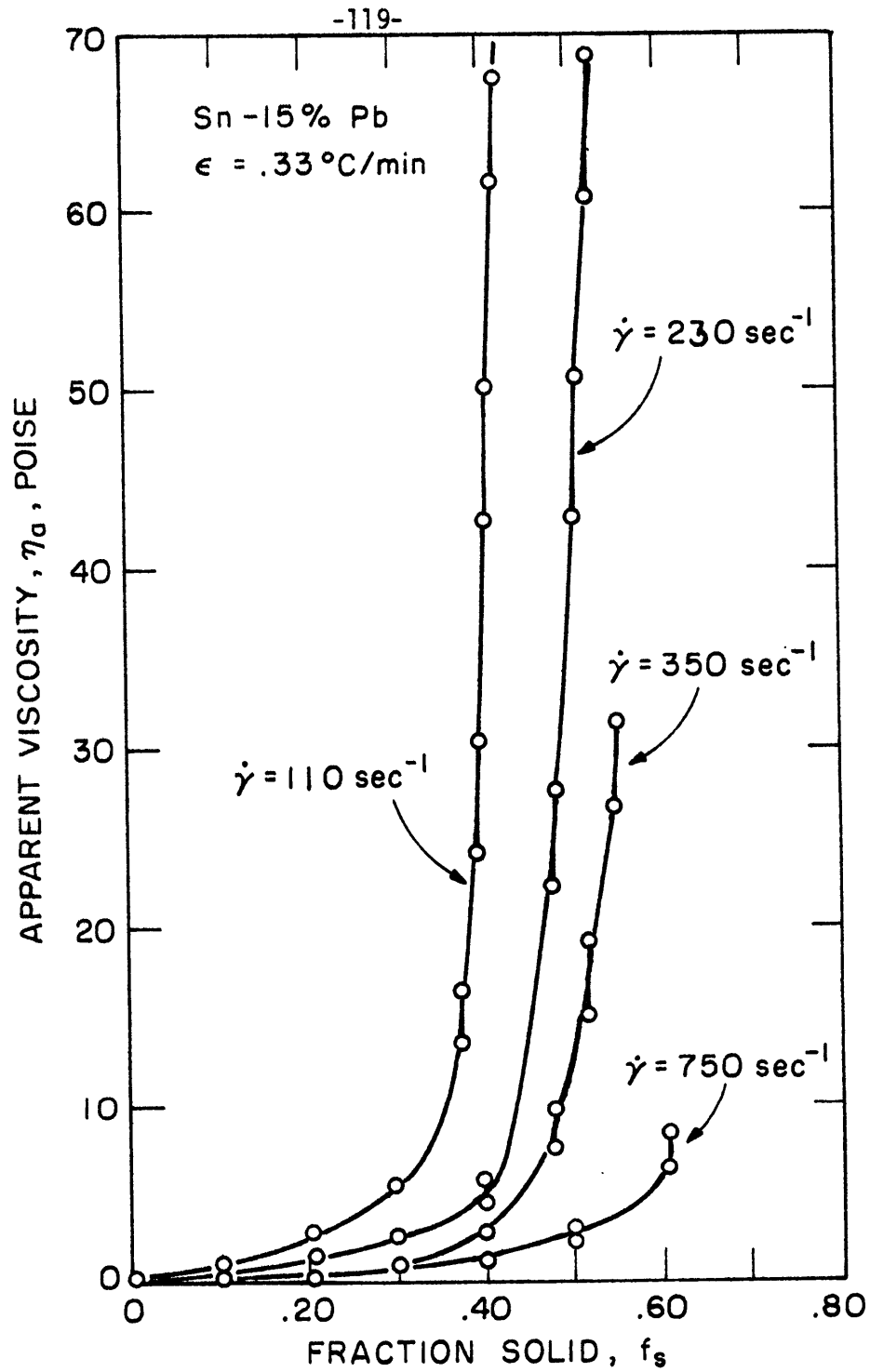
Figure 17. Effect of fraction solid on the apparent viscosity of a Sn-15%Pb slurry. Effect of four different shear rates; 115, 230, 350 and 750 sec⁻¹ at a slow cooling rate of 0.33°C/minute.
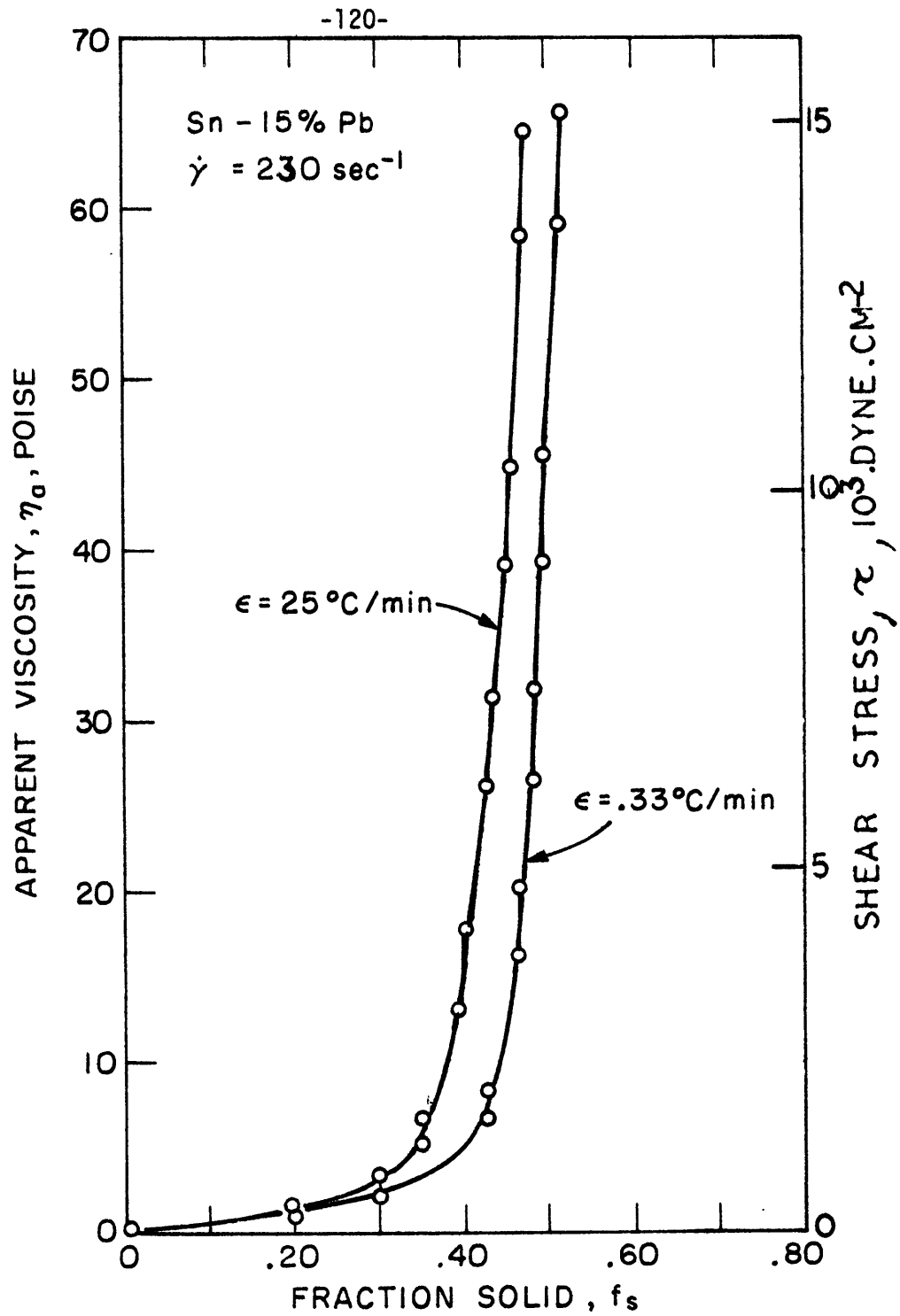
Figure 18. Effect of fraction solid on the apparent viscosity of a Sn-15%Pb slurry. Effect of three different cooling rates; 25, 1.0 and 0.33°C/minute at a slow shear rate of 230 sec^{-1}.
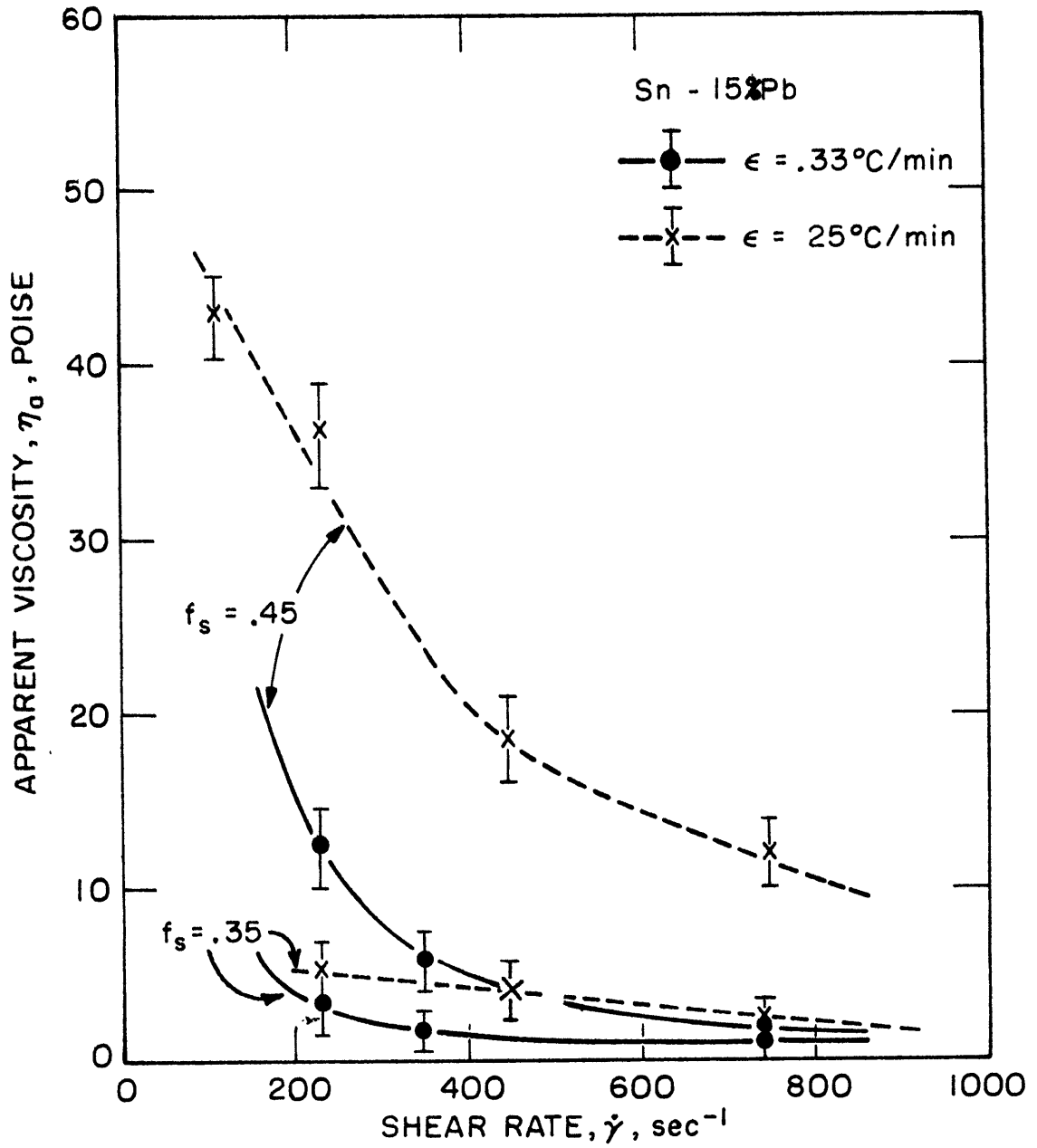
Figure 19. Effect of shear rate used during cooling of a Sn-15%Pb slurry on the apparent viscosity at two different fractions solid, 0.35 and 0.45 and for two different cooling rates of 25 and 0.33°C/minute.
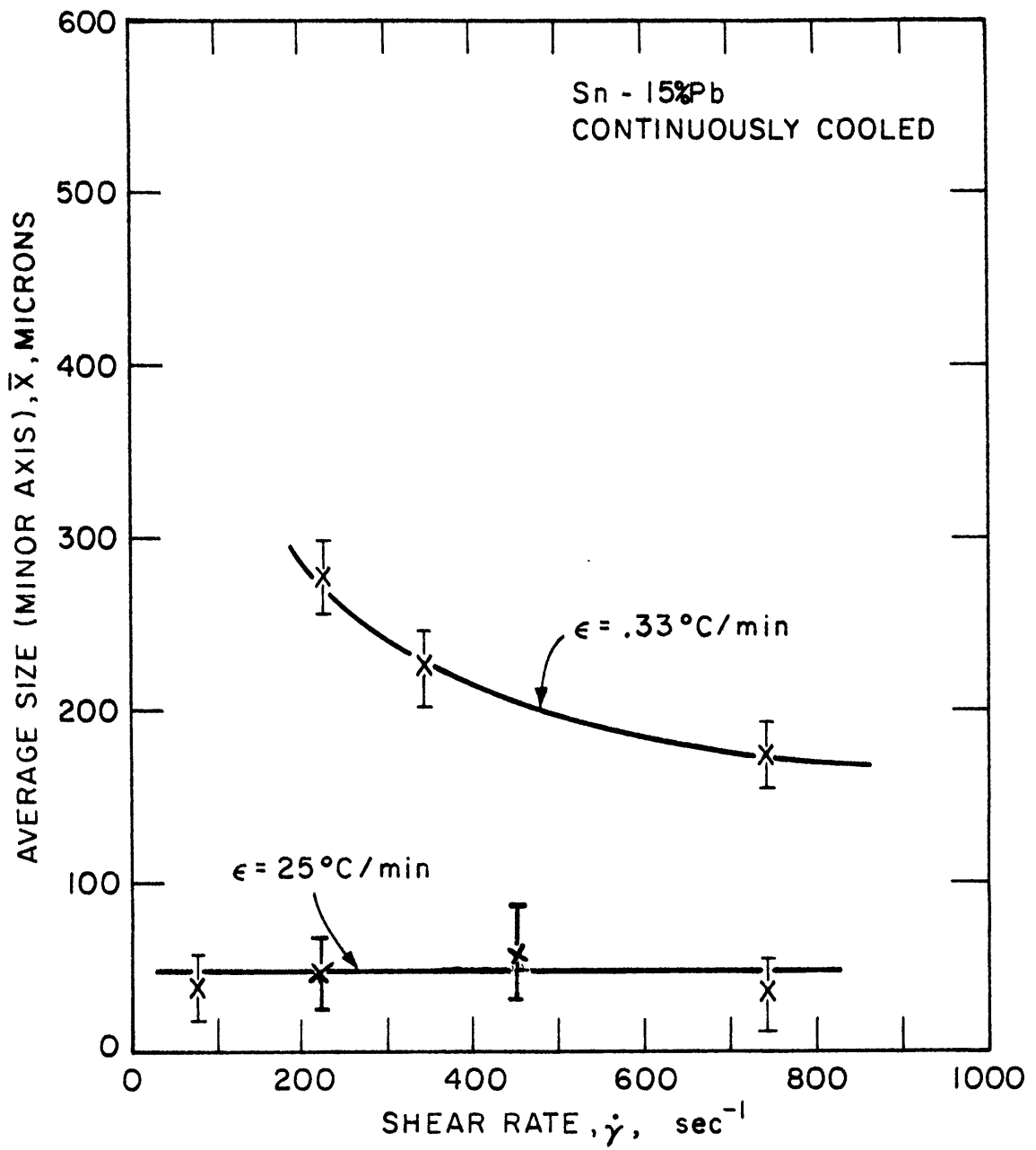
Figure 20. Effect of shear rate on the size of primary solid particles of Sn-15%Pb slurries at two different cooling rates of 25 and 0.33°C/minute.
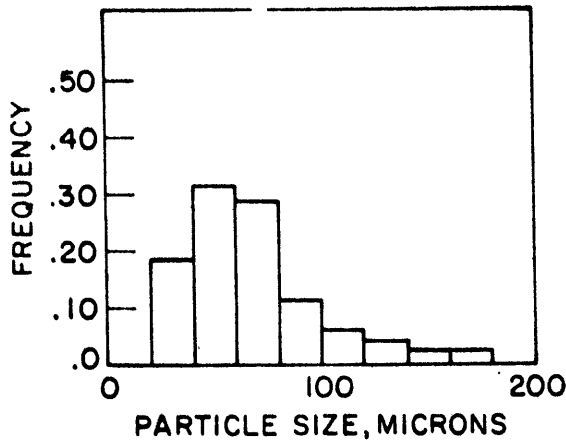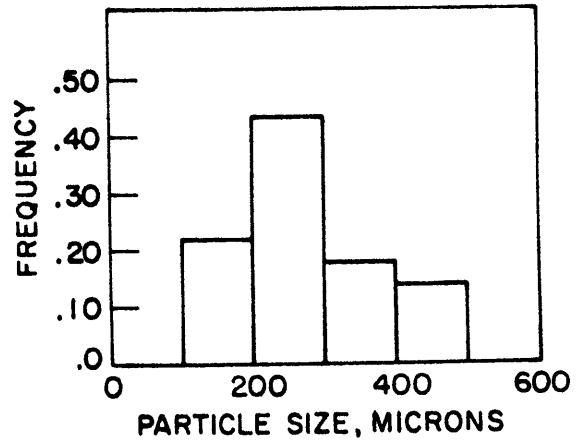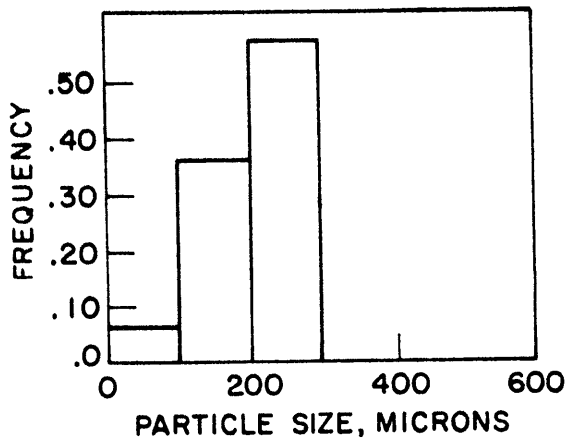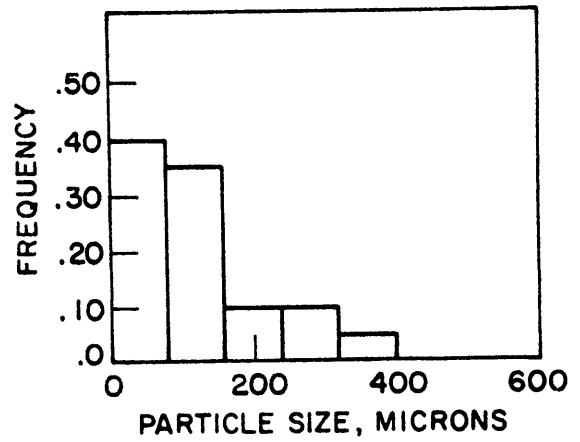
Figure 21. Distribution of size of primary solid particles
of continuously cooled slurries of Sn-15%Pb. Effect
of cooling rate, shear rate and fraction solid.
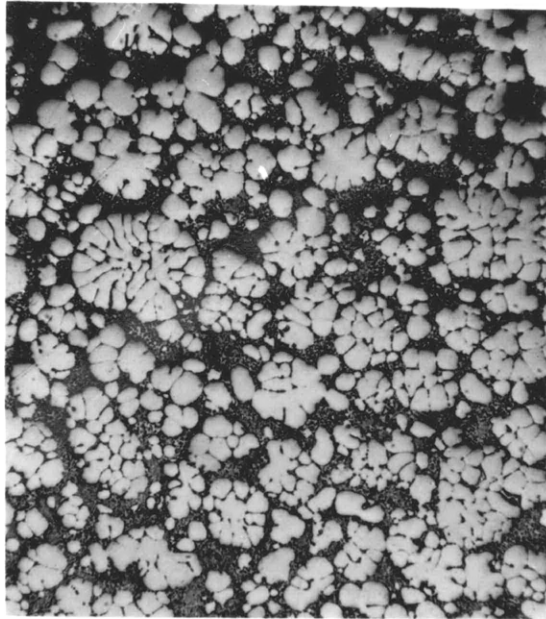
(a)
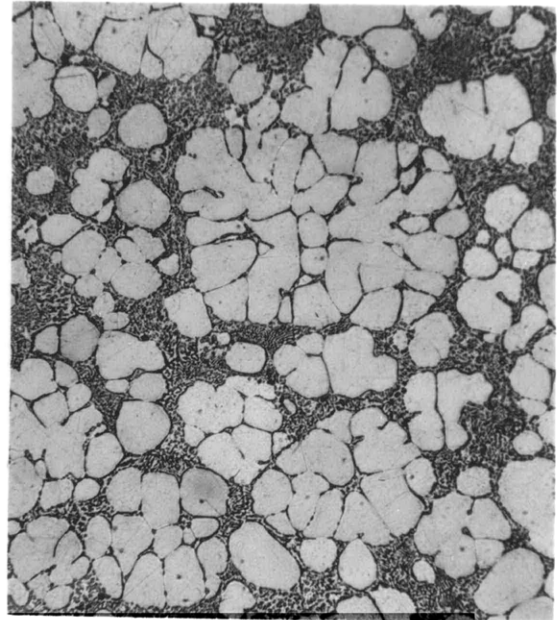
(b)
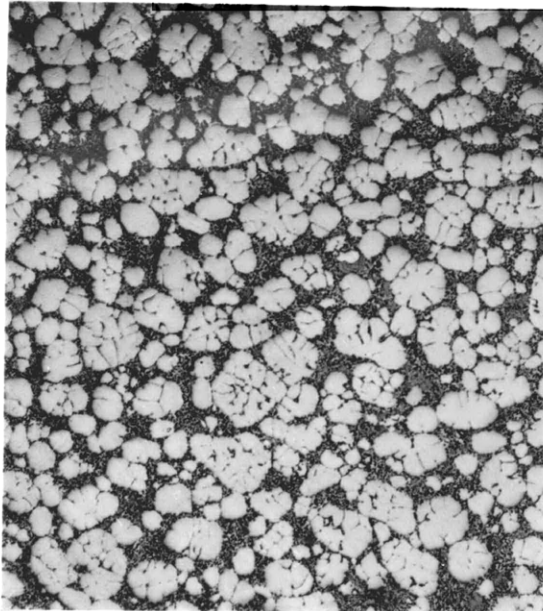
(c)
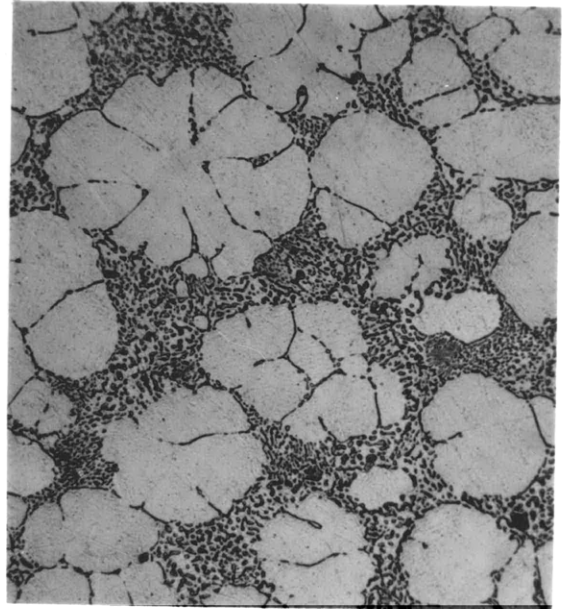
(d)

Figure 22.Microstructures of Sn-15%Pb slurries for a cooling rate of25°C/min
and a fraction solid of 0.55;(a) and (b) at a shear rate of 230
sec^{-1},at 50X and 100X respectively;(c) and (d) at a shear rate of
750sec^{-1},at 50X and 100X respectively.
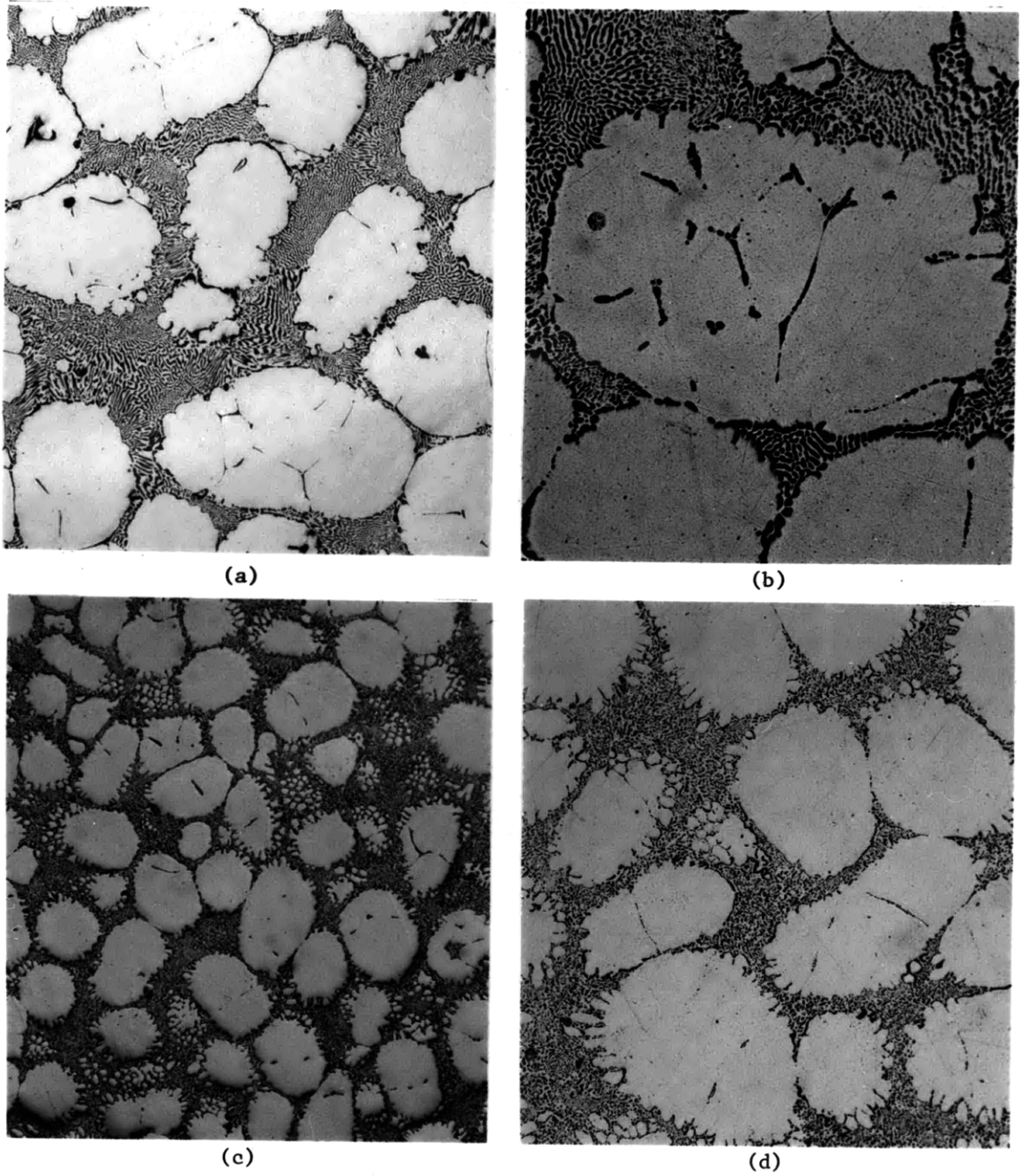
Figure 23.Microstructures of Sn-15%Pb slurries for a cooling rate of 0.33°C/min
and a fraction solid of 0.55;(a) and (b) at a shear rate of $230sec^{-1}$,
at 50X and 100X respectively;(c) and (d) at a shear rate of $750sec^{-1}$,
at 50X and 100X respectively.
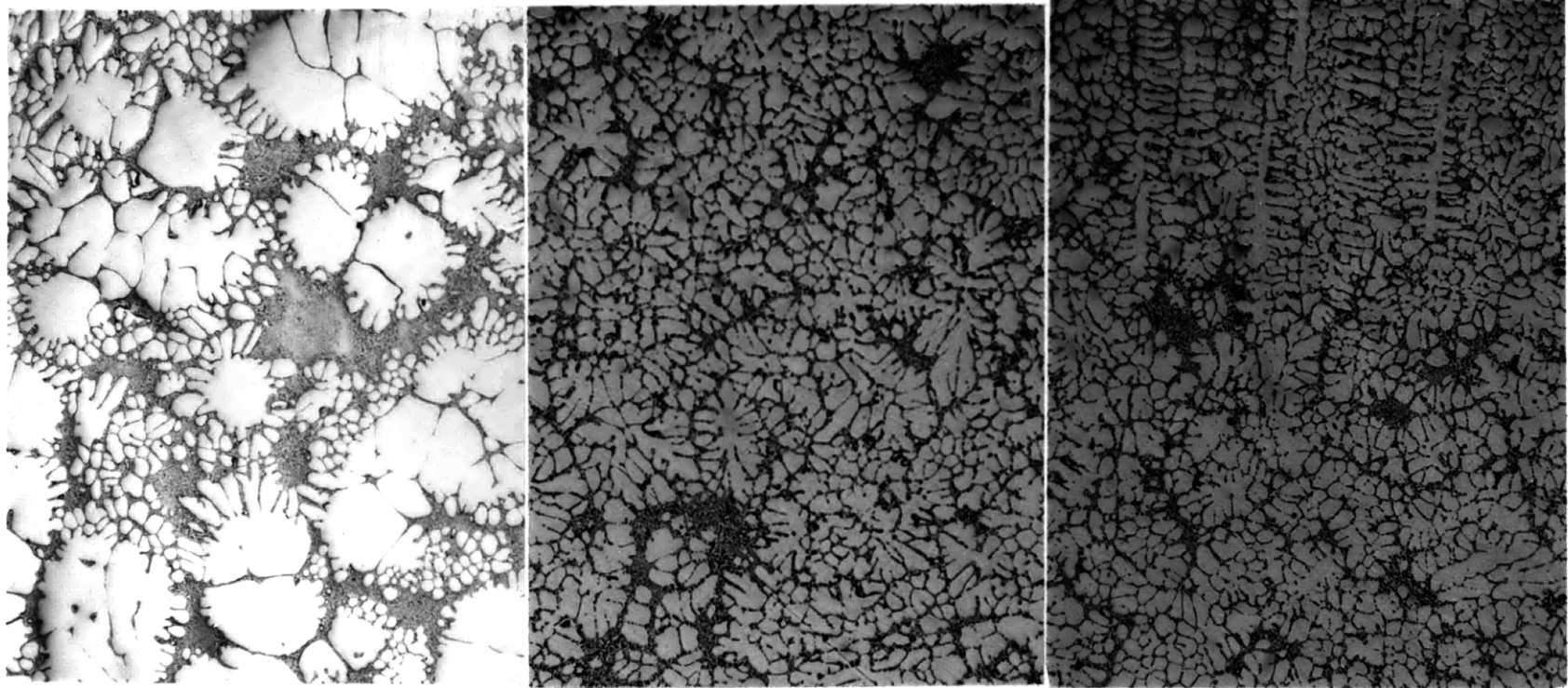
(a)   (b)   (c)

Figure 24.Microstructures of Sn-15%Pb slurries;(a) at a cooling rate of 0.33°C/min and
shear rate of 750sec^{-1} and fraction solid of 0.30;(b) and (c) at a cooling
rate of 25°C/min,shear rate of 230sec^{-1} and fraction solid of 0.25,away and
near the crucible wall,respectively;50X.
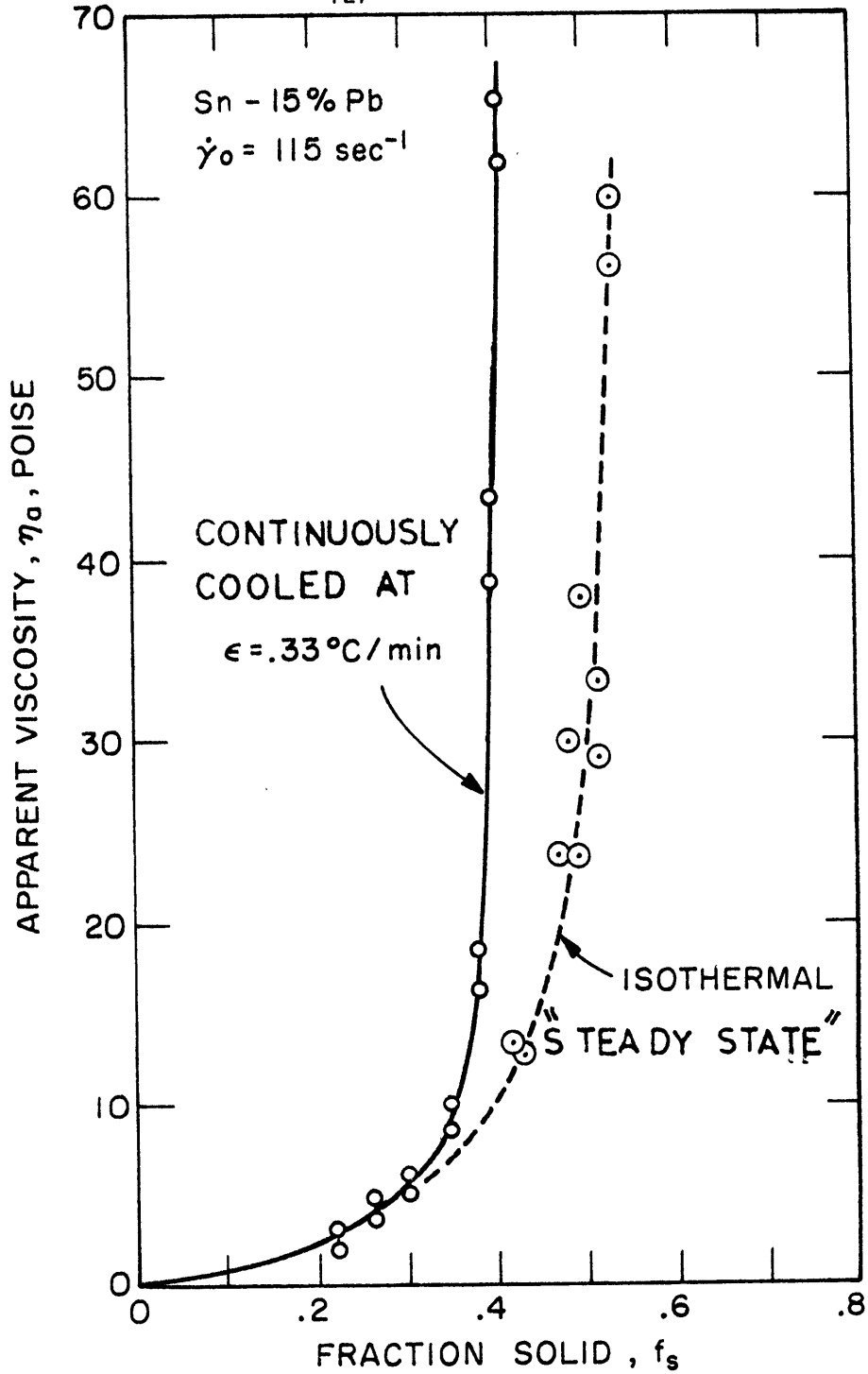
Figure 25. Comparison of the effect of fraction solid on the apparent viscosity of Sn-15%Pb slurries continuously cooled at 0.33°C/minute and isothermally held at different fractions solid; shear rate of 115 sec^{-1}.
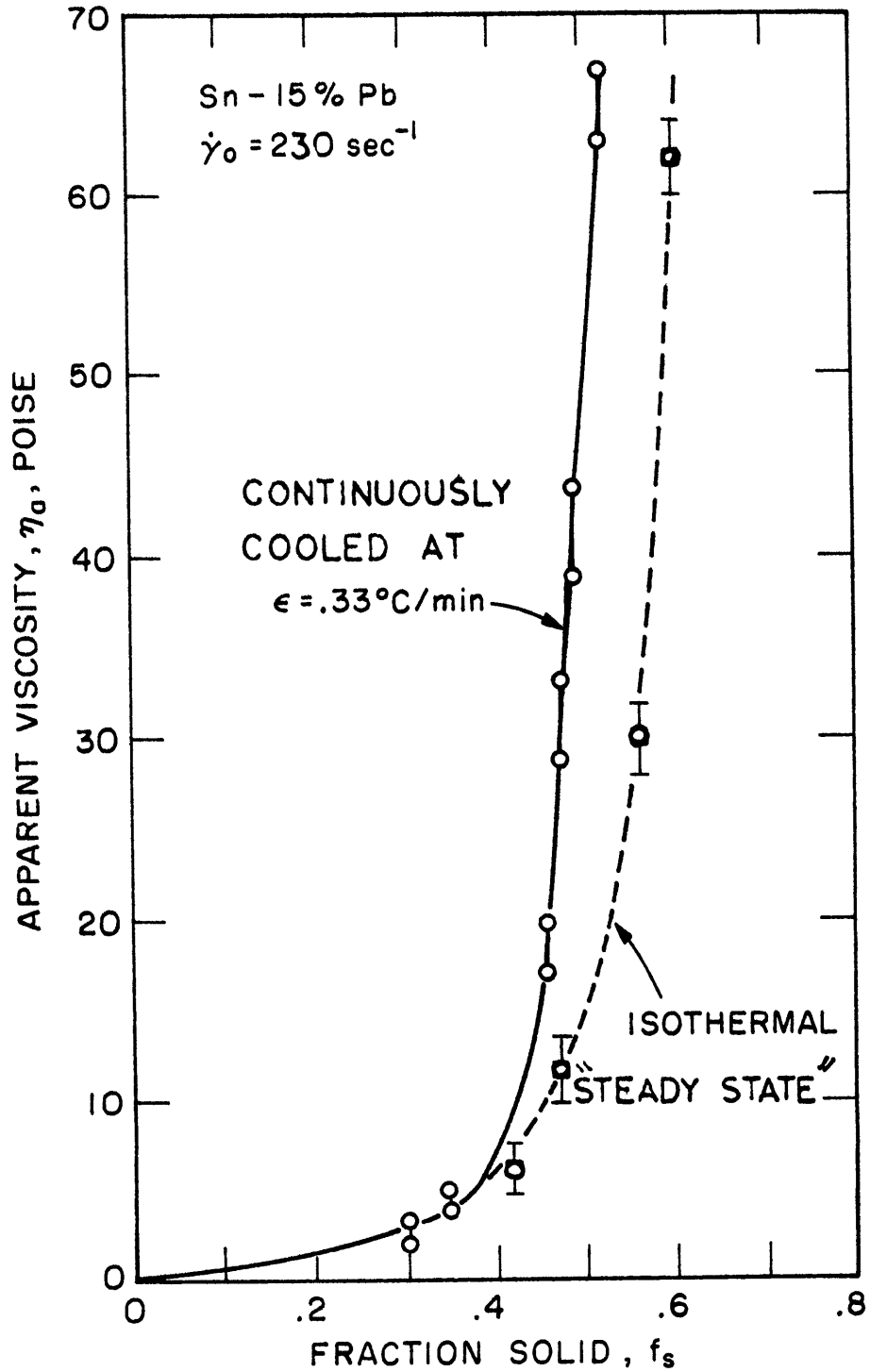
Figure 26. Comparison of the effect of fraction solid on the apparent viscosity of Sn-15%Pb slurries continuously cooled at 0.33°C/minute and isothermally held at different fractions solid; shear rate of 230 sec⁻¹.
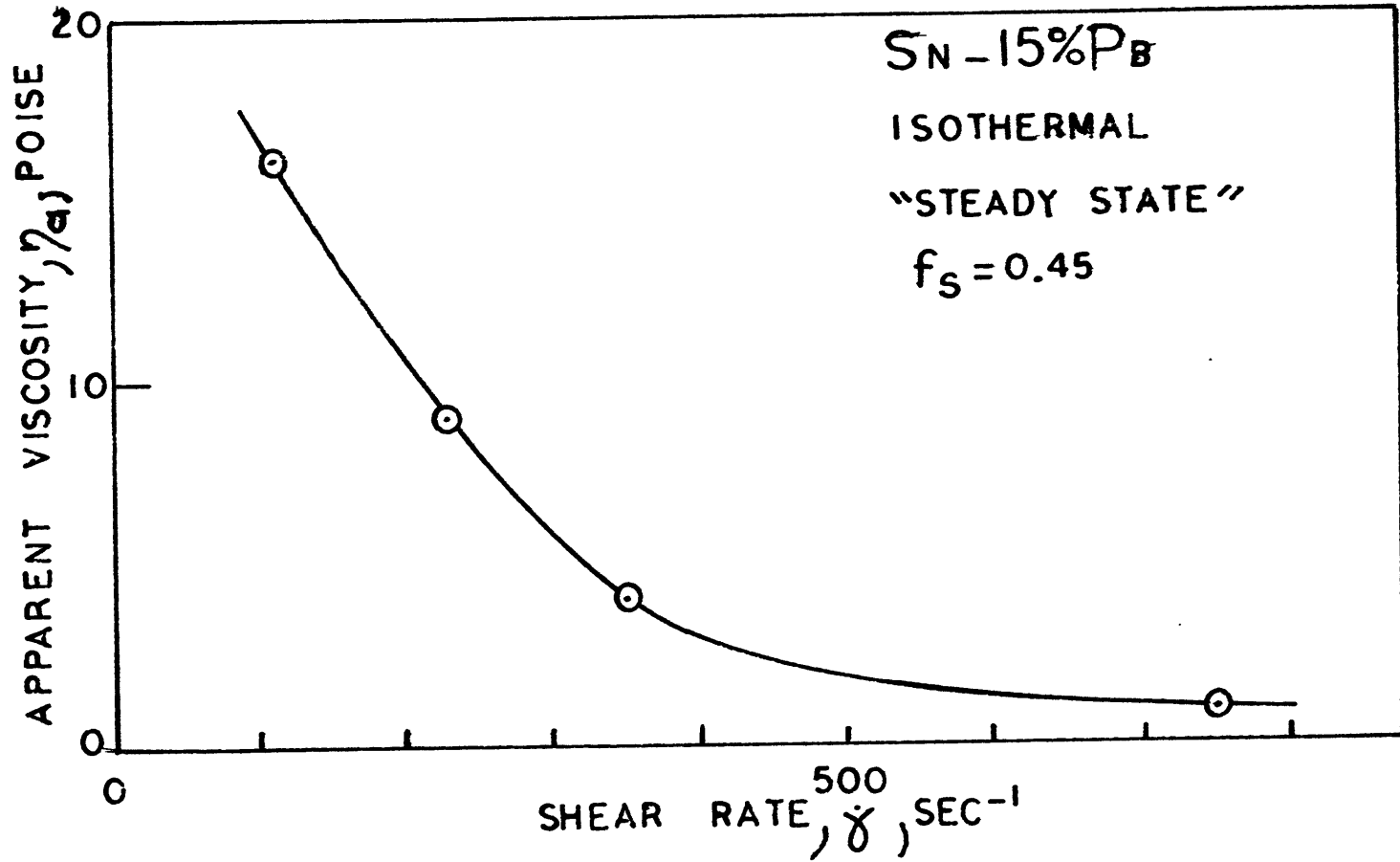
Figure 27. Effect of shear rate on the apparent viscosity of Sn-15%Pb slurries held isothermally at a fraction solid of 0.45; total time spent in the liquid-solid range of 90 minutes.
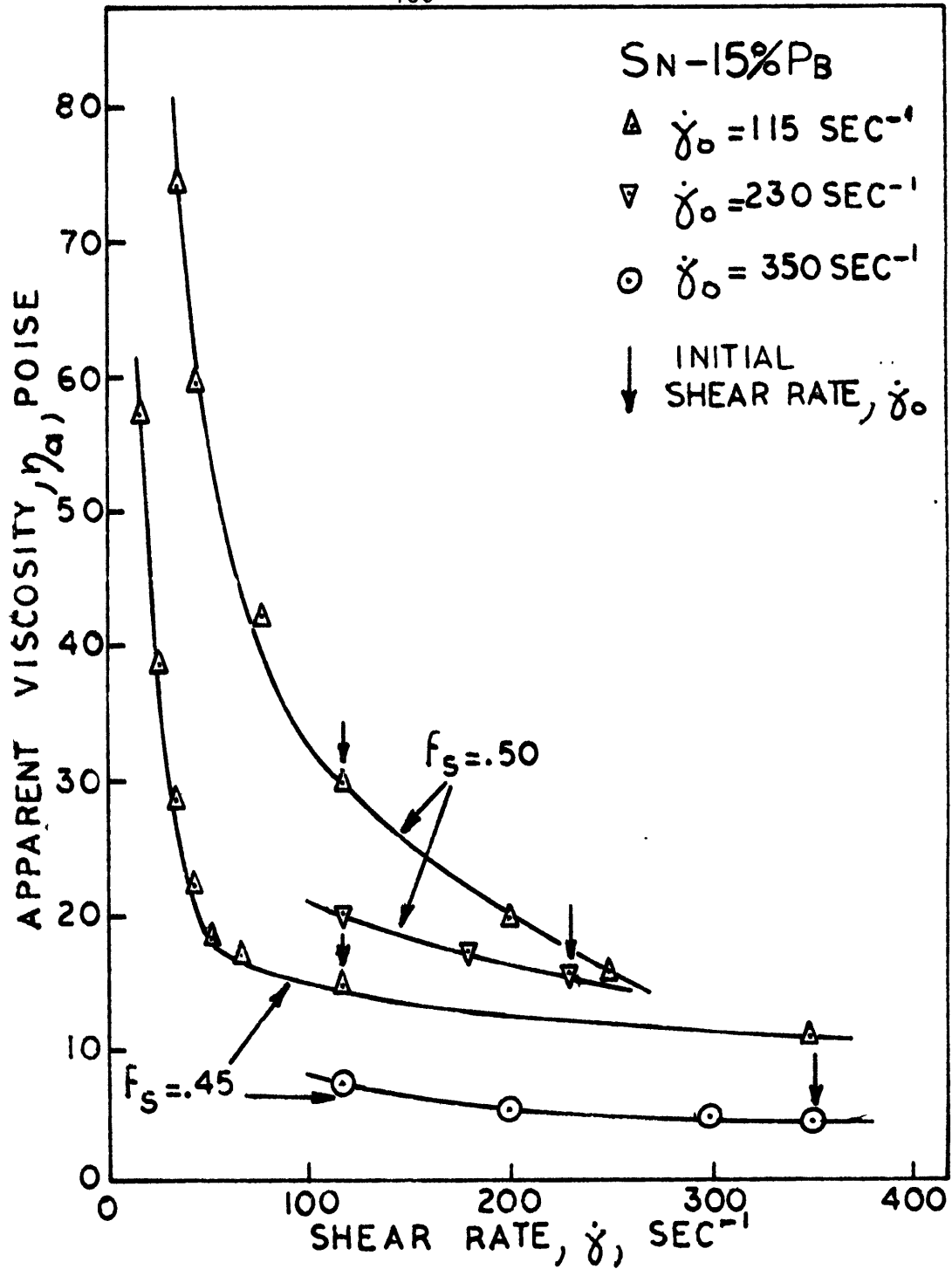
Figure 28. Effect of change of shear rate on the apparent viscosity of Sn-15%Pb slurries held isothermally at fractions solid of 0.50 and 0.45 after a total time of 90 minutes in the liquid-solid range.
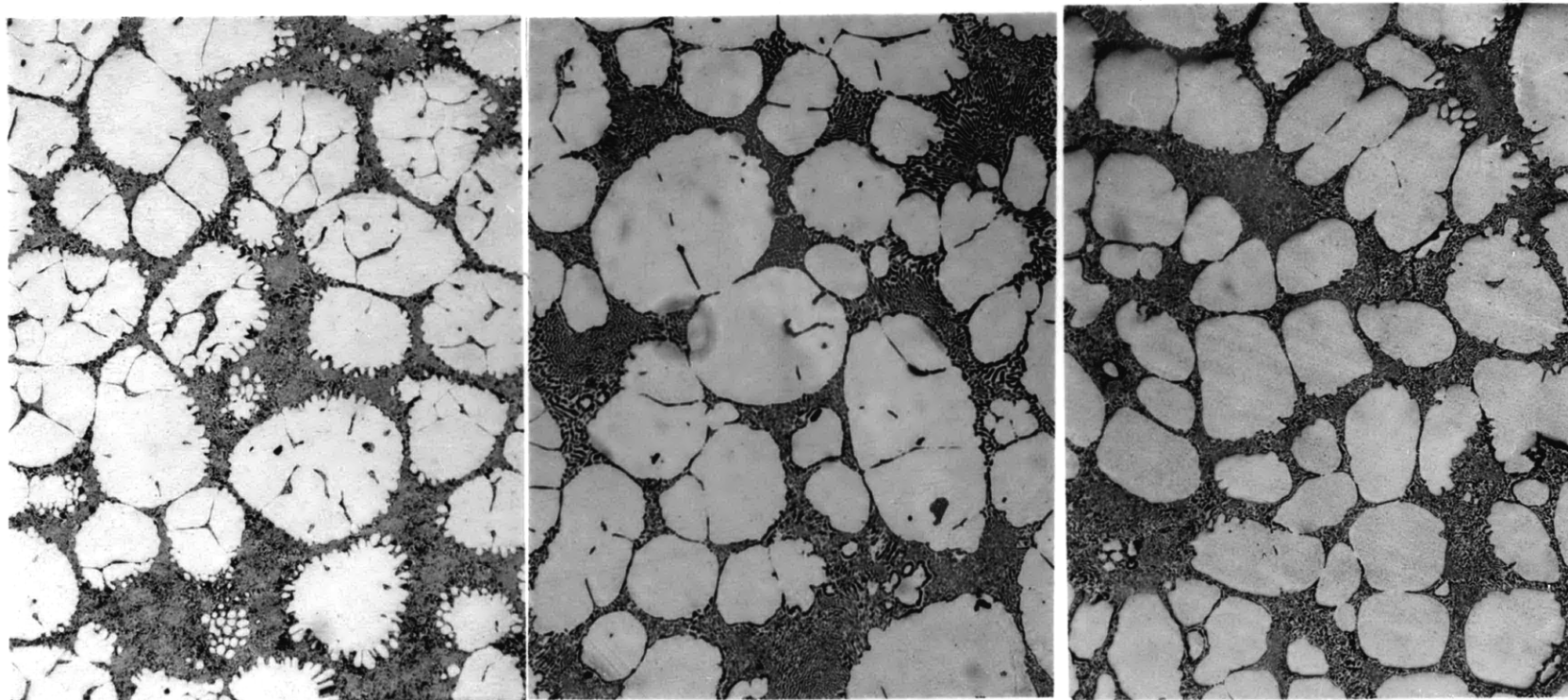
(a)   (b)   (c)

Figure 29.Effect of total time in the liquid-solid range on the microstructures of
Sn-15%Pb slurries at a shear rate of $230sec^{-1}$ and fraction solid of 0.45;
total time of (a) 13min,(b) 40min and (c) 90min;50X.
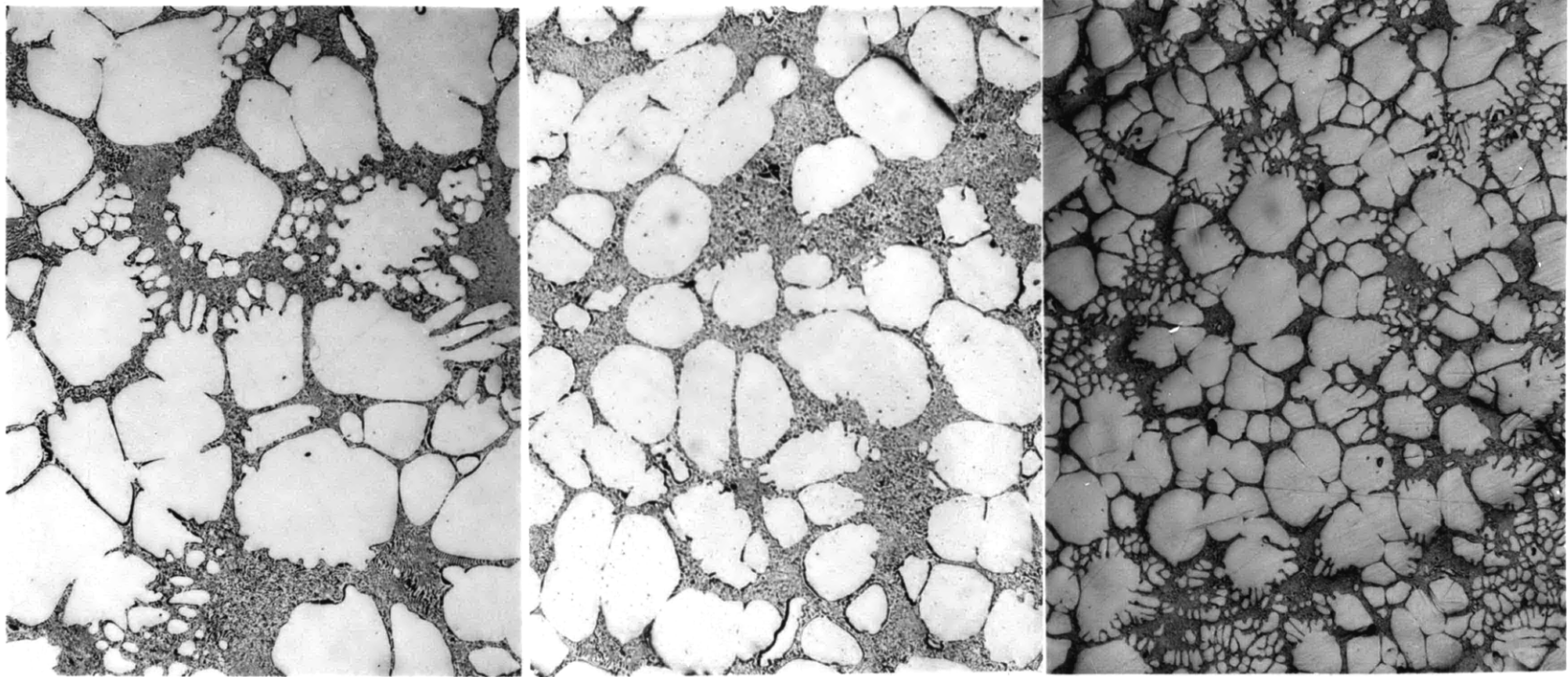
(a)   (b)   (c)

Figure 30. Effect of initial shear rate on the microstructures of Sn-15%Pb slurries after 90 minutes in the liquid-solid range at a fraction solid of 0.45; initial shear rate of (a) $115sec^{-1}$, (b) $230sec^{-1}$ and (c) $750sec^{-1}$; 50X.
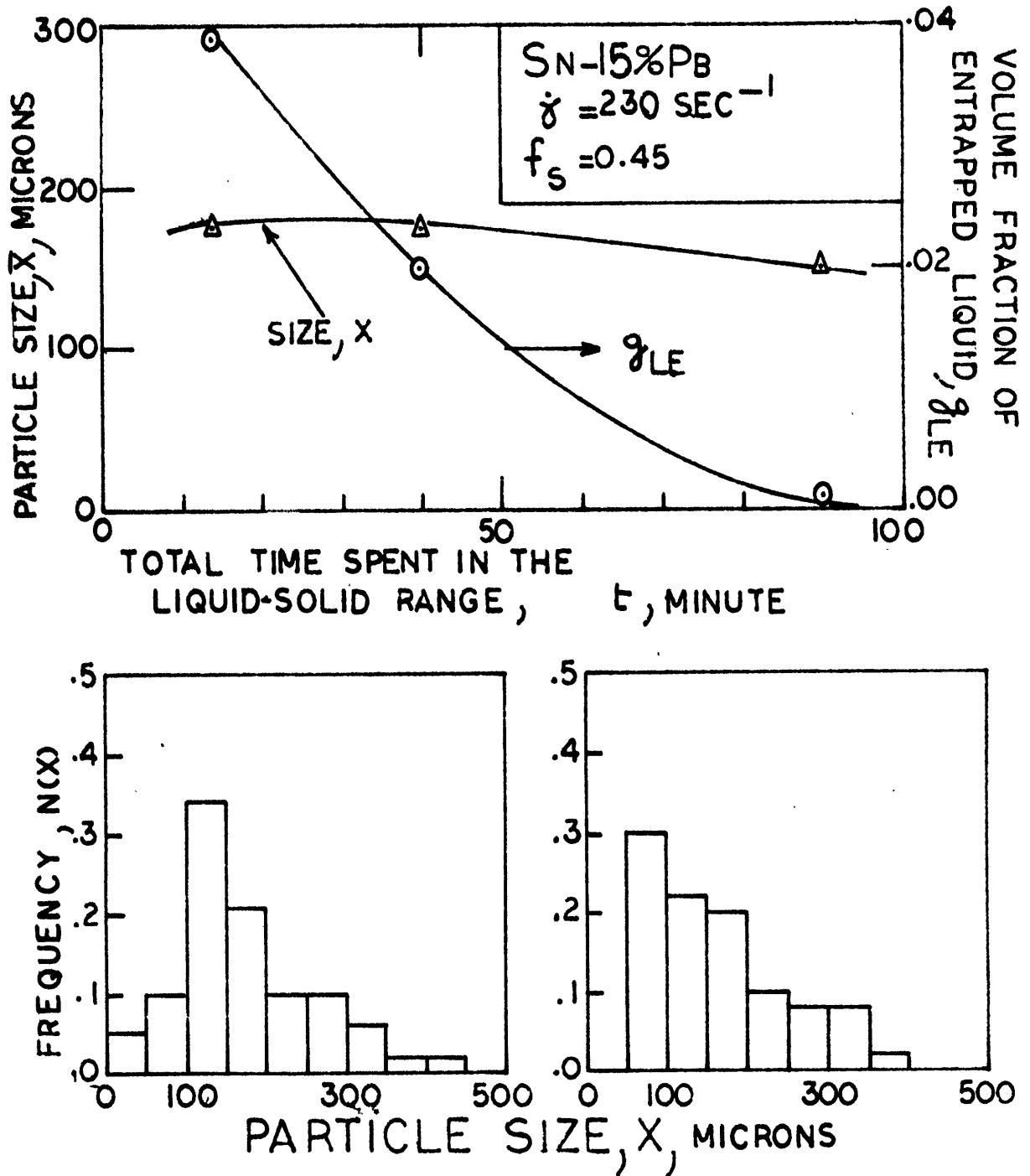
Figure 31. Effect of total time spent in the liquid-solid range on the size, distribution of size and volume fraction of entrapped liquid in primary solid particles of Sn-15%Pb slurries at 230 sec⁻¹ and fraction solid of 0.45. (a) size and entrapped liquid, (b) and (c) distributions of size for total times of 40 minutes and 90 minutes, respectively.
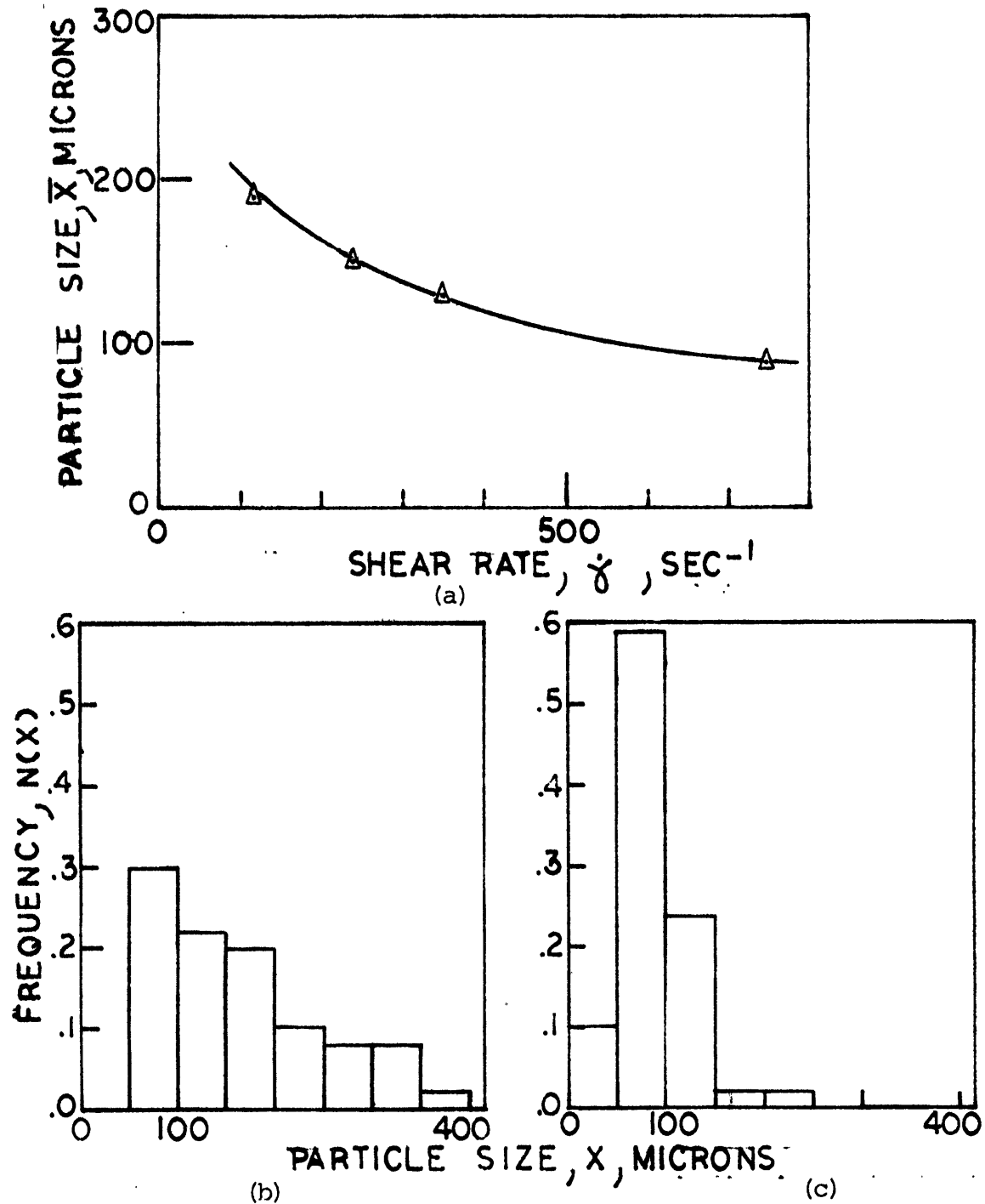
Figure 32. Effect of shear rate on the size and the distribution of size of primary solid particles of Sn-15%Pb slurries held isothermally at a fraction solid of 0.45 after 90 minutes in the solid-liquid range: (a) size, (b) and (c) distributions of size at 230 and 750 sec^{-1}, respectively.
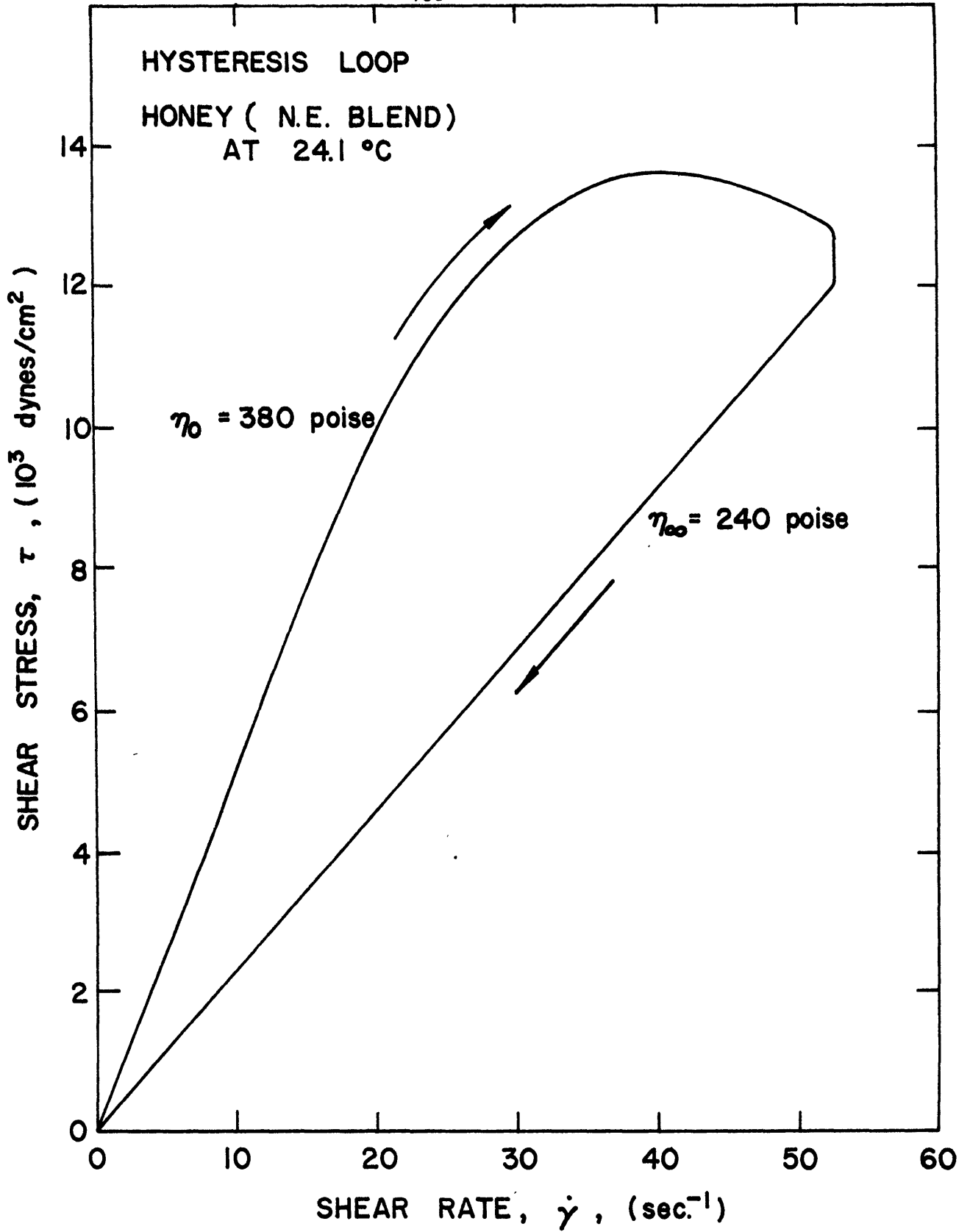
Figure 33. Measured hysteresis loop of New England honey at 24.1°C.
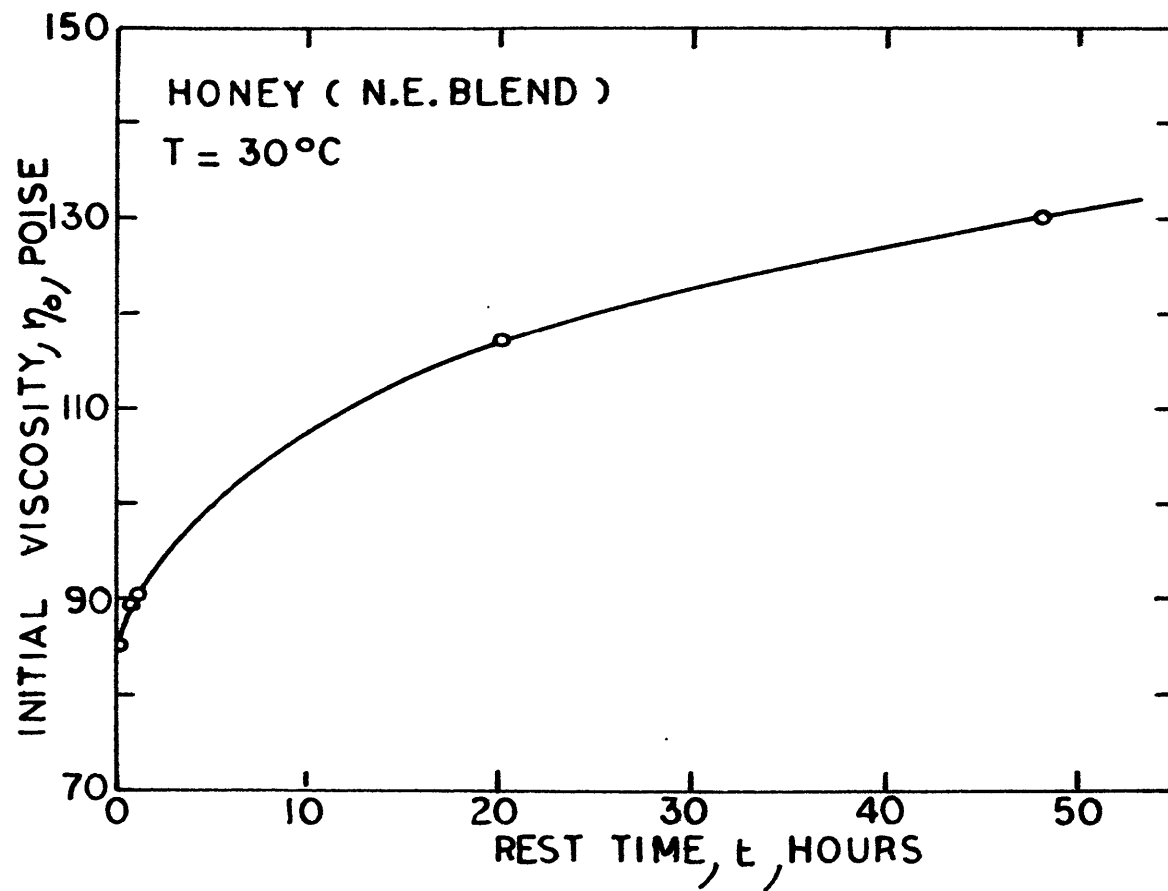
Figure 34.   Effect of rest time on the initial viscosity of honey at 30°C.
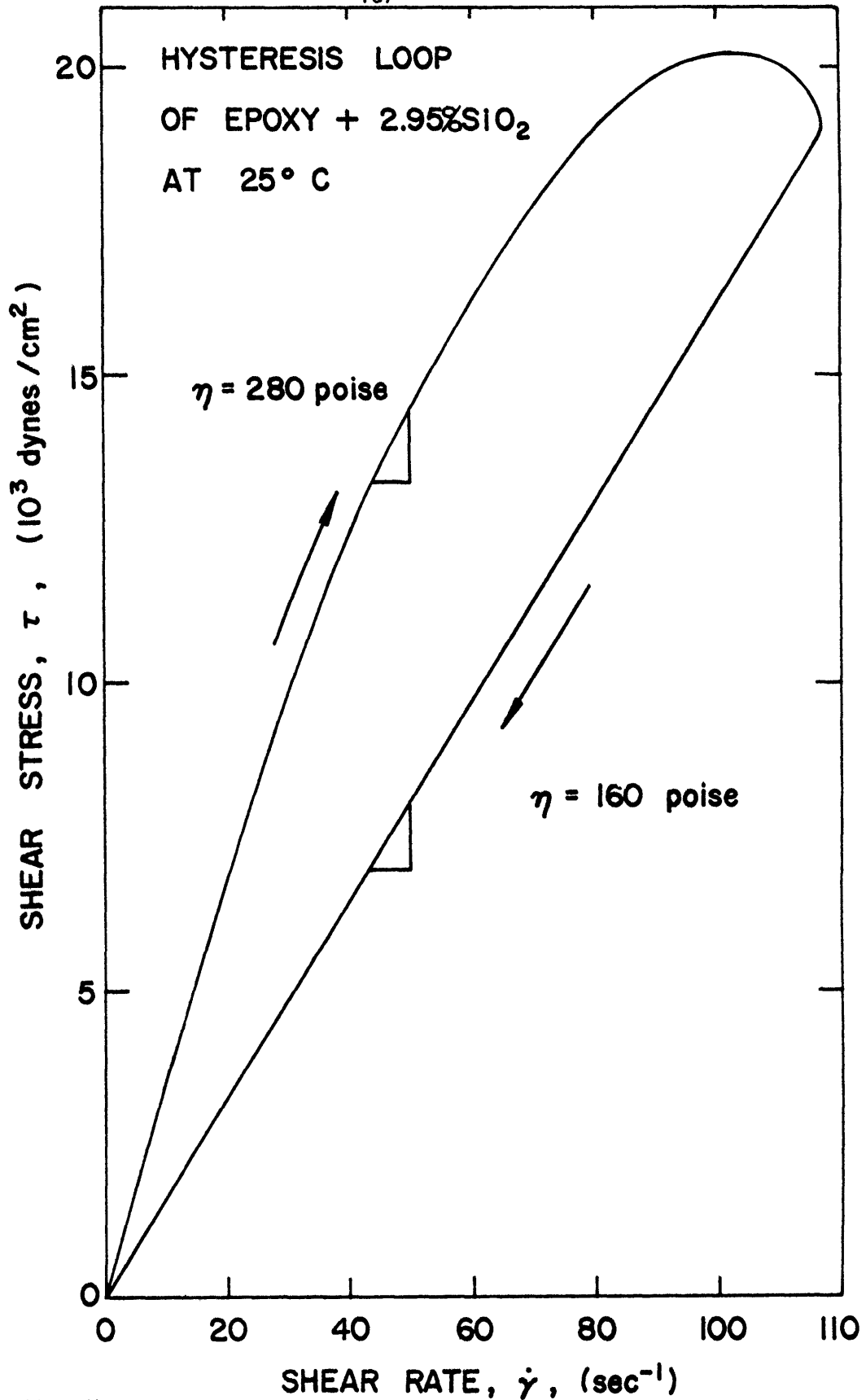
Figure 35. Measured hysteresis loop of a mixture of epoxy and 2.95% SiO$_2$ at 25°C.
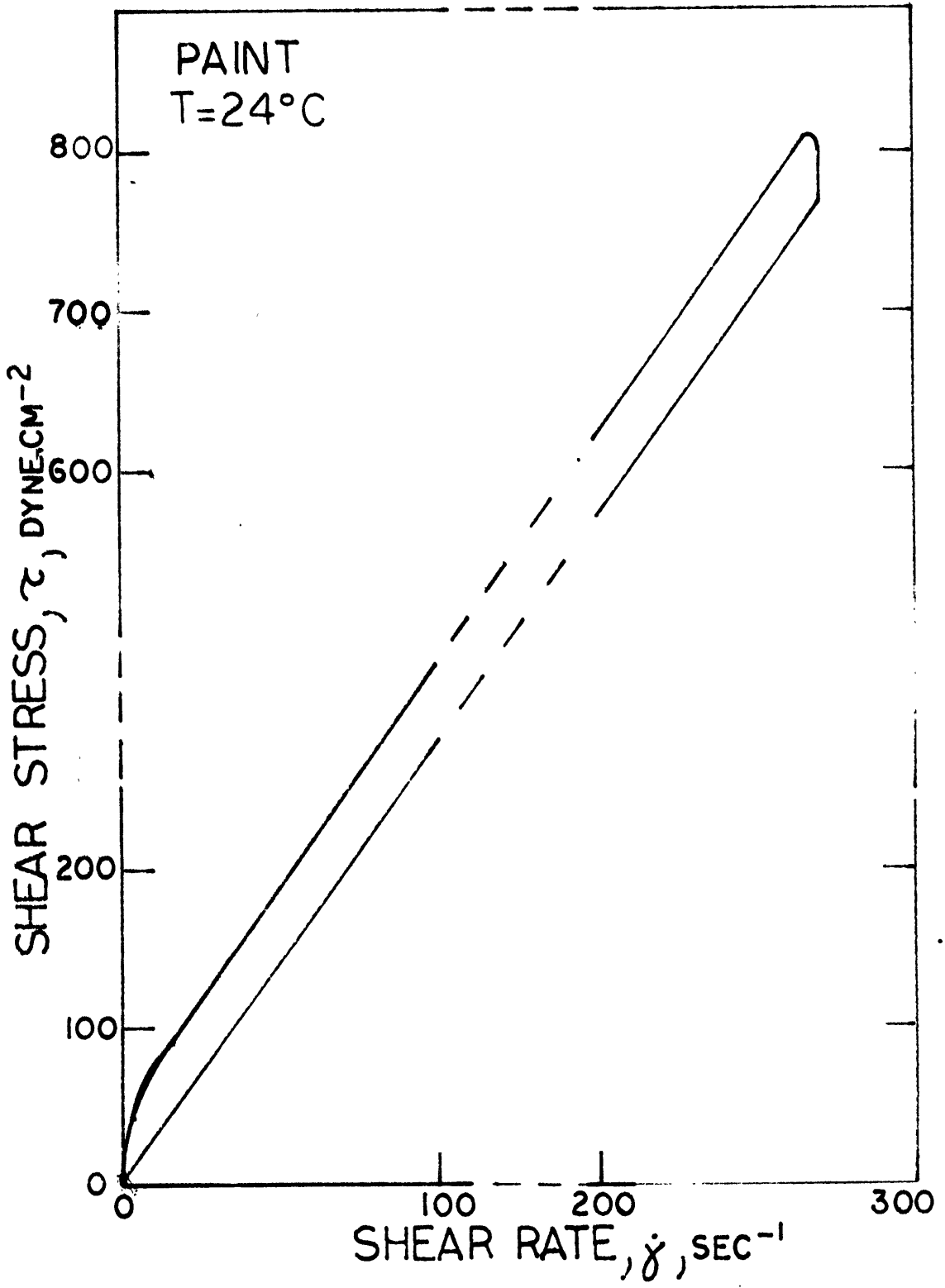
Figure 36.   Measured hysteresis loop of a paint at 24°C.
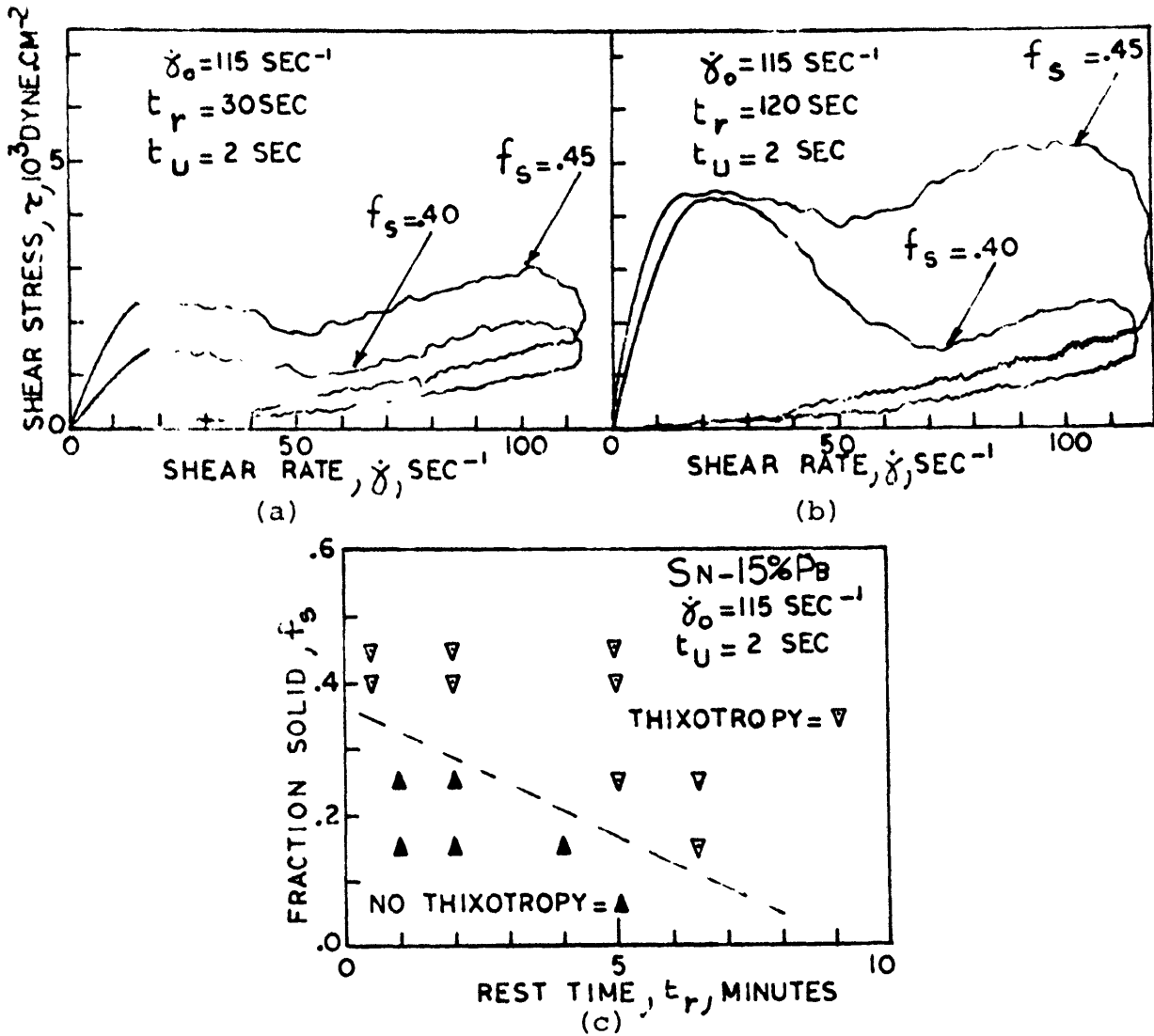
Figure 37. Effect of fraction solid on hysteresis loops of isothermally held slurries of Sn-15%Pb alloy, sheared at 115 sec^{-1}, at 0.40 and 0.45 fraction solid; (a) and (b) loops for 30 sec and 2 min at rest, respectively; (c) thixotropy as a function of fraction solid and time at rest.
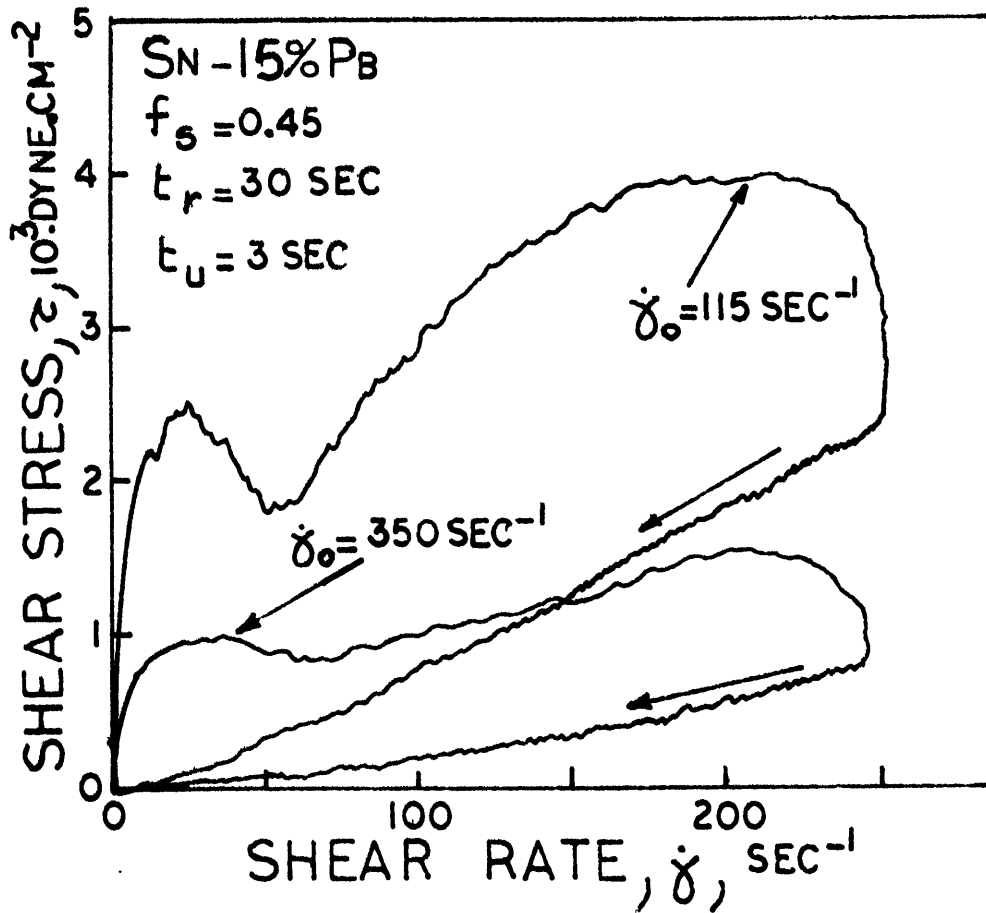
Figure 38. Effect of initial shear rate, $\dot{\gamma}_0$, 115 and 350 sec^{-1}, on hysteresis loops of Sn-15%Pb slurries held at a fraction solid of .45; rest time of 30 seconds.
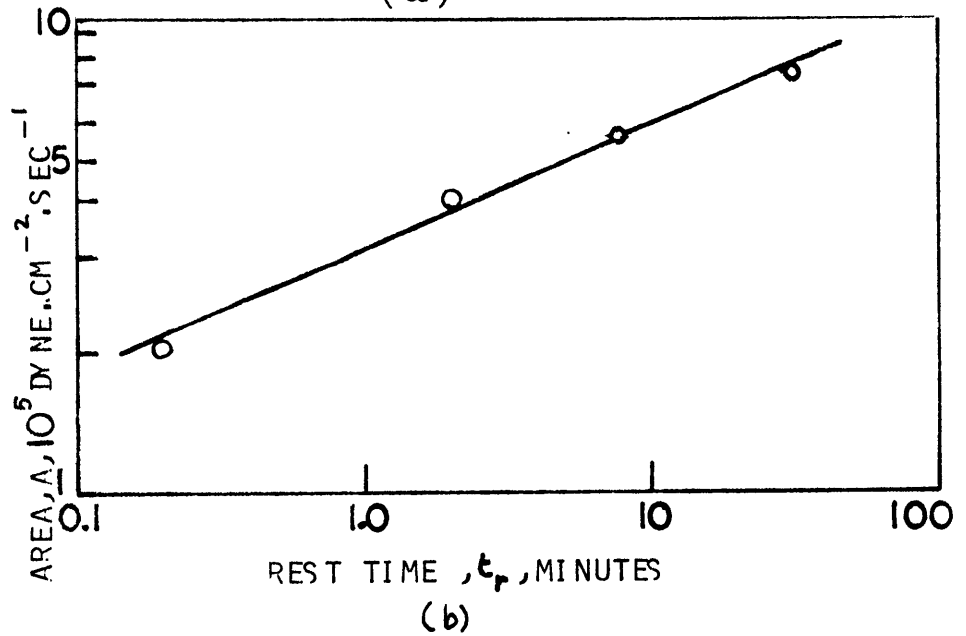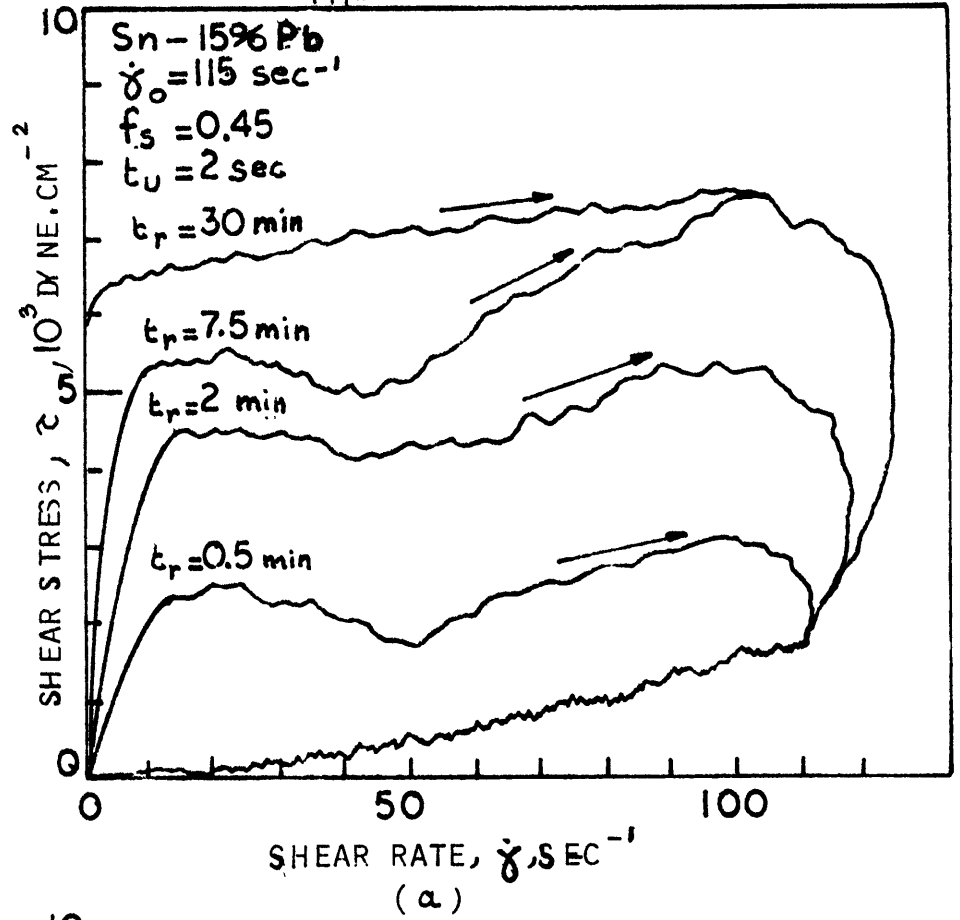
Figure 39. Effect of rest time on hysteresis loops of Sn-15%Pb slurries held at 0.45 fraction solid initially sheared at 115 sec^{-1}; (a) hysteresis loops, (b) areas of hysteresis loop versus rest time.
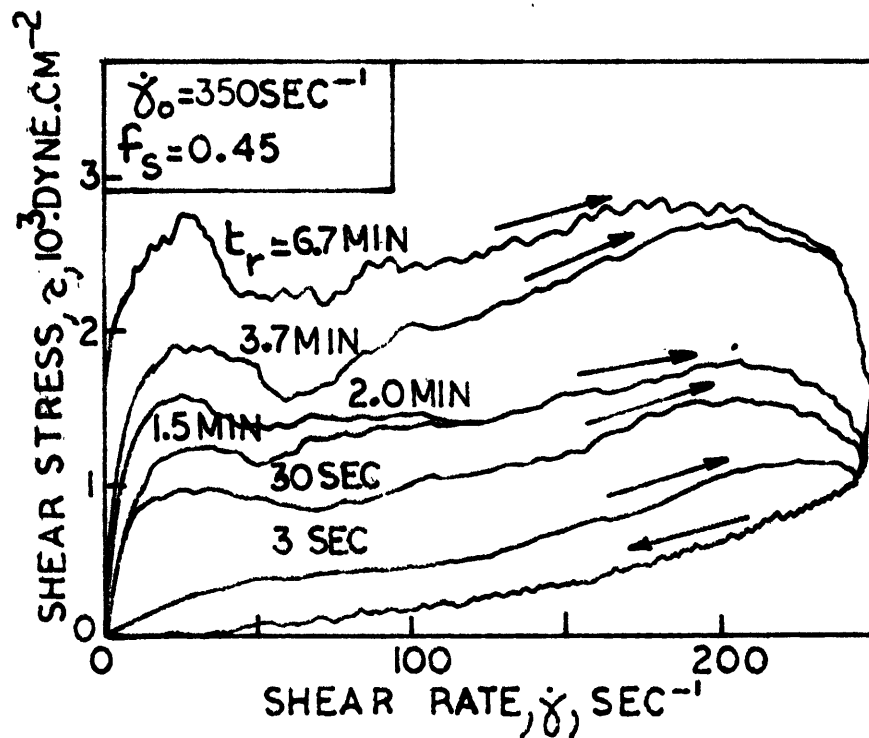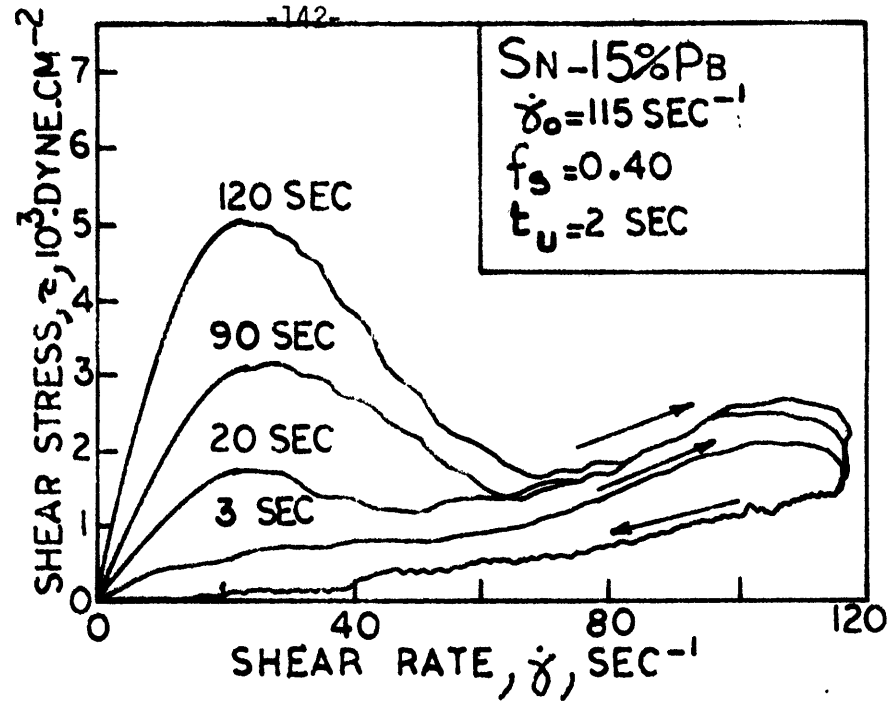
Figure 39 (cont'd). Effect of rest time on hysteresis loops of Sn-15%Pb slurries (c) initial shear rate of 115 sec⁻¹ and fraction solid of 0.40, (d) initial shear rate of 350 sec⁻¹ and fraction solid of 0.45.
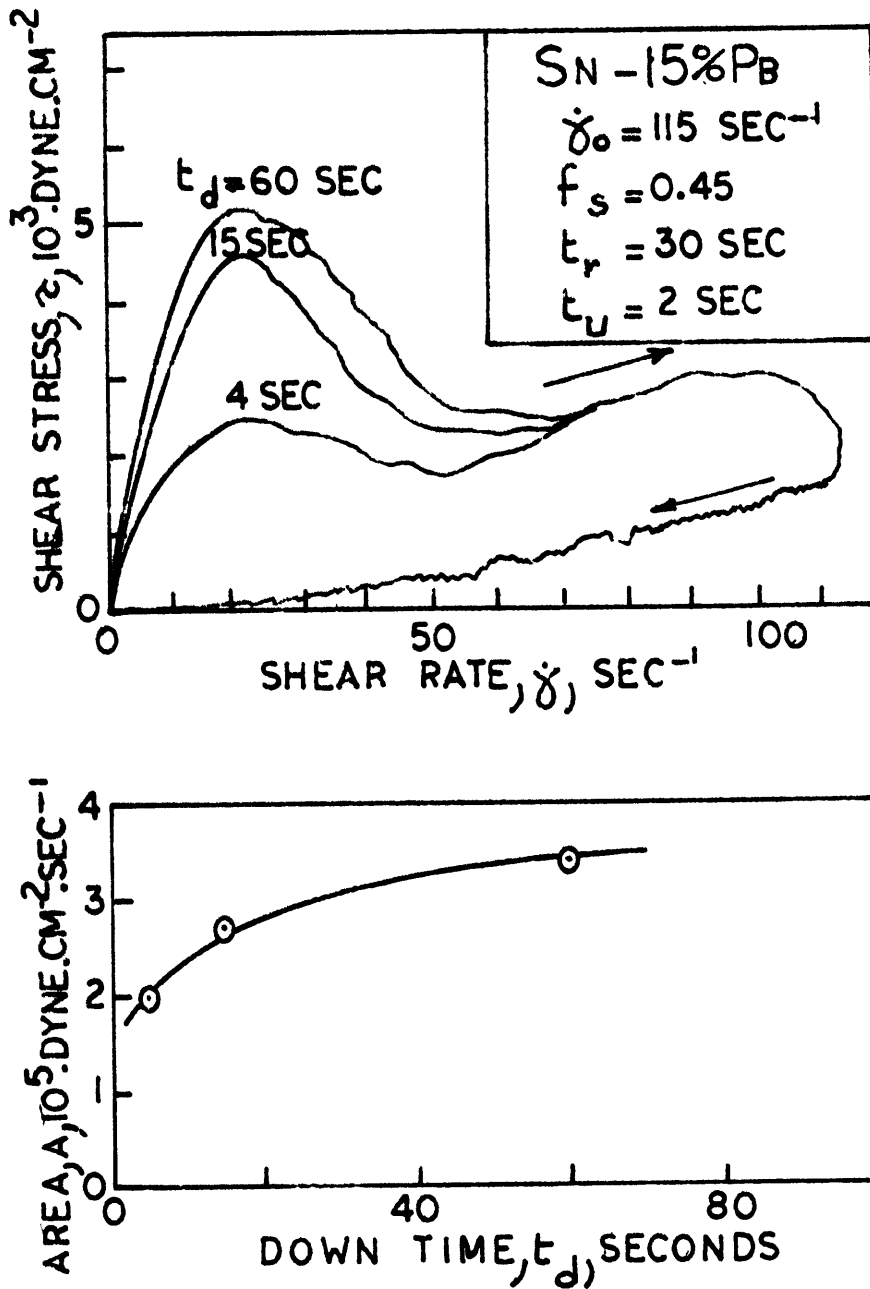
Figure 40. <u>Effect of down-time on hysteresis loops</u> of Sn-15%Pb slurries (a) loops, (b) area versus down-time for an initial shear rate of 115 sec^{-1} and rest time of 30 seconds.
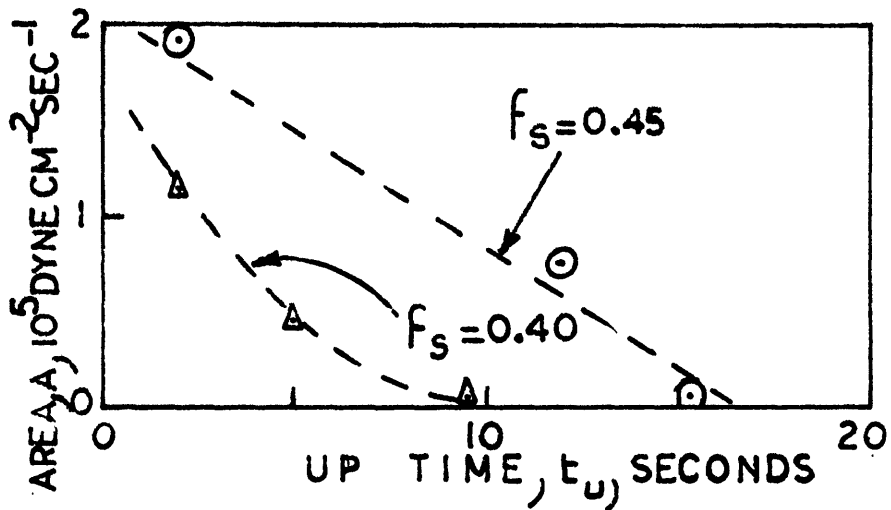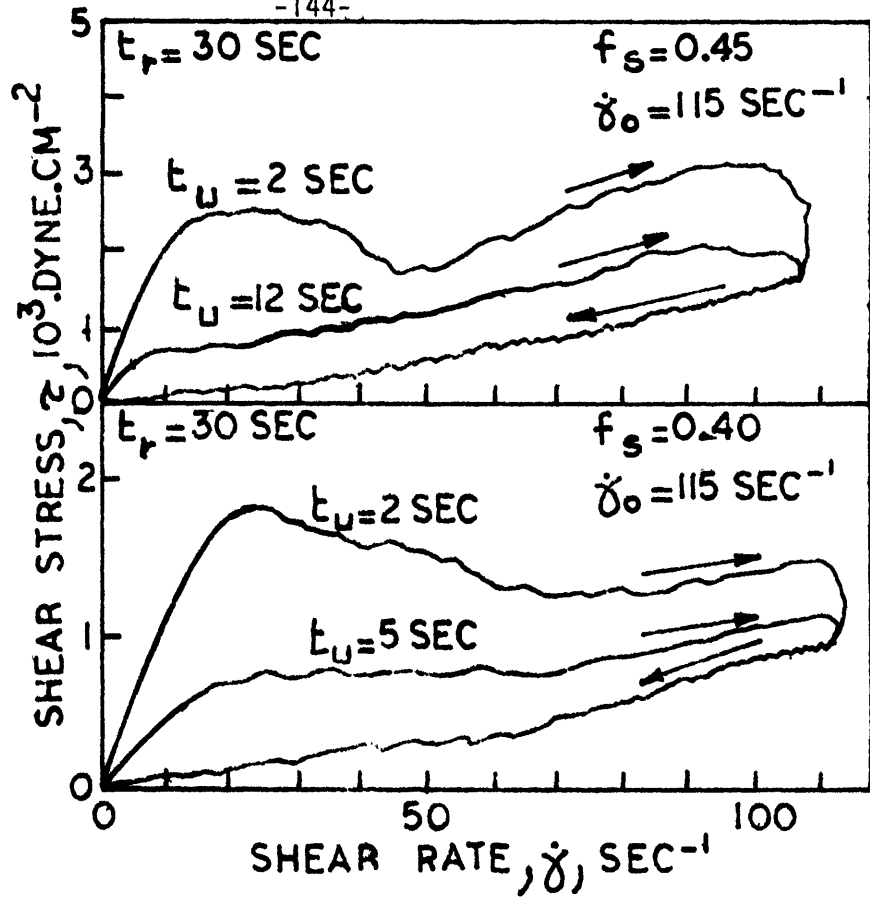
Figure 41. Effect of up-time on hysteresis loops of Sn-15%Pb slurries, initial shear rate of 115 sec⁻¹, fractions solid of 0.45 and 0.40, rest time of 30 seconds (a) loops, (b) loop areas versus up-time.
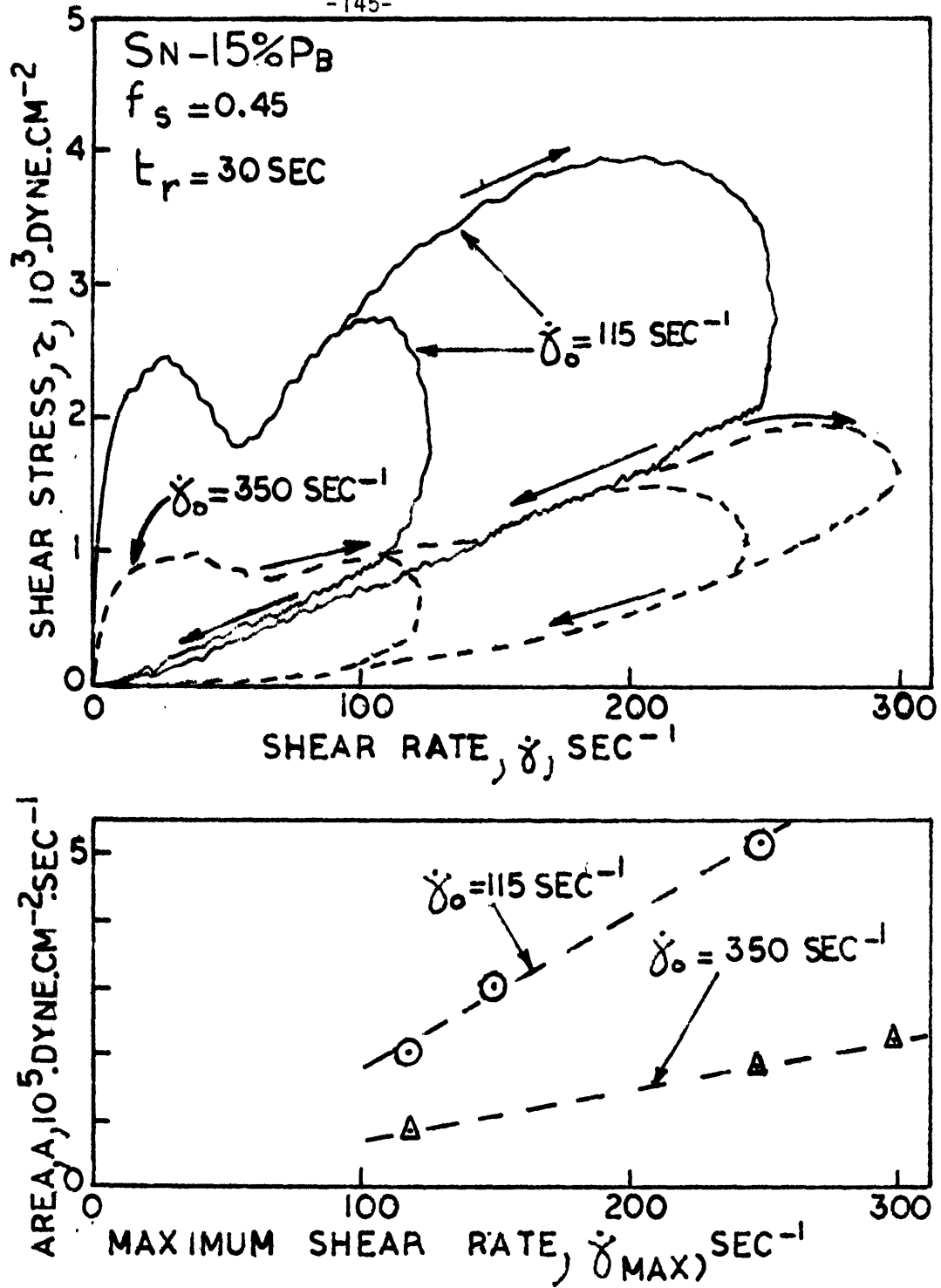
Figure 42. Effect of maximum shear rate on hysteresis loops of Sn-15%Pb slurries, held at a fraction solid of .45 after rest time of 30 seconds (a) loops, (b) area versus maximum shear rate.
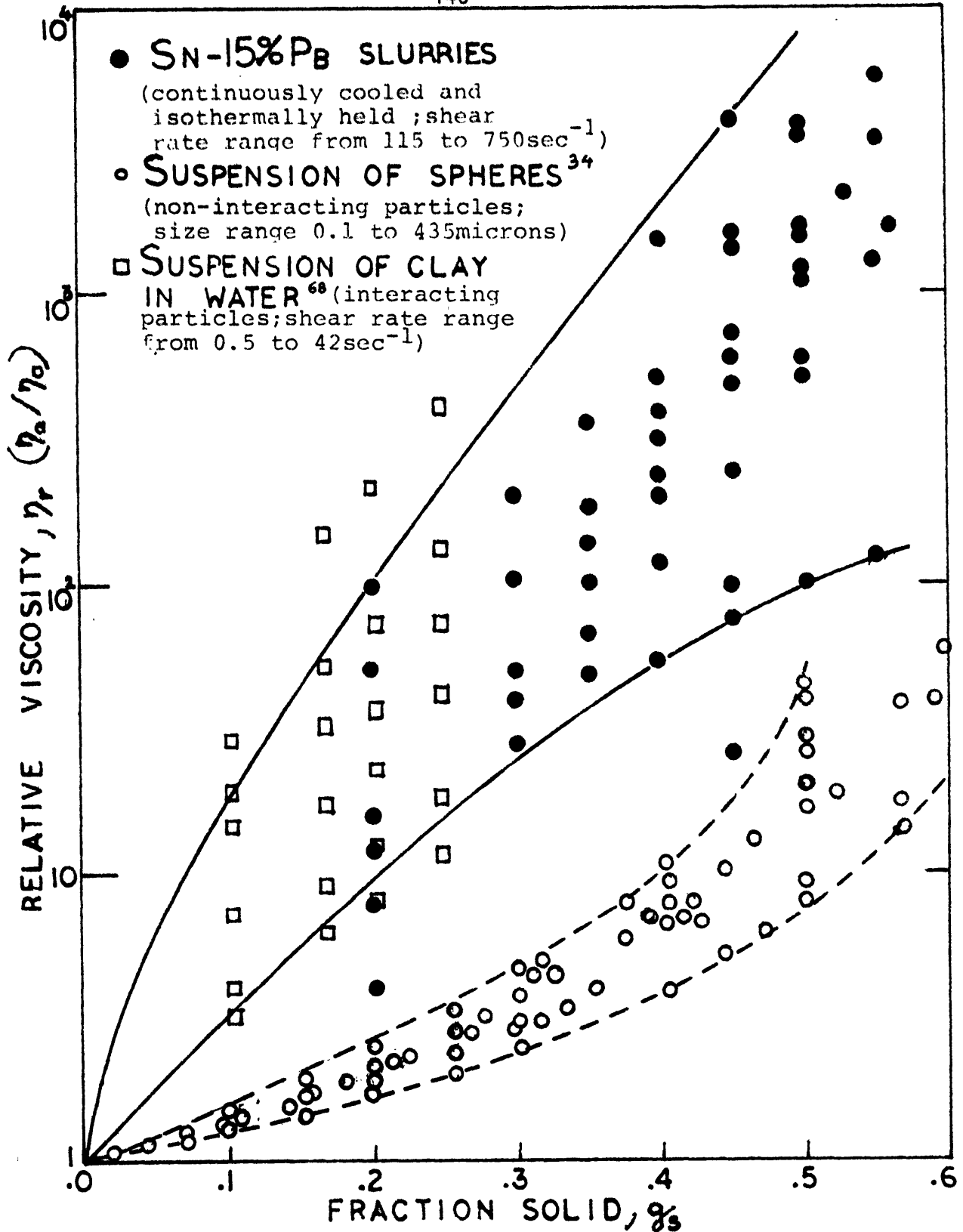
Figure 43. Comparison of the relative viscosity of Sn-15%Pb slurries to that of other suspensions of interacting[68] and non-interacting[34] particles.
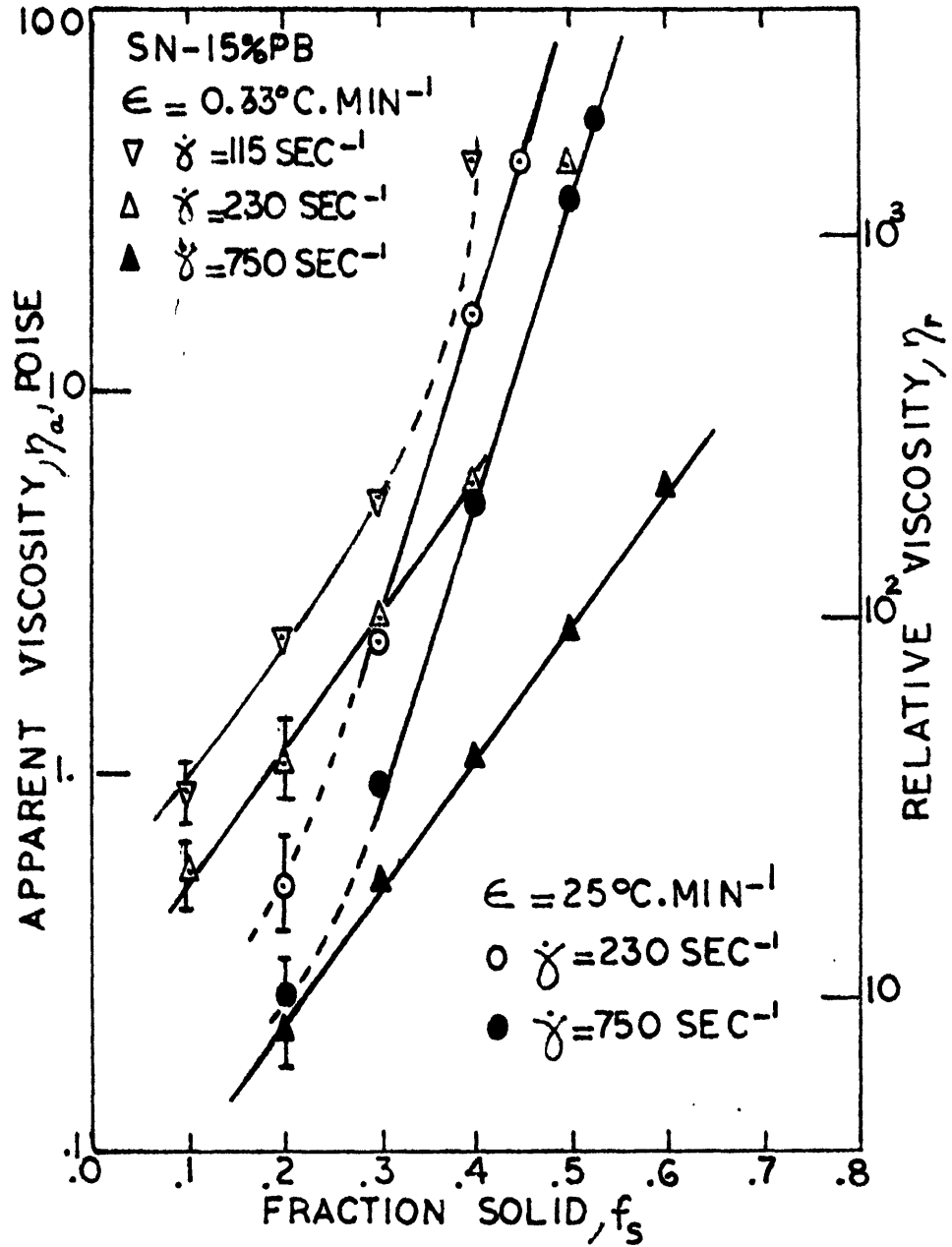
Figure 44. Semi-log plot of the apparent viscosity versus
fraction solid for the continuously cooled
Sn-15%Pb slurries.
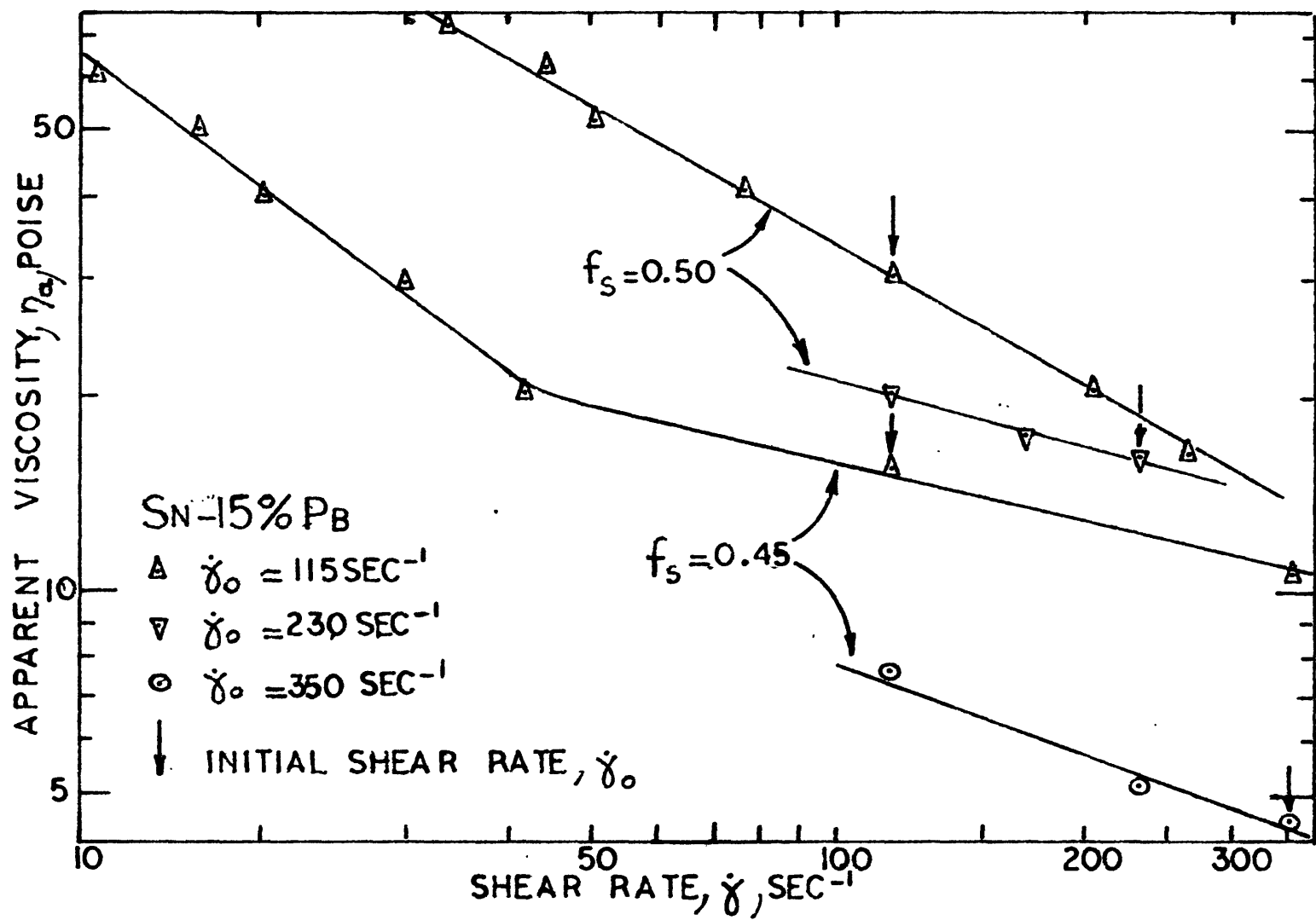
Figure 45 . Log-log plot of apparent viscosity versus shear rate for isothermally held slurries of Sn-15%Pb alloy.

AGGREGATE

PARTICLE

LOW SHEAR RATE

HIGH SHEAR RATE

(a)

(b)
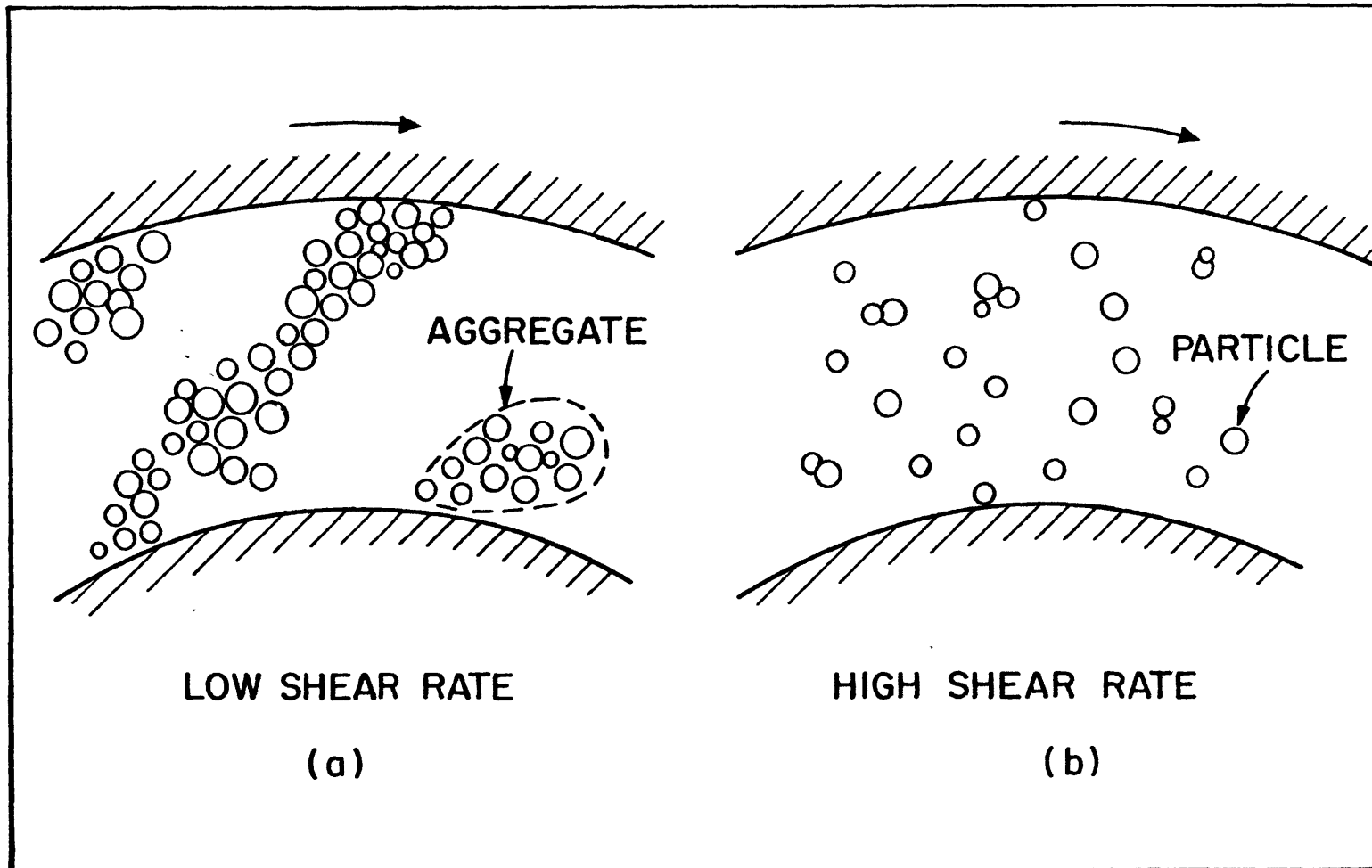
Figure 46. Model for build-up and breakdown of interacting particles,after Michaels[168].
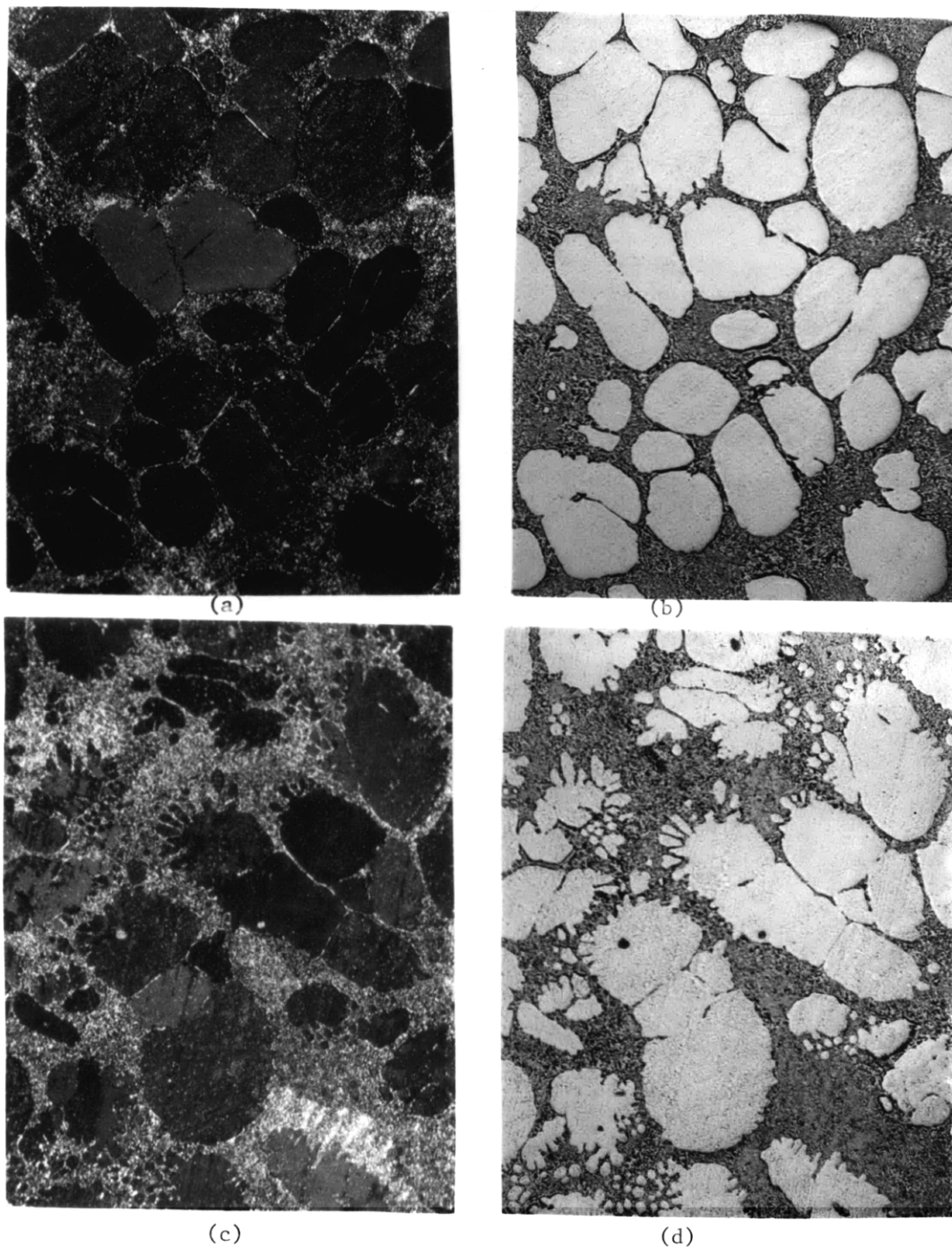
Figure 47 Structures of isothermally held slurries of Sn-15%Pb alloy at a
fraction solid of 0.45,sheared at 230 sec^{-1},after a total time in
the liquid-solid range of 90 minutes;(a) and (b) no change in shear
rate,(c) and (d) increase of shear rate to 350 sec^{-1} for 5 minutes
and back to 230 sec^{-1};(a) and (c) same as (b) and (d) under pola-
rized light;50 X.
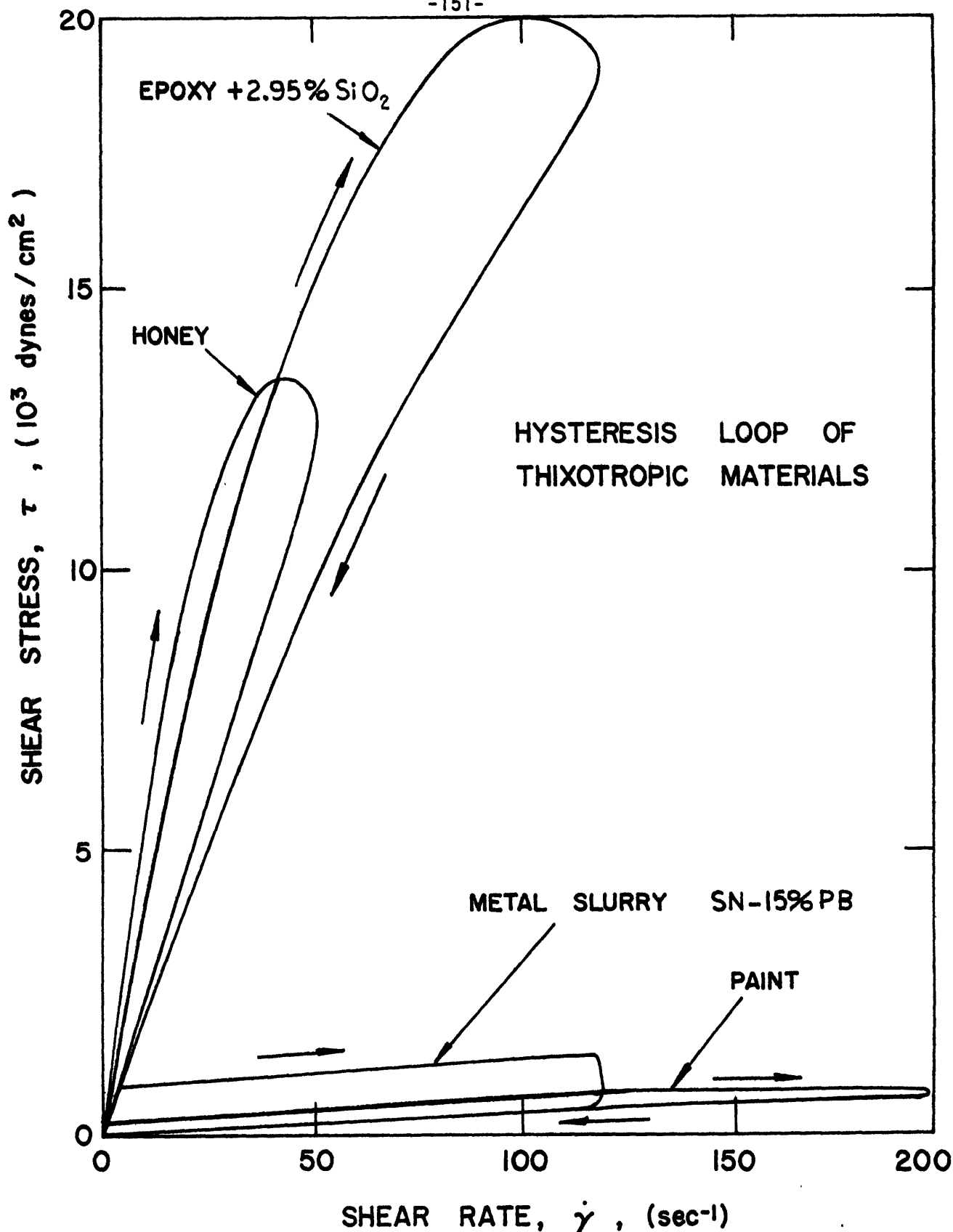
Figure 48. Comparison of the hysteresis loop of Sn-15%Pb slurries and non-metallic systems, generated in this viscometer.

Primary solid particle

Contact point-weld(negative curvature)

R_1

(a) 2 spherical primary solid particles in contact

R_3 R_2

Flux(diffusion distance,R_3)

Area,A,over which solid grows

Volume ,V,of weld

(b)Enlarged view of contact area
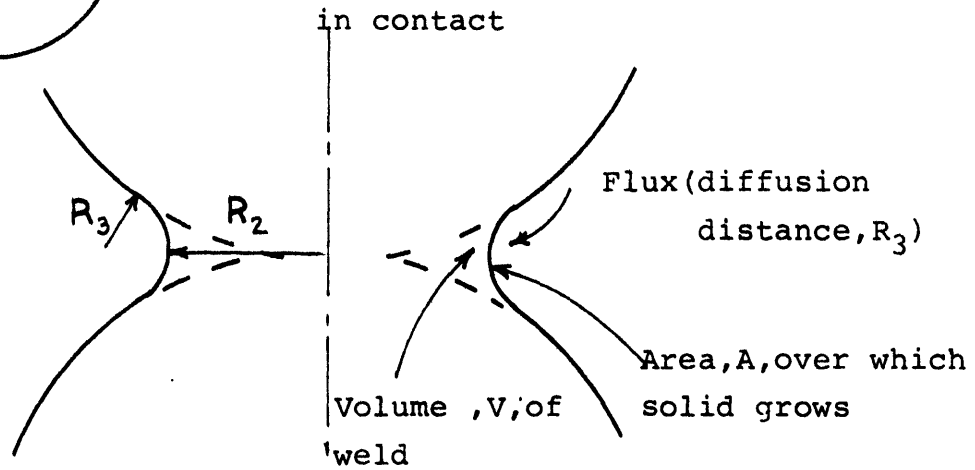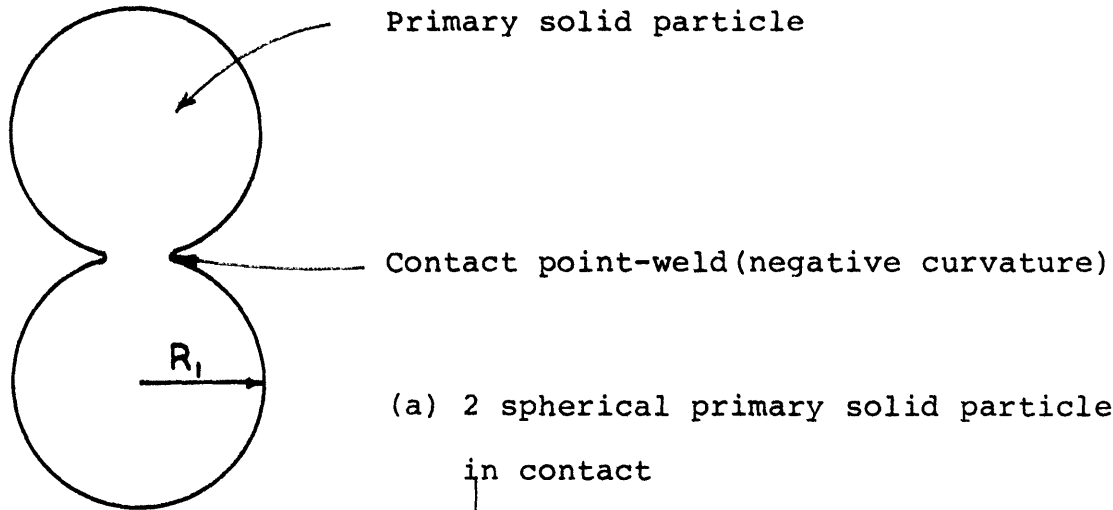
$$R_1 \lll R_2 \lll R_3$$

$$R_3 = \frac{R_2^2}{2R_1}$$

$$A = \frac{\pi^2 R_2^3}{R_1}$$

$$V = \frac{\pi R_2^4}{2R_1}$$

(c)Relationship pertaining to his geometry[105]

Figure 49.Model for the coalescence of two primary solid particles of isothermally held slurries of Sn-15%Pb alloy.
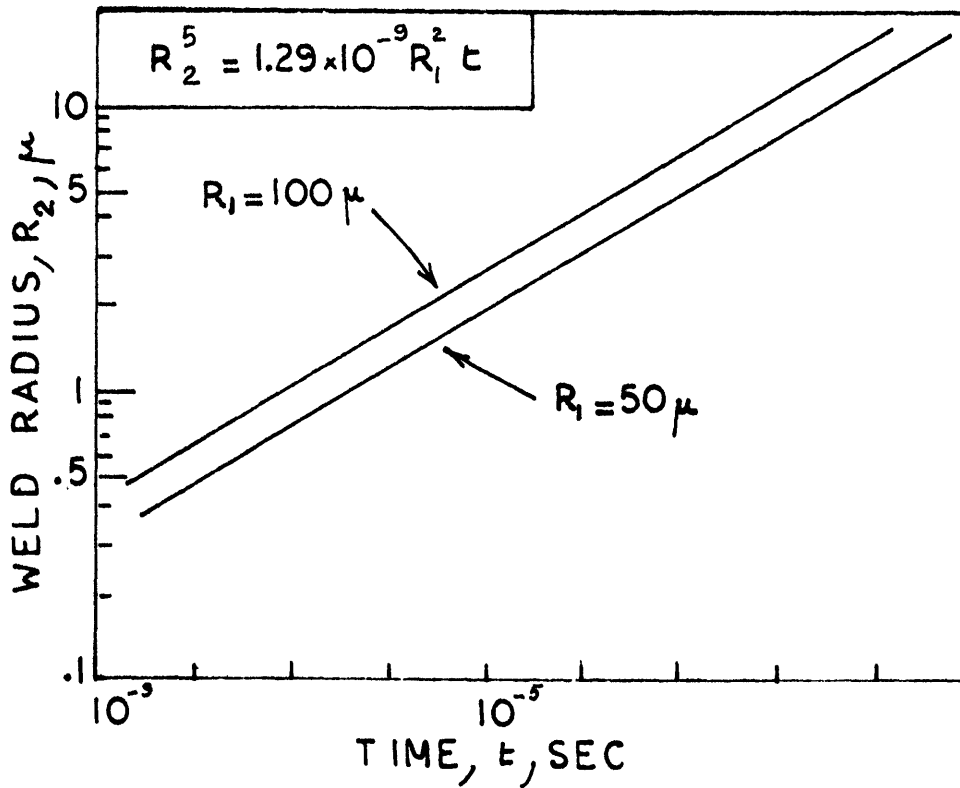
Figure 50. Log-log plot of weld radius versus time of
growth, t, (time of true contact between the
two primary solid particles of Sn-15%Pb
alloy).

FLOW DIRECTION
(Fluid, η)

$\longrightarrow$

SHEAR RATE, $\dot{\gamma}$

$\uparrow$

$\longrightarrow$ F_1

$\longrightarrow$ $F = F_1 - F_2 = 12\pi R_1^2 \eta \dot{\gamma}$

$\longrightarrow$ F_2

$$\tau = \frac{F}{\pi R_2^2} = 12 \left(\frac{R_1}{R_2}\right)^2 \eta \dot{\gamma}$$
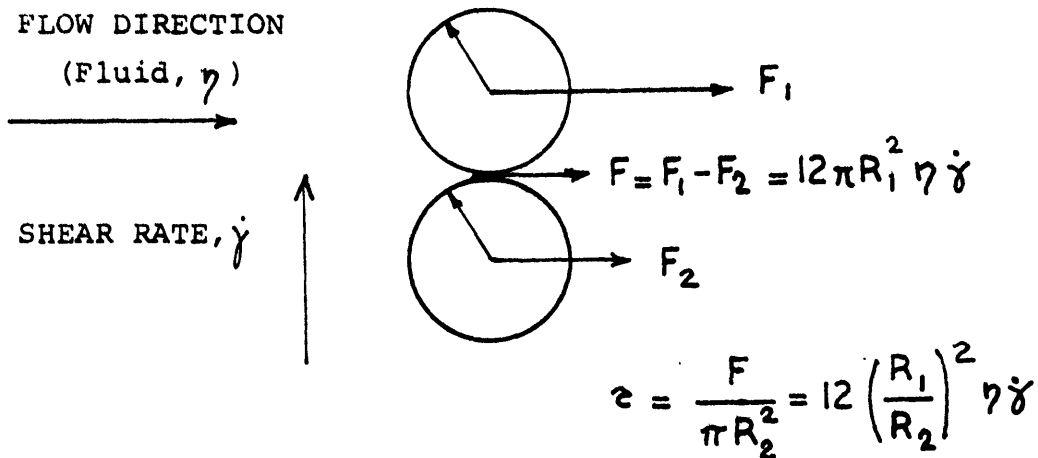
(a) Fluid flo force on a weld between two particles

FLOW DIRECTION

$\longrightarrow$

(i) Collision   (ii) Weld   (iii) Creep of   (iv) Rupture

t=0   grows   weld
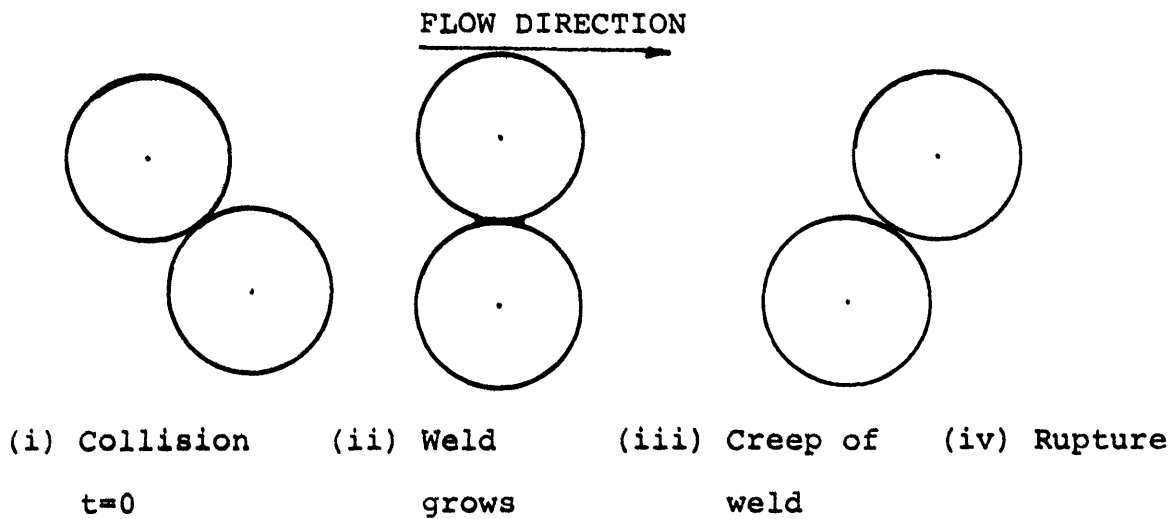
(b) Mechanisms of formatiom and fracture of a weld between
two primary solid particles.

Figure 51.Formation and Fracture of a weld between two primary

solid particles.Model of pseudoplasticity.

FRACTURE TIME, t_f, SEC

STRESS, τ, DYNE.CM^{-2}

$t_f = 4 \times 10^{10} \tau^{-2}$

$\dot{\varepsilon} = 2.5 \times 10^{-12} \tau^2$

$S_n - 38\% P_b$

$T = 183°C$
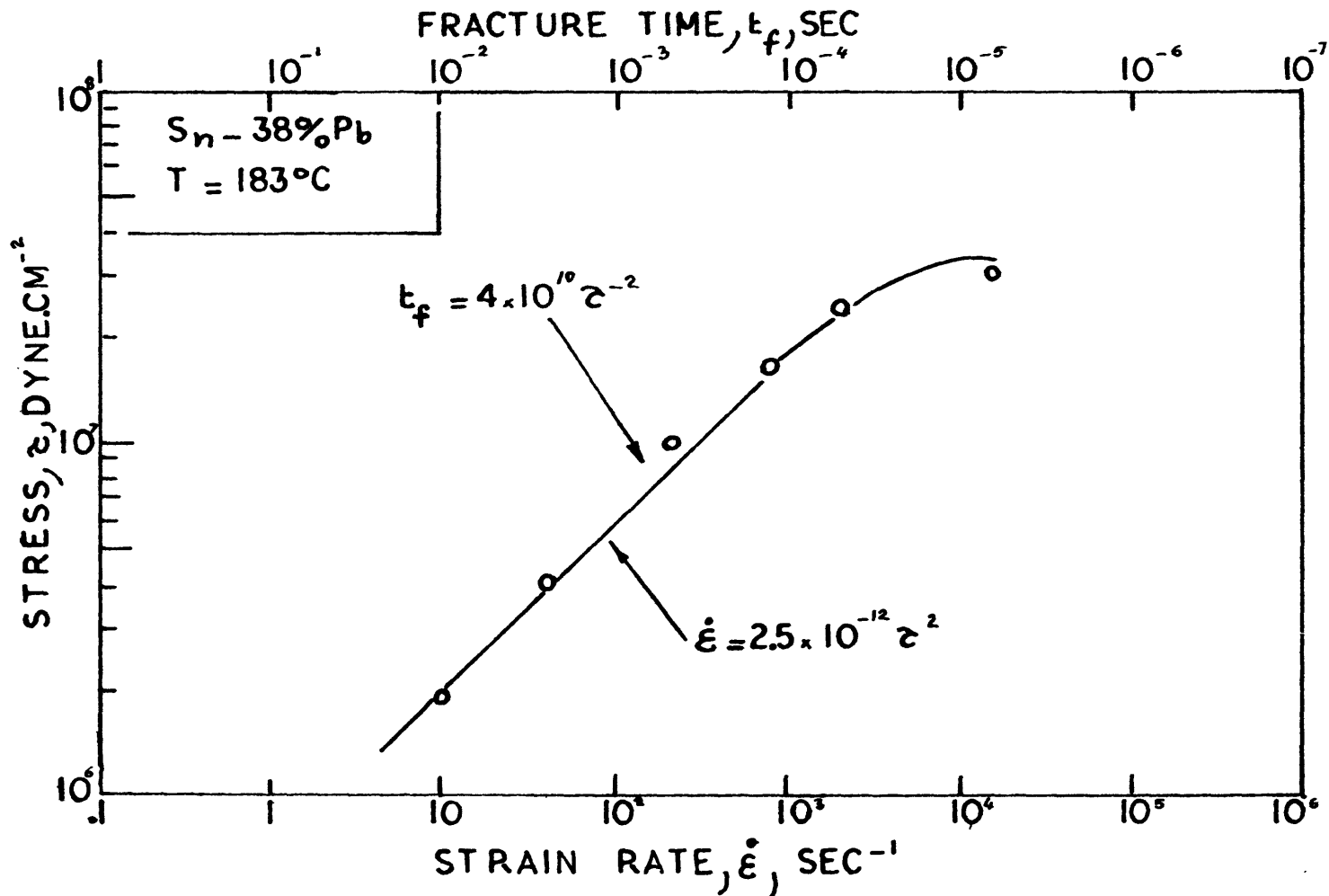
STRAIN RATE, $\dot{\varepsilon}$, SEC^{-1}

Figure 52. Creep behavior (stress versus strain rate) of Sn-38%Pb alloy at the solidus temperature,T-183°C,calculated from its equivalent at T=20°C[111] using Larson-Miller relation with C=20[109] and a time t corresponding to a strain of 0.10.
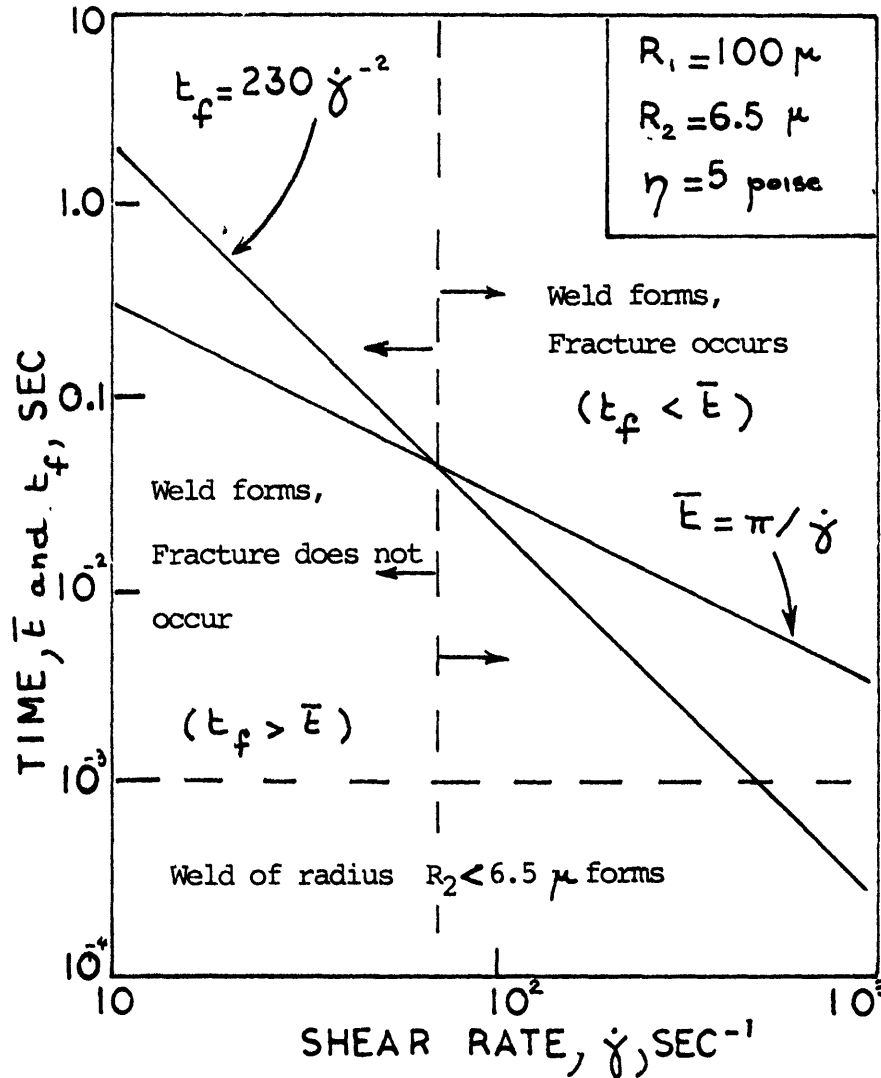
Figure 53. Comparison of the fracture time, t_f, (time necessary for fracture to occur) and life time of a doublet, t, as a function of shear rate.
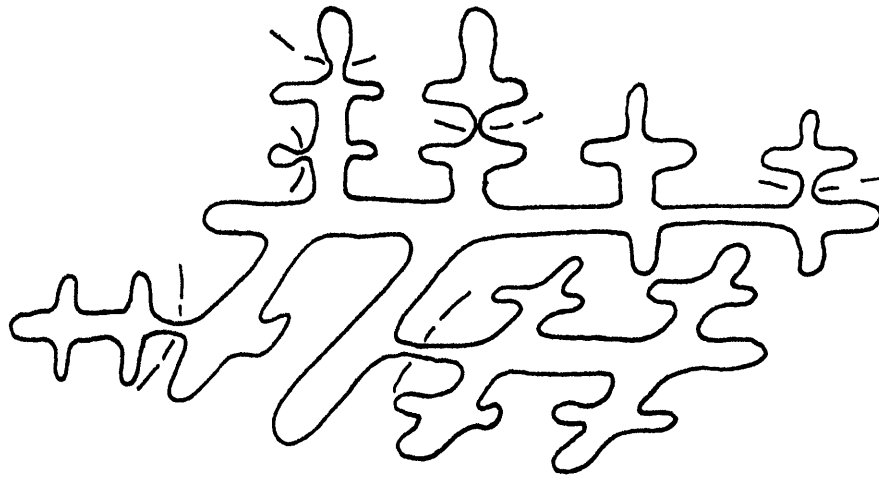
(a)
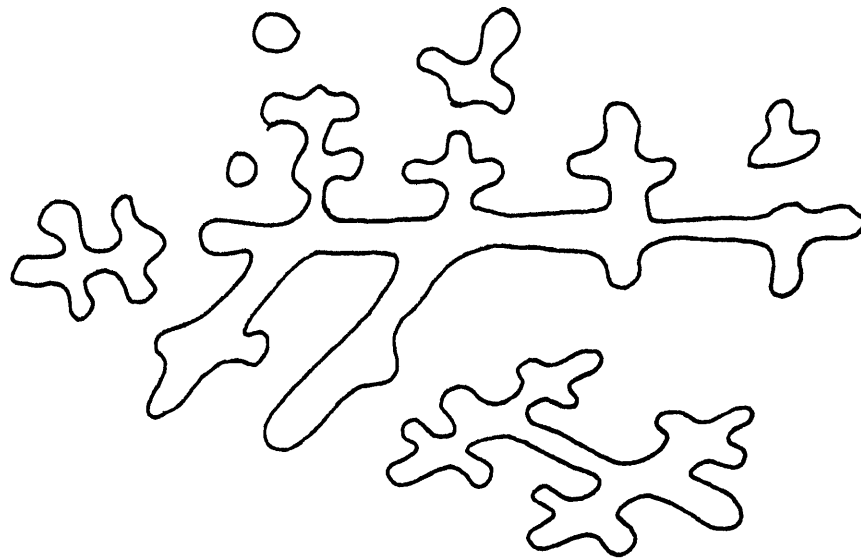
(b)

Figure 54 .Dendrite multiplication mechanism
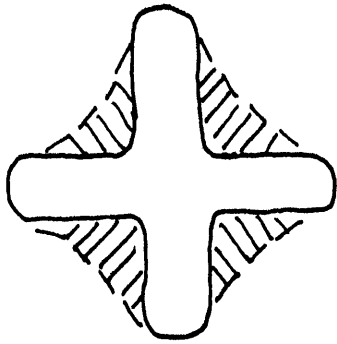
(a)
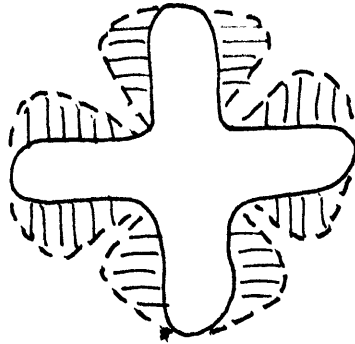
(b)
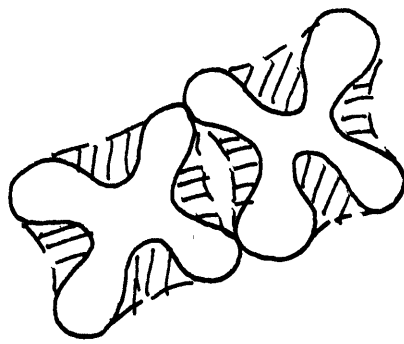
(c)

Figure 55 . Coarsening Models

(a)

(b)

(c)

(d)
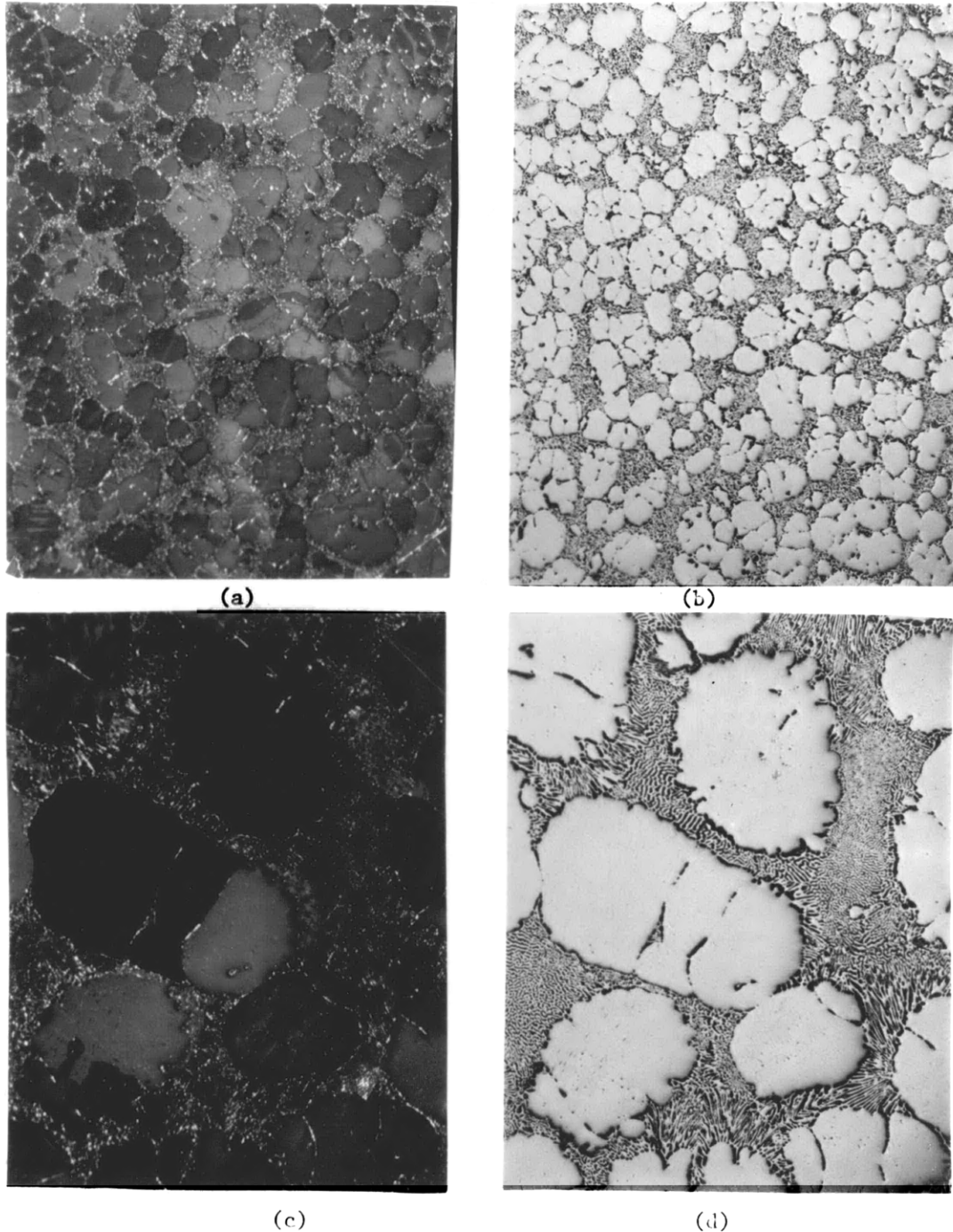
Figure 56. Structures of continuously cooled slurries of Sn-15%Pb alloy, quenched at a fraction solid of 0.55; (a) and (b) sheared at 750 sec^{-1}, cooled at 25°C/min; (c) and (d) sheared at 230 sec^{-1}, cooled at 0.33°C/min; (a) and (c) same as (b) and (d) under polarized light; 50 X.

TABLE I - Effect of Shear Rate on the Viscosity of Coarse Suspensions.

Particle	Ref.	Dispersion Medium	Particle Size, μ	Flow Behavior	Fraction Solid, g_s	Maximum		Viscometer
						Shear stress τ, $\dfrac{dynes}{cm^2}$	Shear rate γ, sec^{-1}	
glass beads	36	Sucrose solution $\eta=.42$ poise	25-150	Newtonian	.65	6.5	1300	Rotational
quartz	38	Water $\eta=.01$ poise	50-200	Dilatant	.10-.30	–	350	Rotational
glass spheres	37	P.I.B.* $\eta=20$poise	50-230	Pseudo-plastic	.45-.60	140	1	Orifice D=.30-.45 mm
TiO_2	36	Sucrose solution η .42poise	.2-1.0	pseudo-plastic $\gamma<400$ sec^{-1} Dilatant $\gamma>1000$ sec^{-1}	.0-.40	100	–	Rotational

* P.I.B. = poly-isobutylene

TABLE II - Effect of Particle Size and Shape on the Viscosity of Coarse Suspensions.

Particle	Ref.	Dispersion Medium	Particle Size, X microns	Flow Behavior		Fraction Solid, g_s	Viscometer
quartz ρ=2.6g/cc	38	Water η =.01	30-180 <16	$\eta\uparrow$ $X\uparrow$ $\eta\uparrow$ $X\downarrow$		0-.30	Rotational 0-350sec^{-1}
glass ρ=2.6g/cc	24	Glucose Sucrose Oil	4-230	$\eta\uparrow$ $X\downarrow$		0-.50	-
PMMA*	41	Aqueous Solution η = .06	Spheres 30-200 Irregular Shape	no effect of size $\eta\uparrow$ $X\uparrow$		.25	Rising Sphere
Clay $q\lesssim 1$ $^\Delta$	42	Water η = .01	.4-.8	$\eta\downarrow$ $q\uparrow$		.10	MacMichael
SiO$_2$ q=10^4	43	Oil η=2poise	.025x250	$\eta\uparrow$ $q\uparrow$		up to .002	Capillary

* PMMA = polymethylmethacrylate

$^\Delta$ q = axial ratio of particle

TABLE III

Effect of Cooling Rate, Shear Rate and Fraction Solid on the Apparent Viscosity of Sn-15%Pb Slurries

Fraction Solid, f_s	Apparent Viscosity, η_a, poise							
	Cooling Rate, $\varepsilon = 0.33°C/min$				Cooling Rate, $\varepsilon = 25°C/min$			
	Shear Rate, $\dot{\gamma}$, sec^{-1}				Shear Rate, $\dot{\gamma}$, sec^{-1}			
	115	230	350	750	115	230	450	750
0.20	2.5	1.2	0.4	0.3	1.2	1.2	0.2	0.1
0.30	5.0	2.5	1.0	0.7	2.5	2.5	1.2	1.0
0.35	8.7	3.5	1.7	1.2	4.5	4.5	4.0	2.5
0.40	40.0	5.0	3.0	1.3	13	10	8	6.0
0.45	100	15	6.2	2.0	40	37	18	12
0.50	-	40±10	12.5	2.6	85±10	100±10	42	30
0.55	-	80±15	32	3.0	-	-	-	80

TABLE IV

Thixotropy Data of Sn-15%Pb Slurries and Non-Metallic Systems

System	Temperature T, °C	Apparent Viscosity η_a, poise	Rest Time, t_r hours	Maximum Shear Rate $\dot{\gamma}_{max}$, sec^{-1}	Up Time t_u, sec	Hysteresis Loop Area, 10^5 dyne cm^{-2}sec^{-1}	Transient Time, t seconds
Honey	24	240	12	55	1.0	1.0	30
Epoxy +2.95% SiO_2	25	160	12	100	2.0	3.00	15
Paint	24	4	2	270	10	0.15	300
Sn-15%Pb f_s=0.45	196	15	0.008-0.5 (30 sec- 30 min)	115	2	2-8	0-20

TABLE V

Relative Viscosity Data for Sn-15%Pb Slurries (Figure 50)
And Non-Metallic Systems

Low Molecular Weight Polyethylene[52]

$\dot{\gamma}_{sec}^{-1}$ T°C	109	96	90	84	80	70
30	1	-	87	850	3020	9350
100	1	-	31.3	347	930	3540
300	1	-	16.6	151	398	1520
1000	1	3.98	9.1	63	158	575

Isothermally Held Slurries of Sn-15%Pb

T°C	209.5	197.6	196.3	195.2	192	187
$\dot{\gamma}_{sec}^{-1}$ fs	0	.42	.45	.47	.53	.60
115	1	540	600	940	2400	-
230	1	240	400	480	800	2480
350	1	-	160	-	-	-
750	1	-	40	-	-	-

TABLE VI

Rheological Properties and Structure of Sn-15%Pb Slurries

	At a Given Fraction Solid								
	Isothermal			Slow Cooling Rate			Fast Cooling Rate		
$\dot{\gamma}$	η	$\bar{X}$	g_{Le}	η	$\bar{X}$	g_{Le}	η	$\bar{X}$	g_{Le}
$\uparrow$	$\downarrow$	$\downarrow$	$\leftrightarrow$	$\downarrow$	$\downarrow$	$\downarrow$	$\downarrow$	$\leftrightarrow$	$\downarrow$

At a Given Fraction Solid and
a Given Shear Rate

$$\frac{\eta \text{ fast}}{\eta \text{ slow}} > 1 \qquad \frac{\bar{X} \text{ fast}}{\bar{X} \text{ slow}} < 1 \qquad \frac{g_{Le} \text{ (fast)}}{g_{Le} \text{ (slow)}} > 1$$

List of Symbols

$\dot{\gamma}$ = shear rate

η_a = apparent viscosity

$\bar{X}$ = average size of primary solid particle

g_{Le} = volume fraction of entrapped liquid

$\uparrow$ increase, $\downarrow$ decrease, $\leftrightarrow$ no change

TABLE VII

Experimentally Determined Coefficients of Equation (27)
$\log \eta_a = \alpha + \beta fs$ and equation (28) $\eta_a = A \exp (Bfs)$ where,
$A = \exp (2.3\alpha)$ and $B = 2.3\beta$. Apparent viscosity is in
poise. The data is for the continuously cooled
slurries of Sn-15%Pb alloy.

Cooling Rate	25°C/minute		0.33°C/minute		
Shear Rate $\dot{\gamma}$, sec^{-1}	230	750	115	230	750
α	-2.0	-2.4	-0.4	-0.62	-1.37
β	8.0	8.0	3.5	3.5	3.5
$A = \exp (2.3\alpha)$	0.01	0.004	0.4	0.24	0.043
$B = 2.3\beta$	18.4	18.4	8.05	8.05	8.05
Range of Fractions Solid	0.2-0.45	0.2-0.55	0.1-0.3	0.1-0.4	0.2-0.6

TABLE VIII

Experimentally Determined Coefficients of equation (29),
$\eta_a = k\dot{\gamma}^n$, relating the apparent viscosity η_a (poise)
to the shear rate, $\dot{\gamma}$ (sec^{-1})

Data for Isothermally Held Slurries of Sn-15%Pb Alloy

Fraction Solid	$f_s = 0.50$		$f_s = 0.45$		
Initial Shear Rate, $\dot{\gamma}_0$, sec^{-1}	115	230	115	115	350
Constant, k unit: cgs	830	100	380	63	55
Exponent, n	-0.70	-.34	-.82	-.30	-.44
Range of Shear Rates, sec^{-1}	30-300	100-250	10-40	40-400	100-400

Data for Kaolin Particles in Water[68]

Fraction Solid	0.10	0.16	0.20	0.24
n	-.65	-.74	-.74	-.86
Range of Shear Rates, $\dot{\gamma}$, sec^{-1}	.5-10	1-10	1-10	1-10

Data for Partially Crystalline Polymer[52]

Temperature	90°C	80°C
n(cgs)	-.50	-.81
Range of Shear Rates, $\dot{\gamma}$, sec^{-1}	100-1000	100- 1000

Data for TiO$_2$ in Water[39]

Fraction Solid, f_s = .40   n = -.75   between 0 and 400 sec^{-1}

TABLE IX

Thixotropy Data for Non-Metallic Systems

System	Ref.	Conditions		Hysteresis Loop Area, A, 10^5 dyne. $cm^{-2}sec^{-1}$	Remarks
		t_u, sec	γ_m, sec^{-1}		
Printing Ink (0.10-0.40 fraction solid)	(57)	30-2000	200	7.8-0.10	Depend on previous history.
Heather honey	(100)	1800	14.5	-	No absolute measurement.
Attalpugite/water (20% solid phase) (needle: 3µ X 10Å)	(62)	30	700	2.95	Isothermal recovery in 12 hours.
Lithium Stearate in Oil	(60)	500	500	0.78	No isothermal recovery.

TABLE X

Experimentally Determined Coefficients to Equation (13) $A = N_0 - N\,t_u$,
Relating the Area of Hysteresis Loops A to the Up Time t_u, of Equation (14)
$A = Q\dot{\gamma}^n$ Relating the Area to the Maximum Shear Rate $\dot{\gamma}_m$, of Equation (30)
$A = A_0 t_r^m$ Relating the Area A to the Rest Time t_r

Data for Isothermally Held Slurries of Sn-15%Pb Alloy

Variable	Relationship Area, A, dyne cm^{-2} sec^{-1}	Conditions	
Rest Time t_r, t_r, minutes	$A = 3.0 \times 10^5\, t_r^{.25}$	$f_s = .45$ $t_u = 2$ sec $\dot{\gamma}_0 = 115$ sec^{-1} $t_d = 4$ sec $\dot{\gamma}_m = 115$ sec^{-1}	
Up Time t_u, sec	$A = 2.0 \times 10^5 - .13 \times 10^5\, t_u$	$f_s = .45$	$\dot{\gamma}_0 = 115$ sec^{-1} $t_r = 30$ sec
	$A = 1.3 \times 10^5 - .13 \times 10^5\, t_u$	$f_s = .40$	$t_d = 4$ sec $\dot{\gamma}_m = 115$ sec^{-1}
Maximum Shear Rate, $\dot{\gamma}_m$, sec	$A = .76 \times 10^3\, \dot{\gamma}_m$	$f_s = .45$ $t_r = 30$ sec $\dot{\gamma}_0 = 350$ sec^{-1} $t_d = 5$ sec $t_u = \min$	

Data for Rotary Printing Ink (Yellow Ink)[57]

Up Time t_u, sec	$A = .22 \times 10^5 - 37.6\, t_u$	$\dot{\gamma}_m = 168$ sec^{-1}
Maximum Shear Rate, $\dot{\gamma}_m$, sec^{-1}	$A = .2\, \dot{\gamma}_m^2$	$t_u = 468$ sec for $\dot{\gamma}_m = 168$ sec^{-1}

TABLE XI

Effect of Structural Parameters and Thermo-Mechanical History
on the Degree of Thixotropy (Area of Hysteresis Loop) of
Isothermally Held Slurries of Sn-15%Pb Alloy

Variable	$f_s \uparrow$	$\dot{\gamma}_o \uparrow$	$t_r \uparrow$	$t_d \uparrow$	$t_u \uparrow$	$\dot{\gamma}_m \uparrow$
Area	A $\uparrow$	A $\downarrow$	A $\uparrow$	A $\uparrow$	A $\downarrow$	A $\uparrow$

A = area of hysteresis loop,

$\dot{\gamma}_o$ = initial shear rate,

t_r = rest time,

t_d = down time,

t_u = up time,

$\dot{\gamma}_m$ = maximum shear rate,

$\uparrow$ increase

$\downarrow$ decrease

TABLE XII

Selected Values for Sn-15%Pb Alloy

f_s = 0.45

C_L = 26 wt % Pb

T_L = 196.2°C = 469.3°K

k = 0.10   APPENDIX A

m = 1.2°C/wt %Pb

ρ = 7.3 g/cc

D_{Pb} = 2.1 X 10⁵ cm²/sec (diffusion of Pb in molten Sn-16.1at%Pb
        at T = 196°C[106]

H = 14 cal/g[107]

σ_{S-L} = σ_{L-V} = 520 erg/cm² at T = 220°C for Sn-12%Pb (sessile drop
        method)[108]

TABLE XIII

Effect of Shear Rate on Doublet Life, $\bar{t}$, and Fracture Time, t_f, (time necessary for fracture of a weld between two primary solid particles to occur). Assumptions include: particles are spheres of radius $R_1 = 100\mu$, slurry viscosity is 5 poise, and fracture occurs at a strain of 0.10.

Shear Rate, $\dot{\gamma}$, sec^{-1}	50			100			500		
Doublet life time $\bar{t} = \pi/\dot{\gamma}$, sec	0.06			0.03			0.006		
Time of true contact, t, sec	0.06	0.03	0.001	0.03	0.015	0.001	0.006	0.003	0.001
Weld radius, R_2, μ $R_2^5 = 1.29 \times 10^{-9}\, R_1^2 t$ Eq(35)	15	13	6.5	13	11.5	6.5	9.5	8.0	6.5
Shear stress, τ, 10^6 dyne.cm^{-2} $\tau = 12(R_1/R_2)^2\eta\dot{\gamma}$ Eq (37)	.013	.017	.708	.035	.046	1.41	3.3	4.68	7.05
Shear stress, τ, psi	.19	.25	10.3	.52	.67	20.4	46.5	68	102
Strain rate, $\dot{\varepsilon}$, sec^{-1} $\dot{\varepsilon} = 2.5 \times 10^{-2}\tau^2$ Eq (38b)	.0004	.0008	1.25	.003	.005	5	27.5	55	125
Fracture time, t_f, sec $t_f = 4 \times 10^{10}\tau^{-2}$ Eq (38)	250	125	0.08	33	20	0.02	.003$_6$	.0018	.0008
Criterion for fracture $t_f - t \gtrless 0$	$t_f - t > 0$ DO NOT BREAK						$t_f - t < 0$ BREAK		

APPENDIX A

SOLIDIFICATION OF TIN-LEAD ALLOYS

There is good agreement (1°C at the most)[112,113,114] between the
data points giving the liquidus of Sn-rich alloys of Sn and Pb, Figure A1.
The main feature of the liquidus line is the existence of a positive curva-
ture (liquidus lies below the straight line joining the melting point of
pure tin and that of the eutectic), Figure A1. This curvature results in a
variation of the k's (ratio of the solid composition to that of the liquid)
which added to that of the solidus makes the k's vary greatly from 0.10
to 0.07.

Fraction Solid

The fraction solid, present at a given temperature in the liquid-solid
range, depends on the conditions of the solidification.

If complete mixing of the liquid occurs and if enough time is allowed
for the diffusion in the solid to be completed, a mass balance results in
the lever rule, expressed as

$$f_s = \frac{1}{1 - k} (1 - C_0/C_L) \qquad (A1)$$

If there is no diffusion in the solid, the same mass balance results
in the Scheil equation

$$\int_0^{f_s} \frac{df_s}{1 - f_s} = \int_{C_0}^{C_L} \frac{1}{1 - k} \frac{dC_L}{C_L} \qquad (A2)$$

Since the k's vary, the integration must be performed step by step.
Results of both methods are shown in Figure A2. As expected, the lever

rule gives higher temperatures for the same fraction solid since the diffusion in the solid impoverishes the liquid or raises the equilibrium temperature. Figure A2 shows that the difference is at its maximum 0.01.

Density of Solid Solution of Pb in Sn

As solidification takes place, the densities of the solid and liquid phases change and most likely are not equal. There are two factors that contribute to the density of solid solution of Pb in Sn: (1) the decreasing temperature with the increasing content of Pb, (2) the expansion of the lattice due to the appearance of Pb atoms in the Sn network. The first factor increases the density (volumetric contraction[105]) whereas the second factor decreases the density (Pb atoms are larger than Sn atoms[106]).

After computation of the mass, volume of a unit cell, their variations with temperature and composition, one gets the density of the solid phase along the solidus line

$$\rho_s = 7.22_2 \ (1 + .792_6 \ N_{Pb}) \eqno(A3)$$

where N_{Pb} is the atomic fraction of Pb; results of equation A3 are given in Figure A3 and Table Al as well as data of the density of the liquid phase along the liquidus line.

Weight Fraction-Volume Fraction

Since the Scheil equation or the lever rule are deduced from a mass balance they give a value of the weight fraction solid, f_s. However the important factor for the study of rheology is the volume fraction, g_s. It is easily derived as

$$g_s = \left(1 + \frac{1 - f_s}{f_s} \times \frac{\rho_S}{\rho_L}\right)^{-1} \qquad (A4)$$

Using known values of ρ_L[105] and the values of ρ_S derived earlier, it is found out that the differences are very small (due to the small difference in density), Table A2.

Experimental Verification of f_s Versus T

Two slurries of Sn-15%Pb alloy were held isothermally at T = 202.0°C and T = 197.0°C for two hours under a shear rate of 230 sec^{-1} and were further quenched. The measured volume fractions of primary solid particles, V_V, were 0.31 and 0.46 which correspond to 0.30 and 0.45 in weight fraction solid. These results are plotted in Figure A2 and agree well with the computed values of 0.30 and 0.44.

TABLE A1

N_{Pb},S	.00	.00741	.0095	.0118	.0145
N_{Pb},L	.00	.100	.145	.200	.261
T_L,°C	232	207	200	192	183

TABLE A2

f_s	.0	.20	.30	.40	.50	.60	$.61_6$
g_s	.0	$.20_6$	$.31_0$	$.41_4$	$.51_8$	$.62_1$	$.63_9$
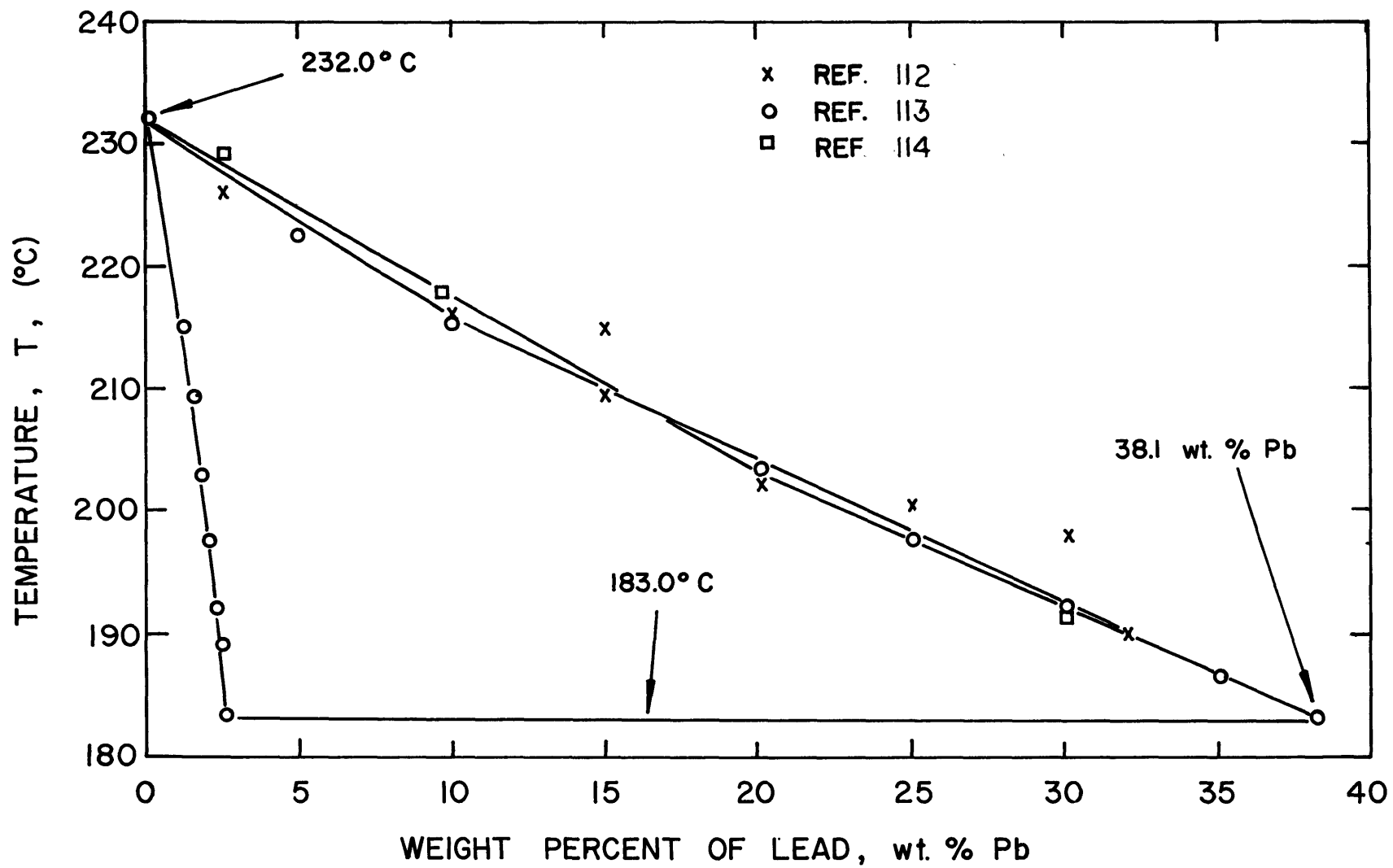
Figure A1.Phase diagram of Sn-Pb alloys;Sn-rich alloys.

FIGURE A2. SOLIDIFICATION OF SN-15%PB ALLOY

× SCHEIL EQUATION

⊙ LEVER RULE

△ EXPERIMENTAL DATA
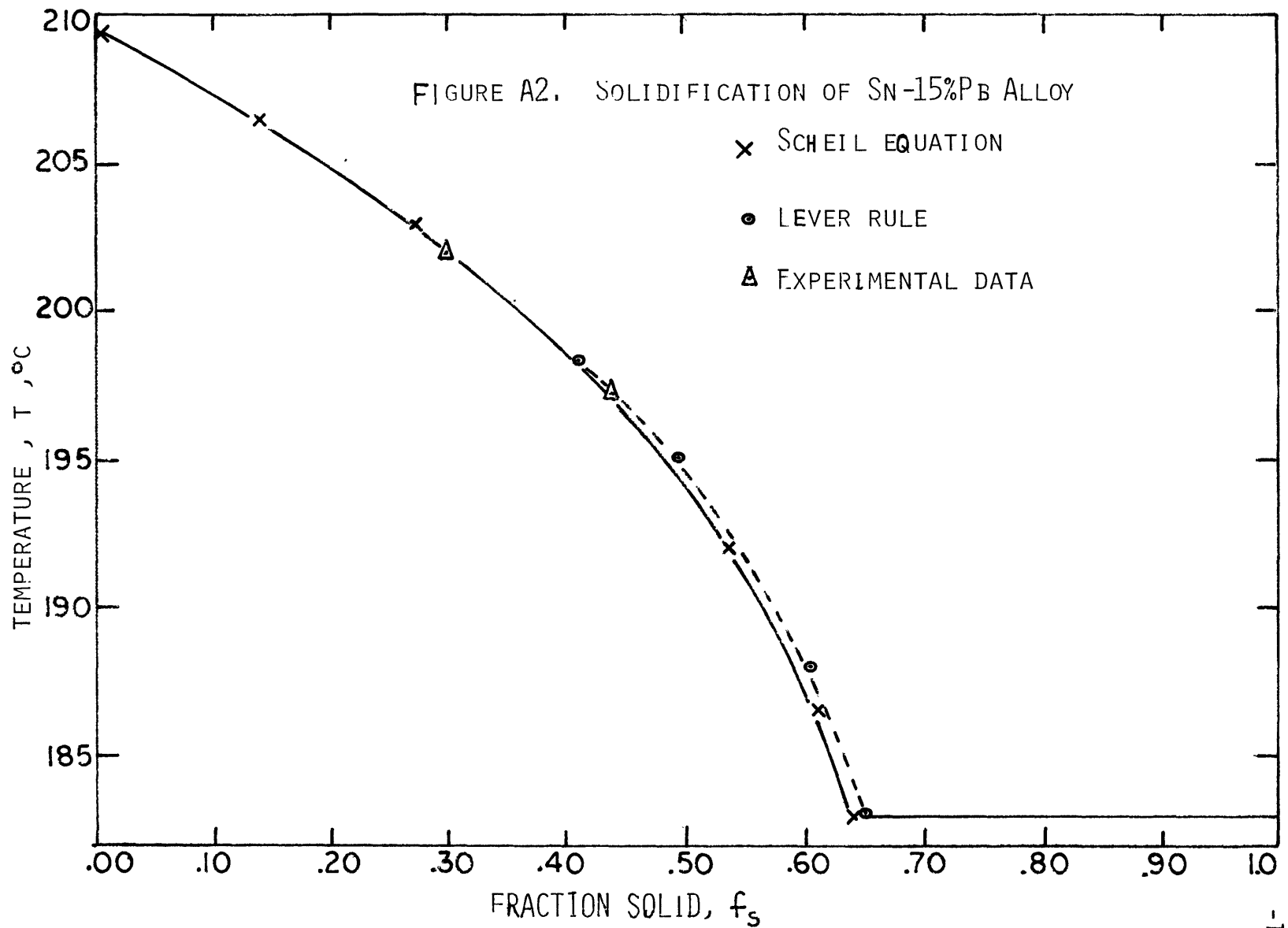
Figure A2.Solidification of Sn-15%Pb alloy;Temperature versus fraction solid.
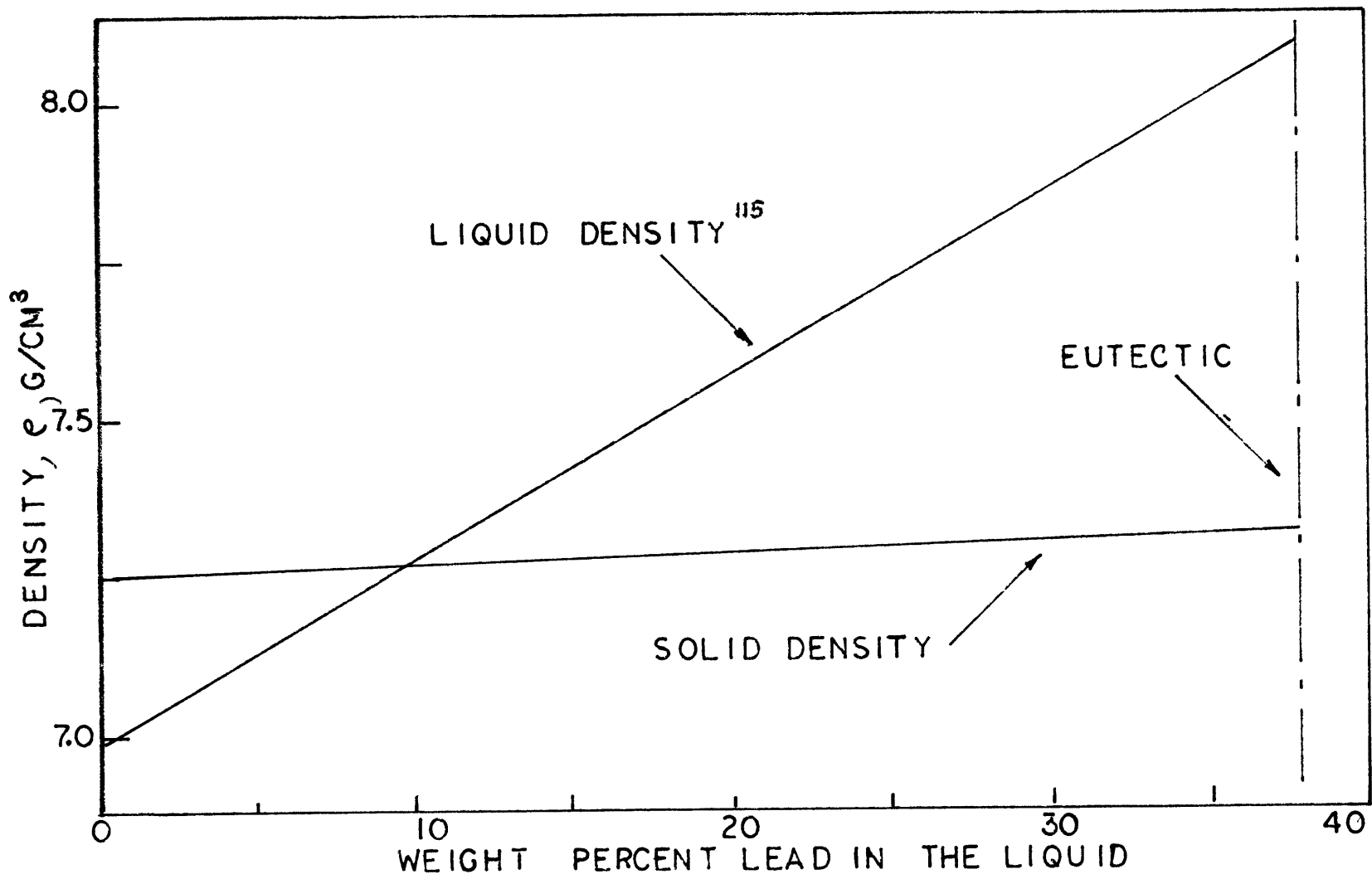
Figure A3. Densities of solid and liquid alloys of Sn-Pb in equilibrium as a function of the weight percent lead in the liquid.

APPENDIX B

COMPOSITION ANALYSIS

LEAD

	Antimony and tin	0.00400
	Arsenic	0.00002
	Bismuth	0.00003
	Copper	0.00010
	Iron	0.00100
	Nickel	0.00010
	Silver	0.00010

TIN		99.925
	Lead	0.020
	Antimony	0.003
	Arsenic	0.025
	Bismuth	0.006
	Copper	0.010
	Iron	0.010
	Nickel	0.001

Lead was obtained from Fisher Scientific Company, Fair Lawn, New Jersey, in Reagent grade sticks.

Tin was obtained from Tin Plate Corporation, Somerville, Massachusetts.

APPENDIX C

MEASUREMENT OF NUMBER AND AVERAGE SIZE IN VOLUME

DeHoff[98] summarizes the problem and states: "The general quantitative metallographic problem of relating measurements that can be made on a random plane section to the number of particles in the three dimensional structure has not been solved to date."

However, it is possible to derive a general equation relating the number of particles to measurement on a plane section, but the resulting relationship is purely formal and involves properties of the particles that depend upon their shape and size.

Assuming the particles to have a constant shape, it is possible to derive the exact relationship even when a size distribution exists but it becomes necessary to measure the length of some characteristic dimension on every particle.

For ellipsoid the relationship between the average minor axis, $\overline{X}$, and the average of the reciprocal of the minor axis of each particle, $\overline{z}$, is

$$\overline{X} = k_4/\overline{z} \qquad\qquad (C1)$$

where k_4 is a shape parameter depending on the axial ratio of the ellipsoid, q; it has been determined by de Hoff and is found to be constant for prolate ellipsoid and equal to $\pi/2$.

As pointed out by de Hoff there are two disadvantages to this method (1) $\overline{z}$ is the average of the reciprocal of the minor axis; it is a harmonic mean and its accurate determination is very sensitive to errors (i.e. the

particle sections which are below the resolution of the microscope may have an important effect). (2) The accurate determination of $\bar{z}$ requires roughly the same number of measurements of section as does the determination of particle size distribution.

So it is more informative to treat the data in such a way as to obtain the size distribution, and obtain the total number of particles and their average as a by product.

Provided particles have the same shape, ellipsoidal, de Hoff[117] has extended the method of Schwartz-Saltykov[97] to the determination of the size distribution from measurements on a random plane. He derived:

$$N_V(j) = \frac{1}{k(q)\Delta} \sum_{i=j}^{k} N_A(i) \; \beta(j,i) \qquad (C2)$$

Δ is the size of a class,

$k(q)$ is the shape factor depending on the axial ratio q,

$\beta(i,j)$ are the coefficients determined by Schwartz-Saltykov[97],

$N_V(j)$ is the number per unit volume of particles of the class j,

$N_A(i)$ is the number per unit area of particles of the class i.

So the average size (minor axis) is

$$\bar{X} = \Delta \frac{\sum_{j=1}^{k} (j - 1/2) \; N_V(j)}{\sum_{j=1}^{k} N_V(j)} \qquad (C3)$$

From those data the standard deviation of the distribution can be determined

$$\sigma_x = \sqrt{\frac{\sum_{i=1}^{k} [(i - 1/2)\Delta - \overline{X}]^2 \, N_V(i)}{\sum_{i=1}^{k} N_V(i)}}$$

(C4)

Etching of Sn-15%Pb Structures

First polish on grinding paper down to number 600 (using soap on the paper), then polish with Alumina down to 0.06 microns (using clean cloth), rinse and dry.

Immerse for 20 seconds in a solution of

        80% glycerol

        10% acetic acid

        10% nitric acid

rinse under hot water, and repolish with a solution of Alumina 0.06 microns very briefly to remove overetched top surface.

To reveal the different orientations of Sn grains, proceed as follows:

- polish as usual

- rub for 1 to 2 minutes the specimen with a cotton swab dipped in a solution of 10% HCl in distilled water

- rinse and dry

- look at specimen under polarized light.

APPENDIX D

FLOW EQUATION OF AN UNKNOWN FLUID

The flow equation of an unknown fluid is obtained by analysis of plots of experimental data relating rate of shear to shear stress[83]. Shear stress, τ, and rate of shear, $\dot{\gamma}$, depend on position in the fluid. Obviously, we must compare values at the same position. The most convenient position is at one of the boundaries: the stress at the wall of the inner cylinder of a coaxial cylinder instrument is easily calculated from the applied force or torque, T; it is

$$\tau = \frac{T}{2\pi h \kappa^2 R^2} \qquad (D1)$$

where the symbols have their usual meanings. From this relation, we note that the distribution of stress across the gap of the instrument is not dependent on the properties of the fluid.

The shear rate is defined as

$$\dot{\gamma} = r \, d\dot{\theta}/dr \qquad (D2)$$

where $\dot{\theta}$ is the angular velocity at the distance r; even for Newtonian materials $\dot{\gamma}$ varies across the annulus of the viscometer and falls off with the square of the radius, Figure D1.

The problem is how to arrive at the rate of shear at a given position in the gap so that a valid expression for the equation $\dot{\gamma} = f(\tau)$ may be obtained from a plot of rate of shear versus shear stress.

Derivation of Some Basic Equations

From the equations of change and assuming:

(1) an incompressible fluid,

(2) a laminar motion,

(3) circular streamlines,

(4) a steady motion,

(5) no slippage at the walls,

(6) a two-dimensional motion,

(7) an isothermal system,

it is possible to derive the basic equations. We will just outline the

basic steps of derivation:

(a) v_θ is constant with respect to θ,

(b) the product τr^2 is constant and equal to $T/2\pi h$, so that $\tau_{bob}/\tau_{cup} = \kappa^2$,

(c) the shear rate is defined as $\dot{\gamma} = r(d\theta/dr)$.

We simply write that the angular velocity, Ω, is the sum of the differen-

tial angular velocity going from the inner wall to the outer wall; after

transformation, it gives

$$\Omega = \frac{1}{2} \int_{\tau_{bob}}^{\tau_{cup}} f(\tau) \frac{d\tau}{\tau} \qquad (D3)$$

Since we have no knowledge of $f(\tau)$, we need to differentiate this equation

and then develop the function $f(\tau)$ at a particular location. We will use

a Euler-MacLaurin development based on logarithms. We derive,

$$f(\tau_{bob}) = \frac{\Omega}{\ln\varepsilon} \left[1 + \ln\varepsilon \frac{d\ln\Omega}{d\ln\tau_b} + \frac{(\ln\varepsilon)^2}{3} \frac{d^2\ln\Omega}{d(\ln\tau_b)^2} - \frac{(\ln\varepsilon)^4}{45} \frac{d^4\ln\Omega}{d(\ln\tau_b)^4} + \cdots \right.$$

$$(D4)$$

where $\varepsilon = \frac{1}{\kappa}$

A quick analysis of this infinite series tells us that for a Newtonian fluid, the first derivative, $d\ell n\Omega/d\ell n\tau_{bob}$ is equal to 1 and that the terms of second or higher order will be equal to zero. For non-Newtonian fluid, the error involved in terminating the series at any point is dependent on κ. It is then important to follow a procedure as follows:

(1) Obtain measurements of torque and angular velocity over the desired range.

(2) The torque is converted to shear stress at the inner cylinder wall by

$$\tau_{bob} = T/2\pi h\kappa^2 R^2.$$

(3) A log-log plot of Ω versus τ_{bob} is constructed. Derive the slope

$$m = d\ell n\Omega/d\ell n\tau_{bob}.$$

(4) If $m\ell n\varepsilon < .2$, third and higher order terms may be dropped and obtain

$$\dot{\gamma}_{bob} = f(\tau_{bob}) = \Omega/\ell n\varepsilon(1 + m\ell n\varepsilon)$$ with an error less than 1%.

(5) If $.2 < m\ell n\varepsilon < 1.0$, plot m versus $\ell n\tau_{bob}$ and get $dm/d\ell n\tau_{bob}$. The equation of flow is then

$$\dot{\gamma}_{bob} = f(\tau_{bob}) = \frac{\Omega}{\ell n\varepsilon} [1 + m\ell n\varepsilon + \frac{(\ell n\varepsilon)^2}{3} (m^2 + \frac{dm}{d\ell n\tau_b})] \qquad (D5)$$

with an error less than 1%.

Application to Metal Slurries

This method is applied to the data of Figure 28 for a slurry initially sheared at 115 sec^{-1} and held isothermally at $f_s = 0.45$. Figure D2 shows a plot of log Ω versus log τ_{bob} which gives a straight line of slope $m = 1.56$.

Application of equation D5 to the viscometer (see Table D1 for the

values of the instrument constants) gives

$$\dot{\gamma}_{bob} = 4.80\Omega \qquad (D6)$$

instead of

$$\dot{\gamma}_{bob} = 4.40\Omega \qquad (D7)$$

and the error committed is $\Delta\dot{\gamma}/\dot{\gamma}$ = 8.3%. Not only is the relative error small but it is constant in the range of shear rates used. This value is taken as the maximum ever committed since the flow curve of the other slurries are flatter than that described above.

TABLE D1

Instrument Characteristics

h_{cm}	κR_{cm}	R_{cm}	κ	κ^2	$1/\kappa$	Instrument Constant, C $10^{-3}.cm^{-3}$
8.9	2.225	3.015	.739	.545	1.35	3.65
8.9	2.860	3.175	.900	.810	1.11	2.40

End Effect

The end effect may be considered as equivalent to an increase in the effective depth of immersion from h to h + Δh, where Δh, the end correction is in general a function of R, κ, h and the end gap. L.S. Oka[86] has found that

$$\frac{\Delta h}{R} = \frac{1}{8} \frac{\kappa^2 R}{\ell} [1 - \kappa^2]\{1 + 4\frac{\ell}{\kappa R} X (\kappa, R, \ell) + \frac{8}{\pi} \frac{\ell}{\kappa R} Y (\kappa, R, \ell) \qquad (D8)$$

where the first term in the braces corresponds to the end correction due to the bottom of the inner cylinder without the edge effect, the second

term to the edge effect, and the third term to the effects of both the end and the free surface.

Experimental values have been reported by R.N. Weltmann[87] in the study of rheology of pastes and paints:

R,cm	κR,cm	h,cm	Instrument Constant, C, 10^{-3}cm^{-3}	End effect $\Delta h/h$	κ
2.4	2.20	3.60	.75	.134	.91
1.75	1.56	3.53	1.76	.142	.89
1.50	1.30	5.10	2.33	.021	.86
1.45	1.30	5.10	1.82	.017	.89
1.40	1.30	5.10	1.25	.016	.93
1.35	1.30	5.10	.66	.015	.96
.60	.55	5.10	.84	.012	.91

This table shows that the higher the bob is, the smaller the correction is, everything else being equal. As the height of the bob that was used in these experiments was 8.9 cm, no correction was added for the end effects.

VELOCITY PROFILE

$$V_\theta = \frac{\Omega}{1-K^2} \cdot \frac{r^2 - K^2 R^2}{r}$$

SHEAR STRESS

$$\tau_{r\theta} = \frac{T}{2\pi h} \cdot \frac{1}{K^2 r^2}$$

ROTATION
SPEED

Ω

$$\dot{\gamma} = \frac{2\Omega}{1-K^2} \cdot \frac{K^2 R^2}{r^2}$$

SHEAR RATE

FIXED
CYLINDER

r

KR

R
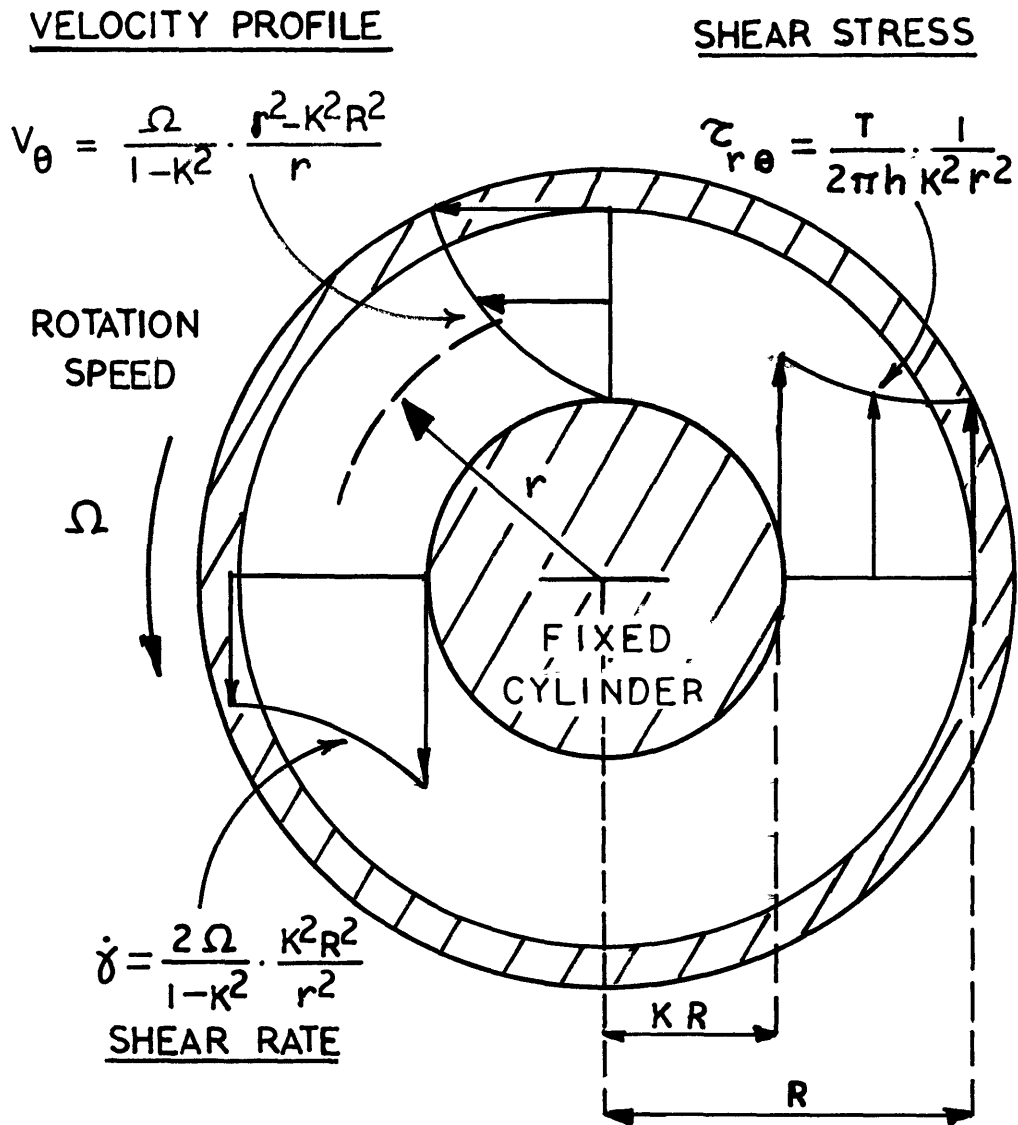
Figure DI . SCHEMATIC DIAGRAM OF TANGENTIAL
ANNULAR FLOW
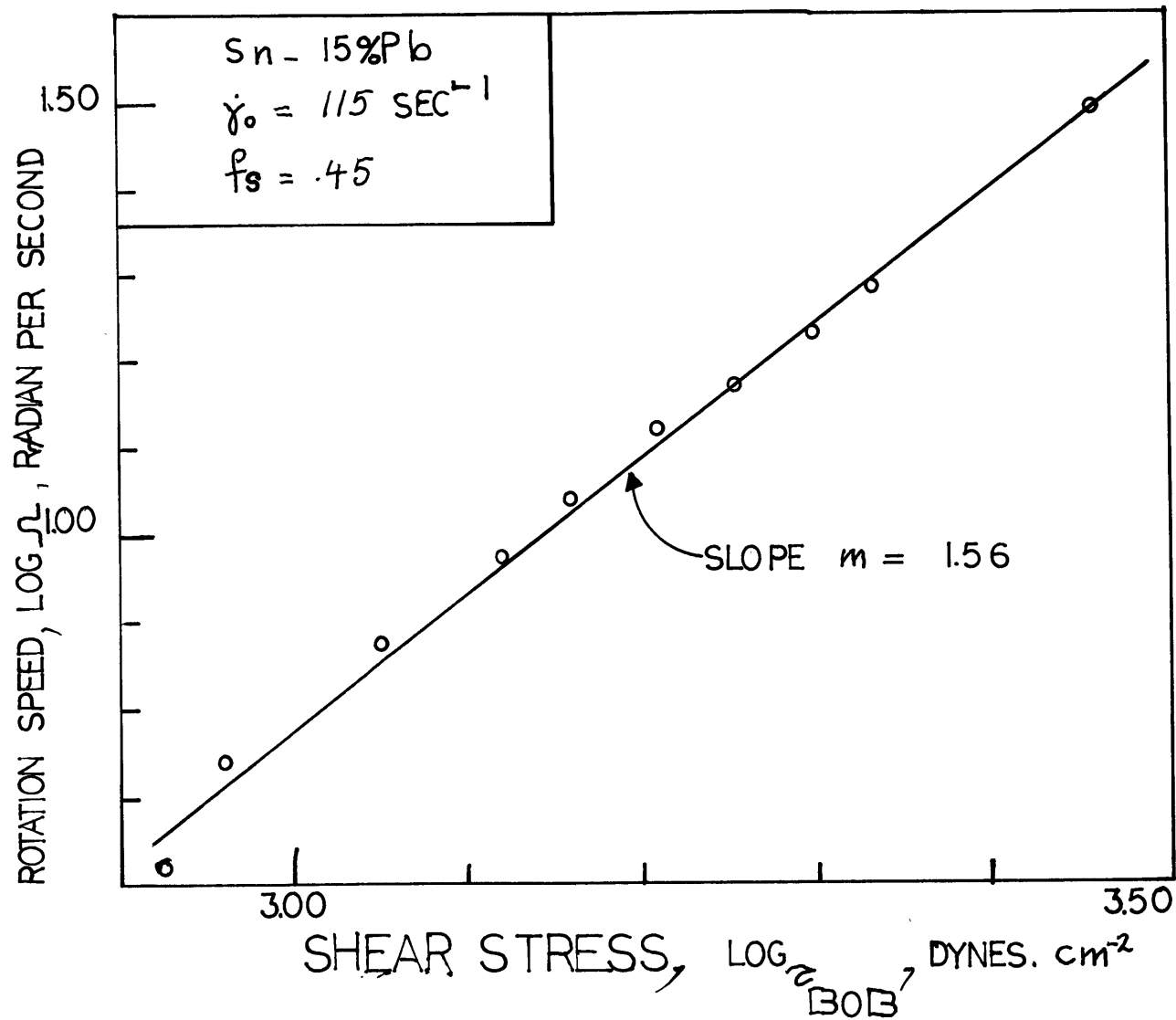
Figure D2.Flow curve of Sn-15%Pb slurry;log-log plot using data
shown in Figure **28**.

APPENDIX E

TURBULENCE AND TEMPERATURE EFFECTS

Turbulence

It is well known that as the velocity of a fluid increases, a transition from laminar to turbulent flow occurs. However, in the case of Couette flow, external forces such as centrifugal forces stabilize the tendency for a fluid particle to move inwards and as shown by H. Schlichting[90] there is no limit to the Reynolds number at which laminar steady flow can occur. However, if the outer cylinder is set in motion impulsively there is a theoretical upper limit

$$Re_{crit} = 66 \times 10^3 \qquad (E1)$$

calculated for $\kappa = 1$. This value is an underestimate of any of the experimental results reported in Figure E1, for different values of the ratio κ. Schlichting also established that, although transition does occur during the starting process, the flow reverts to a laminar pattern when a steady state is established. Schultz-Grunow[91] showed that the persistence of turbulence in steady state regime was due to imperfections in the geometrical shape such as eccentricity and vibrations, Figure E1.

Very little is known about the effect of particles on the onset of turbulence. H. Hatschek and R.S. Jane[92] showed one case where turbulence occurred at two-thirds of the critical Reynolds number. In another study[93], the reverse phenomenon was found: the critical Reynolds number is multiplied by 2 for poly-acrylic acid in water up to 0.08 g/cm^3 in

concentration. It is believed the presence of polymer may help to damp out minor disturbances which could lead to premature turbulence.

Application to Metal Slurries

The Reynolds number is defined as:

$$Re = \Omega R^2 / \nu \qquad (E2)$$

where R is the cup radius, 3 cm

Ω is the rotation speed of the cup, in radians per second,

ν is the kinematic viscosity of the system, cm^2/sec

Applying equation E2 to Sn-15%Pb slurry of viscosity greater than 0.10 poise the flow is found to be laminar up to 1000 rpm.

Temperature Effect

The viscous flow of the liquid phase generates energy that is dissipated by the conduction to the surrounding; as a result the temperature, T_0, rises and reaches a maximum, T, at the center of the annulus. It has been shown[109] that

$$\Delta T = T - T_0 = \frac{1}{8} \eta_0 \frac{\Omega^2 R^2}{k} \qquad (E3)$$

where η_0 is the viscosity of the fluid, 0.025 poise

Ω is the rotation speed of the cup, in radians per second,

R is the radius of the cup, 3 cm,

k is the thermal conductivity of the alloy, 0.04 cal/g.cm°K.

No one has studied the effect of particles on the dissipation of viscous energy. However the presence of particles merely results in an increase of the local shear rate easily derived from geometrical considerations. For instance at g_s = 0.45 it is found that the shear rate is

increased by 4.

Application to Metal Slurries

Application of equation E3 to an Sn-15%Pb slurry at f_s = 0.45 and for a rotation speed of 250 rpm gives

$$\Delta T = 0.45°C \tag{E4}$$

which corresponds to a decrease of 0.01 of fraction solid.
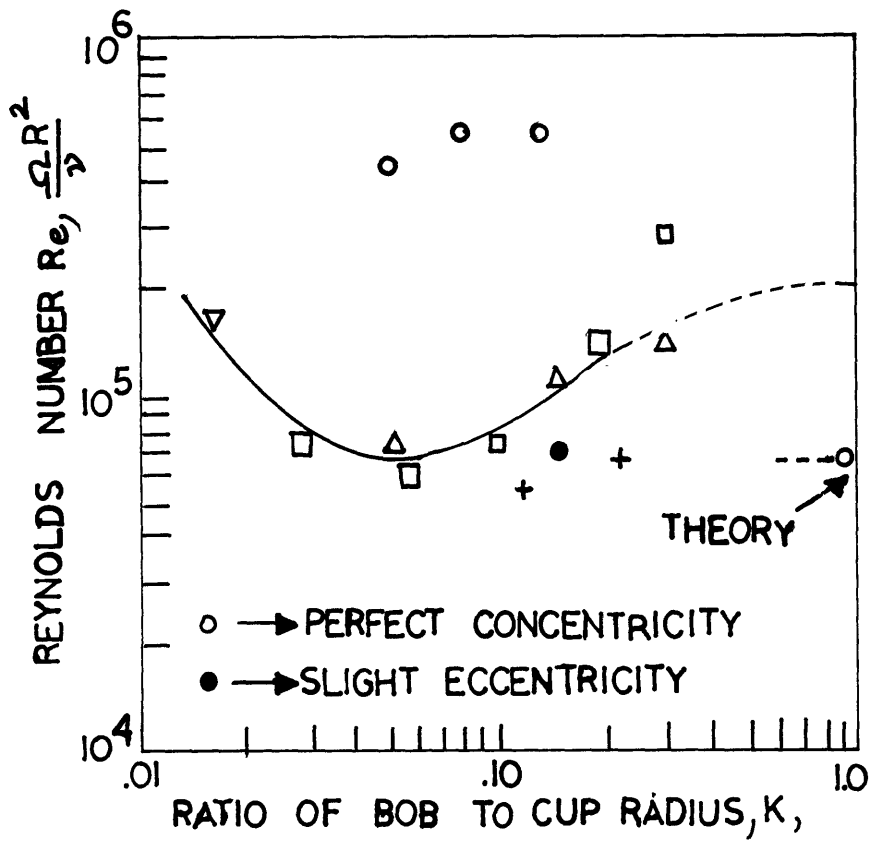
Figure E1. Transition from laminar to turbulent
flow in concentric cylinder visco-
meter, after H. Schlichting[90].

APPENDIX F

SETTLING OR FLOATING OR SOLID PARTICLES IN
A FLUID OF DIFFERENT DENSITY[119]

1.   Stokes Law

The motion of a particle settling under gravity is governed by Newton's second law

$$m \frac{du}{dt} = m'g - F \tag{F1}$$

where m and m' are the masses of the particle and fluid displaced by the particle, u the velocity of the particle, g the intensity of the gravity field at that point and F the frictional force resisting the particle's motion. If the particle is spherical and the resistance entirely due to frictional effects, the magnitude of F is $3\pi\eta ud$ according to Stokes Law, where η is the viscosity of the fluid, d the diameter of the particle.

We get

$$\frac{du}{dt} = \frac{\rho - \rho_0}{\rho} g - \frac{18\eta u}{\rho d^2} \tag{F2a}$$

and in steady motion

$$u = \frac{d^2}{18\eta} (\rho - \rho_0)g \tag{F2b}$$

Effect of particle shape

If the particles are not spherical an equivalent diameter d_2 has to be used.

Effect of concentration

If the concentration of particles in the medium is high enough to

create interference the process of settling does not follow Stokes Law. The suspension as a whole settles at a constant rate with a well defined interface between fluid and settled particles. This form of settling is referred to as "hindered settling" or "mass subsidence". All particles move at the same rate regardless of size and the suspension does not change concentration until it reaches the bottom of its container.

2. Hindered Settling

Steinour[120] obtained the velocity of hindered settling, on the basis of an extensive series of experiments with spheres and irregular particles of different sizes and densities,

$$u_o = u_s \ \varepsilon^2 \ 10^{1.82(1-\varepsilon)}$$ (F3)

where u_s is the velocity of a single particle in the fluid in accordance with Stokes Law, ε is the void fraction.

Using the Kozeny-Carman[121] equation which gives the pressure drop, Δp, due to a fluid flowing with a velocity, u, through a bed of packed particles of depth, L, and porosity, ε

$$\frac{\Delta p}{L} = \frac{k}{g} \ \eta \ \frac{u}{d_s} \ \frac{(1-\varepsilon)^2}{\varepsilon^3}$$ (F4)

where k is a packing constant, d_s the specific surface diameter, Clyde Orr[119] derived the formula

$$u_o = 2 \ \frac{\varepsilon^3}{1-\varepsilon} \ g \ d^2 k' \ \frac{\Delta p}{\eta}$$ (F5a)

$$u_o = \frac{36 \ k' \varepsilon^3}{1-\varepsilon} \ u_s$$ (F5b)

From experimental data they found $k' = .0065$. It is possible to write equation F5 in dimensionless numbers $(1-\varepsilon/\varepsilon^3) \ F_r = R_e$ where F_r is the Frounde Number and R_e the Reynolds Number.

3. Application to Sn-15%Pb Slurries

Using equation F5 and values of η_o[85] and $\Delta\rho$ (Appendix A), one can calculate the initial settling velocity of the solid particles as a function of the fraction solid and the size of the particles, Table F1. To further calculate the distance settled, one needs to take into account the decrease of settling velocity with time because of the increase of the fraction solid.

More accurately if dz is the distance settled in the time dt

$$dz = u_o \ dt \qquad (F6)$$

where the velocity u_o is approximated in the range of fraction solid from 0.45 to 0.50 by the equation

$$u_o = A - B \ g_s \qquad (F7)$$

where A and B are constants. The dependence of g_s upon the distance settled is

$$g_s = g_{so}/(1 - z/z_o) \qquad (F8)$$

where g_{so} is the fraction solid, at time zero, and z_o the height of the slurry in the viscometer. Integrating equation F8 gives

$$z = z_o(1 - g_{so} \ B/A) \cdot (1 - e^{-At/z_o}) \qquad (F9)$$

Application

Given a metal slurry with g_s = .45 at t = 0, d = 200 microns, A = .013 cm/sec and B/A = 1.54 cm/sec and z_o = 10 cm, one gets z = 1 cm after 5 minutes at rest.
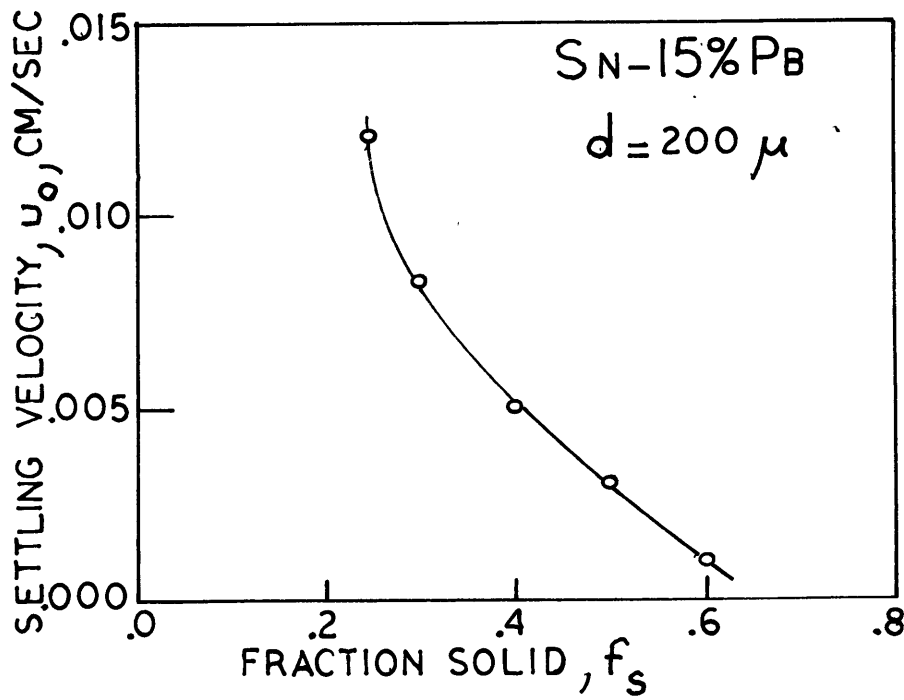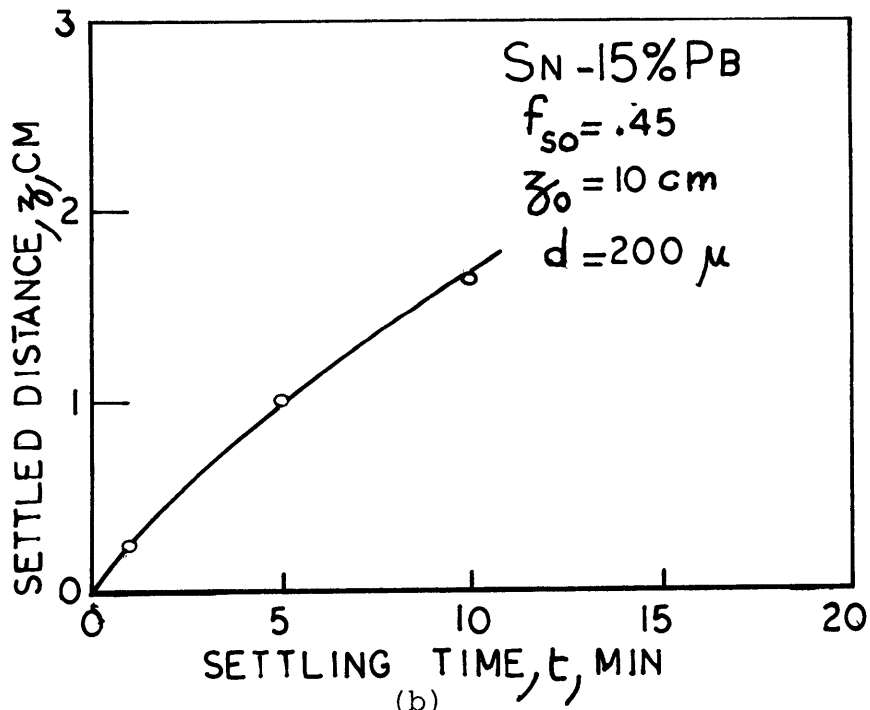
Figure F1. Hindered settling of spherical particles
of Sn-15%Pb slurries, Table F1; (a) settling
velocity, equation (F5b), (b) settled distance
equation (F9).

TABLE F1

Hindered Settling

g_s	.25	.30	.40	.45	.50	.55	.60
Δp g/cm³	.25	.27	.40	.45	.50	.57	.67
η_o poise	.019	.019	.C21	.022	.023	.024	.025

Particle Diameter, d, μ	Settling Velocity, u_o, cm/sec						
100	.003	.002	$.001_2$	.001	$.000_7$	$.000_5$	$.000_2$
200	.012	.008	.005	.004	.003	.002	.001

Settling Time t, min	Settled Distance, z, cm for d = 200μ						
1	-	.45	-	.23	-	.17	-
5	-	1.85	-	1.00	-	.74	-
10	-	2.99	-	1.67	-	1.24	-

APPENDIX G

EFFECT OF SHEAR ON THE STRUCTURE OF SUSPENSIONS

1. Introduction

It is well known that the rheological properties of a system are affected by its structure; this effect was first observed by Ostwald[122] and named structural viscosity and occurs whenever particles in a suspension can form aggregates. Reciprocally it is possible to calculate the effect of shear on the structure of a suspension.

If n_i is the number per cm^3 of aggregates made of i particles, type i, the variations with time of the number of aggregates containing s particles is given[123] by

$$\frac{dn_s}{dt} = \frac{1}{2} \sum_1^{s-1} A_{i,s-i} n_i n_{s-i} - n_s \sum_1^{\lambda} A_{i,s} n_i - B_s(s-1)n_s$$

$$+ 2 \sum_{s+1}^{\lambda} B_i n_i \qquad (G1)$$

where $A_{1,m}$ is the association frequency of aggregates of type 1 and m, B_q is the dissociation frequency of an aggregate of type q, and λ is the maximum number of particles per aggregate. $A_{1,m} n_1 n_m$ is the number per second and cm^3 of collisions of type 1 and type m aggregates giving rise to an aggregate of type $1+m$; $B_q n_q$ is the number of type q aggregates that dissociate in a second.

If x is the average number of particles per aggregate

$$x = \sum_1^{\lambda} sn_s / \sum n_s \qquad (G2)$$

and if the A's and the B's are independent of the type of aggregates, it can be shown[123]

$$x = \sqrt{\frac{n_0 A}{2B}} \qquad (G3)$$

where n_0 is the initial number of particles equal to $\sum_1^\lambda sn_s$.

To predict the size of aggregates one must know the values of the A's and the B's and their variations with shear rate and fraction solid.

2. Collision Frequency

The collision of two particles of size a_i and a_j occurs at a frequency

$$A_{i,j} = \frac{4}{3} R_{ij}^3 \dot{\gamma} \qquad (G4)$$

where $\dot{\gamma}$ is the shear rate, R_{ij} is the radius of collision equal to $a_i + a_j/2$, and where a_i and a_j are the diameters of the aggregates of types i and j, respectively.

The number of collisions per second and unit volume is

$$F_{i,j} = A_{ij} \, n_i \, n_j \qquad (G5)$$

where n_i and n_j are the number of aggregates of type i and j per unit volume. For particles of same size, a, it becomes

$$F = \frac{24 \, g_s^2 \, \dot{\gamma}}{\pi^2 a^3} \qquad (G6)$$

where g_s is the fraction solid.

3. Life Time of Aggregated Particles

Once particles are aggregated, they stay in that state until the fluid flow forces are strong enough to pull them apart. In the case of

non-interacting particles this happens after a certain time T; this time, T, depends on the angle made by the line joining the particle center with the direction of flow and on the shear rate (Figure 58). On the average, this angle is 45° and the time T is equal to $\pi/\dot{\gamma}$[124]. In the case of interacting particles, the aggregates break when

$$F_{cohesion} = F_{fluid\ flow} \tag{G7}$$

where the fluid flow force may be calculated from Stokes Law

$$F_f = \frac{3\pi}{4} \eta\dot{\gamma} \, a_o a_i \tag{G8}$$

where a_i is the size of the aggregate to which the i particles of size a_o are aggregated. When the shear rate is greater than a critical value

$$\dot{\gamma}_c = F_c/\frac{3\pi}{4} \eta a_o a_i \tag{G9}$$

where F_c is the cohesion force , the particles will be pulled out of the aggregate as if there was no interaction; the time spent in the aggregated state is still T (equal to $\pi/\dot{\gamma}$ on the average). If the shear rate is lower than $\dot{\gamma}_c$, the aggregates do not break and the life time is infinite. Aggregation continues until a_i is large enough for $\dot{\gamma}_c$ to equal $\dot{\gamma}$.

4.   Dissociation Frequency

The dissociation frequency is equal to the inverse of the life time of an aggregate; hence,

$$B = \dot{\gamma}/\pi \tag{G10}$$

in the case of non-interacting particles.

5.   Equilibrium Size of Aggregate

At any time, there are in a suspension some particles forming

temporary aggregates (interacting or non-interacting particles); only in the case of interacting particles are there permanent aggregates.

Most of the temporary aggregates[124] are doublets of size $a_2 = 2a_0$ and their concentration is $g_{s2} = 4g_{s1}^2$; there are also triplets of size $a_3 = 3a_0$ and in concentration $g_{s3} = 15.3g_{s1}g_{s2}$.

In the case of interacting particles the permanent aggregates are of size a_i such that the fluid flow forces are just balanced by the forces of cohesion

$$a_i = \frac{4F_c}{3\pi\eta\dot{\gamma}\,a_0} \quad \text{or} \quad x = \frac{4F_c}{3\pi\eta\dot{\gamma}\,a_0^2} \tag{G11}$$

6.   Estimates at High Fraction Solid

At high fraction solid, the collisions probably occur according to the relationships outlined above. However, the life time T of the aggregates and the fluid flow forces are likely to change because some of the assumptions made are no longer valid:

(1) It was assumed that there was no collision during the time of aggregation, but at high fraction solid there are many collisions that either disrupt the pair or contribute to the formation of higher aggregates.

(2) The particles were assumed to have reached their maximum velocity to calculate the fluid flow forces.

In summary, at low fraction solid it is possible to calculate the size of the aggregates as a function of shear rate, equation (G11). However as fraction solid increases, the model cannot describe the mechanisms taking place.

APPENDIX H

VISCOSITY OF A SUSPENSION OF INTERACTING PARTICLES

Part of the dissipated energy in shearing a suspension of interacting particles is used to break network bonds between particles[58]. At a given shear rate, $\dot{\gamma}$, it makes a contribution to the viscosity of the suspension equal to

$$\eta = E/\dot{\gamma}^2 \qquad (H1)$$

where E is the energy dissipation rate expressed as

$$E = N \cdot W \qquad (H2)$$

where N is the number of broken bonds per cm^3 and sec and W is the energy dissipated during the breaking of a bond. N is the product[58] of the collision probability, $(2/\pi)g_s\dot{\gamma}$, times the number of particles per cm^3, $6g_s/8\pi R_1^3$, where g_s is the volume fraction solid and R_1 is the radius of the primary solid particles.

In the following section a model is presented to calculate the term W for Sn-15%Pb slurries.

1. First there is the mechanical energy (energy absorbed before fracture of a weld; area under a stress-strain curve) expressed as

$$W_1 = \tau\varepsilon v \qquad (H3)$$

where τ is the stress acting on the weld resulting from the fluid flow forces (see equation (J3) of Appendix J), ε is the strain of the weld at the time of rupture and v is the volume of the weld equal to $\pi R_2^4/2R_1$[103].

Rearranging equations (H1) to (H3), one gets

$$\eta_1/\eta_0 = \frac{3}{4\pi} \, g_s^2 \, \epsilon (\frac{R_2}{R_1})^4 \qquad \text{(H4)}$$

When applied to Sn-15%Pb slurries, held at 0.45 fraction solid, taking R_1 = 50 and R_2 = 5 microns and ϵ equal to 0.10, one gets η_1/η_0 = 5×10^{-7}.

2. The second type of energy to be dissipated arises from the change in chemical potential, $\Delta\mu$, that the solvent atoms of the weld undergo as they melt back into the fluid at a different equilibrium temperature

$$W_2 = n \, \Delta\mu \qquad \text{(H5)}$$

with n being the number of moles of solvent in the weld. The difference, $\Delta\mu$, is given by the following equation[103]

$$\Delta\mu = 2\overline{V} \, \sigma (\kappa_1 - \kappa_2) \qquad \text{(H6)}$$

where $\overline{V}$ is the partial molar volume, σ is the interfacial energy between the liquid and the solid, κ_1 and κ_2 are the curvatures near and away from the weld. The curvatures κ_1 and κ_2 are given by the following expression

$$\kappa_1 = R_1/R_2^2 \quad \text{and} \quad \kappa_2 = 1/R_1 \qquad \text{(H7)}$$

Rearranging equations (H5) to (H7) one gets for the viscosity

$$\eta_2 = \frac{3}{2\pi} \, \sigma \, g_s^2 \, \frac{R_2^2}{R_1^3} \, \frac{1}{\dot{\gamma}} \qquad \text{(H8)}$$

Table H1 gives the result of equation (H8) when selected values of the Sn-15%Pb alloy are chosen, Table XII. For instance, at a shear rate of 100 sec^{-1}, at a fraction solid of 0.45, for R_1 = 50 and R_2 = 5 microns, the value of viscosity is η_2 = 2 poise.

TABLE H1

Values of the Apparent Viscosity as Calculated

From Equation (H9): $\eta_a = \dfrac{3}{2\pi} \cdot \sigma \cdot \dfrac{g_s^2}{\dot{\gamma}} \cdot \dfrac{R_2^2}{R_1^3}$

Fraction Solid 0.45; Shear Rate 100 sec^{-1}

R_1, microns	10	50	100
R_2, microns	apparent	viscosity,η_a,poise	
1	4.85	0.039	0.005
5	121	.97	.12

APPENDIX I

WELD FORMATION BETWEEN TWO PRIMARY SOLID
PARTICLES OF Sn-15%Pb SLURRIES

The following model describes the formation of a weld between two

primary solid particles of a Sn-15%Pb slurry after the particles have col-

lided, Figure 49. The assumptions are:

(1) The two particles are in true contact - whenever two particles collide,

some liquid is left between them; if, under the pressure exerted by the

particles and caused by the fluid this liquid drains out, then the parti-

cles establish a true contact. The time required by the liquid to drain

will decrease with increasing shear rate, since the fluid flow forces

increase with increasing shear rate (see equation (J1)).

(2) The dihedral angle between the two particles is 180°. This assumes

that the interfacial energy between the solid particles is zero[125], i.e.

there is no lattice misorientation between the two particles[128].

The equilibrium temperature of the solid-liquid interface, at the point of

contact between the particles, depends on the local curvature, and for this

surface of negative curvature, κ, the liquidus temperature is raised by

by[104]

$$\Delta T = - \frac{2\kappa\sigma T_L}{H} \qquad (I1)$$

where $\kappa = \frac{1}{2} (\frac{1}{R_2} - \frac{1}{R_3})$, see Figure 49,

σ = solid-liquid interfacial energy,

T_L = equilibrium liquidus temperature for a planar interface,

H = volumetric heat of fusion.

Assuming equilibrium at the two liquid-solid interfaces (large primary solid particle radius R_1 and area of contact with negative radius of curvature R_3, see Figure 49) a diffusion couple is established in the liquid between the two interfaces such that

$$j = -\rho_L D_L \frac{C_L^c - C_L^p}{R_3} \qquad (12)$$

where j is the flux in $g/cm^2.sec$, D_L is the diffusivity, C_L^p and C_L^c are the weight percents of solute in the liquid in equilibrium with the particle and the area of contact, respectively. From Figure 49, solute is seen to diffuse away from the area of contact. This is equivalent to solvent diffusing to the area of contact, A, so that its volume grows at a rate dV/dt

$$j A dt = \rho_L C_L^c (1 - k) dV \qquad (13)$$

Equations (13) and (12) are now combined recognizing that concentration differences are very small so that $C_L^c = C_L$. Integrating from the start of growth (t = 0, $R_2 = R_{20}$) to the time, t, over which the particles are in contact gives the following expression,

$$R_2^5 - R_{20}^5 = 10\pi R_1^2 \frac{D_L \sigma T_L t}{C_L (1 - k)M_L H} \qquad (14)$$

When R_2 is much larger than R_{20} equation (14) reduces to

$$R_2^5 = 10\pi R_1^2 D_L \sigma T_L t/C_L(1 - k)m_L H \qquad (15)$$

Using selected values of Sn-15%Pb alloy listed in Table XII, equation (15) gives

$$R_2^5 = 1.29 \times 10^{-9} R_1^2 t \tag{16}$$

Equation (16) is plotted in Figure 50 and gives for $R_1 = 100\mu$, a radius $R_2 = 6.5\mu$ after a time $t = 10^{-3}$ seconds.

APPENDIX J

MECHANISM FOR FRACTURE OF A WELD BETWEEN
TWO PRIMARY SOLID PARTICLES

A model is presented to describe the effect of shear rate on fracture of a weld formed between two primary solid particles. The fluid flow forces result in stresses that cause the metallic weld between the primary solid particles to deform (creep) and eventually fracture.

1. Fluid Flow Force

Given two spherical particles of radius, R_1, whose center line is perpendicular to the direction of flow in a liquid of viscosity, η, in shear motion at a rate, $\dot{\gamma}$, there is a net force operating on the weld between these two particles equal to the difference of the drag forces operating on each particle by the fluid. This difference of force may be approximated from Stokes's Law[127] by

$$F = 6\pi R_1 \, \eta \, \Delta v \tag{J1}$$

where Δv is the difference of fluid velocity between the centers of the particles:

$$\Delta v = 2R_1 \dot{\gamma} \tag{J2}$$

The shear stress due to this force operating on the total weld area of πR_2^2 is

$$\tau = 12(R_1/R_2)^2 \, \eta\dot{\gamma} \tag{J3}$$

2. Creep

As a result of this stress, the metallic weld between the two

primary solid particles creeps. The high temperature creep process is essentially limited by the rate of climb of blocked dislocations from their slip planes[109]. Climb is controlled by the rate of diffusion of vacancies to or from the local stress fields. The Dorn-Weertman relation[110] developed from these concppts is usually written

$$\dot{\varepsilon} = A_o e^{-Q_D/RT} \tau^n = A \tau^n \tag{J4}$$

where n, A_o are constants, T the temperature, R the gas content, and where the creep rate, $\dot{\varepsilon}$, during secondary creep (extension at constant strain rate under a constant stress) is expressed as a function of the stress, τ, and the activation energy for self diffusion Q_D. This equation agrees with experimental data for pure metals and dilute alloys in the practical creep stress range.

The creep fracture of alloys occurs when the strain reaches a certain critical value, ε_o, after a time, t_o, which is found empirically to be related to the temperature and stress by the Larson-Miller relation[109]

$$T(C + \log t_o) = f(\tau) \tag{J5}$$

where T is the temperature in degree Rankine (°R), t is in hours and the constant C = 20.

Creep experiments have been performed on the eutectic alloy Sn-15%Pb under stresses up to 2.0 MN/m² (300 psi) at T = 20°C ($T/T_m = 0.65$)[111]. Extension of this curve at high temperature can be obtained using equation (J5) and is plotted in Figure 52. Also plotted in Figure 52 is the fracture time, t_f, time required for the strain to reach the critical limit set as 0.10[126].

$$t_f = \dot{\varepsilon}_0/\varepsilon \qquad \text{(J6)}$$

Between 10^6 and 3×10^7 dyne.cm^{-2} equation (J4) can be rewritten

$$\dot{\varepsilon} = 2.5 \times 10^{-12}\tau^2 \qquad \text{(J7)}$$

and equation (J6)

$$t_f = 4 \times 10^{10} \ \tau^{-2} \qquad \text{(J8)}$$

Now combining equations (J8) and (J3) gives

$$t_f = 230 \times \dot{\gamma}^{-2} \qquad \text{(J9)}$$

3. Fracture

Fracture of a weld will occur if the stress is applied for a time greater than the fracture time (time required for the strain to reach 0.10). The time over which stress is applied may be approximated by the time over which the particles are in contact.

Mason and Bartok[124] have developed an expression relating rate of shear to duration over which two rigid particles (glass) 50 to 300μ, stay in contact in a Couette viscometer. The average doublet life calculated and experimentally determined for fairly dilute suspensions, $f_s \simeq 0.10$, is given by

$$t = \pi/\dot{\gamma} \qquad \text{(J10)}$$

For a shear rate of 100 and 500 sec^{-1}, expression (J10) yields average doublet life of 5×10^{-2} and 6×10^{-3} seconds, respectively.

Calculations of doublet lives and fracture times, from equations (J9) and (J10), are shown in Table XIII and are plotted in Figure 53. Figure 53 shows for this highly simplified model, shear rate conditions under

which a given size weld, formed between two primary solid particles, will have time to fracture or not.

APPENDIX K

EXPERIMENTAL DATA

A. "Continuously Cooled" Results

Run Number	Rotation Speed, Ω r.p.m.	Bob to Cup Radius Ratio, κ	Shear Rate, $\dot{\gamma}$, sec^{-1}	Temp. at Quench, T, °C	Final Fraction Solid, f_{sf}	Cooling Rate $\dot{\epsilon}$ °C/min	Torque at Quench T, 10^6 dyne.cm	Viscosity Data on Figure Number	Structure Data on Figure Number
1	135	.9	115	190.5	.55	25	-	-	20
2	210	.9	230	190.5	.55	25	-	15,18,19	20,21,22
3	360	.9	400	190.5	.55	25	-	19	20,21
4	700	.9	750	190.5	.55	25	-	15,16,19	20,21,22
5	210	.9	230	203.5	.25	25	.120	19	24
6	700	.9	750	203.5	.25	25	.096	19	-
7	700	.9	750	190.5	.55	1.0	-	16	-
8	210	.9	230	196	.45	1.0	-	-	29,31
9	250	.7	115	190.5	.55	0.33	-	17,19,25	20
10	500	.7	230	190.5	.55	0.33	5.05	17,18,19,26	20,21,23
11	500	.7	230	196	.45	0.33	.95	17,18,19	29,31
12	760	.7	350	190.5	.55	0.33	3.08	17,19	20
13	700	.9	750	190.5	.55	0.33	.935	16,17,19	20,21,23
14	700	.9	750	202	.30	0.33	.219	17,19	21,24

B. <u>Viscosity of Isothermally Held Slurries</u> of Sn-15%Pb Alloy After a Total Time in the Liquid-Solid Range of 90 Minutes.

Run Number	Rotation Speed, Ω, rpm	Bob to Cup Radius Ratio, K	Shear Rate sec^{-1}	Temp. T, °C	Fraction Solid, f_s	Torque T, 10^6 dyne/cm	Viscosity Apparent, Poise	Figure Number
15	250	0.7	115	197.6	0.42	.427	13.5	25
16	250	0.7	115	197.2	0.43	.395	12.5	25
17	250	0.7	115	196.3	0.45	.475	15	25,27,30,32
18	250	0.7	115	195.2	0.47	.74	23.5	25,27,30,32
19	250	0.7	115	194.8	0.48	.955	30	25,27,30,32
20	250	0.7	115	194.2	0.49	.74	23.5	25,27,30,32
21	250	0.7	115	193.7	0.50	1.05	33.5	25,27,30,32
22	250	0.7	115	193.7	0.50	1.21	38	25,27,30,32
23	250	0.7	115	193.0	0.51	1.40	47	25,27,30,32
24	250	0.7	115	193.0	0.51	1.77	56	25,27,30,32
25	250	0.7	115	192	0.53	1.89	60	25,27,30,32
26	500	0.7	230	197.6	0.42	.378	6	26
27	500	0.7	230	196.3	0.45	.567	9	26,27,29,30,31,32
28	500	0.7	230	195.2	0.47	.755	12	26,27,29,30,31,32
29	500	0.7	230	190	0.56	1.89	30	26,27,29,30,31,32
30	500	0.7	230	187	0.60	3.90	62	26,27,29,30,31,32
31	320	0.9	350	196.3	0.45	.585	4	27,32
32	700	0.9	750	196.3	0.45	.312	1	27,30,32

C. Pseudoplasticity Experiments. Effect of Change of Shear Rate on the Viscosity of Isothermally Held Slurries of Sn-15%Pb Alloy. (Bob to cup radius ratio of 0.7). Data plotted in Figure 28.

Initial Shear Rate $\dot{\gamma}_0$, sec^{-1}		115		115		230		230		350	
Fraction Solid, f_s		.45		.50		.45		.50		.45	
Rotation Speed, Ω, rpm	Shear Rate, $\dot{\gamma}$, sec^{-1}	Torque, T, 10^6 dyne.cm	Apparent Viscosity η_a, poise	Torque, T, 10^6 dyne.cm	Apparent Viscosity η_a, poise	Torque, T 10^6 dyne.cm	Apparent Viscosity η_a, poise	Torque, T, 10^6 dyne.cm	Apparent Viscosity η_a, poise	Torque, T, 10^6 dyne.cm	Apparent Viscosity η_a, poise
35	16	.252	57.5	-	-	-	-	-	-	-	-
52	24	.257	39	-	-	-	-	-	-	-	-
72	35	.262	29	-	74	-	-	-	-	-	-
102	47	.290	22.5	-	59	-	-	-	-	-	-
152	70	.326	17	-	42	-	-	-	-	-	-
250	115	.472	15	-	30	-	-	.63	20	.236	7.5
435	200	-	-	1.09	20	-	-	-	-	.274	5
500	230	-	-	1.10	17.5	.567	9	.975	15.5	-	-
545	250	-	-	1.10	16	-	-	.99	14.5	-	-
650	300	-	-	-	-	-	-	-	-	.37	4.5
760	350	1.06	11	-	-	.575	6	-	-	.384	4.0

BIBLIOGRAPHY

1. F.R. Eirich, Rheology, Theory and Its Applications, Vol. 1, Academic Press, 1956, New York, p. 1.

2. P. Sherman, Industrial Rheology, Rheology of Dispersed Systems, Chapter III, Academic Press, 1970, New York, p. 97.

3. R.N. Weltmann, Rheology, Theory and Its Applications, Vol. 3, Ed. by F.R. Eirich, Academic Press, 1960, New York, p. 189.

4. A.C. Zettlemeyer and R.R. Myers, Rheology, Theory and Its Applications, Vol. 3, Ed. by F.R. Eirich, Academic Press, 1960, New York, p. 145.

5. S.H. Maron and I.M. Krieger, Rheology, Theory and Its Applications, Vol. 3, Ed. by F.R. Eirich, Academic Press, 1960, New York, p.121.

6. R.S. Lenk, Plastics Rheology, Wiley Interscience, 1968, New York, p. 51.

7. S.A. Metz and M.C. Flemings, Trans. A.F.S., 78, 1970, 453.

8. M.C. Flemings, Solidification Processing, McGraw-Hill, 1974, New York, p. 214.

9. M.N. Galkin and S.V. Lomazov, Russian Castings Production, 8, May, 1970, pp. 241-42.

10. D.B. Spencer, Sc.D. Thesis, Department of Metallurgy and Materials Science, MIT, 1971.

11. D.B. Spencer, R. Mehrabian and M.C. Flemings, Met. Trans., 3, 1972, p. 1925.

12. R. Mehrabian and M.C. Flemings, Fourtieth Intl. Congress on Foundry, Moscow, September 9, 1973.

13. E.F. Fascetta, M.S. Thesis, Department of Metallurgy and Materials Science, MIT, 1973.

14. M. Reiner, Rheology, Theory and Its Applications, Vol. 1, Ed. by F.R. Eirich, Academic Press, 1956, New York, p. 27.

15. M. Reiner, Rheology, Theory and Its Applications, Vol. 1, Ed. by F.R. Eirich, Academic Press, 1956, New York, p. 43.

16. M. Reiner, Deformation and Flow, Ed. by H.K. Lewis, London, 1949, p. 112.

17. P. Sherman, Industrial Rheology, Academic Press, 1970, New York, p. 10.

18. R. Howink, Elasticity, Plasticity and the Structure of Matter, Cambridge University, 1937, London, p. 9.

19. W. Ostwald and R. Auerbach, Kolloid Z., 38, 1926, pp. 261-328.

20. J. Pryce-Jones, J. Oil and Color Chemist's Assoc., 26, 1943, pp. 3-13.

21. W. Eitel, Physical Chemistry of Silicates, University of Chicago Press, 1954, Chicago, p. 347.

22. H.L. Frisch and R. Simha, Rheology, Theory and Its Applications, Ed. by F.R. Eirich, Academic Press, 1956, New York, pp. 594-613.

23. R.B. Bird, W.E. Stewart and E.N. Lightfoot, Transport Phenomena, Wiley, 1960, New York, p. 76.

24. D.I. Lee, Trans. Soc. Rheology, 13, No. 2, 1969, pp. 273-288.

25. I.R. Rutgers, Rheol. Act., 2, 1962, pp. 202-305.

26. A. Einstein, Annalen der Physik, 19, 1909, pp. 289-371.

27. G.B. Jeffery, Proc. Roy. Soc. of London, A 102, 1922, p. 161.

28. W.R. Blakeney, J. Colloid and Interface Science, 22, 1966, pp. 324-30.

29. E. Guth and R. Simha, Kolloid Z., 74, 1936, p. 266.

30. N. Saito, J. Phys. Soc. (Japan), 5, 1950, p. 4.

31. V. Vand, J. Phys. and Colloid Chem., 52, 1948, p. 277.

32. R. Manley and S. Mason, Can. J. Chem., 33, 1955, p. 763.

33. M. Mooney, J. Colloid. Sci., 6, 1951, pp. 162-170.

34. D.G. Thomas, J. of Colloid Sci., 20, 1965, pp. 267-277.

35. H. Eyring, D. Henderson, Statistical Mechanics and Dynamics, Wiley, 1964, New York, p. 460.

36. A.B. Metzner and M. Whitlock, Trans. Soc. Rheology, 2, 1958, pp. 239-254.

37. J.S. Chong, E.B. Christiansen and A.D. Baer, J. Appl. Polymer Science, 15, 1971, pp. 2007-2021.

38. B. Clarke, Trans. Instr. Chem. Engrs., 45, 1967, T pp. 251-256.

39. H.D. Jefferies, J. Oil and Color Chem. Assoc., 45, No. 10, 1962, p. 681.

40. C. Moreland, Can. J. Chem. Eng., 41, Feb., 1963, pp. 24-28.

41. S.G. Ward, Brit. J. Applied Physics, 1, Nov., 1950, pp. 286-290 (Part I), pp. 325-328 (Part II).

42. L.W. Coughanour and F.H. Norton, J. Am. Soc. Ceram., 32, No. 4, 1949, pp. 129-132.

43. G. Baum, J. Composite Materials, 2, No. 1, Oct., 1968, p. 128.

44. G.F. Eveson, Rheology of Disperse Systems, Ed. by C.C. Mill, Pergamon Press, 1959, New York, pp. 61-83.

45. R.J. Farris, Trans. Soc. Rheology, 12, No. 2, 1968, pp. 281-301.

46. T.B. Lewis and L.E. Nielsen, Trans. Soc. Rheology, 12, No. 3, 1968, pp. 421-443.

47. S.G. Ward, Br. J. Applied Physics, 10, 1959, p. 317.

48. H. DeBruijn and P.G. Meerman, Proc. of First Intl. Congress on Rheology, Holland, 1943, Ed. by NHPC, Amsterdam, p. II 60.

49. W. Haller, Kolloid Z., 56, 1931, pp. 257-267.

50. J.M. Burgers, In "Second Report on Viscosity and Plasticity", Nordemann, 1938, New York, pp. 113-184.

51. H.R. Shaw, J. Petrology, 10, 1969, pp. 510-535.

52. R.S. Porter and J.F. Johnson, Trans. Soc. Rheology, 11, No. 3, 1967, pp. 259-266.

53. J. Hermans Jr., J. of Colloid Sci., 17, 1962, pp. 638-648.

54. H. Freundlich, Thixotropy, Herman, 1935, Paris, p. 3.

55. W.H. Bauer and E.A. Collins, Rheology, Theory and Its Applications, Vol. 4, Ed. by F.R. Eirich, Academic Press, 1967, New York, p. 457.

56. T. Alfrey Jr., Mechanical Behavior of High Polymers, Interscience Publishers, 1948, New York, p. 45.

57. H. Green and R.N. Weltmann, Analysis of the Thixotropy of Pigment-Vehicle Suspensions, Ind. Eng. Chem. An. Ed., 15, No. 3, March 15, 1943, pp. 201-206.

58. S.J. Hahn, T. Ree and H. Eyring, Ind. Eng. Chem., 51, No. 7, July, 1959, pp. 856-857.

59. D.A. Denny and R.S. Brodkey, J. Applied Physics, 33, No. 7, 1959, pp. 2269-2274.

60. A.G. Fredrickson, AIChE J., 16, No. 3, May, 1970, pp. 436-441.

61. H.T. Kim and R.S. Brodkey, AIChE J., 14, No. 1, Jan., 1968, pp. 67-68.

62. H. Eyring et al., Trans. Soc. Rheology, V, 1961, pp. 67-84.

63. H.D. Weymann, Proc. of the Fourth Intl. Cong. on Rheology, Ed. by E.H. Lee, Interscience Publishers, 1965, New York, p. 573.

64. R.J. Morgan, Trans. Soc. Rheology, 12, No. 4, 1968, pp. 511-533.

65. D.C.H. Cheng and F. Evans, Brit. J. Appl. Phys., 16, 1965, pp. 1599-1617.

66. C. Goodeve, Trans. Far. Soc., 38, 1938, p. 511.

67. T. Gillespie, J. Colloid Science, 15, 1960, pp. 219-231.

68. A.S. Michaels and J.C. Bolger, I. and E.C. Fundamentals, 1, No. 3, August, 1962, pp. 153-162.

69. R.A. Ritter and G.W. Govier, Can. J. Chem. Eng., 48, 1970, pp. 505-513.

70. G.J. Davies, Solidification and Casting, Wiley, 1973, New York, p. 105.

71. T.Z. Kattamis, J. Coughlin and M.C. Flemings, Trans. AIME, 239, 1967, p. 1504.

72. K.A. Jackson, J.D. Hunt, D.R. Uhlmann and T.P. Steward III, Trans. AIME, 236, 1966, p. 149.

73. R.T. Southin, J. Inst. Metals, 94, 1966, p. 401.

74. W.A. Tiller and S. O'Hara, The Solidification of Metals, ISI Publication, #110, London, 1968, p. 27.

75. R.G. Garlick and J.F. Wallace, Trans. AFS, 67, 1959, p. 366.

76. G.F. Balandin and Y.P. Yakolev, Physics of Metals and Metallography, 13, No. 3, 1962, p. 112.

77. V. Kondic, Acta Metallurgica, 6, 1958, p. 660.

78. F.A. Crosley, R.D. Fischer and A.G. Metcalfe, Trans. AIME, 221, 1961, p. 419.

79. F.C. Langeberg, G. Pestel and C.R. Honeycutt, Trans. AIME, 221, 1961, pp. 993-1001.

80. C. Mascré, Fonderie, 200, 1962, p. 361.

81. F. Sauerwald, Metall., 3, Nos. 23/24, 1949, pp. 414-415.

82. K.E. Mann and E. Riepert, Metall., 10, Nos. 5/6, 1956, pp. 195-199.

83. J.R. Van Wazer et al., Viscosity and Flow Measurement, Interscience Publishers, 1963, New York, p. 55.

84. M. Reiner, Rheology, Vol. 1, Ed. by F.R. Eirich, Academic Press, 1956, New York, p. 34.

85. M.R. Thresh and F.A. Crawley, Met. Trans., 1, 1970, pp. 1531-1535.

86. S. Oka, Bull. Kobayashi Inst. Phys. Research, 7, 1957, p. 13.

87. R.N. Weltmann, Rheology, Theory and Its Applications, Vol. 3, Ed. by F.R. Eirich, Academic Press, 1960, New York, p. 197.

88. H. Green, Ind. Eng. Chem. An. Ed., 14, No. 7, June 15, 1942, p. 576.

89. M.M. Couette, Ann. de Chimie et Physique, 21, 1890, p. 433.

90. H. Schlichting, Boundary Layer Theory, Translated by J. Kestin, McGraw-Hill, 1960, New York, p. 428.

91. F. Schultz-Grunow, ZAMM, 39, 1959, p. 101.

92. Von E. Hatschek and R.S. Jane, Kolloid Z., 38, 1926, p. 33.

93. E.L. Kelley and J.G. Brodnyan, Fourth Intl. Cong. on Rehology, Ed. by E.H. Lee, Interscience Publishers, 1965, New York, p. 57.

94. A.G. Fredrickson, Principle and Applications of Rheology, Prentice Hall, 1964, New Jersey, U.S.A., p. 144.

95. R.B. Bird and C.F. Curtiss, Chemical Engineering Science, 11, 1959, pp. 108-113.

96. E.C. Carver and J.R. Van Wazer, J. of Physical and Colloid Chemistry, 51, 1947, pp. 751-763.

97. S.A. Saltykov, Stereometric Metallography, Second Edition, Metallurgizdat, Moscow, 1958, p. 446.

98. R.T. DeHoff, Quantitative Metallography, McGraw Hill, 1968, New York, p. 128.

99. F. Moore, Trans. Brit. Ceram. Soc., 58, 1959, pp. 470-492

100. J. Pryce-Jones, Kolloid Z., 129, 1952, pp. 96-122.

101. T.C. Patton, Paint Flow and Pigment Dispersion, Interscience Publishers, 1966, New York, p. 109.

102. D.J. Doherty and R. Hurd, J. Oil and Color Chemist's Assoc., 41, 1958, pp. 42-77.

103. M.C. Flemings, Solidification Processing, McGraw Hill, 1974, New York, p. 273.

104. M.C. Flemings, Solidification Processing, McGraw Hill, 1974, New York, p. 266.

105. W.D. Kingery, Introduction to Ceramics, Wiley, 1960, New York, p. 371.

106. G. Doge and K.H. Standke, Z. Naturforsch, 22A, No. 1, 1967, pp. 62-66.

107. P. Pascal, Nouveau Traité de Chimie Minérale, Tome VIII, 3e Fascicule, Masson et Cie, Paris, 1961, p. 301.

108. D.W.G. White, Met. Trans., 2, Nov. 1971, p. 3067.

109. W. Hayden et al., Mechanical Behavior, Wiley, 1965, New York, p. 133.

110. J. Weertman, Trans. AIME, 227, 1963, p. 1475.

111. B. Burton, Scripta Metallurgica, 5, 1971, pp. 669-672.

112. M. Hansen, Constitution of Binary Alloys, McGraw Hill, New York, 1958, and supplements.

113. G.V. Raynor, Annotated Equilibrium Diagrams, No. 6, Institute of Metals, London, January, 1947.

114. H.J. Fisher and A. Phillips, Trans. AIME, 200, 1954, p. 1060.

115. H.R. Thresh, A.F. Crawley and D.W.G. White, Trans. AIME, 242, No. 5, 1968, pp. 819-822.

116. J.A. Lee and G.V. Raynor, Proc. Phys. Soc. (London), 67B, 1954, pp. 737-747.

117. R.T. DeHoff, Trans. AIME, 224, 1962, pp. 474-477.

118. R.B. Bird, W.E. Stewart and E.N. Lightfoot, Transport Phenomena, Wiley, 1960, New York, p. 277.

119. F.C. Orr Jr., Fine Particle Measurement, MacMillan and Co., 1959, New York, p. 43.

120. H.H. Steinour, Ind. Eng. Chem., 36, 1944, pp. 618-624.

121. J. Kozeny, Sitzber. Akad. Wiss. Wien., Math. Naturw. Kl, Abt. IIa 136, 1927, pp. 271-306.

122. Wo. Ostwald and R. Auerbach, Kolloid Z., 38, 1926, pp. 261-228.

123. M. Joly, Rheologica Acta, 1, Nos. 2-3, 1958, pp. 180-185.

124. S.G. Mason and W. Bartok, in Rheology of Dispersed Systems, Ed. by C.C. Mill, Pergamon Press, 1959, New York, p. 16.

125. C.S. Smith, Private communication, Massachusetts Institute of Technology, Department of Metallurgy and Materials Science, April, 1974.

126. R.M. Pelloux, Private communication, Massachusetts Institute of Technology, Department of Metallurgy and Materials Science, April, 1974.

127. W. Albers and J. Th. G. Overbeek, J. Colloid Science, 15, 1960, pp. 489-502.

128. K.T. Aust and B. Chalmers, Proc. of the Royal Society of London, A 201, 1950, p. 210.

129. M.C. Flemings, Solidification Processing, McGraw Hill, 1974, New York, p. 148.

BIOGRAPHICAL NOTE

The author was born on January 23, 1947, in Paris, France. He received his Baccalauréat C with honor from Lycée Hoche, Versailles, where he remained for two years to be sussessfully admitted to Ecole des Mines de Nancy and Ecole Supérieure d'Electricité de Paris in 1966. He received his degree of Ingénieur Civil des Mines in 1969 and went to Carnegie-Mellon University for one year. He joined M.I.T. in 1970 and received his M.S. 1971.

He is a second lieutenant of the Armes Blindées et Cavalerie of the French Army. He was married in 1971 and has one daughter, Léa Desirée.